

Durham E-Theses

Some kinetic and equilibrium studies of the reactions of nitrobenzofurazan derivatives with nucleophiles

Rabbitt, Lynsey C.

How to cite:

Rabbitt, Lynsey C. (2000) *Some kinetic and equilibrium studies of the reactions of nitrobenzofurazan derivatives with nucleophiles*, Durham theses, Durham University. Available at Durham E-Theses
Online: <http://etheses.dur.ac.uk/4623/>

Use policy

The full-text may be used and/or reproduced, and given to third parties in any format or medium, without prior permission or charge, for personal research or study, educational, or not-for-profit purposes provided that:

- a full bibliographic reference is made to the original source
- a [link](#) is made to the metadata record in Durham E-Theses
- the full-text is not changed in any way

The full-text must not be sold in any format or medium without the formal permission of the copyright holders.

Please consult the [full Durham E-Theses policy](#) for further details.

SOME KINETIC AND EQUILIBRIUM STUDIES
OF THE REACTIONS OF NITROBENZOFURAZAN
DERIVATIVES WITH NUCLEOPHILES

by

Lynsey C. Rabbitt, B. Sc. Hons. (Dunelm)

Graduate Society

The copyright of this thesis rests with the author. No quotation from it should be published in any form, including Electronic and the Internet, without the author's prior written consent. All information derived from this thesis must be acknowledged appropriately.

A thesis submitted for the degree of Doctor of Philosophy
in the Department of Chemistry, University of Durham, 2000.



13 JUL 2001

To Mum, Dad, Michelle and Simon.

SOME KINETIC AND EQUILIBRIUM STUDIES OF THE REACTIONS OF NITROBENZOFURAZAN DERIVATIVES WITH NUCLEOPHILES

By Lynsey C. Rabbitt

A thesis submitted for the degree of Doctor of Philosophy in the
Department of Chemistry, University of Durham, 2000.

Abstract

The reactions of 4,6-dinitrobenzofuroxan, (DNBF) with aniline and six of its N- and ring-substituted derivatives have been studied. It is known that aniline usually reacts as a nitrogen nucleophile, forming nitrogen-bonded σ -adducts with trinitrobenzene, (TNB) in the presence of a strong base. However, in acidic solutions, σ -adducts are formed with bonding between a ring carbon atom of the anilines and the 7-position of DNBF. A value of 2.0 for k_H/k_D , the kinetic isotope effect, indicates that bond formation is largely rate determining in the substitution pathway. Estimates were made for the pK_a values relating to carbon protonation of the anilines. In solutions of aniline buffered with aniline hydrogen chloride it was possible to distinguish an initial, rapid reaction via the nitrogen centre to give anionic σ -adducts. The thermodynamically more stable carbon-bonded σ -adducts were observed to form over time. In the presence of excess amine, these zwitterionic σ -adducts were in rapid equilibrium with the deprotonated forms. Equilibrium constants for this acid-base process were measured, and indicate that the negatively charged DNBF moiety is electron withdrawing relative to hydrogen.

Kinetic and equilibrium studies are reported for the reactions of several aliphatic amines with a selection of nitrobenzofurazan derivatives in DMSO. Rapid reaction at the 5-position to yield σ -adducts was followed by slower formation of the thermodynamically more stable adducts at the 7-position. Proton transfer from the zwitterionic intermediates to a second molecule of amine was generally rapid, and the attack of the amine rate determining. This is in direct contrast with reactions involving TNB, where the proton transfer step is usually rate limiting.

The reactions of four nitrobenzofurazan derivatives with sulfite have been studied in aqueous solutions. The stability of the initially formed 5-adducts was remarkably high in comparison with the corresponding σ -adducts formed from attack of sulfite on TNB. A slow isomerisation was observed to yield the thermodynamically more stable 7-adducts, except in the reaction with 4-nitro-7-chlorobenzofurazan, where attack at the 7-position would lead to nucleophilic substitution of the chloro-group to yield the substitution product. The mechanism of the isomerisation was found to occur via an intermolecular rearrangement, and not according to an intramolecular Boulton-Katritzky rearrangement. Sulfite attack on DNBF was also studied. A value for the equilibrium constant for the formation of a 1:1 adduct, K_7 $1.1 \times 10^{13} \text{ dm}^3 \text{ mol}^{-1}$ was determined. This high value is a reflection of the high carbon basicity of the sulfite ion, and the highly electrophilic character of DNBF. Evidence was also obtained for the formation of 1:2 di-adducts in the presence of excess sulfite, which are present in the isomeric cis and trans forms.

Acknowledgements

I would like to thank my Ph.D. supervisor Dr. Mike Crampton, for all his help, support and encouragement over the last three years. His enthusiastic approach to Physical Organic Chemistry has been an inspiration, and his generosity greatly appreciated.

A special “thank you” goes to Colin. His technical wizardry, sense of humour and selfless nature have made large problems into small incidents, and his friendship in times of difficulty has been unfaltering.

Thanks also go to my lab colleagues, past and present. Andy, Ian, Andy “Taffster” Munro, Kathryn “Chicken Dippers” Brown, Seve, Linda “Gibbo” Gibbons, Tony “The Tiger” Holmes, Darren “Dr” Noble, Paul “Big Work Week” Coupe and Dave “Elvis” Parkin. I’ll never forget cheesy chips, “hat power”, that New Inn table and those “big work weeks”!

Special thanks must go to my parents, for their never-ending love, support (both emotional and financial) and belief in my ability, and to Simon, for.....everything.

Declaration

The material in this thesis is the result of research undertaken in the Department of Chemistry, University of Durham, between October 1997 and August 2000. It is the original work of the author except where acknowledged by reference, and has not been submitted for any other degree.

Statement of Copyright

The copyright of this thesis lies with the author. No quotations from it should be published without prior written consent, and information derived from it should be acknowledged.

Contents

1 Introduction	10
1.1 Nucleophilic Aromatic Substitution Reactions	11
1.1.1 The Mechanism of Nucleophilic Aromatic Substitution Reactions	11
1.1.2 Early Mechanistic Investigations	12
1.1.3 Spectroscopic Evidence for the Formation of Intermediates	13
1.1.3.1 NMR Spectroscopy	14
1.1.3.2 X-ray Crystallography	16
1.1.3.3 Theoretical Studies	17
1.1.4 Factors Which Influence Reactivity	19
1.1.4.1 Activation by NO ₂	19
1.1.4.2 Leaving Group Ability	21
1.1.4.3 Influence of the Nucleophile	24
1.1.4.3.1 Nitrogen Nucleophiles	25
1.1.4.3.2 Sulfur Nucleophiles	28
1.1.4.3.3 Carbon Nucleophiles	29
1.1.4.4 Reactivity at Unsubstituted Versus Substituted Ring Carbons	30
1.1.5 Solvent Effects	30
1.2 Electrophilic Aromatic Substitution Reactions	32
1.2.1 The Mechanism of Electrophilic Aromatic Substitution	32
1.2.2 Early Mechanistic Investigations	33
1.2.3 Evidence to Support the Mechanism	33
1.2.3.1 Kinetic Isotope Effects	33
1.2.3.2 Isolation of the Intermediate	34
1.2.4 The Effects of Substituents	35
1.2.5 The Hammett Equation	35
1.2.6 Electrophilic Aromatic Substitutions Involving Aniline	37
1.3 Nitrobenzofurazans and Nitrobenzofuroxans	39
1.3.1 Structure	39
1.3.2 Hydroxide Ion Attack on DNBF	42
1.3.3 Reactivity	45
1.3.3.1 As an Electrophile	45

1.3.3.2 With the "Proton Sponge"	46
1.3.3.3 Formation of Carbon-Bonded Adducts	48
1.3.3.4 With Ketones	49
1.3.3.5 With Nitroalkanes	50
1.3.3.6 In Diels-Alder Reactions	52
1.3.3.7 Formation of Spiro-Cyclic Adducts	53
1.3.4 Applications	54
1.4 References	56
2 Electrophilic Aromatic Substitution in Aniline Derivatives	60
2.1 Introduction	61
2.1.1 Reactions of Trinitrobenzene with Aniline	61
2.1.2 Reactions of 4,6-Dinitrobenzofuroxan with Aniline	62
2.1.3 Reaction of 4,6-Dinitrobenzofuroxan with Phenoxide	66
2.2 Experimental	67
2.3 Results and Discussion	67
2.3.1 NMR Data	67
2.3.2 Kinetic Data for Reaction in HCl	69
2.3.3 Calculation of KH_2O	70
2.3.4 Reaction of DNBF and Aniline	73
2.3.4.1 Kinetic Data	73
2.3.4.2 Kinetic Isotope Effect Studies	78
2.3.5 Reaction of DNBF with Substituted Anilines	80
2.4 Comparison with other π -Excessive Aromatics	86
2.5 Conclusion	88
2.6 References	89
3 The Ambident Reactivity of Aniline Derivatives Towards DNBF	90
3.1 Introduction	91
3.2 Experimental	92
3.3 Results and Discussion	92
3.3.1 Calculation of pK_a Values of Aniline Derivatives in DMSO	94
3.3.2 NMR Data	100
3.3.2.1 Carbon-Adduct Deprotonation in Presence of Excess Aniline	103

3.3.3 Kinetic Data in DMSO	107
3.3.3.1 Measured in the Presence of HCl	107
3.3.3.2 Measured in Solutions Containing Aniline and Aniline Hydrochloride	112
3.4 Comparison with TNB	118
3.5 Conclusion	119
3.6 References	120
4 The Reactions of 4-Nitrobenzofurazan and 4-Nitrobenzofuroxan with Amines in DMSO	121
4.1 Introduction	122
4.2 Experimental	125
4.3 Results and Discussion	125
4.3.1 NMR Data	127
4.3.2 Kinetic Data	130
4.3.2.1 Reactions of Piperidine	134
4.3.2.2 Reactions of Pyrrolidine	139
4.3.2.3 Reactions of Morpholine	141
4.3.2.4 Reactions of n-Butylamine	144
4.3.2.5 Reactions of Benzylamine	147
4.3.2.6 Reactions of N-Methylbenzylamine	149
4.4 Comparison of 4-Nitrobenzofurazan (NBZ) and 4-Nitrobenzofuroxan (NBF)	153
4.5 Comparison with Trinitrobenzene (TNB)	157
4.6 Conclusion	159
4.7 References	159
5 The Reactions of 4-Nitro-7-X-Benzofurazans with Amines in DMSO	161
5.1 Introduction	162
5.2 Experimental	165
5.3 Results and Discussion	166
5.3.1 NMR Data	168
5.3.2 Kinetic Data	170
5.3.2.1 Reactions of Piperidine	178
5.3.2.2 Reactions of Pyrrolidine	183

5.3.2.3 Reactions of n-Butylamine	187
5.3.2.4 Reactions of Benzylamine	193
5.3.2.5 Reactions of N-Methylbenzylamine	199
5.4 Comparisons	203
5.4.1 The Directing Effects and Leaving Group Abilities of the X-Substituents	207
5.4.2 Reactivity of Piperidine and Pyrrolidine	209
5.4.3 Reactivity of Primary and Secondary Amines	210
5.4.4 Amine Attack at Substituted vs Unsubstituted Positions	213
5.5 Conclusion	215
5.6 References	216
6 Kinetic and Equilibrium Studies of the Reactions of 4-Nitrobenzofurazan, and some Derivatives with Sulfite Ions in Water	217
6.1 Introduction	218
6.2 Experimental	220
6.3 Results and Discussion	221
6.3.1 NMR Data	222
6.3.2 Kinetic Data	228
6.3.2.1 Reaction of 4-Nitrobenzofurazan	229
6.3.2.2 Reaction of 4-Nitrobenzofuroxan	234
6.3.2.3 Reaction of 4-Nitro-7-chlorobenzofurazan	237
6.3.2.4 Reaction of 4-Nitro-7-methylbenzofuroxan	239
6.4 Comparisons	241
6.5 Conclusion	243
6.6 References	245
7 Reactions of 4,6-Dinitrobenzofuroxan with Sulfite in Aqueous Solution	246
7.1 Introduction	247
7.2 Experimental	251
7.3 Results and Discussion	252
7.3.1 NMR Data	252
7.3.2 Kinetic and Equilibrium Studies	256
7.3.2.1 Formation of a 1:1 DNBF:Sulfite Adduct	256

7.3.2.2 Reactions of the 1:1 DNBF:Sulfite Adduct with Protons and Hydroxide Ions	258
7.3.2.3 Formation of a 1:2 DNBF:Sulfite Adduct	261
7.3.2.4 Reaction of the 1:1 DNBF:Hydroxide Adduct with Sulfite	267
7.3.2.5 Reaction of DNBF with the Hydrogen Sulfite Ion	269
7.4 Comparisons	276
7.5 Conclusion	279
7.6 References	279
8 Appendix	280
8.1 Measurement Techniques	281
8.1.1 UV/Visible Spectrophotometry	281
8.1.2 Stopped-flow Spectrophotometry	284
8.1.3 NMR Spectroscopy	286
8.1.4 pH Measurements	287
8.2 Derivation of Rate Equations	288
8.2.1 Attack at an Unsubstituted Ring Position	288
8.2.2 Attack at a Substituted Ring Position	292
8.2.3 Formation of the Substitution Product	296
8.3 Publications, Conferences, Examined Lecture Courses and Colloquia	299
8.3.1 Research Publications	299
8.3.2 Conferences Attended	299
8.3.3 Examined Lecture Courses	300
8.3.4 Colloquia, Lectures and Seminars	300
8.4 References	307

Chapter 1

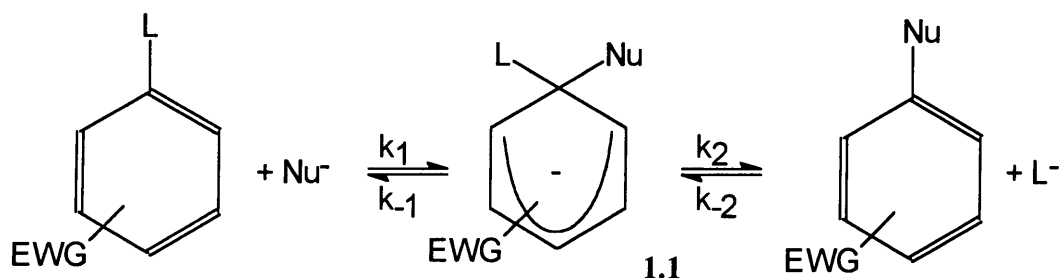
Introduction

1 Introduction

1.1 Nucleophilic Aromatic Substitution Reactions

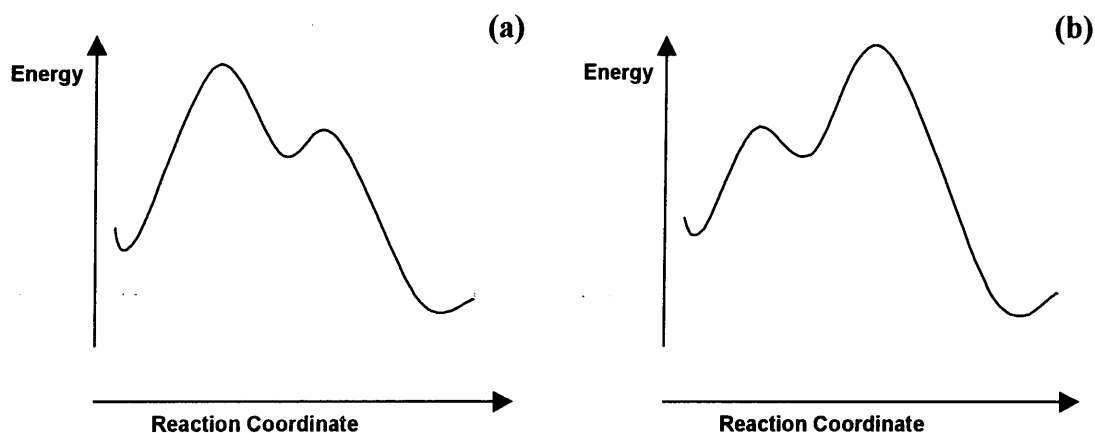
1.1.1 The Mechanism of Nucleophilic Aromatic Substitution Reactions

The general mechanism for nucleophilic aromatic substitution is illustrated in Scheme 1.1,¹ where L represents a leaving group, Nu⁻ an anionic nucleophile, and EWG an electron withdrawing group or groups. Attack of Nu⁻ produces an intermediate cyclohexadienyl anion, **1.1**, (also known as a σ -adduct) which contains an sp³ hybridized carbon atom. The energy of the intermediate, **1.1**, will depend on the number and type of electron withdrawing groups, and the nature of the attacking nucleophile, Nu⁻, and leaving group, L⁻.

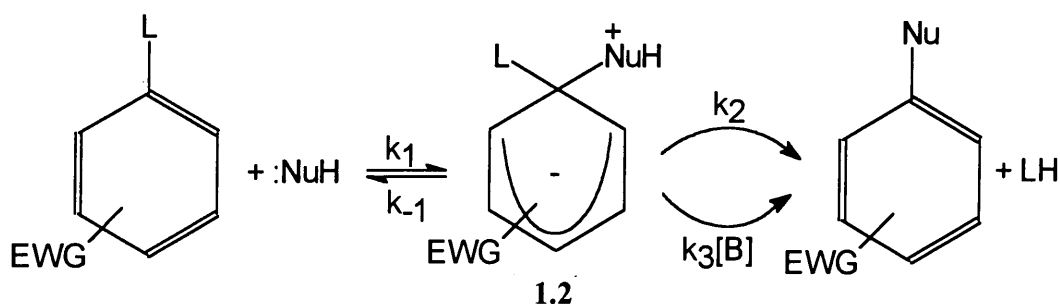


The σ -adduct intermediate subsequently decomposes to yield the substitution product. Either the formation or decomposition of the σ -complex may be rate limiting,² depending on the relative energies of the two transition states, Figure 1.1.¹

Figure 1.1: Energy diagrams for reactions assuming, (a) rate-limiting formation, and (b) rate-limiting decomposition of the intermediates.

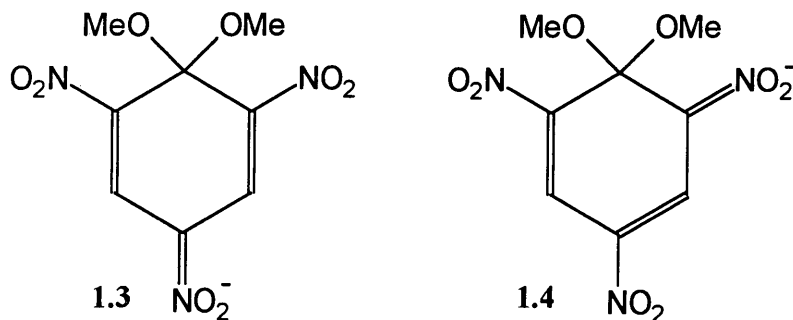


When the attacking nucleophile is neutral, the initially formed σ -adduct intermediate **1.2** is zwitterionic, Scheme 1.2. The acidic proton is removed by a base, which may be the nucleophile itself. Therefore, conversion to products can occur via an uncatalysed or base-catalysed pathway.¹

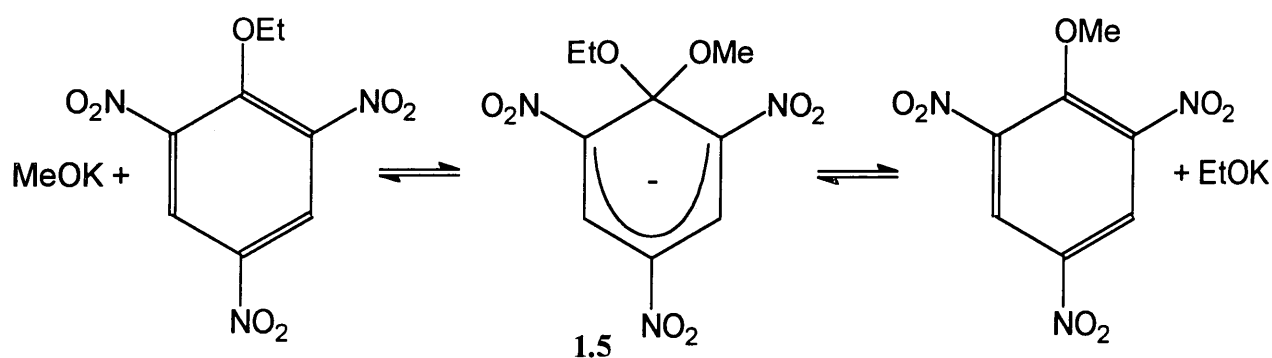


1.1.2 Early Mechanistic Investigations

It was in 1900 that Jackson and Gazzolo first ascribed quinoid resonance structures, **1.3** and **1.4**, to the product formed in the reaction between 2,4,6-trinitroanisole (TNA) and sodium methoxide.³



Shortly afterwards, Meisenheimer obtained chemical evidence which supported these quinoid structures.⁴ The reaction of TNA and potassium ethoxide gave the same product, **1.5**, as the reaction of 2,4,6-trinitrophenetole (TNP) and potassium methoxide, Scheme 1.3. Meisenheimer was able to isolate the product as the potassium salt. He then subsequently decomposed the product (formed by either route) by acid to yield the same mixture of TNA and TNP. Further evidence was gained when the reacting solutions produced identical UV-Visible spectra.⁵ Adducts formed in reactions of nucleophiles with polynitroaromatic compounds are commonly known as Jackson-Meisenheimer complexes,⁶ or σ -adducts.



Scheme 1.3

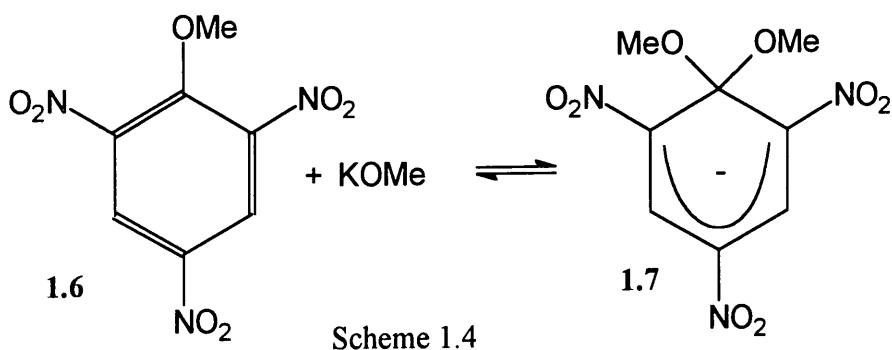
Confirmation of the σ -adduct structure was not obtained until 1964 with the availability of ^1H NMR spectroscopy.⁷

1.1.3 Spectroscopic Evidence for the Formation of Reaction Intermediates

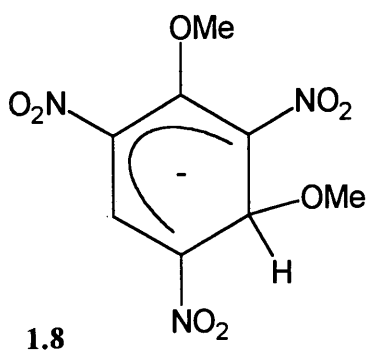
Numerous workers have studied the structure and reactivity of anionic σ -adducts, using them as models for the intermediates formed during nucleophilic aromatic substitution. A variety of spectroscopic techniques have been used, including Infra-red and UV/Visible techniques. However, these methods are usually not as useful as ^1H NMR spectroscopy in determining the structures of adducts.

1.1.3.1 NMR Spectroscopy

In 1964, Crampton and Gold obtained the first unambiguous ^1H NMR data which confirmed the structure of anionic σ -complexes.⁷ The ^1H NMR spectrum of the adduct **1.7**, formed by reaction of potassium methoxide and TNA, **1.6**, Scheme 1.4, contained two peaks.

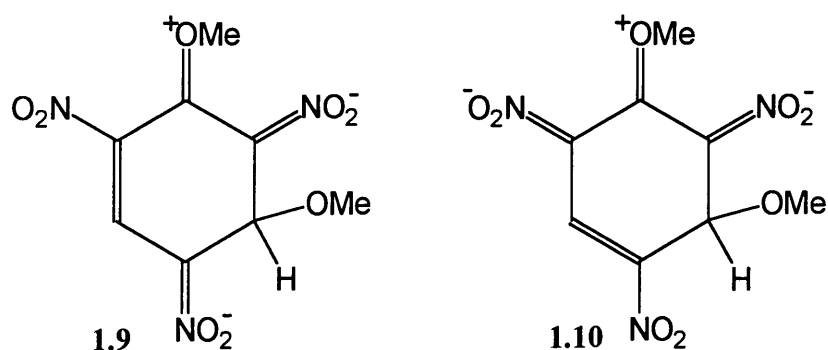


The resonance intensities represented two ring protons and six methoxyl protons. Both resonances were shifted to lower frequency compared to the parent anisole, due to the change in hybridization from sp^2 to sp^3 at the substituted ring carbon. The appearance of only two bands in the spectrum indicated the chemical equivalence of the ring hydrogens and the methoxy groups, ruling out structures such as **1.8**.

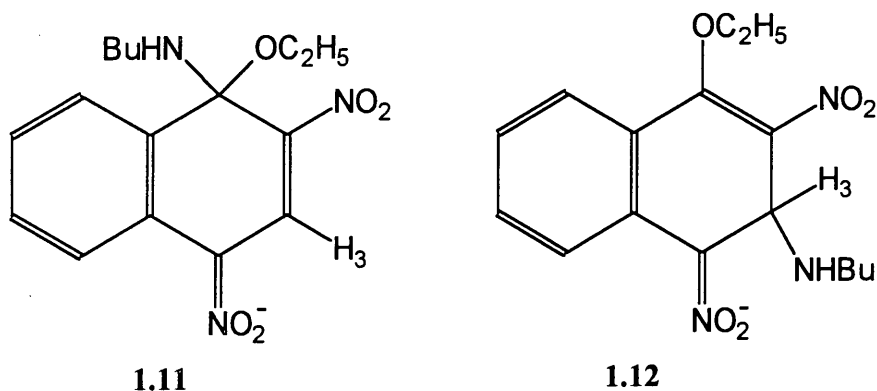


However, in 1965, Servis^{8,9} reported that **1.8** could be observed as the kinetically preferred adduct when concentrated sodium methoxide solution was added to a solution of TNA in d_6 -DMSO. The spectrum of **1.8** showed two pairs of doublets due to the coupling of the ring hydrogens. This 1,3 σ -adduct was extremely labile, and rapidly gave rise to the more thermodynamically stable 1,1 σ -adduct, **1.7**.

In the 1,3 complex the co-planar 1-methoxy and 2,6-dinitro groups are subjected to a steric compression, although there is also the possibility for greater charge delocalisation due to the contribution of resonance structures **1.9** and **1.10**. In the 1,1 complex, the methoxy groups are situated in the plane perpendicular to that of the ring, and hence **1.7** is the more thermodynamically stable form.¹⁰

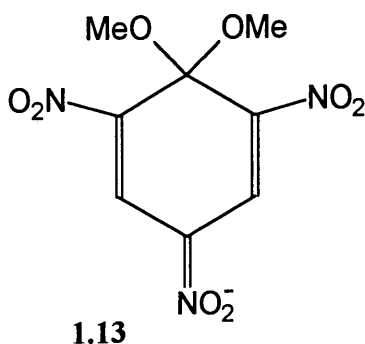


Fyfe and co-workers developed and used the technique of flow NMR spectroscopy to measure high resolution spectra with reliable intensities in rapidly flowing, chemically reacting mixtures.¹¹ The technique was used to detect and assign the structure of the intermediate **1.11** reported previously by Bunnett and Orvik¹² in the reaction of 1-ethoxy-2,4-dinitronaphthalene with *n*-butylamine. The spectrum contained three different resonances due to H_3 , situated at high frequency which were attributed to reactant, intermediate and product respectively. This proved that the intermediate was **1.11**, and not **1.12**, as the resonance due to H_3 in **1.12** would have appeared at lower frequency due to the change in hybridization from sp^2 to sp^3 at C_3 .

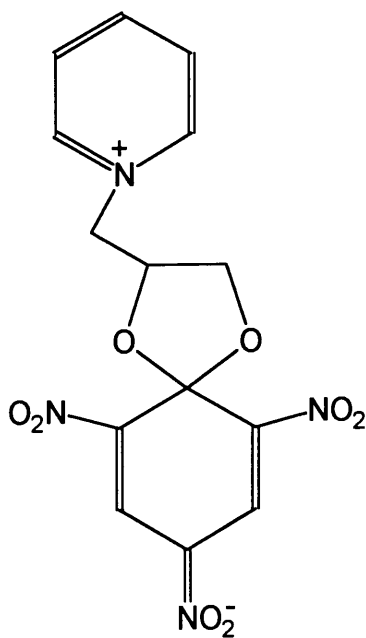


1.1.3.2 X-ray Crystallography

X-ray crystallographic studies have provided information about the bond lengths and angles within σ -complexes.^{13,14,15} The data have been useful, even though the results of such studies do not provide information relating to solvated species in solution, (forces within the crystal lattice may affect measured conformations and bond lengths).² For example, in the crystal structure of 1-methoxyanisole, **1.13**, the C₄-NO₂ bond is much shorter than either the C₂-NO₂ or the C₆-NO₂ bonds. This provides direct evidence that more negative charge resides on the C₄-NO₂ bond. The ring was found to be approximately planar, with both alkoxy oxygens in a plane perpendicular to the ring plane.¹³



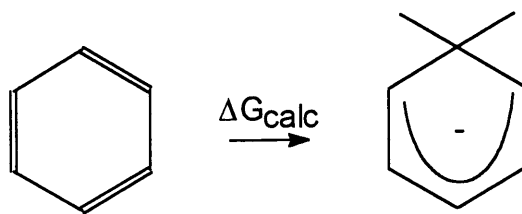
Further evidence that the negative charge in a σ -complex resides on the para nitro-group has recently been provided by Borbulevych.¹⁶ The C₄-NO₂ bond in **1.14** is again shorter than the C₂-NO₂ or C₆-NO₂ bonds, and the C-C bond distances in the ring vary considerably.



1.14

1.1.3.3 Theoretical Studies

Dewar calculated that the formation of a cyclohexadienyl ring from a benzene ring occurs with the loss of only $41.80 \text{ kJ mol}^{-1}$ (ΔG_{calc} in Scheme 1.5) in resonance energy.¹⁷ Therefore, the cyclohexadienyl anion is able to retain a large amount of the original stabilisation energy through resonance delocalisation of charge, Figure 1.2. The resonance structures will be more stable if the negative charge can be dispersed through electronegative atoms of substituents such as NO_2 which undergo conjugation to positions ortho and para to the substituted carbon.



Scheme 1.5

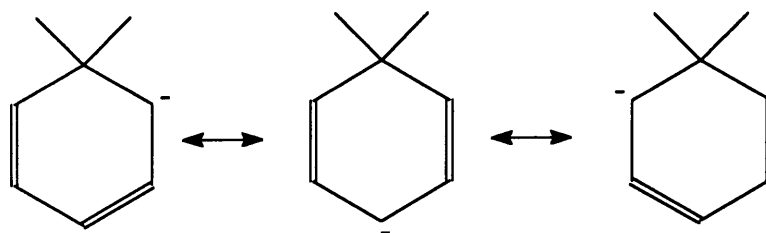


Figure 1.2

Olah and co-workers¹⁸ studied the cyclohexadienyl anions **1.15**, which were formed by proton abstraction from the corresponding 1,3- or 1,4-dienes in liquid ammonia. ^{13}C NMR was used to prove the existence of the resonance structures shown previously in Figure 1.2. ^{13}C chemical shifts are given in Figure 1.3. These show that resonances due to the ortho and para carbons are shifted to lower frequency on formation of the cyclohexadienyl anion. There was no corresponding shift for the meta carbons and so no negative charge is situated at these positions.

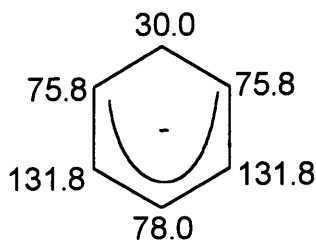
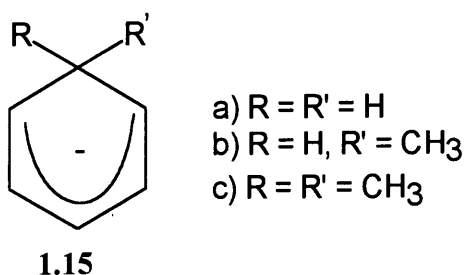
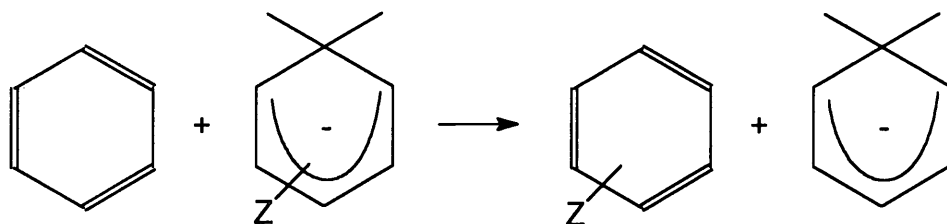


Figure 1.3

In 1980, Birch and co-workers calculated stabilisation energies for substituted cyclohexadienyl anions relative to substituted benzenes,¹⁹ Scheme 1.6. All electron-withdrawing groups were observed to have a stabilising effect, but the effect was greater for NO_2 than for other groups studied.



Scheme 1.6

1.1.4 Factors which Influence Reactivity

1.1.4.1 Activation by NO_2

The presence of electron-withdrawing groups in an aromatic ring is an essential requirement for $\text{S}_{\text{N}}\text{Ar}$ reactions. If there are no NO_2 (or other electron-withdrawing) groups present, there will be repulsion between the π -electron system and the approaching nucleophile.²⁰ The cyclohexadienyl anion will be more favoured if the negative charge generated can be dispersed through electronegative atoms capable of conjugation in positions ortho and para to the sp^3 carbon. Many nitroarene-base interactions cannot proceed further than the addition step, forming potentially stable σ -adducts.

For trinitrobenzene, (TNB), significantly more charge is located on the para- NO_2 group than on the ortho- NO_2 groups, Figure 1.4.²¹ The greater effectiveness of the para- NO_2 group over the ortho- NO_2 group in stabilising a cyclohexadienyl structure may be due to the steric barrier to co-planarity of the ring substituents and ortho- NO_2 groups in the adduct.²²

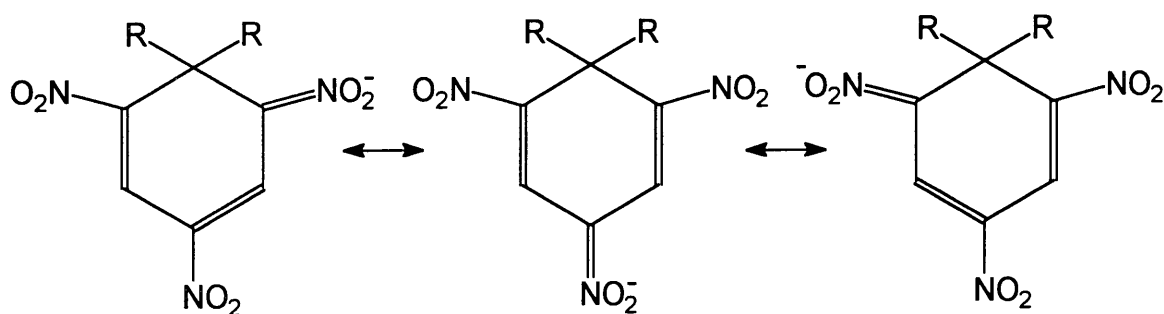


Figure 1.4

Birch showed that nitro-groups have a greater stabilising effect on σ -complexes in comparison with other electron-withdrawing substituents.¹ Cyano-substitution decreases the equilibrium constant for the formation of the dimethoxy-complexes **1.16a-e**, Table 1.1. Substitution of an ortho-NO₂ group by a cyano-group leads to a 7-fold reduction in the value of the equilibrium constant, while substitution of a para-NO₂ group leads to a 70-fold reduction. This provides further evidence for the greater stabilisation of σ -adducts by para-NO₂ groups.²³

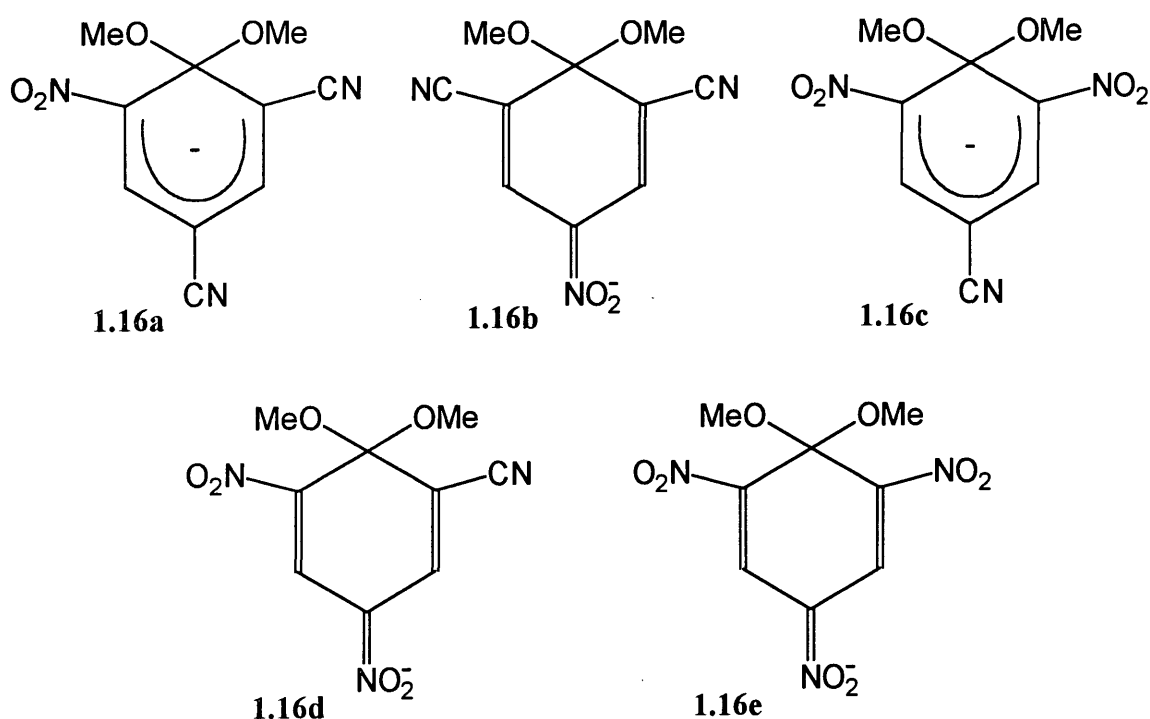
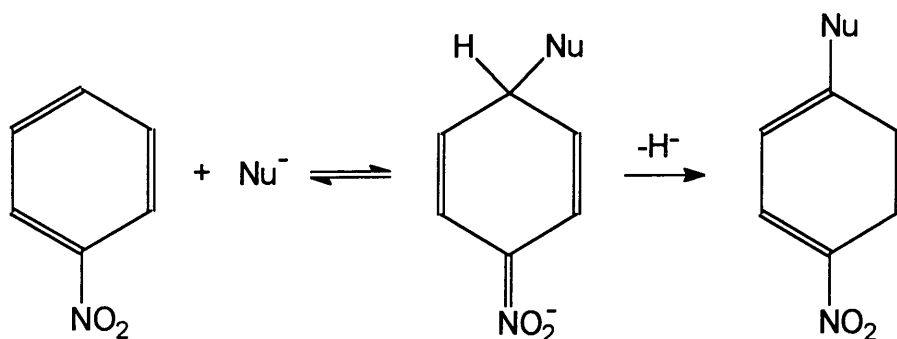


Table 1.1: Measured equilibrium constants for formation of some dimethoxy-adducts in methanol.

complex	K / dm ³ mol ⁻¹ (25°C)
1.16a	10
1.16b	34
1.16c	280
1.16d	2600
1.16e	17000

1.1.4.2 Leaving Group Ability

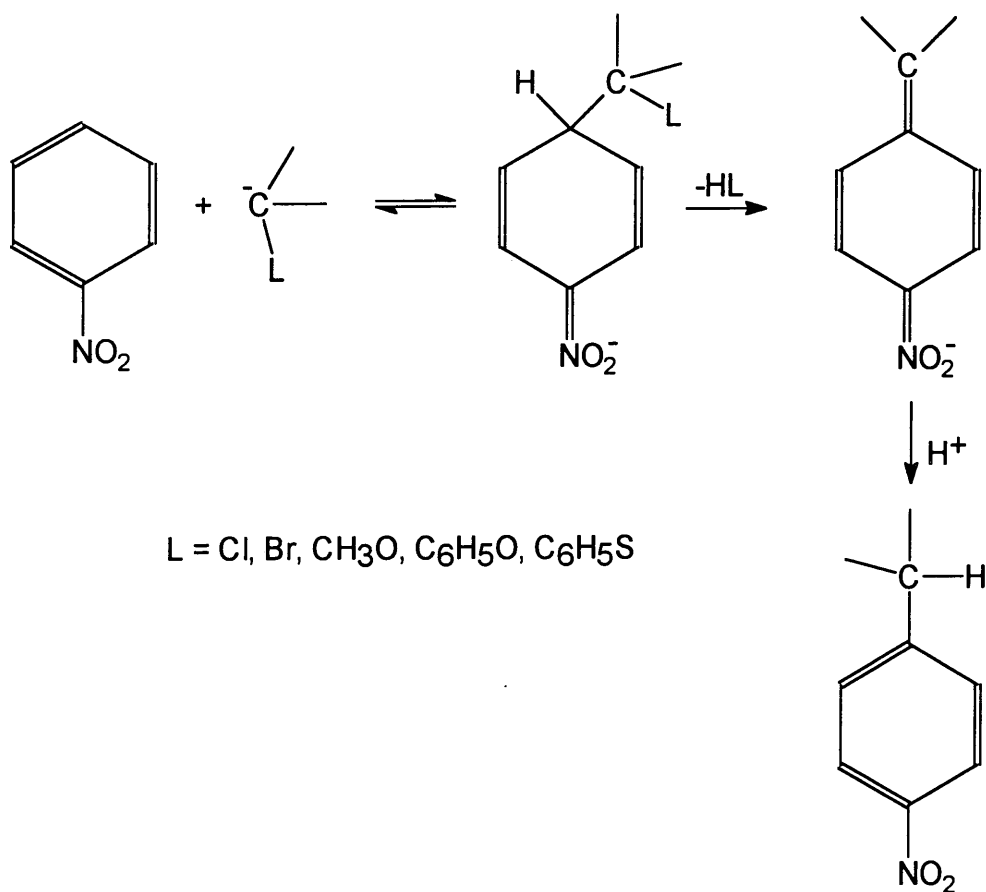
A departing hydride anion has a very low anionic stability ($\text{pK}_a = 36$).²⁴ $\text{S}_{\text{N}}\text{Ar}$ displacements of hydrogen are probably very endothermic, having transition states for C-H bond breaking that are too high to be kinetically accessible. Therefore, nucleophilic displacement of hydrogen in activated aromatic systems, (as shown in Scheme 1.7), can only occur by very specific mechanisms. Since hydrogen is a very poor leaving group,²⁵ reaction at activated C-H ring positions will normally yield the intermediate σ -adduct.²



Scheme 1.7

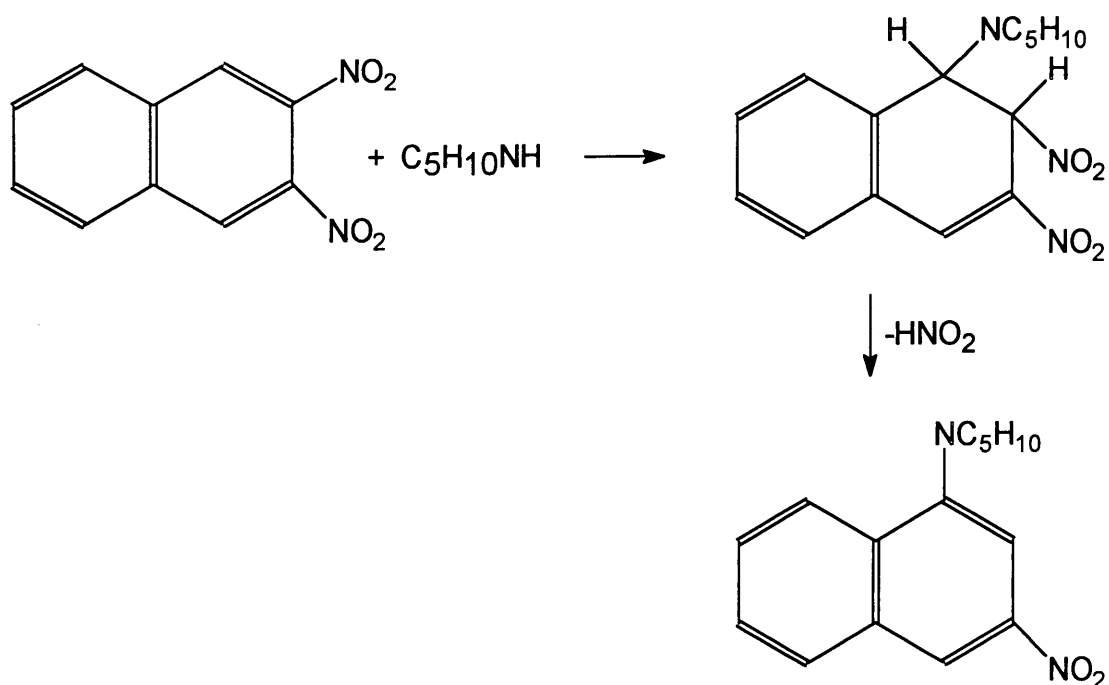
In order for displacement to occur an “oxidation” pathway is necessary.¹ The substrate itself may act as an oxidising agent in basic media, or an external oxidising agent may be required.

An example of the nucleophilic substitution of hydrogen is given in Scheme 1.8. The driving force for this reaction is the elimination of a nucleofugal group present at the reactive centre of the incoming nucleophile.^{26,27} Scheme 1.8 shows a carbanionic nucleophile (which has a leaving group, L at the anionic carbon atom) attacking a nitroarene. The carbanions are generated by the action of base on the corresponding CH acids. For example, Makosza and Winiarski²⁷ used a strong base to generate the carbanion, $\text{PhSO}_2\text{CHCl}^-$ from chloromethylphenylsulfone ($\text{ClCH}_2\text{SO}_2\text{Ph}$). Once formed, the σ -adducts are converted to products by a base induced β -elimination of HL . This mechanism is usually known as the vicarious substitution of hydrogen.



Scheme 1.8

Another example of hydrogen substitution occurs when both a ring hydrogen and a ring substituent must depart in order to achieve rearomatization, as in Scheme 1.9.^{28,29} The reaction is an example of cine-substitution, where the nucleophile attacks at a position α to a leaving group. The nitro-group at C_3 is thought to increase the lability of H_1 through a conjugative interaction with the π -system. The proton transfer step to initiate loss of HNO_2 is assisted by excess piperidine, or an external base such as Dabco.²⁹



Scheme 1.9

There is a strong dependence on the pK_a of the corresponding alcohol for reactions involving alkoxide and aryloxy leaving groups.³⁰ The methoxide anion is small with a highly localised negative charge, while phenoxide is able to delocalise the negative charge throughout the aromatic ring.³¹ Therefore, phenoxide is a better leaving group than methoxide. The rate and equilibrium constants for the formation and stability of **1.17** and **1.18**^{32,33,34} illustrate the greater leaving group ability of phenoxide over methoxide, Table 1.2.

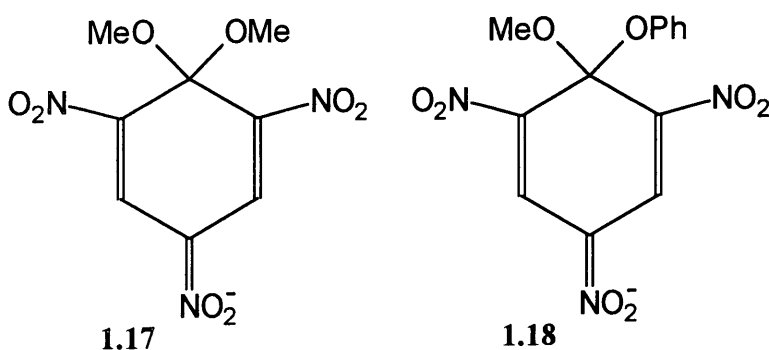


Table 1.2: Rate and equilibrium constants calculated for the formation and decomposition of **1.17** and **1.18**, from 2,4,6-trinitroanisole.

	MeO ⁻	PhO ⁻
$k_1 / \text{dm}^3 \text{mol}^{-1} \text{s}^{-1}$	17	50
$K_1 / \text{dm}^3 \text{mol}^{-1}$	17000	0.026
k_{-1} / s^{-1}	10^{-3}	1900

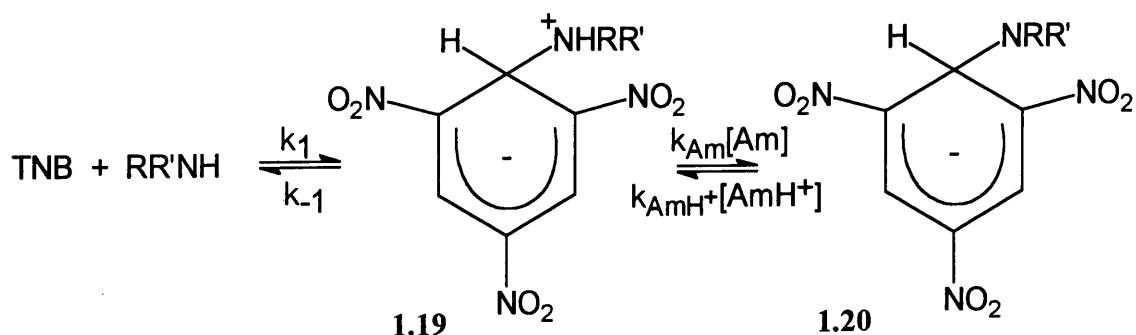
Gravitz and Jencks reported that amines are intrinsically better leaving groups than alkoxide ions.³⁵ However, Bernasconi found evidence that for amines and alkoxide ions of comparable pK_a , the leaving group abilities of the alkoxide ions are similar to, or even greater than those of the amines. He has suggested that the relative leaving group abilities may depend on the nature of the electrophile.³⁶

1.1.4.3 Influence of the Nucleophile

Nucleophilic reactivity is related to the basicity of the attacking nucleophile. However, since σ -adduct formation involves attack at a carbon centre, it is the carbon basicity (rather than the proton basicity) of the attacking species which is important in influencing reactivity. The position of the transition state along the reaction co-ordinate can be described in terms of the sensitivity of the reaction to changes in the basicity of the attacking nucleophile.³⁷

1.1.4.3.1 Nitrogen Nucleophiles

Amine addition at an unsubstituted carbon of TNB occurs very rapidly in aqueous or DMSO solutions to give the zwitterionic σ -complex, **1.19**.^{36,38} The complex is subsequently deprotonated to form the anionic σ -complex, **1.20**, Scheme 1.10.^{39,40}



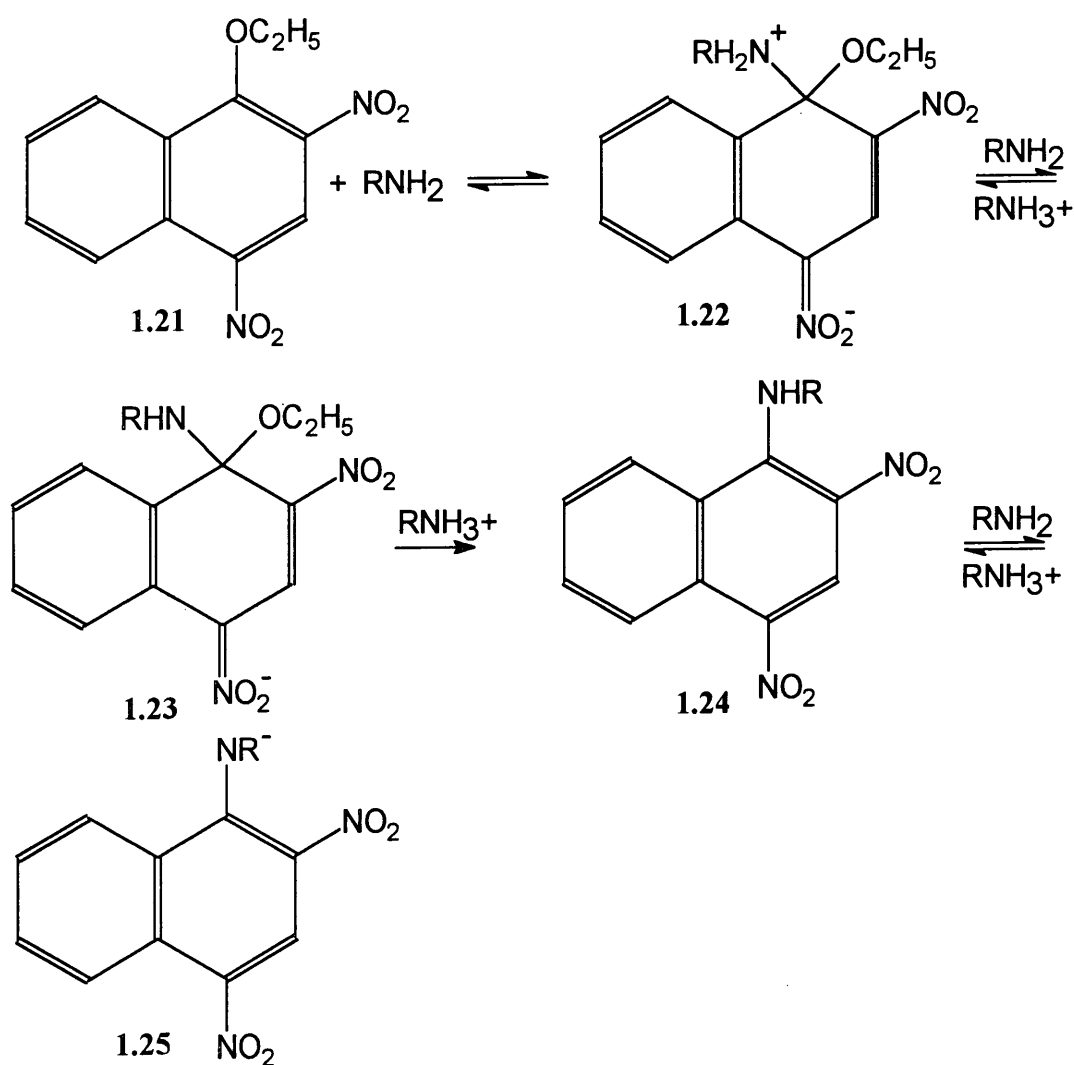
Scheme 1.10

It is interesting that in the formation of **1.20** the proton transfer step may be rate-limiting. Kinetic studies in DMSO³⁸ allowed the calculation of values of k_{Am} , the rate constant for proton transfer from the zwitterion to amine. The values obtained are around $1 \times 10^7 \text{ dm}^3 \text{ mol}^{-1} \text{ s}^{-1}$ for the n-butylamine system, and $1 \times 10^4 \text{ dm}^3 \text{ mol}^{-1} \text{ s}^{-1}$ for the piperidine system and are lower than expected for a diffusion controlled process. It is likely that factors which reduce the rate constant for proton transfer are; i) strong hydrogen bonding of the proton to be transferred to the solvent, DMSO, and ii) steric hindrance to the approach of the reagent. The latter factor accounts for the much lower rate constants observed with the secondary amine than with the primary amine.

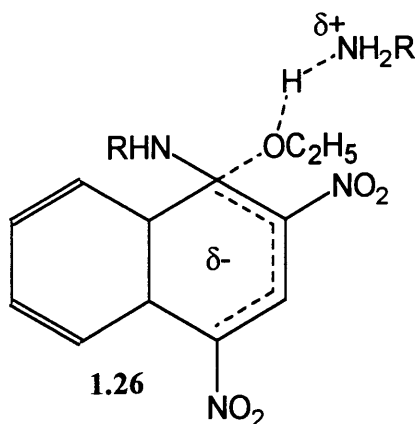
Many nucleophilic substitution reactions involving amines are found to be subject to general base catalysis implying that proton transfer is rate-limiting. Two possibilities are; i) rate-limiting proton transfer from the zwitterionic intermediate, analogous to **1.19**, to base, or ii) rapid equilibration of the zwitterion with its anionic form, followed by general acid catalysed expulsion of the leaving group (the SB-GA mechanism). The evidence is that the nature of the rate determining step may depend on the leaving group. Thus with good leaving groups, such as phenoxide,⁴¹ it is the proton transfer from the zwitterion

which is rate-limiting, while with poorer leaving groups, such as alkoxides, the SB-GA mechanism applies.

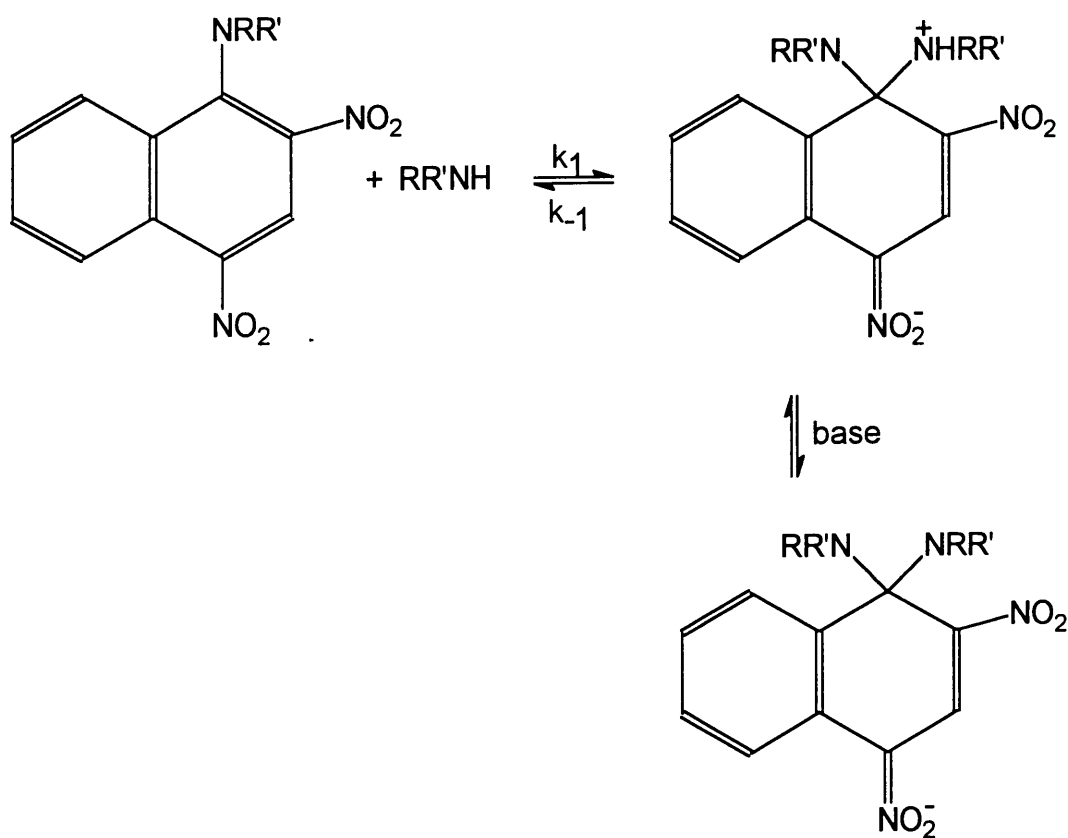
An example of the latter is the classical study by Bunnett and Orvik of the reactions of 2,4-dinitronaphthyl ethyl ethers with aliphatic amines in DMSO, Scheme 1.11. Reaction occurred in two well resolved stages. The first process gave the adduct **1.23** which was identified by UV/Visible spectrophotometry and ^1H NMR spectroscopy. In the second stage of the reaction, general acid catalysed conversion of **1.23** to **1.24** was observed, and a transition state, **1.26** was postulated.¹² Since the transition state contains one molecule of substrate and two molecules of amine, the reaction overall shows general base catalysis. The eventual product in the presence of excess amine was the deprotonated substitution product, **1.25**.



Scheme 1.11



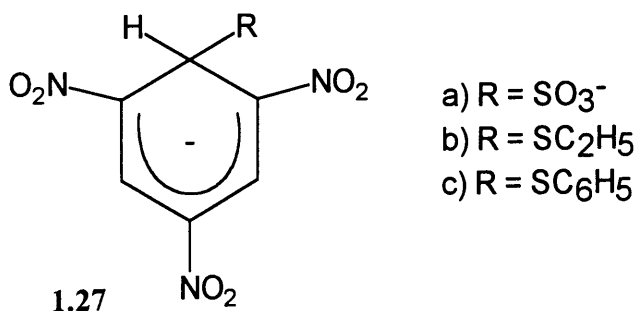
Naphthalene adducts resulting from amine addition at an amino-substituted carbon atom form at much lower rates than the TNB complexes in DMSO, Scheme 1.12. This is due to a ground state stabilisation through resonance interaction with the amino group in the parent, together with steric hindrance to the approach of the amine nucleophile at the amino-substituted carbon.



Scheme 1.12

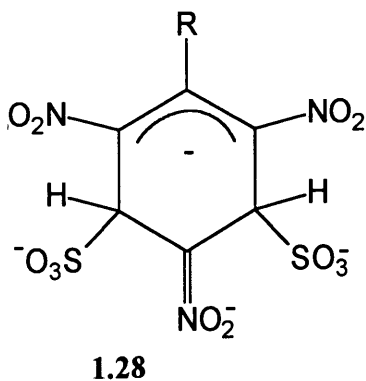
1.1.4.3.2 Sulfur Nucleophiles

Sulfite, thioethoxide and thiophenoxide will all act as nucleophiles with TNB to give complexes **1.27a-c**. The resonance due to the proton at the sp^3 hybridized carbon occurs at significantly higher frequency than for complexes with carbon bases.²²



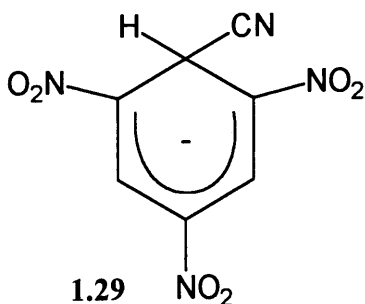
Anionic sulfite has a much greater solvation requirement than singly charged anions such as methoxide, (both in the complex and as a doubly charged anion). Steric hindrance to attack at a substituted position may be quite severe, and so attack at an unsubstituted position is kinetically and thermodynamically favoured. Hence sulfite attack occurs preferentially at C_3 in the 1-substituted 2,4,6-trinitroaromatics studied.^{42,22} For 1-X-substituted trinitrobenzenes, the hydrogen at C_3 shows a large shift to lower frequency in 1H NMR spectroscopy, consistent with a change in hybridisation from sp^2 to sp^3 . The C_5 hydrogen shows a smaller shift to lower frequency due to the increased shielding in the negatively charged complex.⁴³

If there is a high excess of sulfite over the electron-deficient aromatic, 1:2 complexes, **1.28**, may form. These adducts contain more localised negative charge than 1:1 complexes and are not well solvated in aprotic solvents such as DMSO.⁴³

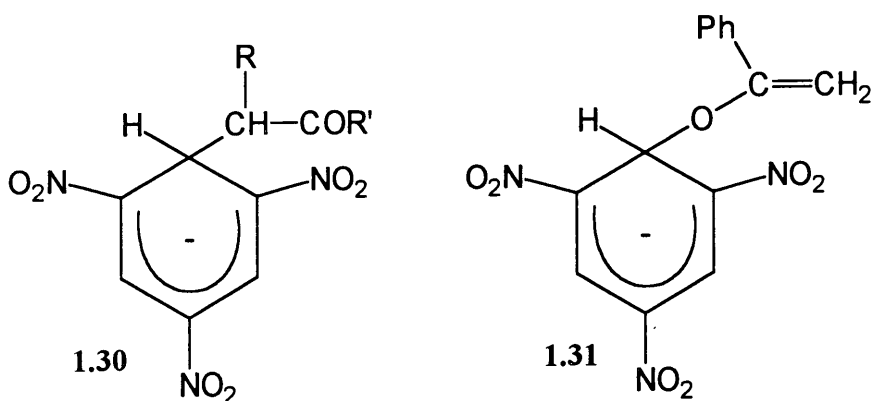


1.1.4.3.3 Carbon Nucleophiles

There are numerous examples of carbon-bonded σ -adducts in the literature.^{20,2} They result from reaction with a large variety of anionic as well as neutral carbon nucleophiles.²⁰ Cyanide will attack an unsubstituted carbon of TNB in many different solvent systems including alcohols, acetone and chloroform to yield **1.29**.



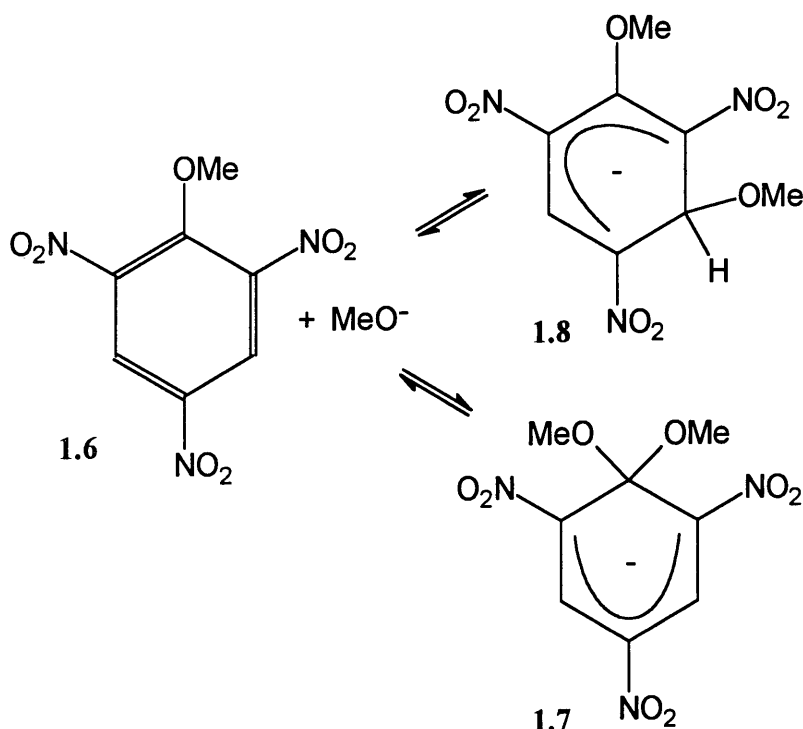
The reactions of electron-deficient aromatics with enolate carbanions such as ketones, aldehydes and esters have also been studied.⁴⁴ There have been several reports of reaction via the carbon centre to give adducts, **1.30**. Recently it was found that the oxygen-bonded adduct, **1.31** could be observed as a transient species before the formation of the thermodynamically more stable carbon-bound adduct. The ^1H NMR spectrum of **1.31**, formed from TNB and the acetophenone enolate anion in acetonitrile-dimethoxyethane at $-50\text{ }^\circ\text{C}$, shows a band at 6.93 ppm for the hydrogen at C_1 . This is shifted considerably from the position of the corresponding hydrogen (5.22 ppm) in the carbon-bonded adduct.⁴⁵



1.1.4.4 Reactivity at Unsubstituted Versus Substituted Ring Carbons

In general, nucleophilic attack at an activated, unsubstituted ring position is kinetically favoured compared to attack at an activated, substituted position. This is due to two factors. First, there is a very low electrostatic repulsion between the hydrogen atom and the incoming nucleophile, and second, there is a lower steric requirement at an unsubstituted compared to a substituted position.²⁰

Occasionally, transient σ -adducts, **1.8**, which are not further converted to substitution products, are formed in side equilibrium reactions prior to the substitution pathway, Scheme 1.13. These transient σ -adducts are sometimes observed spectroscopically.^{46,22,8,9}

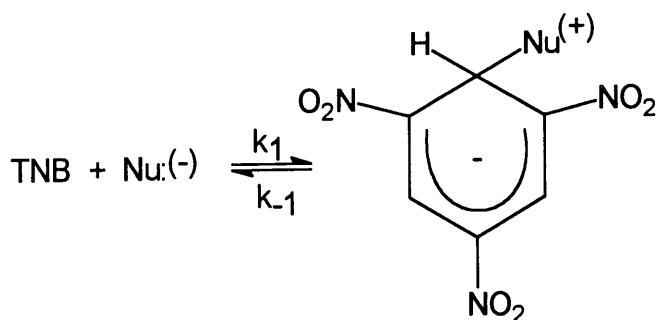


Scheme 1.13

1.1.5 Solvent Effects

The nature of the solvent profoundly effects the rate and equilibrium parameters for the formation and decomposition of σ -adducts. Dimethyl sulfoxide (DMSO) and other dipolar aprotic solvents such as dimethylformamide (DMF) enhance the stability of 1:1 adducts.

The effect of DMSO on K_1 reflects an increase in the rate of formation (k_1) and a decrease in the rate of decomposition (k_{-1}) of the 1:1 adduct, Scheme 1.14.

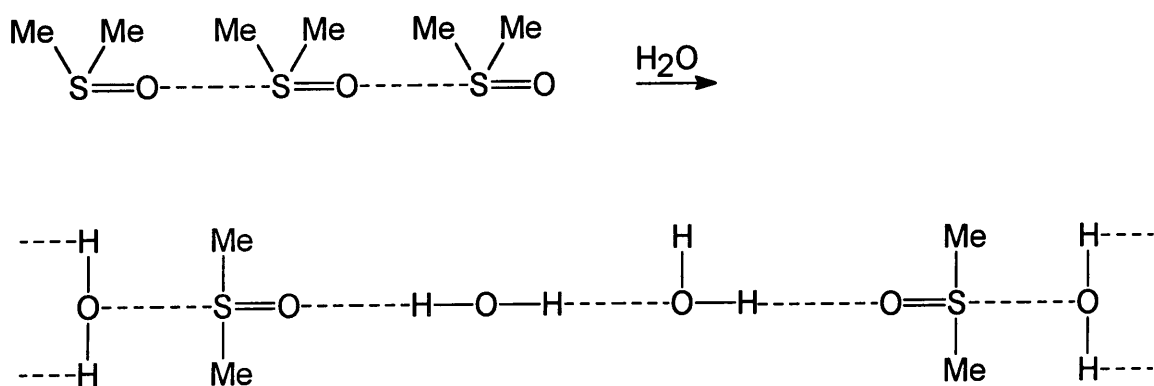


Scheme 1.14

The reactions discussed in this thesis have been performed in DMSO or DMSO-water mixtures. The aqueous solutions of DMSO are of special interest because of their unique biological and physicochemical properties.⁴⁷ Perhaps one of the most significant properties of DMSO is its ability to act as a carrier for transferring drugs through the cell membrane. Many drugs have an enhanced physiological effect when mixed with DMSO, and smaller doses are required.⁴⁸

DMSO is a polyfunctional molecule with a highly polar $\text{S}=\text{O}$ group and two hydrophobic CH_3 groups, in a pyramidal arrangement.⁴⁹ The $\text{S}=\text{O}$ link is almost a covalent double bond, but also contains a minor contribution of polar-coordinated single bond.⁵⁰ The two methyl groups exert an inductive effect, which enhances the polarisation of the sulfoxide group.⁵¹ The negative charge on the oxygen atom of a DMSO molecule will therefore be greater than that on the oxygen atom of a water molecule.

DMSO is similar to water in that it has an ordered structure which involves association between sulfur and oxygen atoms to form chains, which are broken down on addition of water,⁵² Scheme 1.15. All the molecules in the mixture will be more basic than molecules in pure water as the charge on the oxygen atoms of DMSO is transmitted to the water molecules through hydrogen bonding.⁵¹ DMSO-water mixtures have been investigated by a number of techniques including X-ray diffraction,⁵⁰ NMR^{53,54} and electrochemistry.⁵¹



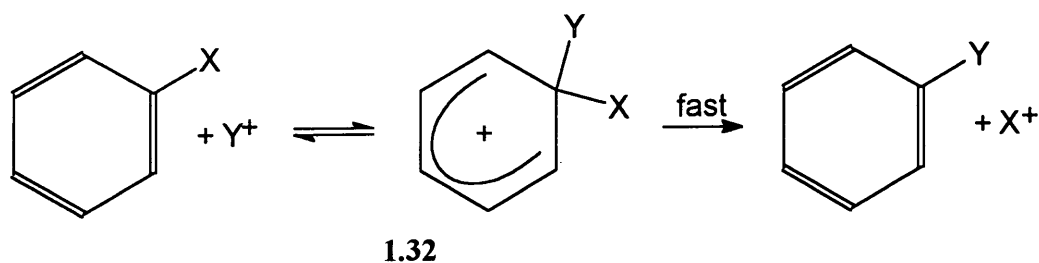
Scheme 1.15

Anions with a localised negative charge (OH^- , RO^- , SO_3^{2-}) are more susceptible to destabilisation by DMSO than large, polarisable species. Therefore the increase in K_1 (Scheme 1.14) for 1:1 complex formation with a given electrophile is much greater for nucleophiles such as hydroxide than for phenoxide.

1.2 Electrophilic Aromatic Substitution Reactions

1.2.1 The Mechanism of Electrophilic Aromatic Substitution

The majority of electrophilic aromatic substitutions proceed by one mechanism with respect to the substrate. The electrophile attacks in the first step, to give a positively charged intermediate, **1.32**, (also known as a Wheland intermediate⁵⁵) with the second step being the departure of the leaving group, Scheme 1.16. Either the addition or the elimination step may be rate-limiting, but the expulsion of the leaving group is generally rapid.



Scheme 1.16

In electrophilic aromatic substitution, the attacking species is a positive ion or the electropositive end of a dipole. The resulting cyclohexadienyl cation is able to achieve a certain amount of stability through resonance, Figure 1.5, but is still highly reactive, and

must undergo a further reaction, the departure of the leaving group. The leaving group must be able to depart without its lone pair electrons. The most common leaving group in electrophilic aromatic substitutions is the proton.

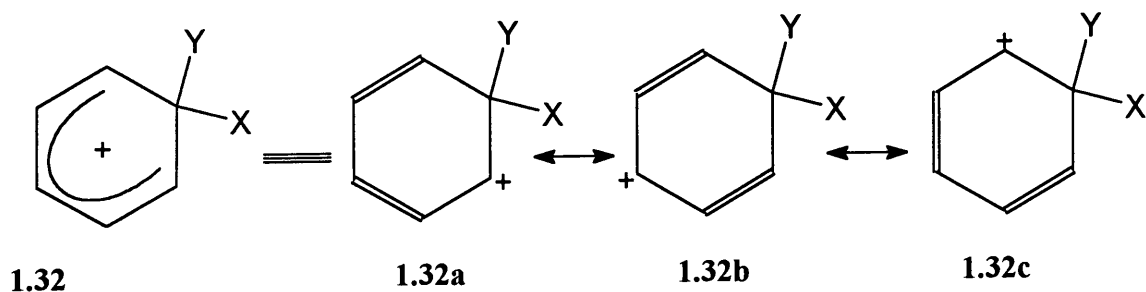
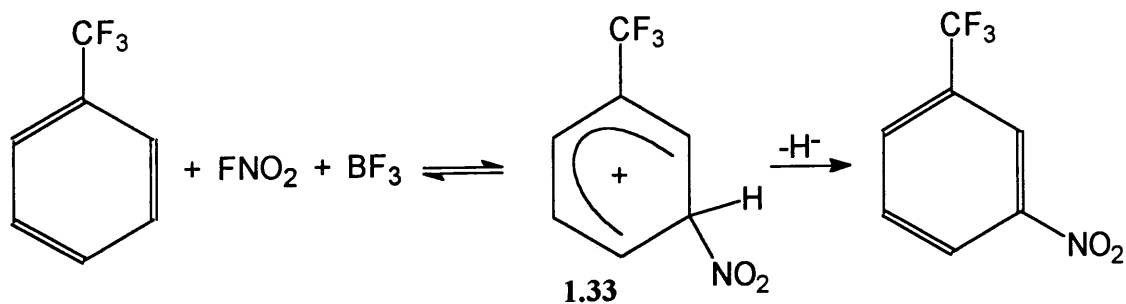


Figure 1.5

1.2.2 Early Mechanistic Investigations

Olah and Kuhn reacted trifluoromethylbenzene with nitril fluoride and boron trifluoride and assigned structure **1.33** to the resulting coloured crystalline complex.⁵⁶ As meta-nitrotrifluoromethylbenzene is the nitration product of trifluoromethylbenzene, Scheme 1.17, the evidence for the structure of the nitration intermediate was indeed convincing.



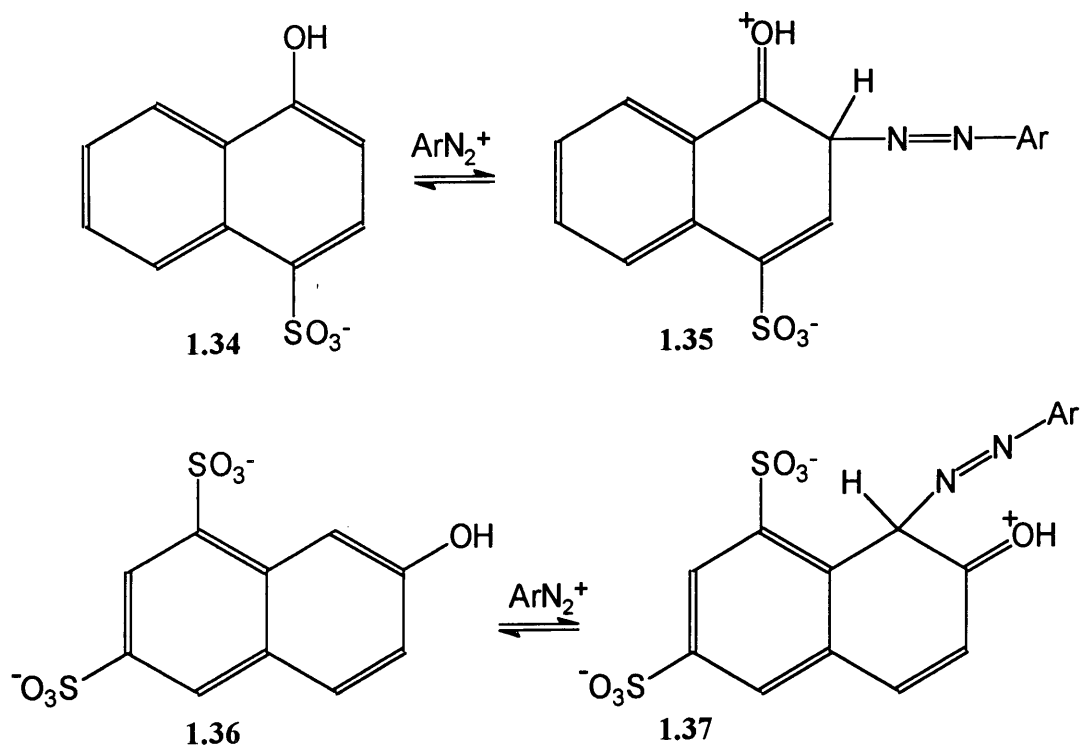
Scheme 1.17

1.2.3 Evidence to Support the Mechanism

1.2.3.1 Kinetic Isotope Effects

In the majority of electrophilic aromatic substitutions a primary kinetic isotope effect is not observed.⁵⁷ This illustrates that the rate-limiting step does not involve carbon-hydrogen bond breaking, and is therefore the initial attack of the electrophile. For example, deuteriobenzene and tritiobenzene are nitrated at almost the same rate as benzene itself,⁵⁸ and there is no observed kinetic isotope effect in many halogenations.⁵⁷

There is evidence that steric hindrance at the reaction centre may reduce the rate of carbon-hydrogen bond cleavage.⁵⁹ Thus the diazonium coupling reaction of **1.34** via the intermediate **1.35** occurs without the observation of a primary isotope effect. However, the reaction of **1.36**, which is more sterically hindered, gives a k_H/k_D ratio of 6.55. It is more difficult for a base to approach the reaction centre in the intermediate **1.37**, so that the rate of C-H bond breaking is reduced.



Isotope effects may be reduced or even eliminated at sufficiently high concentrations of base. Increasing the base concentration increases the rate of conversion of intermediate to product without affecting the rate of reversion of the intermediate to starting materials.

1.2.3.2 Isolation of the Intermediate

Olah and co-workers prepared the benzenonium ion, **1.38**, in HF-SbF₅-SO₂ClF-SO₂F₂ at -134 °C.⁶⁰ The ¹³C NMR spectrum of the ion provided evidence for the charge distribution shown in Figure 1.5.⁶¹ The 2, 4 and 6 carbons of **1.38** have a greater chemical shift in the NMR spectrum as they carry a partial positive charge, Table 1.3.

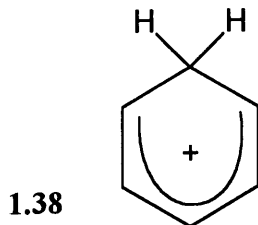


Table 1.3: ^{13}C NMR chemical shifts for the benzonium ion, **1.38**.

C_n	^{13}C NMR chemical shift / ppm
C_1	52.2
C_2	186.6
C_3	136.9
C_4	178.1
C_5	136.9
C_6	186.6

1.2.4 The Effects of Substituents

Some substituents activate the nucleus toward electrophilic attack. These include alkyl groups and nitrogen or oxygen substituents, which cause substitution to occur predominantly in the ortho and para positions. Other substituents deactivate the nucleus, for example, carbonyl, nitro and cyano groups and the halogens, (Cl, Br, I). These substituents cause substitution to occur mainly in the meta position, although the halogens will allow reaction at the ortho and para positions.

1.2.5 The Hammett Equation

It was Hammett who first succeeded in giving numerical values to ring substituents in order to measure their effect on the reactivity of the substrate.⁶² The Hammett equation is given in Equation 1.1. For a given substituent X, K_0 is the equilibrium constant for reaction when $\text{X} = \text{H}$, K the equilibrium constant for X, σ a constant characteristic of X, and ρ a constant for a reaction under a given set of conditions.

Equation 1.1: $\log \frac{K}{K_0} = \sigma \rho$

The equation was based on the study of the ionisation of $\text{XC}_6\text{H}_4\text{COOH}$ in water at 25 °C. The value of ρ was set at 1.00 for this reaction and σ_{meta} and σ_{para} values calculated accordingly. The constant ρ measures the susceptibility of the reaction to electronic effects. The equation has also been used to successfully predict rate constants. Reactions with a positive ρ value exhibit an enhanced rate constant when electron-withdrawing groups are present, while the rate constants of reactions with a negative ρ value are increased in the presence of electron-donating groups. The σ values are the sum of the resonance and field effects of a group X attached to a benzene ring. A positive value of σ indicates an electron-withdrawing group and a negative value an electron-donating group. The Hammett treatment usually fails for substituents at the ortho position because of steric hindrance effects.

Where attack occurs on the benzene ring with a direct resonance interaction between the group, X, and the reaction site in the transition state, two new sets of σ values have been calculated. When an electron-donating group interacts with a developing positive charge in the transition state, σ^+ values are applied, and when electron-withdrawing groups interact with a developing negative charge, σ^- values are used. A selection of σ values is given in Table 1.4.

Table 1.4: σ values for a selection of substituents.

Group	σ_p	σ_m	σ_p^+
H	0	0	0
NH ₂	-0.57	-0.09	-1.3
NMe ₂	-0.63	-0.10	-1.7
Me	-0.14	-0.06	-0.31
OMe	-0.28	0.10	-0.78

1.2.6 Electrophilic Aromatic Substitutions Involving Aniline

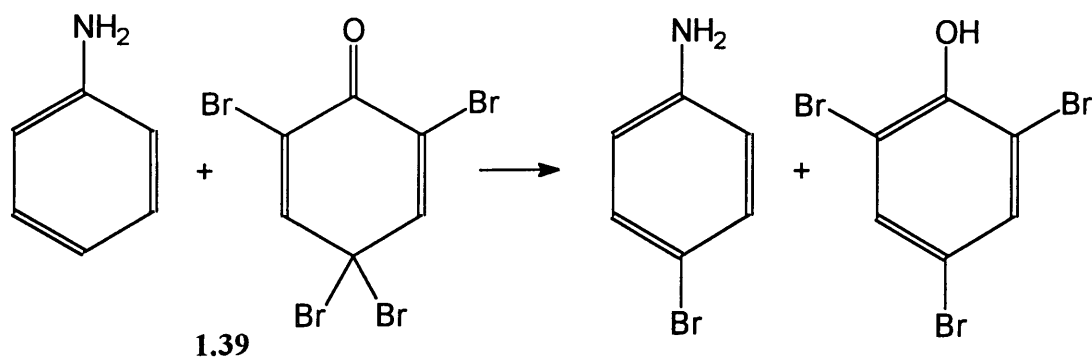
Studies have been reported of the exchange of ring hydrogens in aniline and its substituted derivatives.⁶³ Rate constants for exchange show a dependence on the acidity of the medium. However, different substrates may respond differently to changes in acid concentration, and there is evidence that exchange may occur either in the free base or in protonated forms. An amine with a strong electron-donating substituent will protonate readily and the equilibrium concentration of the conjugate acid will be high. Hence hydrogen exchange will occur via the conjugate acid. Whereas, an amine with a strong electron-withdrawing substituent will be present in the free form at equilibrium, and hydrogen exchange will occur via the free base.⁶³

Ingold showed that electron-donating substituents cause more rapid exchange at the ortho and para than at the meta positions.⁶⁴ Katritzky and Clementi calculated a ρ value of -7.5 for hydrogen exchange in monosubstituted benzenes in aqueous sulfuric acid.⁶⁵ The presence of electron-donating groups increased the rate of hydrogen exchange.

The rate of electrophilic bromination of aniline derivatives has been found to decrease with increasing acidity of the medium, providing evidence that the reactive species is the free amine. 3- and 4-methyl substitution increased the reaction rate, while 2-methyl substitution led to a rate decrease. This was attributed to inhibition of conjugation between the substituent and the aromatic ring.⁶³

Farrell and Mason showed that the bromination of dimethylaniline and its 2,4,6-trideuteriated isomer gave a fairly small isotope effect, $k_H/k_D = 1.8$. Further studies showed that the value of the isotope effect was dependent on the position of attack, being absent at the 3- and 4-positions. However, the 2,6-dideuteriated compound gave a higher isotope effect of 2.6. This indicates that C-H bond breaking may become partially rate-determining for reaction at sterically hindered sites.⁶⁶

Other reactive species have been used to achieve bromination of aniline. For example, 2,4,4,6-tetrabromocyclohexa-2,5-dienone, **1.39**, reacts with aniline to give the 4-bromo-derivative,⁶⁷ Scheme 1.18.

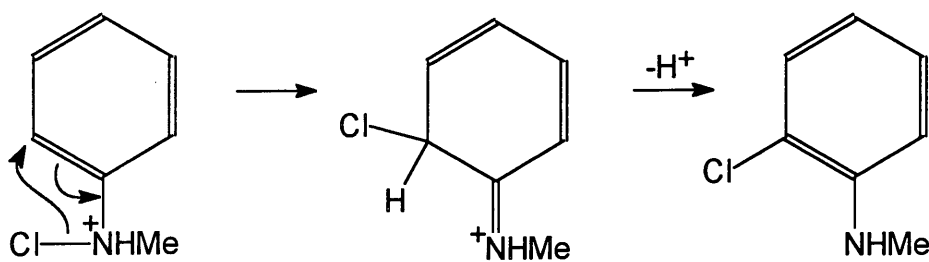


Scheme 1.18

It is probable that this reagent does not normally react directly with unsaturated compounds, but first reacts with small concentrations of nucleophiles, Nu^- , giving brominating species of the type Br-Nu . For example, BrCl may be the brominating species when HCl is used as a catalyst.⁶⁸

Berthelot and co-workers have recently studied the bromination of aniline.⁶⁹ The reaction of tetrabutylammonium tribromide with aniline gave the para-brominated amine exclusively in high yield. They suggested that the brominating species was in fact Br_3^- .

Other species will undergo electrophilic halogenation as a result of the attack of an internal electrophile. For example, the N-chloro-N-methylanilinium ion rearranges to give the ortho-chloro-derivative in carbon tetrachloride, Scheme 1.19.^{70,71}



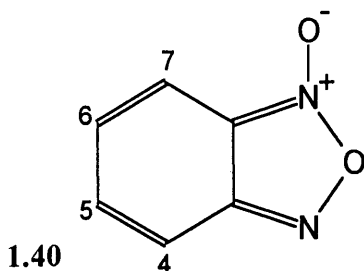
Scheme 1.19

Iodination occurs predominantly at the para-position, and for many aromatic substrates substantial kinetic isotope effects have been established.⁷⁰ Catalysis by nucleophilic bases has also been observed, and proton loss can be important in the rate-determining step of iodination.

1.3 Nitrobenzofurazans and Nitrobenzofuroxans

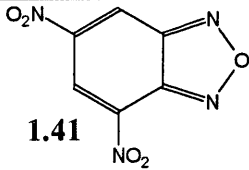
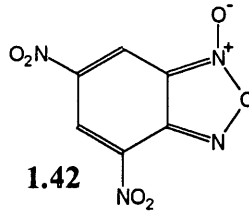
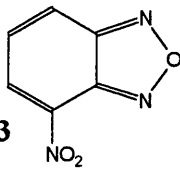
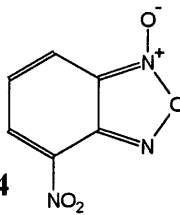
1.3.1 Structure

In the early part of the 20th Century, there was much debate over the structure of benzofuroxan derivatives, and the now generally accepted structure, **1.40**, was first suggested by Green and Rowe in 1912.⁷² Dinitrobenzofuroxan, (DNBF) **1.42**, was first prepared by Drost in 1899, and was named m-dinitro-o-dinitrosobenzene. The structure of this compound was not confirmed until the early 1960's by NMR (Harris and co-workers)⁷³ and by UV and IR (Boulton and co-workers),⁷⁴ and has been recently re-investigated by Terrier and co-workers.⁷⁵ Further studies were carried out by Prout in 1972 to determine the X-ray crystal structure.⁷⁶

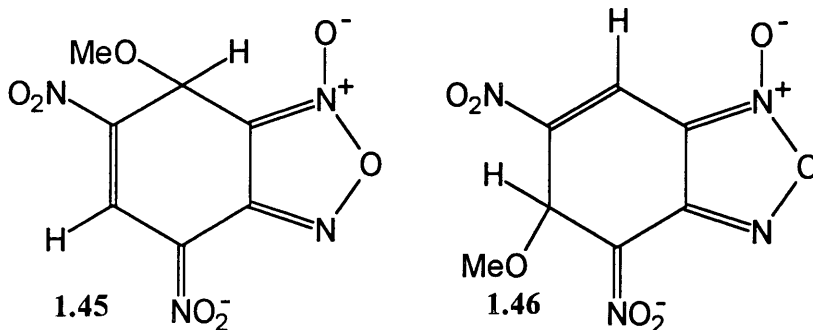


Other nitrobenzofurazan and nitrobenzofuroxan derivatives have been synthesised⁷⁷ and characterised using NMR spectroscopy^{78,73,79} and X-ray crystallography.^{80,81} Table 1.5 summarises the NMR data for a selection of some benzofurazan and benzofuroxan derivatives. Due to the high electrophilicity of these compounds there have been many reports of the formation of σ -adducts resulting from their reactions with nucleophiles. NMR spectroscopy has been widely used to examine the structures of the adducts formed.^{78,79}

Table 1.5: ^1H NMR data for a selection of benzofurazan and benzofuroxan compounds.

Structure	mp / $^{\circ}\text{C}$	H_5	H_6	H_7	Solvent	ref
DNBZ  1.41	133	9.04		9.80	$\text{d}_6\text{-DMSO}$	⁷⁵
DNBF  1.42	173	8.94		9.27	$\text{d}_6\text{-DMSO}$	⁷⁵
NBZ  1.43	93	8.70	7.88	8.59	$\text{d}_6\text{-DMSO}$	⁷⁹
NBF  1.44	143	8.62	7.55	8.13	$\text{d}_6\text{-DMSO}$	⁷⁹

The ^1H NMR spectrum of the methoxide adduct of DNBF, **1.42**, shows doublets, $J = 0.6$ Hz, at 8.70 and 5.89 ppm. The large shift to lower frequency of one of these resonances relative to the parent, indicates that attack has occurred at one of the ring carbon atoms carrying hydrogen. However, the spectrum does not allow the distinction to be made between structures **1.45** and **1.46**.



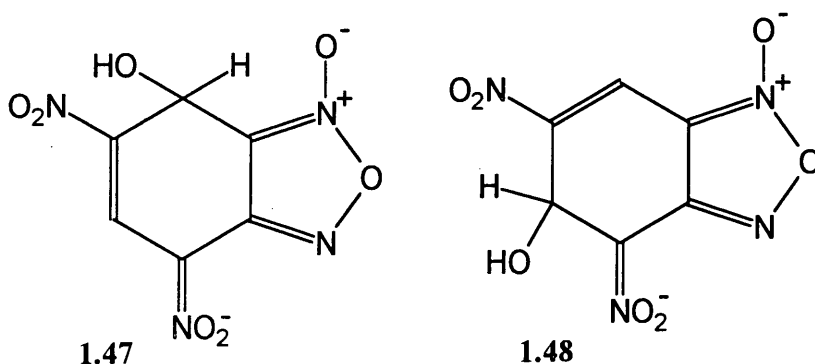
Terrier and co-workers have used ^{15}N and ^{13}C isotope labelling of DNBF, **1.42**, to ascertain the position of attack and to validate other ^1H NMR data. ^{15}N NMR data confirmed that σ -complexation occurs at the 7-position to give **1.45**.⁷⁵ DNBF and its methoxide adduct were

isotopically labelled with ^{15}N at the 6- NO_2 or the 4- and 6- NO_2 groups. In the methoxide adduct ^1H NMR resonances occur at 8.70 (H_A) and 5.89 (H_B) in DMSO. ^{15}N labelling of the 6- NO_2 group left the H_B resonance unchanged while causing a splitting of the H_A resonance. Further splitting of H_A occurred on labelling of the 4- NO_2 group.⁷⁵

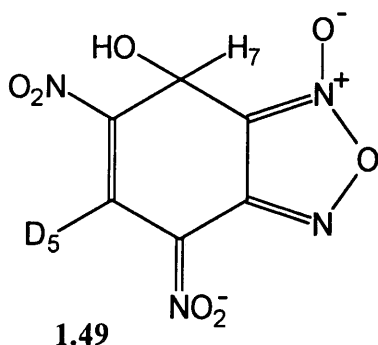
The reactions of 4-nitrobenzofurazan, **1.43**, and 4-nitrobenzofuroxan, **1.44**, with methoxide ions in 30/70 $\text{CH}_3\text{OD}/\text{d}_6\text{-DMSO}$ provided evidence for the formation of isomeric Meisenheimer adducts.⁷⁹ The spectra gained were attributed to the formation of a σ -adduct at the 5-position under kinetic control which isomerised to yield the more thermodynamically stable 7-adduct.⁷⁹

1.3.2 Hydroxide Ion Attack on DNBF

DNBF is able to abstract an hydroxide ion from water to leave an acidic solution. The O-H IR active stretching mode at 3480 cm^{-1} is very sharp and early workers were further drawn to the conclusion that a hydroxide adduct was formed in solution, as water in the potassium salt was not evolved even at $160\text{ }^{\circ}\text{C}$.⁸² Jackson and Earle⁸³ suggested the formation of a metal-hydroxide addition complex to give anions such as **1.47** or **1.48**. Norris and Osmundsen were unable to discriminate between the two proposed structures **1.47** and **1.48** using NMR spectroscopy with deuteriated solvents. After consideration of the possible resonance forms they concluded that the 7-adduct should be more stable than the 5-adduct.⁸⁴ This conclusion was also supported by Boulton and Clifford.⁸⁵



Brown and Keyes prepared 5-deuterio-4,6-dinitrobenzofuroxan. The ^1H NMR and IR spectra indicated that addition of the hydroxide ion had occurred at the 7-position to give **1.47**, rather than the 5-position.⁸² The C-H out-of-plane deformation mode for H_7 was unaffected, occurring at 690 cm^{-1} for **1.47** and **1.49**. While that at 730 cm^{-1} due to H_5 had decreased in intensity by approximately 50% and the corresponding C-D deformation mode appeared at 540 cm^{-1} .⁸²



Terrier and co-workers studied the formation and decomposition of **1.47** using stopped-flow spectrophotometry.⁸⁶ At pH < 7, **1.47** is formed exclusively from the attack of a water molecule on DNBF. Between pH 7 and pH 9 hydroxide ion attack begins to compete with that of water. At pH > 9, adduct formation is solely due to hydroxide ion attack.⁸⁷ A summary of the rate constants corresponding to Equations 1.2 and 1.3, is given in Table 1.6.

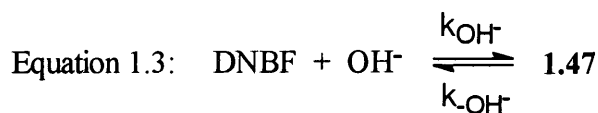
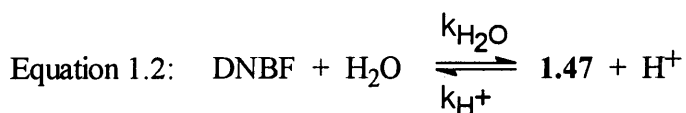
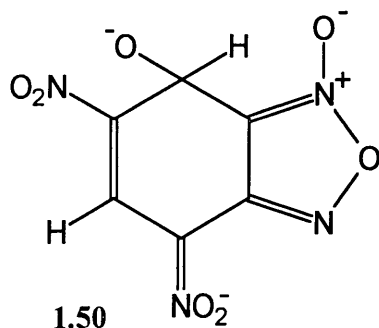


Table 1.6: Rate constants calculated for the formation and decomposition of **1.47**.

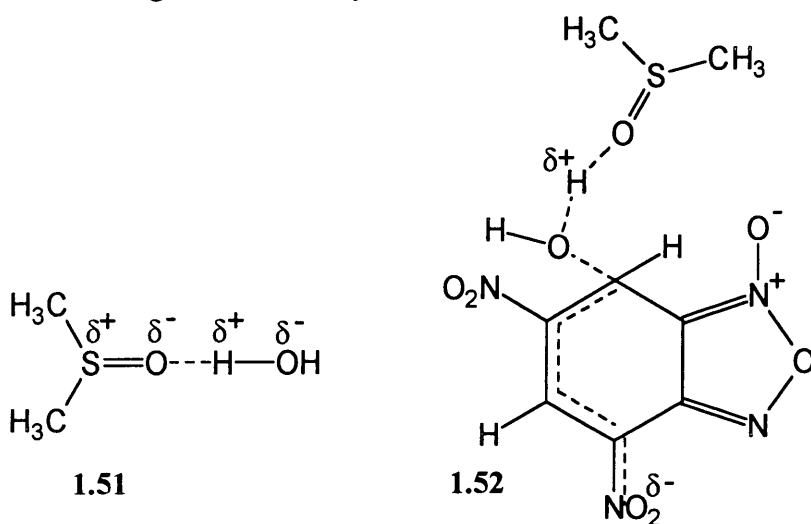
$k_{\text{H}_2\text{O}} / \text{s}^{-1}$	$k_{\text{H}^+} / \text{M}^{-1} \text{s}^{-1}$	$k_{\text{OH}^-} / \text{M}^{-1} \text{s}^{-1}$	$k_{-\text{OH}^-} / \text{s}^{-1}$	pK_a
0.0345	146	33500	2.5×10^{-6}	3.75

Another process was observed to occur in very basic media (pH > 10.6). The decrease in the absorbance due to **1.47** at 465 nm and the corresponding shift in the absorption maxima to 450 nm was attributed to the ionisation of **1.47** to give **1.50**. This is a direct measure of the electron-withdrawing capability of the negatively charged DNBF moiety.



The reaction to produce **1.47** has also been studied in H₂O-DMSO mixtures. The rate constant for nucleophilic attack of water on DNBF, k_{H_2O} , was found to increase with increasing DMSO content of the solvent, indicating that the nucleophilic power of a water molecule increases as the proportion of DMSO increases.⁸⁸

DMSO is able to associate with water to form hydrogen-bonded structures such as **1.51** in which the basic character of the water molecules is strongly enhanced. The reaction to form **1.47** in H₂O-DMSO mixtures may proceed via a transition state such as **1.52** where the DMSO molecule is acting as a base catalyst.⁸⁸



Trinitrobenzene (TNB) is the common reference electrophile. TNB is able to form hydroxide and methoxide adducts from the addition of the ions, but is unable to undergo facile addition of water or methanol.⁸⁹ The hydroxide and methoxide adducts of DNBF are approximately 10^{10} times more stable than the analogous TNB adducts. The greater thermodynamic stability of the DNBF adducts relative to TNB adducts reflects the much higher rates of nucleophilic attack and lower rates of decomposition.

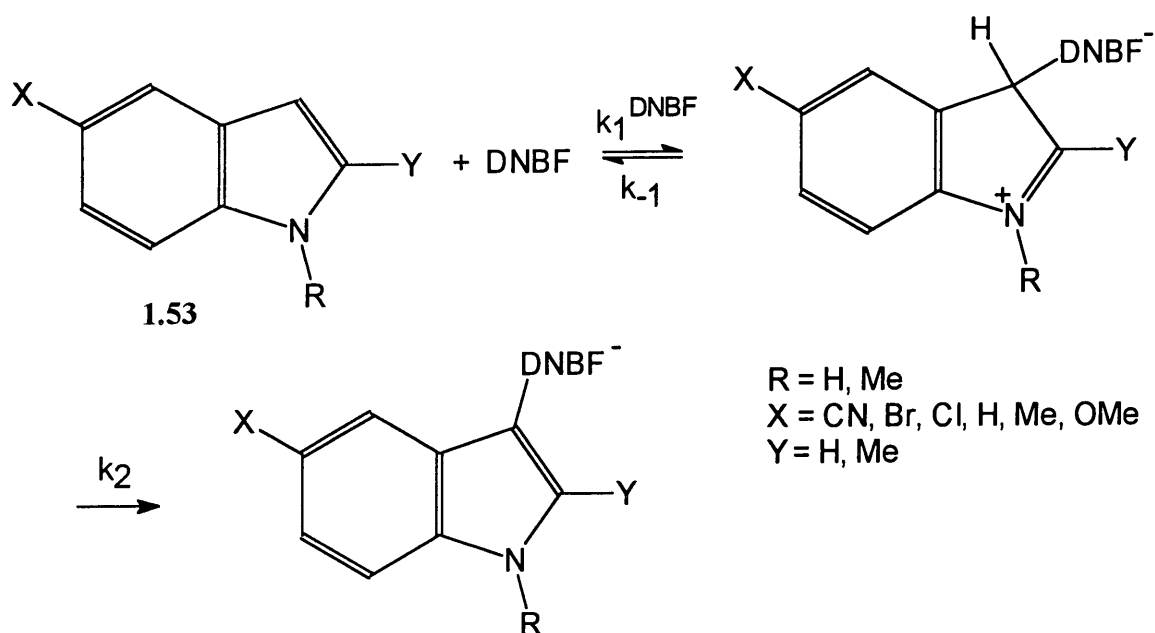
1.3.3 Reactivity

The low aromaticity of the benzofurazan and benzofuroxan systems favours covalent addition of the nucleophile. This effect, together with the combination of the strong electron-withdrawing effects of the nitro-groups and the annelated furoxan ring leads to the exceptional reactivity of these compounds and the stability of the adducts formed. The activating power of heterocyclic rings may be due to several factors: (i) The electron-withdrawing power of an aza-substituent in an aromatic system will increase activation if in a position conjugated to the reaction centre. (ii) Oxygen present in the ring will increase the electron-withdrawing power due to its own high electronegativity. (iii) The annelated ring is able to delocalise charge in the transition state through conjugation with the reaction centre.⁹⁰ The following sections provide further evidence for the high reactivity of DNBF and its versatility as an electrophile.

1.3.3.1 As an Electrophile

DNBF is a more powerful electrophile than the proton or the p-nitrobenzenediazonium cation.⁸⁹ A structural and kinetic study of the reaction of DNBF with a series of 5-X-substituted indoles,⁹¹ **1.53**, allowed the determination of the rate constants k_1^{DNBF} , Scheme 1.20. Proton elimination from the zwitterion is rapid and the rate-determining step is the initial electrophilic attack by DNBF. A direct comparison of the rate constants of electrophilic attack of DNBF on the indoles, with the rate constant for indole protonation, $k_1^{\text{H}_3\text{O}^+}$, (calculated from deuterium and tritium labelling at the C-3 position), highlighted the difference in electrophilic character.⁹¹

The experimental results indicated that the neutral DNBF molecule behaved as a much stronger electrophile than the positively charged hydronium ion. The difference in the electrophilic character was calculated from the ratio $k_1^{\text{DNBF}} / k_1^{\text{H}_3\text{O}^+}$. This ratio was found to increase with increasing basicity of the indole.

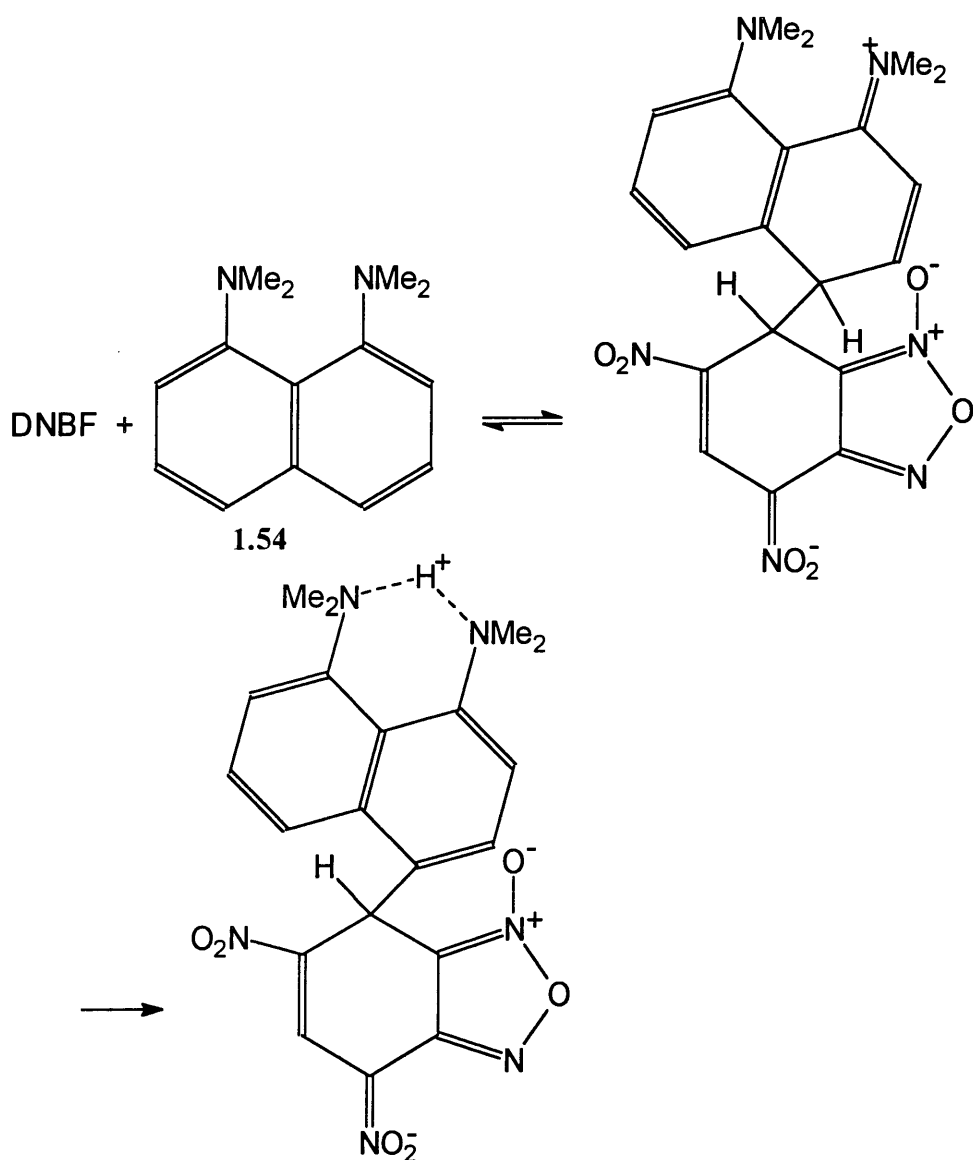


Scheme 1.20

Data are also available⁹¹ for the reaction of indole and N-methylindole with the p-nitrobenzenediazonium cation. The rate constants for complexation of DNBF with indole and N-methylindole (at 25°C in 70/30 (v/v) H₂O/DMSO) are respectively 1.4 and 3 times greater than the rate constants measured for diazo-coupling of these compounds by the nitrobenzenediazonium cation (at 30° in acetonitrile).

1.3.3.2 With the “Proton Sponge”

DNBF has a powerful electrophilic character with the ability to undergo facile σ -complexation in the absence of added base, and as such DNBF and other electron-deficient aromatic compounds have been used to assess the reactivity of weak carbon nucleophiles. For example, the “proton sponge” (1,8-bis(dimethylamino)naphthalene), **1.54**, acts as a carbon nucleophile in reactions with DNBF to produce carbon-bonded adducts, Scheme 1.21. This reaction provided the first evidence that the “proton sponge” was also able to act as a nucleophile.⁹²



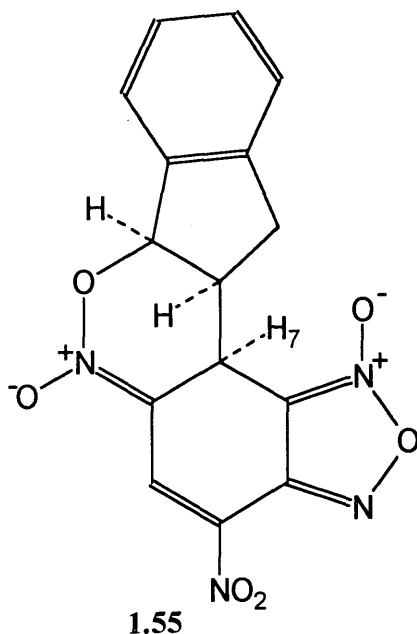
Scheme 1.21

The “proton sponge” has a very high basicity but the steric hindrance due to the two bulky dimethylamino groups makes it a very poor nitrogen nucleophile. The nitrogen lone pairs of an amino group may be delocalised into the aromatic ring and the resonance interaction may lead to carbon basicity. However, there is no reasonable possibility that the dimethylamino groups may be brought into the plane of the ring to aid delocalisation, and the resonance interaction will be small. The observed formation of carbon-bonded DNBF adducts demonstrates that the nucleophilic character of the “proton sponge” is not completely suppressed, and gives further evidence of the electrophilic reactivity of DNBF.

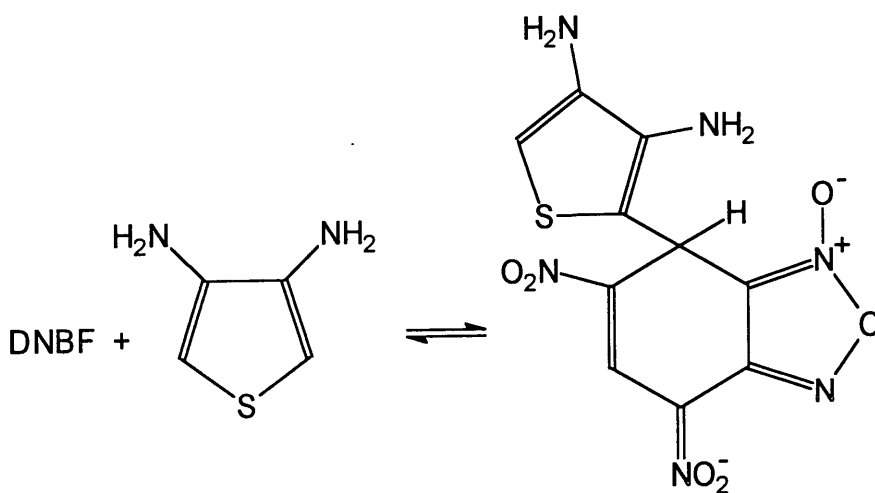
1.3.3.3 Formation of Carbon-Bonded Adducts

A number of π -excessive aromatics and heteroaromatics have been found to react with DNBF to produce stable carbon-bonded σ -adducts which are formally the products of S_EAr substitution of the benzene or heteroarene rings. Anilines,^{93,94} phenols,^{95,96,97} pyrroles,⁸⁹ indoles,⁹¹ and thiophenes^{98,99,100} are just a selection of those aromatics studied. These reactions all provide rare examples of substituent or neighbouring group effects, which are a function of the exceptional reactivity of DNBF.

The reaction of indene with DNBF provides an example of neighbouring nitro group participation with intramolecular nucleophilic attack of an oxygen atom of the 6-NO₂ group at the positively charged carbon of the indene ring, to give an intermediate, **1.55**.¹⁰¹



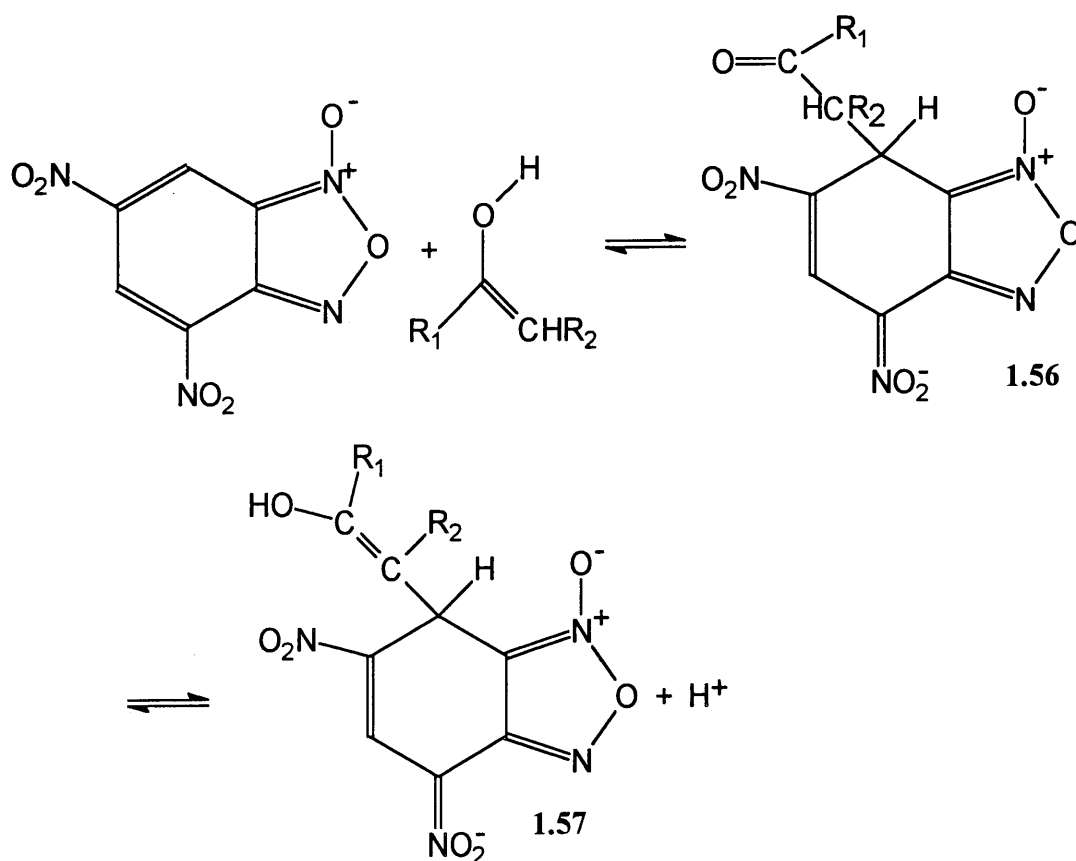
The enaminic character of aminothiophenes has been demonstrated by Terrier.^{98,100} The proton affinity of the amino groups of 3,4-diaminothiophene is considerably greater than that of the α -carbon. However, in the reaction with DNBF, attack by the carbon centre is both kinetically and thermodynamically favoured compared to attack by the amino groups to give the nitrogen-adduct, Scheme 1.22.



Scheme 1.22

1.3.3.4 With Ketones

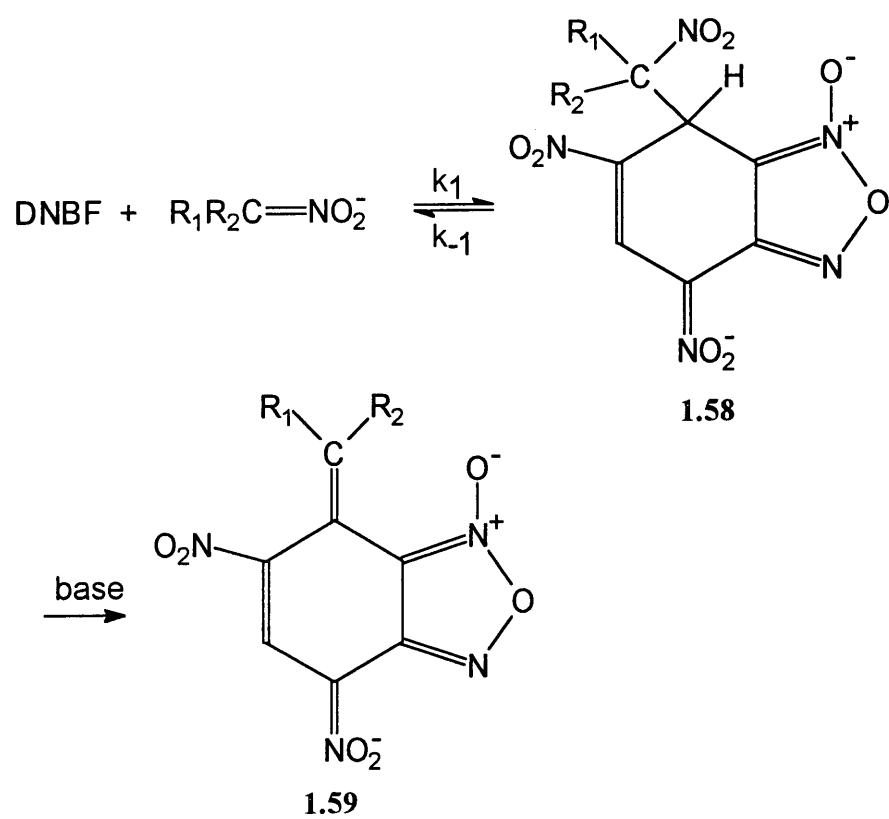
A number of ketones and β -diketones will react with DNBF, in the absence of added base, to yield the keto adducts in their acidic form.¹⁰² The fact that ketones of very low acidity such as acetone and cyclopentanone react with DNBF in the absence of added base underlines the electrophilic character of DNBF. With β -diketones, subsequent enolisation of **1.56** to **1.57** may occur, Scheme 1.23, and is observed through the change in the splitting pattern of the H₇ resonance from a doublet in **1.56**, to a singlet in **1.57**.



Scheme 1.23

1.3.3.5 With Nitroalkanes

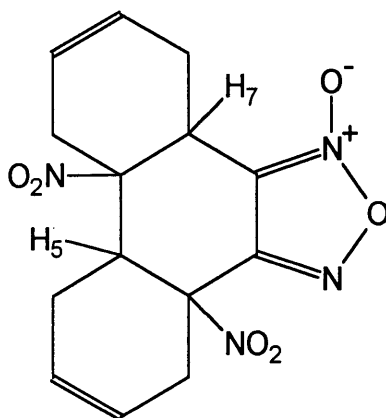
Nitroalkanes also react with DNBF in the absence of added base to give C-adducts, Scheme 1.24. The adducts, 1.58 may undergo a base-catalysed elimination of nitrous acid to yield products, 1.59 in DMSO. Generally, the nitro-group is not a good leaving group and will only be susceptible to base-induced β -eliminations when there is a strong electron-withdrawing group at the β -position.¹⁰³ This reaction provides further evidence that even the negatively charged DNBF moiety is a powerful electron-withdrawing species.



Scheme 1.24

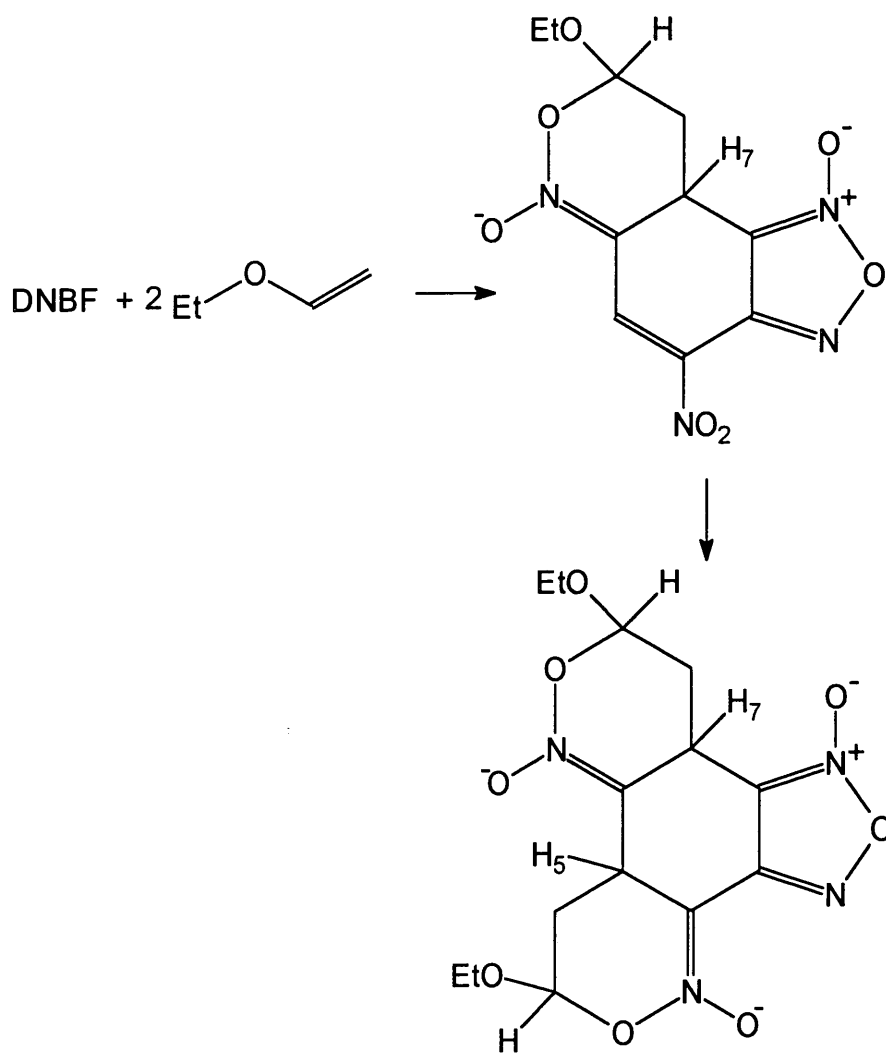
1.3.3.6 In Diels-Alder Reactions

DNBF is also able to act as a dienophile. Reaction with suitable dienes, such as butadiene, may yield di-adducts, **1.60**, by a NEDDA (Normal Electron Demand Diels-Alder) pathway.¹⁰⁴



1.60

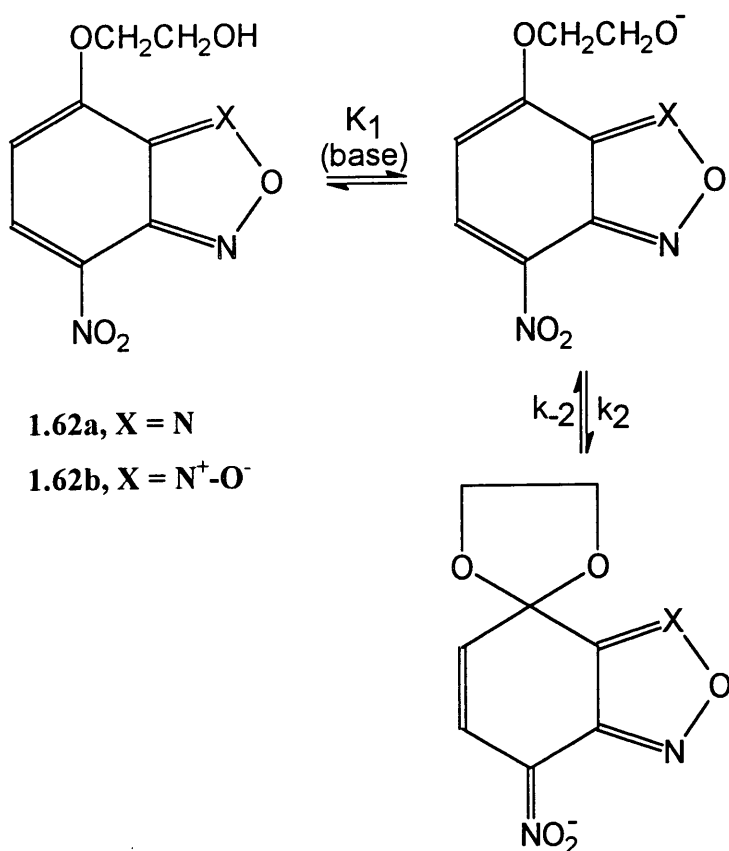
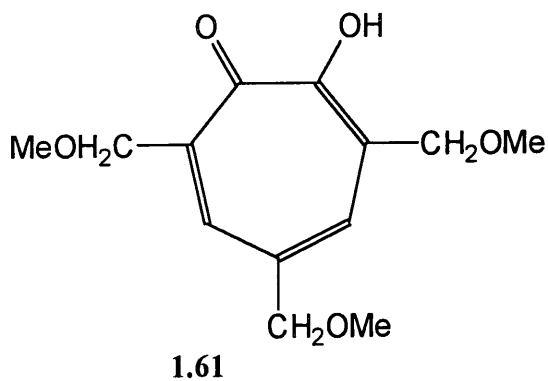
However, Terrier et al found that the reaction with ethyl vinyl ether proceeded according to Scheme 1.25.¹⁰⁵ Here DNBF is acting as a heterodiene in an IEDDA (Inverse Electron Demand Diels-Alder) pathway. This ambident Diels-Alder reactivity is a function of the experimental conditions and the reacting species employed.¹⁰⁶ There is current interest in these reactions as they may lead to the synthesis of new heterocyclic structures.¹⁰⁷



Scheme 1.25

1.3.3.7 Formation of Spiro-Cyclic Adducts

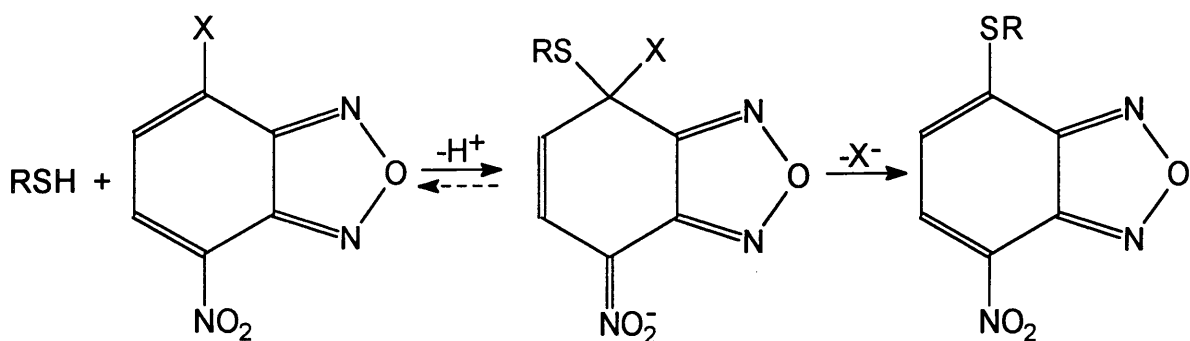
Spiro-cyclic adducts have been observed in the reactions of DNBF with the tropolone derivative¹⁰⁸ **1.61**. Cyclisation also occurs with **1.62a** and **1.62b** in the presence of base, Scheme 1.26.¹⁰⁹ A comparison of the equilibrium constants for spiro-cyclic adduct formation, K_1K_2 , indicated that here the furazan adduct had higher stability than the furoxan derivative.¹⁰⁹ It was argued that the furazan moiety may exhibit a more powerful electron withdrawing effect than the furoxan moiety due to the electron donating effect of the N-oxide group.⁷³



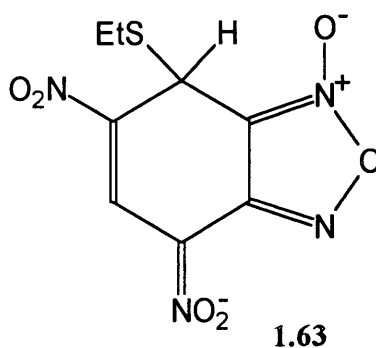
1.3.4 Applications

Some benzofurazan and benzofuroxan derivatives are able to act as powerful inhibitors of nucleic acid and protein biosynthesis. 4-Nitrobenzofuroxan, **1.44** exhibits a toxic effect on the metabolism of leukocytes *in vitro*, and has anitileukemic and immunosuppressive drug potential.¹¹⁰ Various workers have concluded that this potential drug action was related to the interaction of 4-nitrobenzofurazan, **1.43**, or 4-nitrobenzofuroxan, **1.44**, derivatives with

intracellular thiol groups, leading to σ -complex formation, or substitution, Scheme 1.27.^{111,110,112,113,114} Strauss and co-workers have studied the addition of thiol to DNBF to yield **1.63**.¹¹³



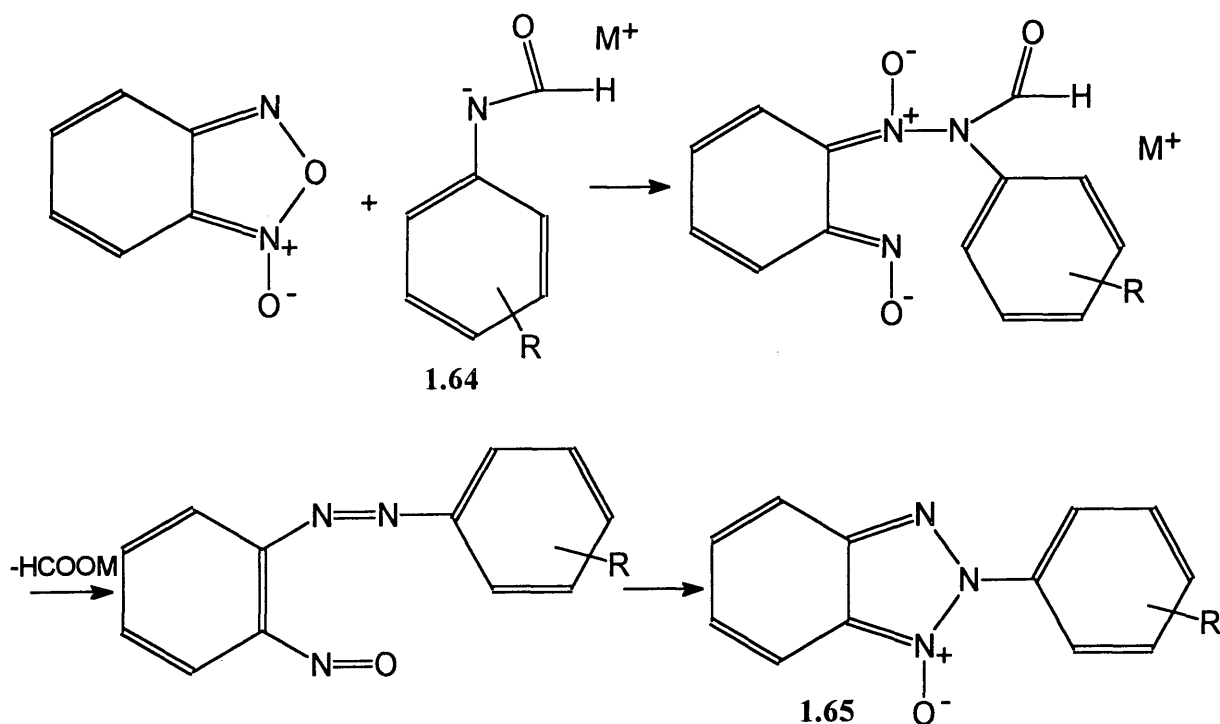
Scheme 1.27



Ghosh and Whitehouse studied the pharmacological activity of some benzofurazans and benzofuroxans.¹¹² The presence of a nitro-group increased the inhibition of the lymphocyte metabolism *in vitro*. The benzofuroxans were generally less potent *in vitro* inhibitors than the corresponding benzofurazans. When X in Scheme 1.27 was a hydrogen atom or a good leaving group (Cl^- , RS^-) the drug action was largely irreversible.¹¹⁴ The drug activity of the compounds was regulated by the introduction of appropriate substituents. *In vitro* activity was diminished by a 5-substituent.

7-Chloro-4-nitrobenzofurazan has been used as a fluorescent labelling reagent for the study of proteins. There is a covalent interaction between a nucleophilic atom in the protein and the C_7 atom, resulting in the formation of a Meisenheimer complex.^{115,116} Benzofuroxan derivatives have also found use as depolarising agents in dry cell batteries, as polymerisation inhibitors and in pest control.¹¹⁷

Niclas and Gohrmann have investigated the reactions of benzofuroxan and formanilides, **1.64**, as a synthetic route to benzotriazoles, **1.65**, Scheme 1.28.^{118,119} Benzotriazoles are useful as fluorescence brighteners and UV light absorbing stabilisers for polymers.¹¹⁸



Scheme 1.28

1.4 References

- ¹ F. Terrier. "Nucleophilic Aromatic Displacement". 1991. VCH.
- ² E. Buncl, M. R. Crampton, M. J. Strauss and F. Terrier. "Electron Deficient Aromatic- and Heteroaromatic-Base Interactions". 1984. Elsevier.
- ³ C. L. Jackson and F. H. Gazzolo., *J. Am. Chem. Soc.*, 1900, **23**, 376.
- ⁴ J. Meisenheimer. *Liebigs Ann. Chem.*, 1902, **323**, 205.
- ⁵ R. Foster. *Nature*. 1955,176, 746.
- ⁶ S. D. Ross., *Progr. Phys. Org. Chem.*, 1963, **1**, 31.
- ⁷ M. R. Crampton and V. Gold., *J. Chem. Soc.*, 1964, 4293.
- ⁸ K. L. Servis., *J. Am. Chem. Soc.*, 1965, **87**, 5495.
- ⁹ K. L. Servis., *J. Am. Chem. Soc.*, 1967, **89**, 1508.
- ¹⁰ C. F. Bernasconi., *J. Am. Chem. Soc.*, 1970, **92**, 4682.
- ¹¹ C. A. Fyfe, A. Koll, S. W. H. Damji, C. D. Malkiewich and P. A. Forte., *Can. J. Chem.*, 1977, **55**, 1468.
- ¹² J. A. Orvik and J. F. Bunnett., *J. Am. Chem. Soc.*, 1970, **92**, 2417.
- ¹³ R. Destro, C. M. Gramaccioli and M. Simonetta., *Acta Cryst.*, B24, 1968, 1369.
- ¹⁴ R. Destro, T. Pilati and M. Simonetta., *Acta Cryst.*, B35, 1979, 733.
- ¹⁵ G. G. Messmer and G. J. Palenik., *Acta Cryst.*, B27, 1971, 316.
- ¹⁶ O. Y. Borbulevych, O. V. Shishkin and V. N. Knyazev., *Acta Cryst.*, 1999, C55, 1704.

- ¹⁷ M. J. Dewar. "The Electronic Theory of Organic Chemistry". Oxford University Press. London. 1949.
- ¹⁸ G. A. Olah, G. Asensio, H. Mayr and P. V. R. Schleyer., *J. Am. Chem. Soc.*, 1978, **100**, 4347.
- ¹⁹ A. J. Birch, A. L. Hinde and L. Radom., *J. Am. Chem. Soc.*, 1980, **102**, 6430.
- ²⁰ F. Terrier., *Chem. Rev.*, 1982, **82**, 77.
- ²¹ P. Caveng, P. B. Fischer, E. Heilbronner, A. L. Miller and H. Zollinger., *Helv. Chim. Acta.*, 1967, **50**, 848.
- ²² M. J. Strauss., *Chem. Rev.*, 1970, **70**, 667.
- ²³ M. R. Crampton., *Adv. Phys. Org. Chem.*, 1969, **7**, 211.
- ²⁴ E. Buncl and B. C. Menon., *J. Am. Chem. Soc.*, 1977, **99**, 4457.
- ²⁵ J. F. Bunnett and R. E. Zahler., *Chem. Rev.*, 1951, **49**, 273.
- ²⁶ M. Makosza, J. Golinski and J. Baran., *J. Org. Chem.*, 1984, **49**, 1488.
- ²⁷ M. Makosza and J. Winiarski., *J. Acc. Chem. Res.*, 1987, **20**, 282.
- ²⁸ G. Guanti, S. Thea and C. Dell' Erba., *Tetrahedron Lett.*, 1976, 461.
- ²⁹ G. Guanti, G. Petrillo and S. Thea., *Tetrahedron.*, 1982, **38**, 505.
- ³⁰ C. F. Bernasconi and H-C. Wang., *J. Am. Chem. Soc.*, 1976, **98**, 6265.
- ³¹ C. F. Bernasconi., *Acc. Chem. Res.*, 1978, **11**, 147.
- ³² C. F. Bernasconi., *J. Am. Chem. Soc.*, 1968, **90**, 4982.
- ³³ C. F. Bernasconi and M. C. Muller., *J. Am. Chem. Soc.*, 1978, **100**, 5530.
- ³⁴ E. J. Fendler, J. H. Fendler and C. E. Griffin., *J. Org. Chem.*, 1969, **34**, 689.
- ³⁵ N. Gravitz and W. P. Jencks., *J. Am. Chem. Soc.*, 1974, **96**, 499.
- ³⁶ C. F. Bernasconi, M. C. Muller and P. Schmid., *J. Org. Chem.*, 1979, **44**, 3189.
- ³⁷ F. G. Bordwell and D. L. Hughes. *J. Am. Chem. Soc.*, 1986, **108**, 5991.
- ³⁸ M. R. Crampton and B. Gibson., *J. Chem. Soc., Perkin Trans. 2.*, 1981, 533.
- ³⁹ C. F. Bernasconi., *J. Am. Chem. Soc.*, 1970, **92**, 129.
- ⁴⁰ C. F. Bernasconi., *J. Phys. Chem.*, 1971, **75**, 3636.
- ⁴¹ R. A. Chamberlin and M. R. Crampton., *J. Chem. Soc., Perkin Trans. 2.*, 1995, 1831.
- ⁴² M. R. Crampton., *J. Chem. Soc. (B).*, 1968, 1208.
- ⁴³ M. R. Crampton., *J. Chem. Soc. (B).*, 1967, 1341.
- ⁴⁴ G. A. Artamkina, M. P. Egarov and I. P. Beletsyaya., *Chem. Rev.*, 1982, **82**, 427.
- ⁴⁵ E. Buncl, J. M. Dust and R. A. Manderville., *J. Am. Chem. Soc.*, 1996, **118**, 6072.
- ⁴⁶ L. DiNunno, S. Florio and P. E. Todesco., *J. Chem. Soc., Perkin Trans. 2.*, 1975, 1469.
- ⁴⁷ S. W. Jacobs, E. E. Rosenbaum and D. C. Wood., "Dimethyl Sulphoxide", Eds., Marcel Dekker. 1971.
- ⁴⁸ A. K. Soper and A. Luzar., *J. Chem. Phys.*, 1992, **97**, 1320.
- ⁴⁹ I. I. Vaisman and M. L. Berkowitz., *J. Am. Chem. Soc.*, 1992, **114**, 7889.
- ⁵⁰ G. J. Safford, P. C. Schaffer, P. S. Leing, G. F. Doebbler, G. W. Brady and E. F. X. Lyden., *J. Chem. Phys.*, 1969, **50**, 2140.
- ⁵¹ K. H. Khoo., *J. Chem. Soc. (A).*, 1971, 2932.
- ⁵² A. J. Parker., *Quart. Rev.*, 1962, **16**, 163.
- ⁵³ J. A. Glasel., *J. Am. Chem. Soc.*, 1970, **92**, 372.
- ⁵⁴ E. S. Baker and J. Jonas., *J. Phys. Chem.*, 1985, **89**, 1730.
- ⁵⁵ G. G. Wheland., *J. Am. Chem. Soc.*, 1942, **64**, 900.
- ⁵⁶ G. A. Olah and S. J. Kuhn., *J. Am. Chem. Soc.*, 1958, **80**, 6541.
- ⁵⁷ R. Taylor. "Electrophilic Aromatic Substitution". Wiley. 1990.
- ⁵⁸ W. M. Lauer and W. E. Noland., *J. Am. Chem. Soc.*, 1953, **75**, 3689.
- ⁵⁹ H. Zollinger., *Helv. Chim. Acta.*, 1955, **38**, 1617.
- ⁶⁰ G. A. Olah, R. H. Schlosberg, R. D. Porter, Y. M. Mo, D. P. Kelly and G. D. Mateescu., *J. Am. Chem. Soc.*, 1972, **94**, 2034.
- ⁶¹ G. A. Olah, J. S. Staral, G. Asencio, G. Liang, D. A. Forsyth and G. D. Mateescu., *J. Am. Chem. Soc.*, 1978, **100**, 6299.
- ⁶² L. P. Hammett., *J. Am. Chem. Soc.*, 1937, **59**, 96.
- ⁶³ Comprehensive Chemical Kinetics., 1972, vol 13.
- ⁶⁴ C. K. Ingold, C. G. Raisin and C. L. Wilson., *J. Chem. Soc.*, 1936, 915.
- ⁶⁵ S. Clementi and A. R. Katritzky., *J. Chem. Soc., Perkin Trans. 2.*, 1973, 1077.
- ⁶⁶ P. G. Farrell and S. F. Mason., *Nature.*, 1959, **183**, 250.
- ⁶⁷ G. Hallas and J. D. Hepworth., *Educ. Chem.*, 1974, **11**, 25.

- ⁶⁸ V. Calo, L. Lopez, G. Pesce and P. E. Todesco., *J. Chem. Soc., Perkin Trans. 2.*, 1974, 1192.
- ⁶⁹ J. Berthelot, C. Guette, P-L. Desbene and J-J. Basselier., *Can. J. Chem.*, 1989, **67**, 2061.
- ⁷⁰ P. B. D. de la Mare., "Electrophilic Halogenation", Cambridge University Press. London. 1976.
- ⁷¹ P. Haberfield and D. Paul., *J. Am. Chem. Soc.*, 1965, **87**, 5502.
- ⁷² A. G. Green and F. M. Rowe., *J. Chem. Soc.*, 1912, **101**, 2452.
- ⁷³ R. K. Harris, A. R. Katritzky, S. Oksne, A. S. Bailey and W. G. Paterson., *J. Chem. Soc.*, 1963, **197**.
- ⁷⁴ A. J. Boulton and P. B. Ghosh., *Adv. Heterocycl. Chem.*, 1969, **10**, 1.
- ⁷⁵ F. Terrier, J-C. Halle, P. MacCormack and M-J. Pouet., *Can. J. Chem.*, 1989, **67**, 503.
- ⁷⁶ C. K. Prout, O. J. R. Hodder and D. Viterbo., *Acta Crystallogr. Sect. B.*, 1972, **28**, 1523.
- ⁷⁷ R. J. Gaughran, J. P. Picard and J. V. R. Kaufman., *J. Am. Chem. Soc.*, 1954, **76**, 2233.
- ⁷⁸ E. Buncel, N. Chuaqui-Offermans and A. R. Norris., *J. Chem. Soc., Perkin Trans. 1.*, 1977, 415.
- ⁷⁹ F. Terrier, F. Millot, A-P. Chatrousse, M-J. Pouet and M-P. Simonnin., *Org. Mag. Res.*, 1976, **8**, 56.
- ⁸⁰ G. G. Messmer and G. J. Palenik., *Chem. Commun.*, 1969, 470.
- ⁸¹ F. Terrier, J. Lelievre, A-P. Chatrousse, T. Boubaker, B. Bachet and A. Cousson., *J. Chem. Soc., Perkin Trans. 2.*, 1992, 361.
- ⁸² N. E. Brown and R. T. Keyes., *J. Org. Chem.*, 1965, **30**, 2452.
- ⁸³ C. L. Jackson and R. B. Earle., *Am. Chem. J.*, 1903, **29**, 89.
- ⁸⁴ W. P. Norris and J. Osmundsen., *J. Org. Chem.*, 1965, **30**, 2407.
- ⁸⁵ A. J. Boulton and D. P. Clifford., *J. Chem. Soc.*, 1965, 5414.
- ⁸⁶ F. Terrier, F. Millot and W. P. Norris., *J. Am. Chem. Soc.*, 1976, **98**, 5883.
- ⁸⁷ F. Terrier, F. Millot and W. P. Norris., *Bull. Soc. Chim. France.*, 1975, 55
- ⁸⁸ F. Terrier, H. A. Sorkhabi, F. Millot, J-C. Halle and R. Schaal., *Can. J. Chem.*, 1980, **58**, 1155.
- ⁸⁹ F. Terrier, E. Kizilian, J-C. Halle and E. Buncel., *J. Am. Chem. Soc.*, 1992, **114**, 1740.
- ⁹⁰ D. DalMonte, E. Sandri, L. DiNunno, S. Florio and P. E. Todesco., *J. Chem. Soc. (B).*, 1971, 2209.
- ⁹¹ F. Terrier, M-J. Pouet, J-C. Halle, S. Hunt, J. R. Jones and E. Buncel., *J. Chem. Soc., Perkin Trans. 2.*, 1993, 1665.
- ⁹² F. Terrier, J-C. Halle, M-J. Pouet and M-P. Simonnin., *J. Org. Chem.*, 1986, **51**, 409.
- ⁹³ M. J. Strauss, R. A. Renfrow and E. Buncel., *J. Am. Chem. Soc.*, 1983, **105**, 2473.
- ⁹⁴ R. W. Read, R. J. Spear and W. P. Norris., *Aust. J. Chem.*, 1984, **37**, 985.
- ⁹⁵ E. Buncel, R. A. Manderville and J. M. Dust., *J. Chem. Soc., Perkin Trans. 2.*, 1997, 1019.
- ⁹⁶ E. Buncel, R. A. Renfrow and M. J. Strauss., *J. Org. Chem.*, 1987, **52**, 488.
- ⁹⁷ E. Buncel and K. T. Park., *Phys. Org. Chem.*, 1986, 247.
- ⁹⁸ F. Terrier, M-J. Pouet, E. Kizilian, J-C. Halle, F. Outurquin and C. Paulmier., *J. Org. Chem.*, 1993, **58**, 4696.
- ⁹⁹ E. Kizilian, F. Terrier, A-P. Chatrousse, K. Gzouli and J-C. Halle., *J. Chem. Soc., Perkin Trans. 2.*, 1997, 2667.
- ¹⁰⁰ F. Terrier, M-J. Pouet, K. Gzouli, J-C. Halle, F. Outurquin and C. Paulmier., *Can. J. Chem.*, 1998, **76**, 937.
- ¹⁰¹ P. MacCormack, J-C. Halle, M-J. Pouet and F. Terrier., *J. Org. Chem.*, 1988, **53**, 4407.
- ¹⁰² F. Terrier, M. P. Simonnin and M-J. Pouet., *J. Org. Chem.*, 1981, **46**, 3537.
- ¹⁰³ F. Terrier, R. Goumont, M-J. Pouet and J-C. Halle., *J. Chem. Soc., Perkin Trans. 2.*, 1995, 1629.
- ¹⁰⁴ G. Kresze and H. Bathelt., *Tetrahedron.*, 1973, **29**, 1043.
- ¹⁰⁵ J-C. Halle, D. Vichard, M-J. Pouet and F. Terrier., *J. Org. Chem.*, 1997, **62**, 7178.
- ¹⁰⁶ D. Vichard, J-C. Halle, B. Huguet, M-J. Pouet, D. Riou and F. Terrier., *Chem. Commun.*, 1998, 791.
- ¹⁰⁷ P. Sepulcri, D. Riou and F. Terrier., *J. Chem. Soc., Perkin Trans. 2.*, 2000, 51.
- ¹⁰⁸ S. V. Kurbatov, Z. N. Budarina, G. Svaslyayeva, N. I. Borisenko, A. P. Knyazev, V. I. Minkin, Yu. A. Zhdanov and L. P. Olekhovich., *Russian Chemical Bulletin.*, 1997, **46**, 1445.
- ¹⁰⁹ G. Ah-Kow, F. Terrier and F. Lessard., *J. Org. Chem.*, 1978, **43**, 3579.
- ¹¹⁰ E. Buncel, N. Chuaqui-Offermans, B. K. Hunter and A. R. Norris., *Can. J. Chem.*, 1977, **55**, 2852.
- ¹¹¹ E. Buncel, N. Chuaqui-Offermans, R. Y. Moir and A. R. Norris., *Can. J. Chem.*, 1979, **57**, 494.
- ¹¹² P. B. Ghosh and M. W. Whitehouse. *J. Medicinal Chem.*, 1968, **11**, 305.
- ¹¹³ M. J. Strauss, A. DeFusco and F. Terrier., *Tetrahedron Lett.*, 1981, **22**, 1945.

-
- ¹¹⁴ M. W. Whitehouse and P. B. Ghosh., *Biochem. Pharmacol.*, 1968, **17**, 158.
¹¹⁵ E. Buncel, J. M. Dust and F. Terrier., *Chem. Rev.*, 1995, **95**, 2261.
¹¹⁶ B. S. Baines, G. Allen and K. Brocklehurst., *Biochem. J.*, 1977, **163**, 189.
¹¹⁷ C. K. Lowe-Ma, R. A. Nissan and W. S. Wilson., *J. Org. Chem.*, 1990, **55**, 3755.
¹¹⁸ H-J. Niclas and B. Gohrmann., *Synth. Commun.*, 1989, **19**, 2141.
¹¹⁹ J. Kind and H-J. Niclas., *Synth. Commun.*, 1993, **23**, 1569.

Chapter 2

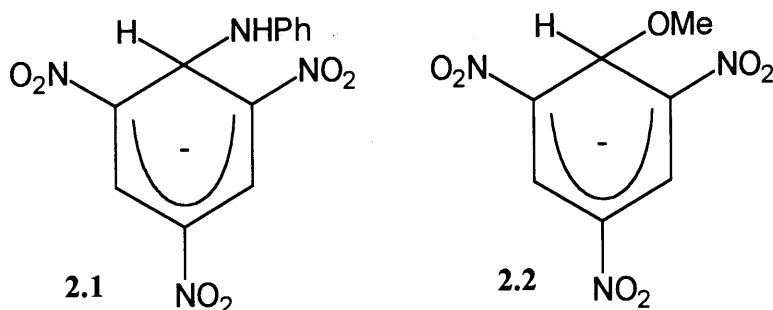
Electrophilic Aromatic Substitution in Aniline Derivatives

2 Electrophilic Aromatic Substitution In Aniline Derivatives

2.1 Introduction

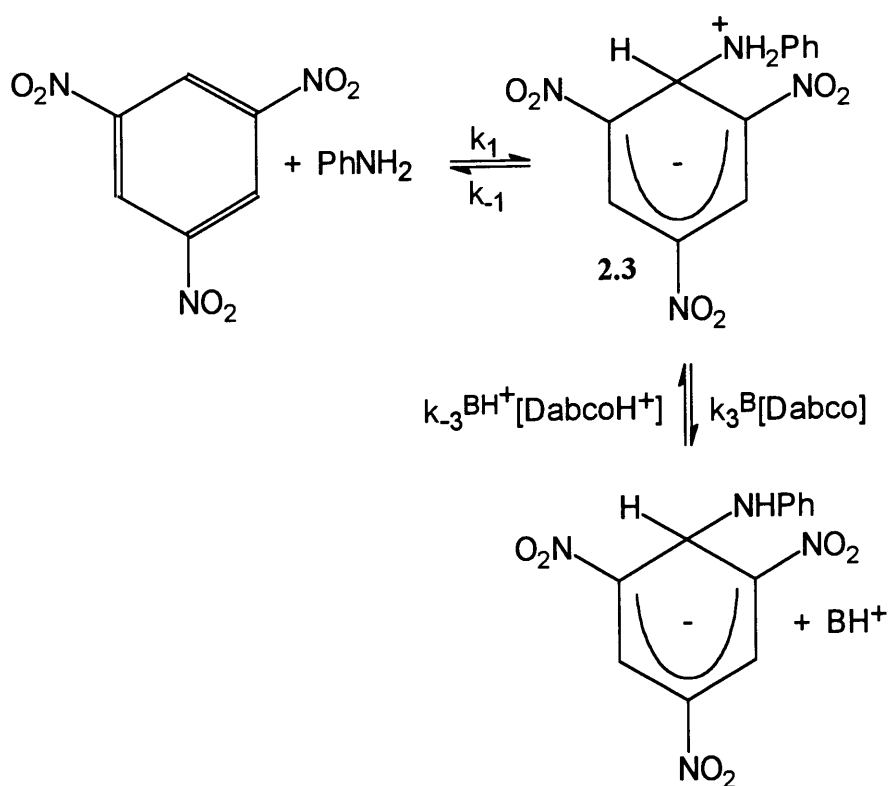
2.1.1 Reactions of Trinitrobenzene with Aniline

Primary and secondary aliphatic amines react with 1,3,5-trinitrobenzene (TNB) in dimethylsulfoxide (DMSO) to give σ -adducts.¹ However, aromatic amines such as aniline do not react spontaneously with TNB to give **2.1**, as shown by UV/Visible spectrophotometry, where there is an absence of a colour development characteristic of σ -complexation on mixing the two reagents.² Meisenheimer complex formation between aniline and TNB to give **2.1** has been achieved by reaction of the methoxide adduct, **2.2**, with aniline in DMSO,^{3,4,2,5} and directly using tertiary amines such as 1,4-diazabicyclo[2.2.2]octane (Dabco) to afford base catalysis.^{6,7,8}



Displacement⁹ and dissociative³ mechanisms have been proposed for the conversion of **2.2** to **2.1**. Detailed investigations by Buncel showed that the reaction of **2.2** with aniline² or ring-substituted anilines⁵ proceeded via a dissociative mechanism.

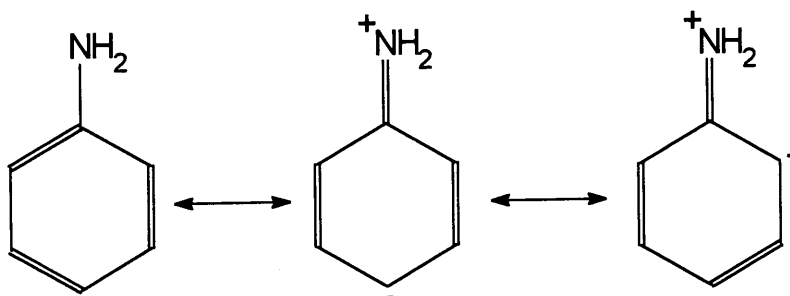
The reaction of TNB and aniline to form a σ -complex in the presence of Dabco or Et₃N was studied by Buncel in 1975, Scheme 2.1.¹⁰ Dabco is a tertiary amine which will function solely as a proton transfer agent due to its inability to form stable σ -complexes with nitroaromatics.⁶ The first step is thermodynamically unfavourable, due to the low basicity of aniline. The presence of Dabco enables the formation of the anionic σ -adduct through a thermodynamically favourable proton-transfer.¹¹ Proton transfer from the zwitterion, **2.3** is rate-limiting as $k_{-1} > k_3^B[\text{Dabco}]$.^{6,7} The reverse reaction will involve the conjugate acid, DabcoH⁺.⁶



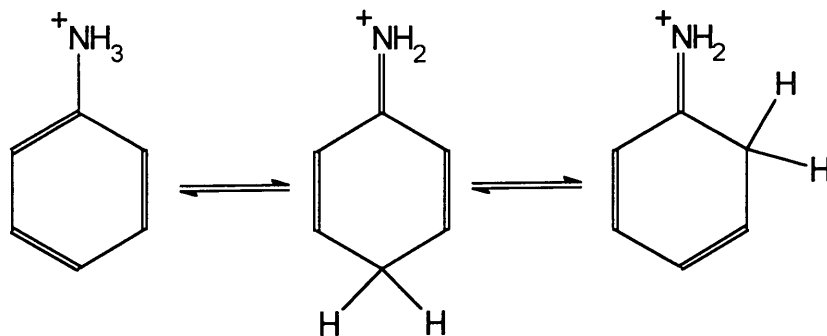
Scheme 2.1

2.1.2 Reactions of 4,6-Dinitrobenzofuroxan with Aniline

Aniline and its substituted derivatives usually act as nitrogen nucleophiles. Nevertheless, aniline may exhibit ambident reactivity, as the lone-pair electrons are delocalised into the aromatic ring, Scheme 2.2. Aniline is able to undergo protonation at the nitrogen centre or in the ring at the ortho and para carbons which are weakly basic, Scheme 2.3.

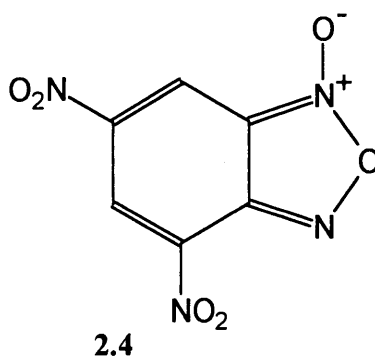


Scheme 2.2

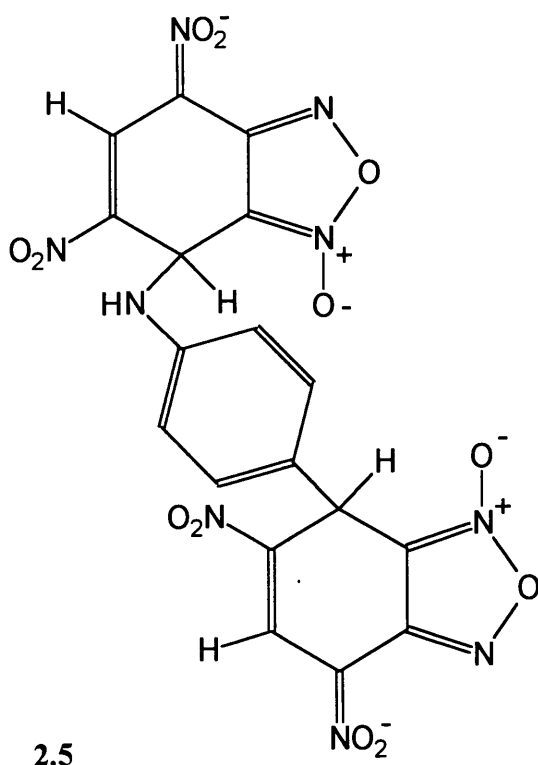


Scheme 2.3

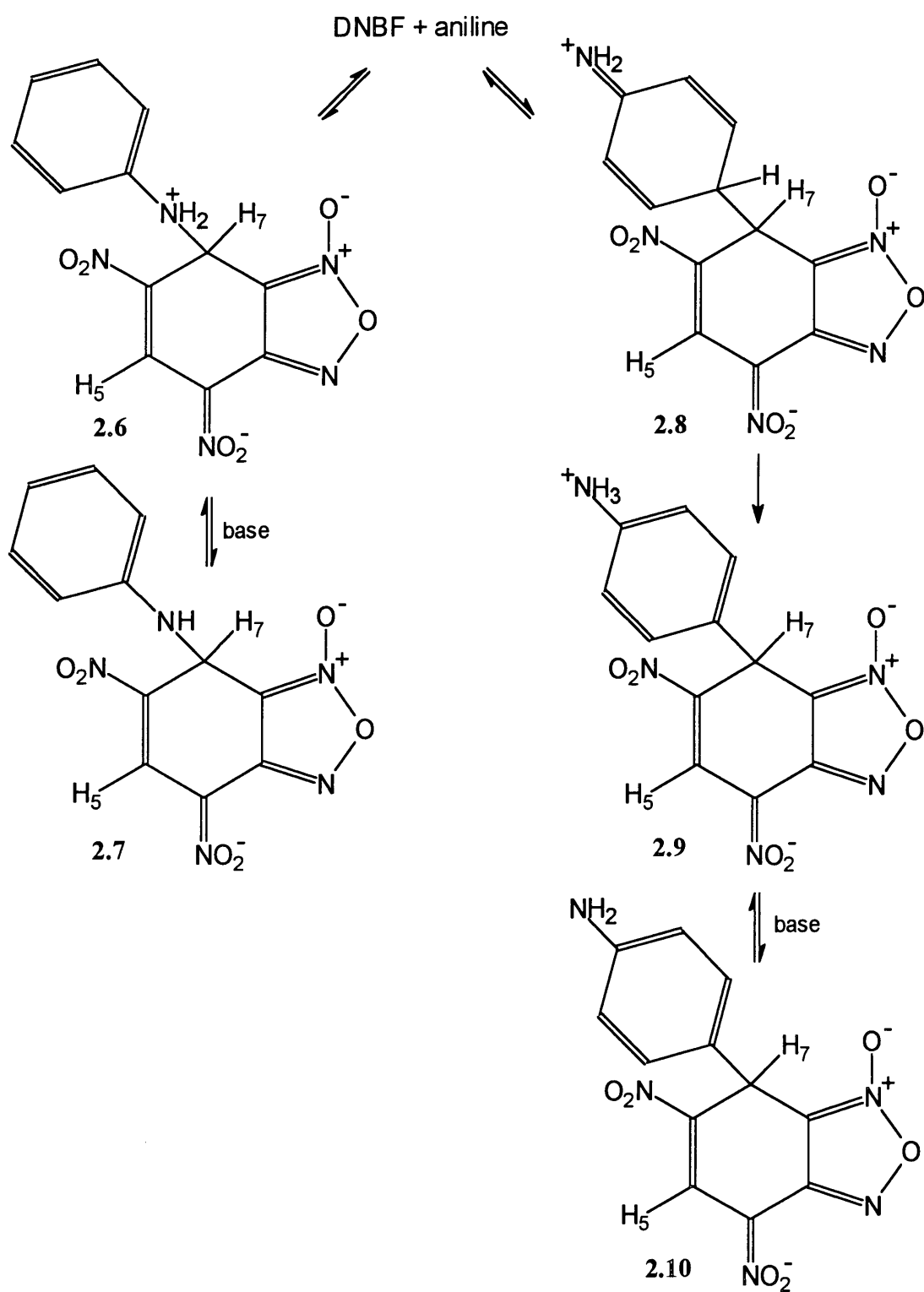
In the early 1980s two separate research groups independently discovered that aniline reacted through its weakly nucleophilic para carbon centre to form a σ -adduct with DNBF, **2.4**.^{12,13} The reaction provided the first reported instance where aniline reacted with an aromatic carbon through the para-position, and not through the amino-nitrogen.¹⁴ If the para-position was blocked by a methyl group, the reaction occurred at the ortho position, although at a reduced rate.¹²



Strauss and co-workers performed ^1H NMR experiments using 1:2 mole ratios of DNBF:aniline to show that formation of the nitrogen-bonded adduct does occur, and is kinetically favoured, but is reversible, while the carbon-bonded adduct is obtained as the thermodynamically controlled product.¹³ The same researchers also prepared the di-adduct, **2.5**, from the reaction of DNBF with the DNBF-aniline carbon-bonded adduct and two equivalents of triethylamine.¹³

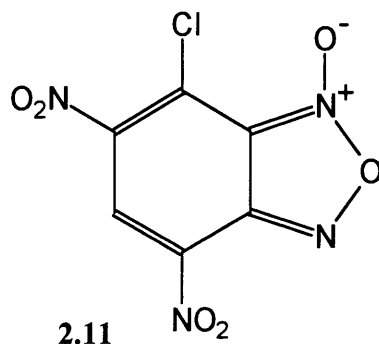


A dissociative mechanism for the conversion of **2.7** to **2.10** was proposed, Scheme 2.4, analogous with the previously studied reaction of aniline with **2.2**.^{13,15} Buncel and co-workers rationalised the scheme by showing that when one equivalent of aniline is used, the reaction to give nitrogen-bonded adducts is unfavourable, since the deprotonation of the initially formed zwitterion, **2.6**, requires a further equivalent of aniline. However, carbon-adduct formation can occur in the presence of one equivalent of aniline, as re-aromatisation of the quinoid intermediate yields the zwitterionic form of the product.¹⁶



Scheme 2.4

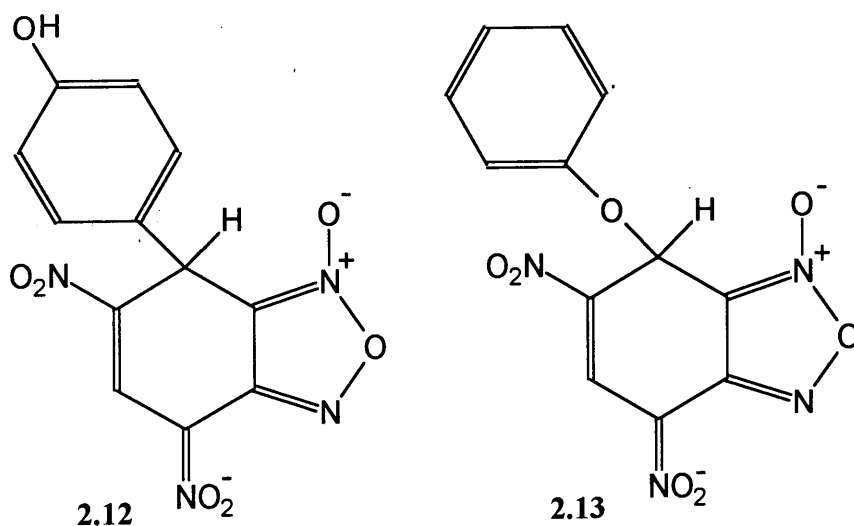
Read and Norris have also observed a nitrogen-bonded substitution product in the reaction of 7-chloro-4,6-dinitrobenzofuroxan, **2.11**, with excess aniline. N,N-dimethylaniline produced only the carbon-bonded product, due to steric hindrance of the lone pair electrons.¹⁷



DNBF is a more reactive electrophile than TNB and so will lower the energy barrier of the reaction pathway, utilising the less reactive carbon nucleophilic site in the aniline system.¹⁶ Hence DNBF can differentiate less between the two nucleophilic centres of aniline in comparison to TNB.¹⁸

2.1.3 Reaction of 4,6-Dinitrobenzofuroxan with Phenoxide

Early investigations of the reaction of DNBF with phenoxide in DMSO, led to the observation of a carbon-bonded adduct, **2.12**. No evidence was obtained for the formation of an oxygen-bonded adduct, **2.13**.^{18,16} However, Buncel and co-workers proposed that the formation of an oxygen-bonded adduct would be kinetically preferred over the carbon-bonded adduct. They believed that the absence of the oxygen-bonded adduct was due to its transient nature, and that conversion to the carbon-bonded adduct was rapid, thus rendering characterisation by ¹H NMR in DMSO at room temperature impossible. It was not until recently that Buncel succeeded in observing the transient oxygen-bonded adduct by altering the solvent from DMSO to a 1:1 acetonitrile:dimethoxyethane mixture which allowed measurements at -40°C.¹⁹ The oxygen-bonded adduct was the only spectrally observable species under these conditions. This evidence clearly established the kinetic preference of DNBF for the oxygen centre of phenoxide.



2.2 Experimental

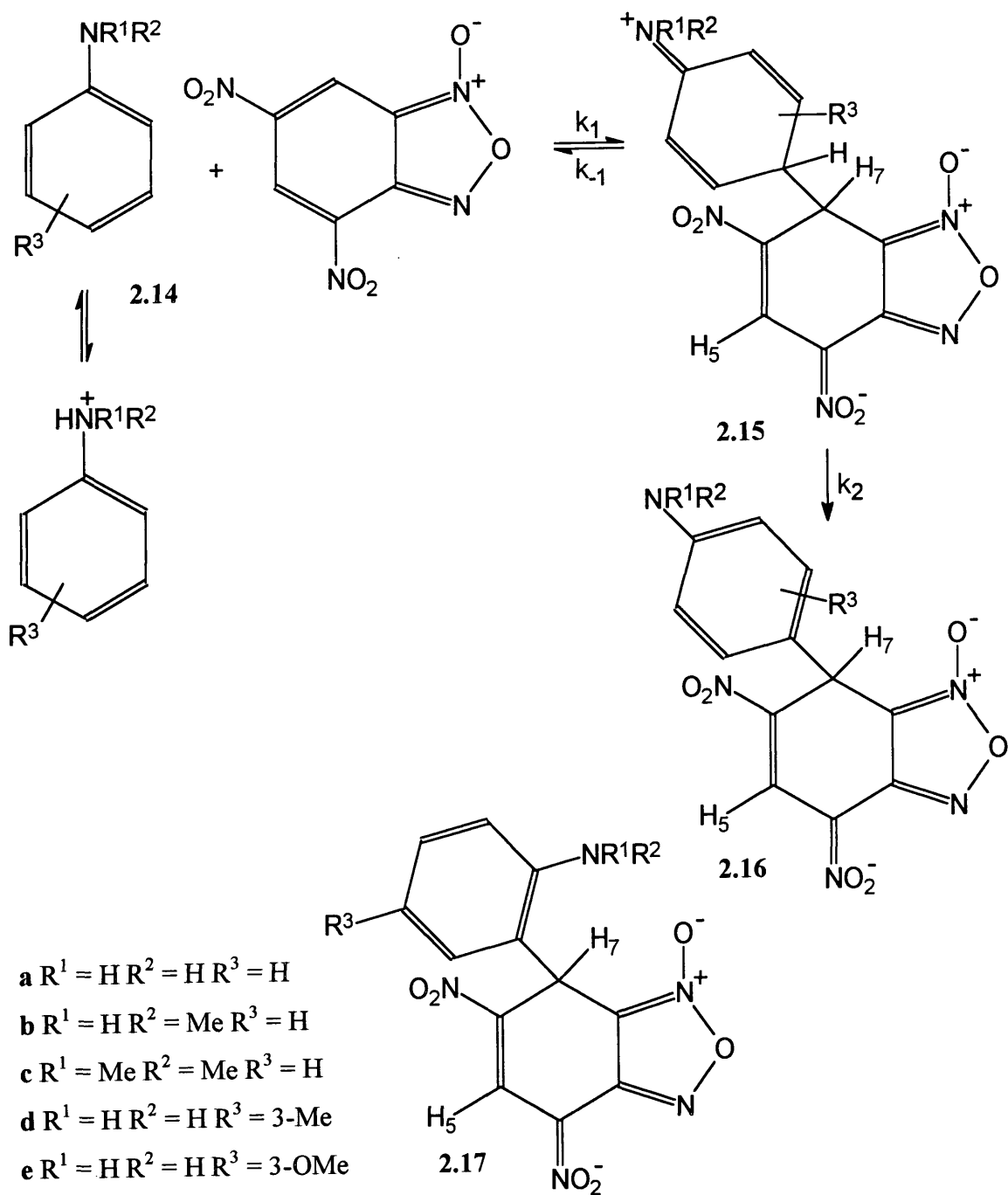
A sample of 4,6-Dinitrobenzofuroxan; mp 172 °C (lit 172-174^{20,21} °C) prepared according to the Drost method,²⁰ was available from previous work. All other reagents and solvents were the purest available commercial products.

¹H NMR spectra were recorded using a Varian Mercury 200 MHz spectrometer. UV/Visible spectra and kinetic measurements were made at 25 °C using either a Perkin Elmer Lambda 2 spectrophotometer or an Applied Photophysics SX-17 MV stopped-flow spectrophotometer. Potassium chloride solutions were used to maintain constant ionic strength ($I = (1/2)\sum c_i z_i^2$) 0.1 mol dm⁻³ in those solutions of lower ionic concentration.

2.3 Results and Discussion

2.3.1 NMR Data

In order to simplify the possible equilibria outlined in Scheme 2.4, NMR studies were performed using 1:1 mole ratio mixtures of DNBF to anilines **2.14a-g** in [²H₆]DMSO, Table 2.1. Nitrogen-bonded adduct formation is thus restricted by the absence of excess aniline necessary to deprotonate the zwitterion, **2.6**. The major reaction product is therefore the carbon-bonded adduct, **2.16** or **2.17**, according to Scheme 2.5.



- a** $\text{R}^1 = \text{H}$ $\text{R}^2 = \text{H}$ $\text{R}^3 = \text{H}$
b $\text{R}^1 = \text{H}$ $\text{R}^2 = \text{Me}$ $\text{R}^3 = \text{H}$
c $\text{R}^1 = \text{Me}$ $\text{R}^2 = \text{Me}$ $\text{R}^3 = \text{H}$
d $\text{R}^1 = \text{H}$ $\text{R}^2 = \text{H}$ $\text{R}^3 = 3\text{-Me}$
e $\text{R}^1 = \text{H}$ $\text{R}^2 = \text{H}$ $\text{R}^3 = 3\text{-OMe}$
f $\text{R}^1 = \text{H}$ $\text{R}^2 = \text{H}$ $\text{R}^3 = 4\text{-Me}$
g $\text{R}^1 = \text{H}$ $\text{R}^2 = \text{H}$ $\text{R}^3 = 4\text{-OMe}$

Scheme 2.5

Table 2.1: ^1H NMR shifts for σ -adducts, **2.16** or **2.17**, in $[\text{}^2\text{H}_6]\text{DMSO}$.

Compound	H ₇	H ₅	Aromatic	Other
DNBF	8.94	9.27		
2.16a	5.36	8.74	7.19 (d), 7.33 (d), J = 8 Hz	
2.16b	5.38	8.74	7.30 (d), 7.37 (d), J = 8.5 Hz	2.90 (NMe)
2.16c	5.39	8.74	7.40 (m)	3.12 (NMe ₂)
2.16d	5.60	8.72	7.08 (m)	2.58 (Me)
2.16e	5.56	8.66	6.89 (s), 6.87 (d), 7.34 (d), J = 7.4 Hz	3.68 (OMe)
2.17f	5.84	8.74	6.92 (s), 7.10 (d), 7.16 (d), J = 8 Hz	2.20 (Me)
2.17g	5.84	8.74	6.53 (s), 6.95 (d), 7.18 (d), J = 8.5 Hz	3.67 (OMe)

Anilines **2.14a-e** reacted with one equivalent of DNBF to give **2.16** where reaction occurred through the para-carbon. The H₅ and H₇ resonances are consistent with **2.16a-e** and typical of carbon-adduct formation.^{22, 23,24} There is a large shift to lower frequency of the H₇ resonance on adduct formation due to the change in hybridisation of C₇ from sp² to sp³.

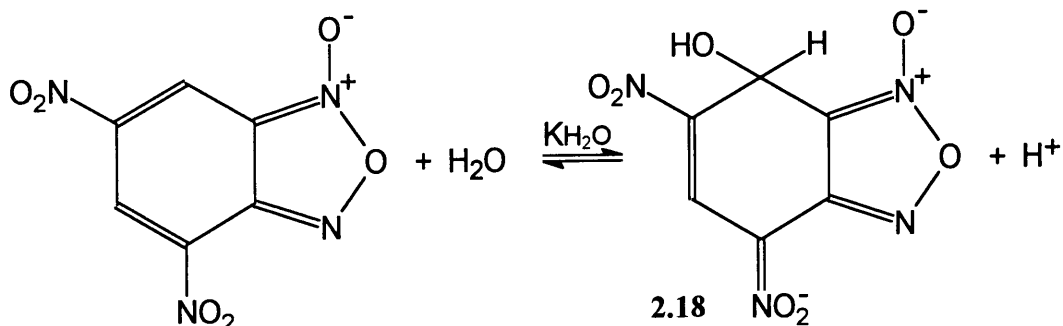
Reaction of the 4-substituted anilines with DNBF produced the ortho-carbon adducts, **2.17f** and **g**. The H₇ resonance for these adducts occurred at 5.8 ppm.

2.3.2 Kinetic Data for Reaction in HCl

Kinetic measurements were made in water-DMSO mixtures, under acidic conditions where the anilines occur largely in the protonated form. These conditions ensured that the data obtained correspond to Scheme 2.5, as there was no evidence for nucleophilic attack via the nitrogen centre of the anilines.

2.3.3 Calculation of K_{H_2O}

The acidic media used in all reactions also reduced the equilibrium concentration of the DNBF.OH⁻ adduct, **2.18**, formed even under neutral conditions²⁵ according to Scheme 2.6. It was necessary to calculate a value for K_{H_2O} in each of the solvent systems studied in order to allow for the possible formation of **2.18** in Scheme 2.5.



Scheme 2.6

The formation of **2.18** was measured spectrophotometrically using the absorbance values at 470 nm, the absorption maximum, in a variety of acid concentrations. K_{H_2O} was then calculated according to Equation 2.1.

$$\text{Equation 2.1: } K_{H_2O} = \frac{[\text{DNBF.OH}^-][\text{H}^+]}{[\text{DNBF}]} = \frac{(\text{Abs} - A_0)[\text{H}^+]}{(A_\infty - \text{Abs})}$$

The absorbance values measured at 470 nm for solvents containing 50%, 70% and 99% DMSO by volume are given in Tables 2.2, 2.3 and 2.4 respectively. The spectra gained for the 70/30 (v/v) DMSO/water solvent system are shown in Figure 2.1. A summary of the calculated K_{H_2O} values is given in Table 2.5 together with some literature values.

Table 2.2: Determination of KH_2O for the 50/50 (v/v) DMSO/water solvent system.

HCl / mol dm ⁻³	Abs at 470 nm	KH_2O^a / mol dm ⁻³
0.002	0.729	
0.010	0.310	0.00482
0.015	0.246	0.00426
0.02	0.223	0.00456
0.03	0.191	0.00460
0.04	0.158	0.00438

^a Calculated according to Equation 2.1, $A_0 = 0.108$, $A_\infty = 0.729$, $[\text{DNBF}] = 4 \times 10^{-5}$ mol dm⁻³.

Table 2.3: Determination of KH_2O for the 70/30 (v/v) DMSO/water solvent system.

HCl / mol dm ⁻³	Abs at 470 nm	KH_2O^a / mol dm ⁻³	^b
0.002	0.779		1
0.010	0.559	0.0191	2
0.015	0.493	0.0186	3
0.02	0.466	0.0208	
0.03	0.396	0.0200	
0.04	0.318	0.0193	4

^a Calculated according to Equation 2.1, $A_0 = 0.14$, $A_\infty = 0.779$, $[\text{DNBF}] = 4 \times 10^{-5}$ mol dm⁻³.

^b numbers correspond to labelled spectra in Figure 2.1.

Figure 2.1: UV/Visible spectra for the equilibrium conversion of **1.18** to DNBF in acidic solution in 70/30 (v/v) DMSO/water.

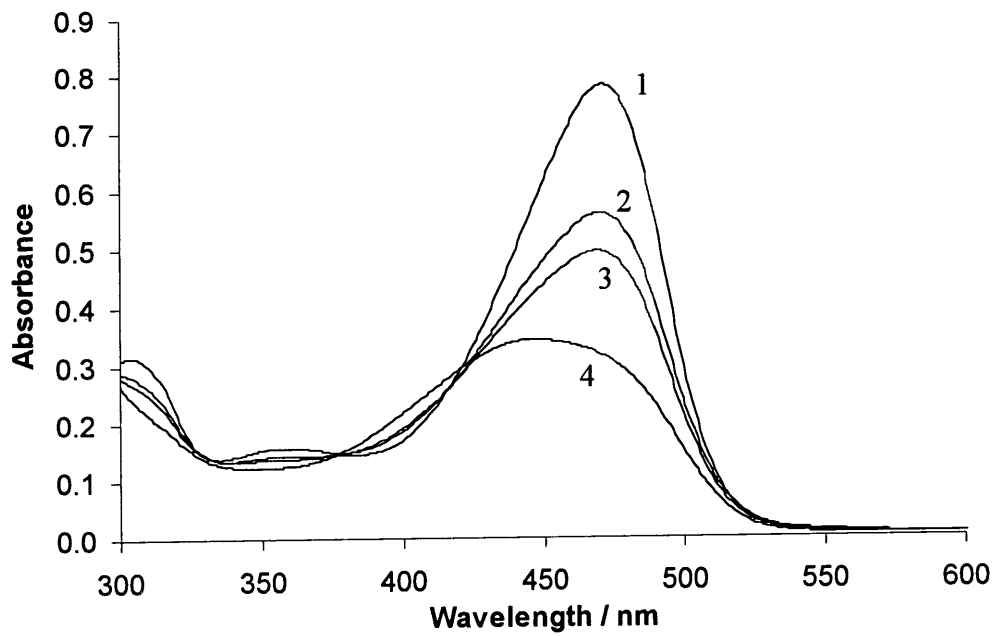


Table 2.4: Determination of KH_2O for the 99/1 (v/v) DMSO/water solvent system.

HCl / mol dm ⁻³	Abs at 470 nm	KH ₂ O ^a / mol dm ⁻³
0.002	0.318	
0.016	0.266	0.0594
0.024	0.240	0.0514
0.040	0.219	0.0413
0.10	0.073	

^a Calculated according to Equation 2.1, $A_0 = 0.073$, $A_\infty = 0.318$, $[\text{DNBF}] = 4 \times 10^{-5} \text{ mol dm}^{-3}$.

Table 2.5: The dependence of KH_2O on the DMSO content of the solvent.

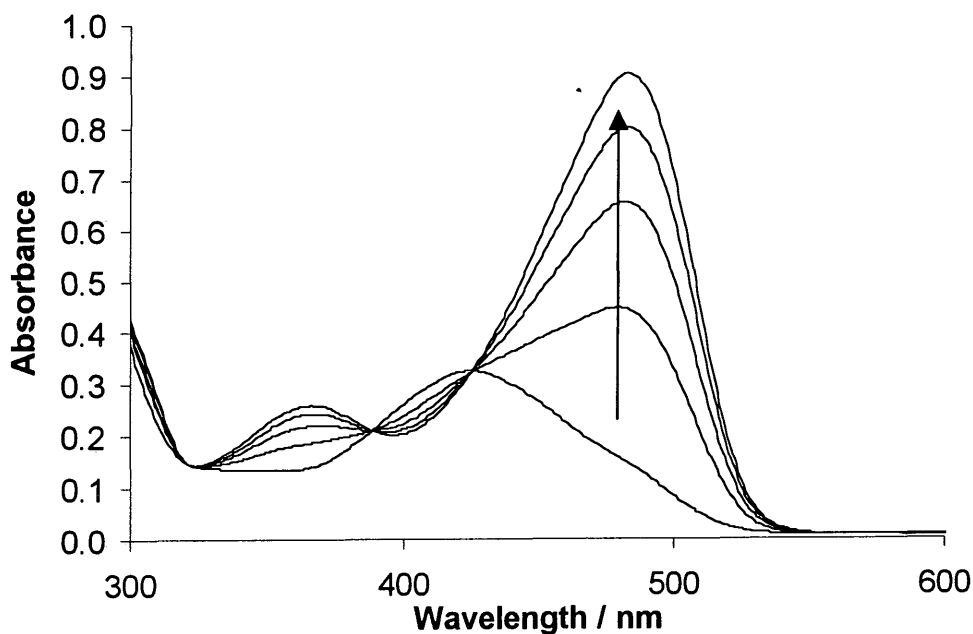
% DMSO by Volume	KH_2O / mol dm ⁻³ (this work)	KH_2O / mol dm ⁻³ (literature values) ²⁶
30		0.0008
50	0.0045 ± 0.0002	0.0041
70	0.0196 ± 0.0008	0.019
90		0.036
99	0.051 ± 0.008	

2.3.4 Reaction of DNBF and Aniline

2.3.4.1 Kinetic Data

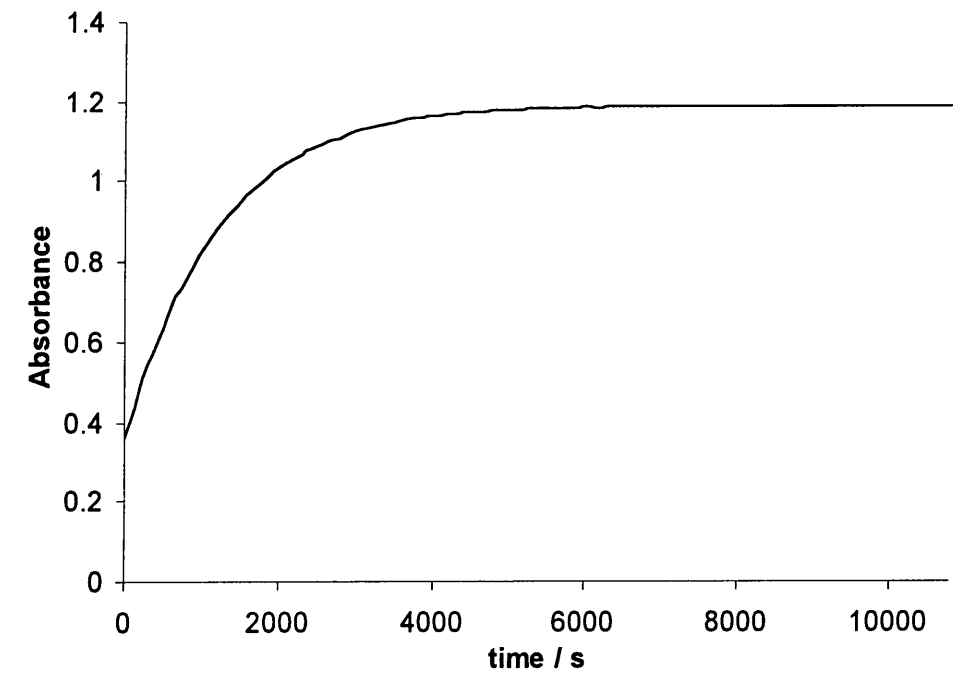
The reaction between DNBF and aniline in acidic solutions is slow, giving a UV/Visible maximum at 489 nm, Figure 2.2. This band is in the region 480-490 nm expected for formation of carbon-bonded adducts.^{22,23} The spectra obtained showed no evidence of the accumulation of **2.15**, the intermediate in the substitution pathway. There was also no evidence for the formation of a 1:2 di-adduct, **2.5**¹³ as very low concentrations of DNBF were used.

Figure 2.2: UV/Visible spectra for the reaction of DNBF, $4 \times 10^{-5} \text{ mol dm}^{-3}$ with aniline hydrochloride, 0.05 mol dm^{-3} and hydrochloric acid 0.03 mol dm^{-3} , in 70/30 (v/v) DMSO/water. Absorbance at 489 nm increases with time.



Kinetic data for the reaction in 70/30 (v/v) DMSO/water are given in Table 2.6. Aniline hydrochloride and free hydrochloric acid were in large excess over DNBF to ensure that adduct formation was a first order process. A specimen plot of the increase in absorbance with time is given in Figure 2.3. The values of the rate constant, k_{obs} , measured at 489 nm, increase linearly with aniline hydrochloride at a constant free acid concentration. However, values decrease as the acid concentration is increased. The reaction is therefore likely to involve free aniline rather than its protonated form.

Figure 2.3: Plot of absorbance versus time, illustrating the increase in absorbance at 489 nm due to carbon-bonded adduct formation between DNBF, $4 \times 10^{-5} \text{ mol dm}^{-3}$ and aniline hydrochloride, 0.05 mol dm^{-3} , in the presence of hydrochloric acid, 0.05 mol dm^{-3} , in 70/30



(v/v) DMSO/water.

Table 2.6: Kinetic data for the reaction of DNBF^a with aniline, in acidic solution in 70/30 (v/v) DMSO/water at 25 °C.

[anilineH ⁺ Cl ⁻] / mol dm ⁻³	[HCl] / mol dm ⁻³	10 ⁴ k _{obs} / s ⁻¹ ^b	k / dm ³ mol ⁻¹ s ⁻¹ ^c
0.02	0.033	4.76	3.2
0.04	0.033	9.60	3.2
0.07	0.033	15.68	3.0
0.10	0.033	23.1	3.1
0.10	0.31	5.12	4.3
0.05	0.059	8.28	3.3
0.05	0.117	5.15	3.6
0.05	0.146	4.30	3.7
0.05	0.200	3.58	4.0
0.05	0.242	3.10	4.2
0.05	0.30	2.44	4.0

^a DNBF concentraion is 4 x 10⁻⁵ mol dm⁻³.

^b measured at 489 nm.

^c calculated using Equation 2.11.

The rate equation for the reaction in Scheme 2.5 is defined by Equation 2.2. The rate constant k , Table 2.6, is related to the constants for the individual steps shown in Scheme 2.5 by Equation 2.3.

$$\text{Equation 2.2: } \frac{-d[\text{DNBF}]}{dt} = k[\text{DNBF}][\text{aniline}]$$

$$\text{Equation 2.3: } k = \frac{k_1 k_2}{k_{-1} + k_2}$$

The stoichiometric concentration of DNBF is given by Equation 2.4, which allows for the small concentration of the hydroxy-adduct, **2.18**, in equilibrium with DNBF as calculated in Section 2.3.3.

$$\text{Equation 2.4: } [\text{DNBF}]_{\text{stoich}} = [\text{DNBF}] + \frac{K_{\text{H}_2\text{O}}[\text{DNBF}]}{[\text{H}^+]}$$

Equation 2.4 can be rearranged to give Equation 2.5 and subsequently Equation 2.6.

$$\text{Equation 2.5: } [\text{DNBF}]_{\text{stoich}} = [\text{DNBF}] \left(1 + \frac{K_{\text{H}_2\text{O}}}{[\text{H}^+]} \right)$$

$$\text{Equation 2.6: } [\text{DNBF}] = [\text{DNBF}]_{\text{stoich}} \left(\frac{[\text{H}^+]}{[\text{H}^+] + K_{\text{H}_2\text{O}}} \right)$$

As the reaction is performed in excess acid, the aniline is largely protonated. Hence the free aniline concentration is given by Equation 2.7, where K_a is the acid dissociation constant of the anilinium ion.

$$\text{Equation 2.7: } [\text{aniline}] = \frac{K_a[\text{anilineH}^+]}{[\text{H}^+]}$$

Substitution of Equations 2.6 and 2.7 into Equation 2.2 gives Equation 2.8.

$$\text{Equation 2.8: } \frac{-d[\text{DNBF}]}{dt} = kK_a \frac{[\text{anilineH}^+]}{[\text{H}^+]} \frac{[\text{DNBF}]_{\text{stoich}}[\text{H}^+]}{([\text{H}^+] + K_{\text{H}_2\text{O}})}$$

Under the experimental conditions with aniline hydrochloride and acid in large excess of the stoichiometric concentration of DNBF, first order kinetics are observed, Equation 2.9.

$$\text{Equation 2.9: } \frac{-d[\text{DNBF}]}{dt} = k_{\text{obs}}[\text{DNBF}]_{\text{stoich}}$$

Comparison of Equations 2.8 and 2.9 gives Equation 2.10, which yields Equation 2.11.

$$\text{Equation 2.10: } k_{\text{obs}} = k \frac{K_a[\text{anilineH}^+]}{[\text{H}^+]} \frac{[\text{H}^+]}{([\text{H}^+] + K_{\text{H}_2\text{O}})}$$

$$\text{Equation 2.11: } k = \frac{k_{\text{obs}}(\text{KH}_2\text{O} + [\text{H}^+])}{K_a[\text{anilineH}^+]}$$

Values of k are given in Table 2.6 for the reaction in 70/30 (v/v) DMSO/water. There is no dependence of these values on the aniline hydrochloride or acid concentrations, confirming that the reaction involves free aniline rather than the anilinium ion. The calculated rate constant is therefore a function of two solvent dependent equilibrium constants, KH_2O , Table 2.5 and K_a , Table 2.7.

Table 2.7: Solvent dependence of the acid dissociation constant.

% DMSO by Volume	Acid dissociation constant (K_a) for aniline / mol dm ⁻³	Reference
70	3.89×10^{-4}	27
50	1.86×10^{-4}	21
30	8.3×10^{-5}	21

2.3.4.2 Kinetic Isotope Effect Studies

The kinetic isotope effect k_H/k_D on the substitution reaction was measured using the reaction of pentadeuterioaniline, $\text{C}_6\text{D}_5\text{NH}_2$ with DNBF for comparison with aniline. Measurements were made simultaneously on deuteriated and nondeuteriated adducts, using the multicell facility in the spectrophotometer, in solvent systems containing 30, 50 and 70% DMSO by volume, Table 2.8. These values, rather than those measured previously for k_H , were then used in the calculation of the kinetic isotope effect.

There is only a small change in the acidity of anilinium ions on ring-deuteration. Values of the $\text{p}K_a$ have been reported as 4.71 for $\text{C}_6\text{H}_5\text{NH}_3^+$ and 4.74 for $\text{C}_6\text{D}_5\text{NH}_3^+$.²⁸ It was therefore assumed that the values for K_a in the DMSO-water mixtures are unaffected by deuteration. Therefore, values of k reported in Table 2.8 were calculated using the KH_2O values in Table 2.5, and the K_a values in Table 2.7.

Table 2.8: Solvent and isotope effects on the reaction of DNBF^a with aniline.

% DMSO by volume	[C ₆ D ₅ NH ₃ ⁺ Cl ⁻] / mol dm ⁻³	[C ₆ H ₅ NH ₃ ⁺ Cl ⁻] / mol dm ⁻³	[HCl] / mol dm ⁻³	10 ⁴ k _{obs} / s ⁻¹	k / dm ³ mol ⁻¹ s ⁻¹	k _H /k _D
70	0.050		0.3	1.31	2.13	2.1 ± 0.1
	0.100		0.3	2.22	1.85	
		0.050	0.3	2.51	4.10	
		0.100	0.3	5.12	4.27	
50	0.030		0.030	1.90	1.17	2.0 ± 0.1
	0.050		0.030	3.10	1.15	
		0.030	0.030	3.87	2.39	
		0.050	0.030	5.71	2.12	
30	0.030		0.030	0.45	0.55	2.1 ± 0.1
	0.050		0.030	0.70	0.52	
		0.030	0.030	0.91	1.13	
		0.050	0.030	1.54	1.14	

^a DNBF concentration is 4 × 10⁻⁵ mol dm⁻³.

Equation 2.3 shows how the overall value of the rate constant k consists of contributions from the rate constants for the individual steps, k_1 , k_{-1} and k_2 . It is likely that k_1 and k_{-1} will show only small changes with isotopic substitution, since these involve secondary isotope effects. The rate constant for rearomatisation of the intermediate, **2.15**, involves carbon-hydrogen bond cleavage, and is likely to show a kinetic isotope effect of around 7. These assumptions, together with the observed value of $k_H/k_D = 2.1$, lead to a value of 0.2 for k_{-1}/k_2 for aniline with $k_1 = 1.2k$. The results indicate that the k_1 step is largely rate-determining as is the case with most electrophilic substitution reactions.²⁹

However, a significant kinetic isotope effect has been observed ($k_H/k_D = 3.7$ in 50/50 (v/v) DMSO/water) for the reaction of 1,3,5-trimethoxybenzene with DNBF.²⁴ Therefore, in this case, the addition of DNBF to the aromatic is not rate-determining, and formation and decomposition of the intermediate produced occurs at comparable rates.

Table 2.8 also contains information regarding the effect of the solvent composition. The kinetic isotope effect is independent of the solvent composition in the range 30-70% DMSO. The value of k increases slightly as the DMSO content of the solvent increases, and k_1 is likely to follow this pattern. DMSO will probably be more capable of solvating the charged, polarisable intermediate, **2.15**, than water. Terrier and co-workers have shown that the rate constant for attack of water on DNBF increases with increasing DMSO content of the solvent.²⁶

2.3.5 Reaction of DNBF with Substituted Anilines

The data obtained for the reaction of DNBF, $4 \times 10^{-5} \text{ mol dm}^{-3}$, with the substituted anilines **2.14b-g** are reported in Tables 2.9-2.14. The values of k were calculated from Equation 2.11 using the appropriate value of K_a .²⁷ All data pertain to a 70/30 (v/v) DMSO/water solvent system, where KH_2O has a value of $0.0196 \text{ mol dm}^{-3}$. A summary of the calculated rate constants is given in Table 2.15.

Table 2.9: Rate data for the reaction of DNBF with **2.14b**, N-methylaniline, in acidic solution at 25 °C.

$[\text{N-methylanilineH}^+\text{Cl}^-] / \text{mol dm}^{-3}$	$[\text{HCl}] / \text{mol dm}^{-3}$	$10^4 k_{\text{obs}} / \text{s}^{-1} \text{ }^a$	$k / \text{dm}^3 \text{ mol}^{-1} \text{ s}^{-1}$
0.050	0.014	136	10.6
0.050	0.025	104	10.6
0.050	0.036	85	10.8
0.050	0.102	42	11.4
0.050	0.15	26	9.9
0.050	0.20	19	9.8
0.050	0.35	12	10.1

^a measured at 494 nm.

Table 2.10: Rate data for the reaction of DNBF with **2.14c**, N,N-dimethylaniline, in acidic solution at 25 °C.

$[\text{N,N-dimethylanilineH}^+\text{Cl}^-] / \text{mol dm}^{-3}$	$[\text{HCl}] / \text{mol dm}^{-3}$	$10^4 k_{\text{obs}} / \text{s}^{-1} \text{ }^a$	$k / \text{dm}^3 \text{ mol}^{-1} \text{ s}^{-1}$
0.020	0.024	30.6	6.5
0.020	0.044	20.5	6.4
0.020	0.055	15.8	5.8
0.020	0.108	9.3	5.8
0.020	0.15	6.8	5.6
0.020	0.20	5.3	5.8
0.020	0.23	5.0	6.2
0.020	0.25	4.2	5.6
0.020	0.28	3.8	5.6

^a measured at 486 nm.

Table 2.11: Rate data for the reaction of DNBF with **2.14d**, 3-methylaniline, in acidic solution at 25 °C.

$[3\text{-methylanilineH}^+\text{Cl}^-] / \text{mol dm}^{-3}$	$[\text{HCl}] / \text{mol dm}^{-3}$	$10^4 k_{\text{obs}} / \text{s}^{-1} \text{ }^a$	$k / \text{dm}^3 \text{mol}^{-1} \text{s}^{-1}$
0.050	0.036	56	27.6
0.050	0.070	36	28.5
0.050	0.153	18.5	28.5
0.050	0.20	14.2	27.7
0.050	0.241	11.1	26.8
0.050	0.30	9.7	27.5
0.050	0.35	8.3	27.2

^a measured at 485 nm.

Table 2.12: Rate data for the reaction of DNBF with **2.14e**, 3-methoxyaniline, in acidic solution at 25 °C.

$[3\text{-methoxyanilineH}^+\text{Cl}^-] / \text{mol dm}^{-3}$	$[\text{HCl}] / \text{mol dm}^{-3}$	$10^4 k_{\text{obs}} / \text{s}^{-1} \text{ }^a$	$k / \text{dm}^3 \text{mol}^{-1} \text{s}^{-1}$
0.010	0.090	1100	1470
0.030	0.070	3700	1350
0.050	0.050	7170	1220
0.030	0.170	1660	1280

^a measured at 487 nm using stopped-flow spectrophotometry.

Table 2.13: Rate data for the reaction of DNBF with **2.14f**, 4-methylaniline, in acidic solution at 25 °C.

$[4\text{-methylanilineH}^+\text{Cl}^-] / \text{mol dm}^{-3}$	$[\text{HCl}] / \text{mol dm}^{-3}$	$10^4 k_{\text{obs}} / \text{s}^{-1} \text{ }^a$	$k / \text{dm}^3 \text{mol}^{-1} \text{s}^{-1}$
0.050	0.0142	1.63	1.10
0.050	0.0249	1.28	1.14
0.050	0.0356	1.06	1.17
0.050	0.0570	0.75	1.15

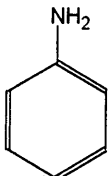
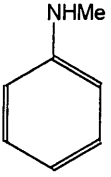
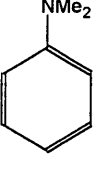
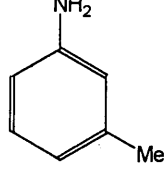
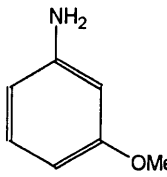
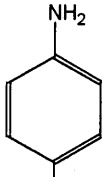
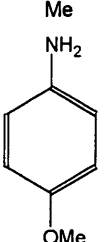
^a measured at 485 nm.

Table 2.14: Rate data for the reaction of DNBF with **2.14g**, 4-methoxyaniline, in acidic solution at 25 °C.

[4-methoxyanilineH ⁺ Cl ⁻] / mol dm ⁻³	[HCl] / mol dm ⁻³	10 ⁴ k _{obs} / s ⁻¹ ^a	k / dm ³ mol ⁻¹ s ⁻¹
0.050	0.0142	0.62	1.24
0.050	0.0356	0.47	1.54
0.050	0.0570	0.38	1.72

^a measured at 490 nm.

Table 2.15: Summary of kinetic data for the reaction of DNBF with substituted anilines in 70/30 (v/v) DMSO/water at 25 °C.

Aniline	pK_a^{27}	λ_{max} / nm^a	$k / dm^3 mol^{-1} s^{-1}$
2.14a 	3.41	489	4.0 ± 0.7
2.14b 	3.06	494	10.3 ± 0.6
2.14c 	2.99	486	6.0 ± 0.8
2.14d 	3.65	485	27 ± 1
2.14e 	3.09	487	1300 ± 100
2.14f 	4.00	485	1.14 ± 0.03
2.14g 	4.47	490	1.5 ± 0.2

^a Absorption maximum of adducts.

The results in Table 2.15 show that the value of k , the rate constant for carbon-adduct formation, increases on N-methylation. However, a second methylation to give **2.14c**, N,N-dimethylaniline results in a reduction in the measured rate constant. Increased N-methylation would be expected to increase the nucleophilicity of the derivative, as methyl groups are inductively electron donating. The expected reactivity is mirrored by the σ^+ -values,^{30,31} which are -1.30 for para-NH₂ and -1.70 for para-NMe₂, with the NHMe group showing intermediate behaviour.³² However these values relate to aqueous solutions whereas the rate constants reported here were measured in media rich in DMSO.

The DMSO-water solvent system is able to delocalise the positive charge on the intermediate **2.15**, via hydrogen bonding with the N-H hydrogen atoms. Therefore, the greater the number of N-H hydrogens, the greater the extent of delocalisation of the positive charge, and hence, stabilisation of the intermediate **2.15**. The isotope effect indicates that nucleophilic attack will be largely rate-limiting in the substitution process. In the transition state leading to **2.15** there will be partial charge development on the side chain nitrogen. Hence the stabilisation of the transition state by DMSO will increase with the number of NH⁺ hydrogens present.

These two opposing effects will contribute to the trend in the measured values of k for the reaction of DNBF with **2.14a-c**.

The reactions of **2.14d** and **2.14e** with DNBF result in carbon-adduct formation at the 4-position. The electron-releasing 3-substituents will activate the derivative to electrophilic attack resulting in considerably larger values of k than for aniline. The methyl and methoxy groups will inductively donate electrons to the 2- and 4-positions, whilst the amino group will activate the 2- and 4-positions through resonance donation of π -electrons. The 4-position will be most reactive as there is less steric hindrance at this site, although the 3-substituents are ortho to the reaction centre, which may cause some retardation of the reaction rate.

When the 4-position is blocked by a substituent, as is the case for **2.14f** and **2.14g**, carbon-adduct formation occurs at the 2-position, ortho to the amino function. The values of k are

then reduced relative to aniline. This reduction is probably due to steric hindrance to electrophilic attack of DNBF, although there may also be some steric inhibition to solvation of the intermediate, **2.15**, leading to a reduction of k .

2.4 Comparison with other π -Excessive Aromatics

The relative nucleophilicity of the aniline derivatives towards DNBF can be compared with other nucleophiles. It has been shown previously that there is an approximately linear relationship between the rate constant for carbon-adduct formation and the pK_a values measured for carbon protonation in aqueous solution.³³ However, most of the literature data refer to a 50/50 (v/v) DMSO/water solvent system, while the data measured here for the aniline derivatives pertain to a 70/30 (v/v) DMSO/water system. The rate constant for the reaction of aniline with DNBF was measured in both of these media, and the assumption that solvent effects will be similar for the substituted derivatives allows a direct comparison with the literature. By multiplying the k values measured in 70/30 (v/v) DMSO/water by 2.3/4.0 (Table 2.8), new values were obtained which are comparable with the literature values for a selection of arenes measured in 50/50 (v/v) DMSO/water, Table 2.16.

Figure 2.4 illustrates the linear Brønsted-type relationship between the carbon nucleophilicities towards DNBF, and the pK_a values in water for carbon protonation, and shows how the pK_a values for the aniline derivatives were estimated.

Table 2.16: Carbon nucleophilicity of aniline derivatives and a selection of π -excessive aromatics towards DNBF in 50/50 (v/v) DMSO/water.

Arene ^a	$k / \text{dm}^3 \text{mol}^{-1} \text{s}^{-1}$	$\log_{10}k$	$\text{pK}_a^{\text{a, b}}$
3-Methoxythiophene	0.5	-0.30	-6.5
5-Cyanoindole	1.1	0.04	-6.0
Aniline	2.3	0.36	(-5.8) ^d
N,N-Dimethylaniline ^c	3.5	0.54	(-5.6) ^d
N-Methylaniline ^c	6.0	0.78	(-5.4) ^d
3-Methylaniline ^c	16	1.20	(-5.0) ^d
5-Bromoindole	46	1.66	-4.4
5-Chloroindole	52	1.72	-4.5
Pyrrole	520	2.72	-3.8
Indole	560	2.74	-3.5
3-Methoxyaniline ^c	750	2.88	(-3.4) ^d
5-Methylindole	2100	3.32	-3.3
5-Methoxyindole	2600	3.42	-2.9

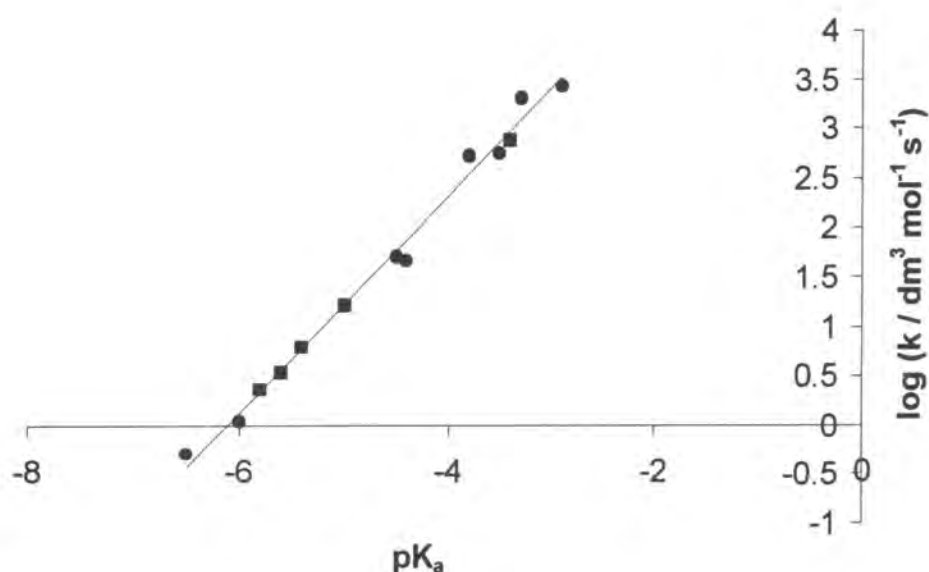
^a Literature data.³³

^b pK_a values in water for protonation on carbon.

^c Values of k in 70/30 (v/v) DMSO/water were multiplied by 2.3/4.0.

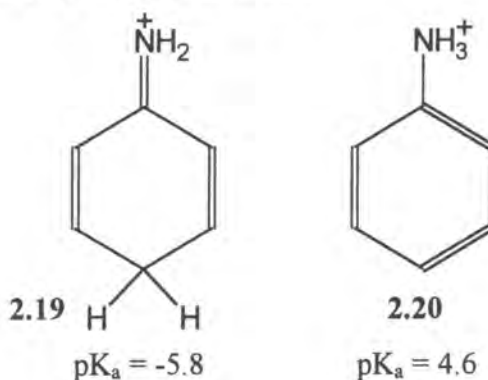
^d Estimated pK_a values for carbon protonation from Figure 2.4.

Figure 2.4: Carbon nucleophilicity of aniline derivatives (■) and a selection of π -excessive aromatics (●) towards DNBF in 50/50 (v/v) DMSO/water.



2.5 Conclusion

These results indicate the possibility of ambident reactivity at the nitrogen and carbon centres of aniline. Hence in the reaction with DNBF adducts **2.7** and **2.10** may be formed. This chapter has largely been concerned with the kinetics of the carbon-carbon bond forming process. However, the results do lead to an estimate for the pK_a for ring protonation of aniline. The value of -5.8 for **2.19**, obtained from Figure 2.4, differs by approximately 11 pK_a units from the value for nitrogen protonation, **2.20**, and shows that nitrogen protonation is very strongly favoured.



2.6 References

- ¹ M. R. Crampton and V. Gold., *J. Chem. Soc. B.*, 1967, 23.
- ² E. Buncel, J. G. K. Webb and J. F. Wiltshire., *J. Am. Chem. Soc.*, 1977, **99**, 4429.
- ³ E. Buncel and J. G. K. Webb., *Tetrahedron Lett.*, 1976, 4417.
- ⁴ E. Buncel and J. G. K. Webb., *Can. J. Chem.*, 1972, **50**, 129.
- ⁵ E. Buncel and J. G. K. Webb., *Can. J. Chem.*, 1974, **52**, 630.
- ⁶ E. Buncel and W. Eggimann., *J. Am. Chem. Soc.*, 1977, **99**, 5958.
- ⁷ E. Buncel, W. Eggimann and H. W. Leung., *J. Chem. Soc., Chem. Commun.*, 1977, 55.
- ⁸ E. Buncel and W. Eggimann., *J. Chem. Soc., Perkin Trans. 2.*, 1978, 673.
- ⁹ A. R. Butler., *Annu. Rep. Chem Soc. B.*, 1972, **69**, 114.
- ¹⁰ E. Buncel and H. W. Leung., *J. Chem. Soc., Chem. Commun.*, 1975, 19.
- ¹¹ M. R. Crampton and I. A. Robotham., *Can. J. Chem.*, 1998, **76**, 627.
- ¹² R. J. Spear, W. P. Norris and R. W. Read., *Tetrahedron Lett.*, 1983, **24**, 1555.
- ¹³ M. J. Strauss, R. A. Renfrow and E. Buncel., *J. Am. Chem. Soc.*, 1983, **105**, 2473.
- ¹⁴ F. Terrier., *Spec. Pub. Chem. Soc.*, 1995, 399.
- ¹⁵ R. W. Read, R. J. Spear and W. P. Norris., *Aust. J. Chem.*, 1984, **37**, 985.
- ¹⁶ E. Buncel, R. A. Renfrow and M. J. Strauss., *J. Org. Chem.*, 1987, **52**, 488.
- ¹⁷ R. W. Read and W. P. Norris., *Aust. J. Chem.*, 1985, **38**, 435.
- ¹⁸ E. Buncel and K-T. Park., *Phys. Org. Chem.*, 1986, 247.
- ¹⁹ E. Buncel, R. A. Manderville and J. M. Dust., *J. Chem. Soc., Perkin Trans. 2.*, 1997, 1019.
- ²⁰ P. Drost., *Justus Liebigs Ann. Che.*, 1899, **307**, 49.
- ²¹ F. Terrier, M-J. Pouet, E. Kizilian, J-C. Halle, F. Outurquin and C. Paulmier., *J. Org. Chem.*, 1993, **58**, 4696.
- ²² F. Terrier, E. Kizilian, J-C. Halle and E. Buncel., *J. Am. Chem. Soc.*, 1992, **114**, 1740.
- ²³ F. Terrier, M-J. Pouet, J-C. Halle, S. Hunt, J. R. Jones and E. Buncel., *J. Chem. Soc., Perkin Trans. 2.*, 1993, 1665.
- ²⁴ F. Terrier, M-J. Pouet, J-C. Halle, E. Kizilian and E. Buncel., *J. Phys. Org. Chem.*, 1998, **11**, 707.
- ²⁵ F. Terrier, F. Millot and W. P. Norris., *J. Am. Chem. Soc.*, 1976, **98**, 5883.
- ²⁶ F. Terrier, H. A. Sorkhabi, F. Millot, J-C. Halle and R. Schaal., *Can. J. Chem.*, 1980, **58**, 1155.
- ²⁷ K. Yates and G. Welch., *Can. J. Chem.*, 1972, **50**, 474.
- ²⁸ C. F. Bernasconi, W. Koch and H. Zollinger., *Helv. Chim. Acta.*, 1963, **46**, 1184.
- ²⁹ R. Taylor. *Electrophilic Aromatic Substitution*. Wiley, New York. 1990.
- ³⁰ H. C. Brown and Y. Okamoto., *J. Am. Chem. Soc.*, 1958, **80**, 4979.
- ³¹ S. Clementi and A. R. Katritzky., *J. Chem. Soc., Perkin Trans. 2.*, 1973, 1077.
- ³² M. Charton., *Prog. Phys. Org. Chem.*, 1981, **13**, 211.
- ³³ E. Kizilian, F. Terrier, A-P. Chatrousse, K. Gzouli and J-C. Halle., *J. Chem. Soc., Perkin Trans. 2.*, 1997, 2667.

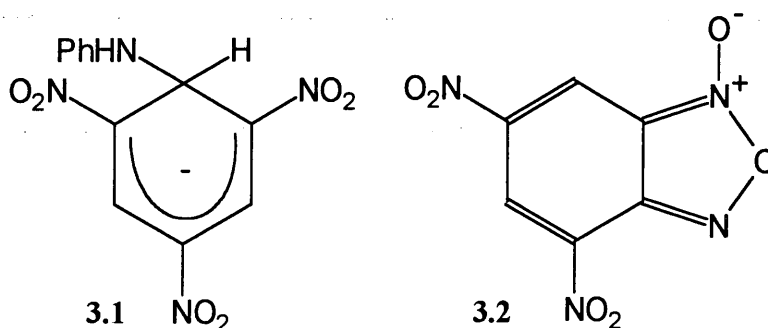
Chapter 3

The Ambident Reactivity of Aniline Derivatives Towards DNBF

3 The Ambident Reactivity of Aniline Derivatives Towards DNBF

3.1 Introduction

Aniline normally reacts as a nitrogen nucleophile and may form σ -adducts, such as **3.1**, with 1,3,5-trinitrobenzene and other ring-activated aromatic compounds. Nevertheless, aniline is a soft base, holding its valence electrons loosely, and has the ability to show ambident reactivity using either the nitrogen or ring-carbon centres. DNBF, **3.2**, may be considered as a soft acid, being highly polarisable and having low electronegativity. It is known that aniline and **3.2** will react together in the absence of base, to give a carbon-bonded σ -adduct resulting from attack at the 4-position of aniline.^{1,2} This adduct may be considered as the product of electrophilic substitution on the aniline ring.³ Nitrogen-bonded adducts have also been observed in the presence of excess aniline from the reaction of DNBF and aniline.²



This chapter investigates the reaction of DNBF, **3.2**, with excess aniline to form nitrogen-bonded σ -adducts which are kinetically preferred. The carbon-bonded adduct is thermodynamically more stable, and its formation is observed over time.

Particular aims were; (i) to determine values of equilibrium constants for the formation of nitrogen-bonded adducts, and to compare these with pK_a values for the protonated forms of the parent amines, (ii) to determine values of the equilibrium constants for proton transfer involving the zwitterionic and anionic forms of the carbon-bonded adducts. These values are expected to measure the electronic effect of the negatively charged DNBF moiety.

3.2 Experimental

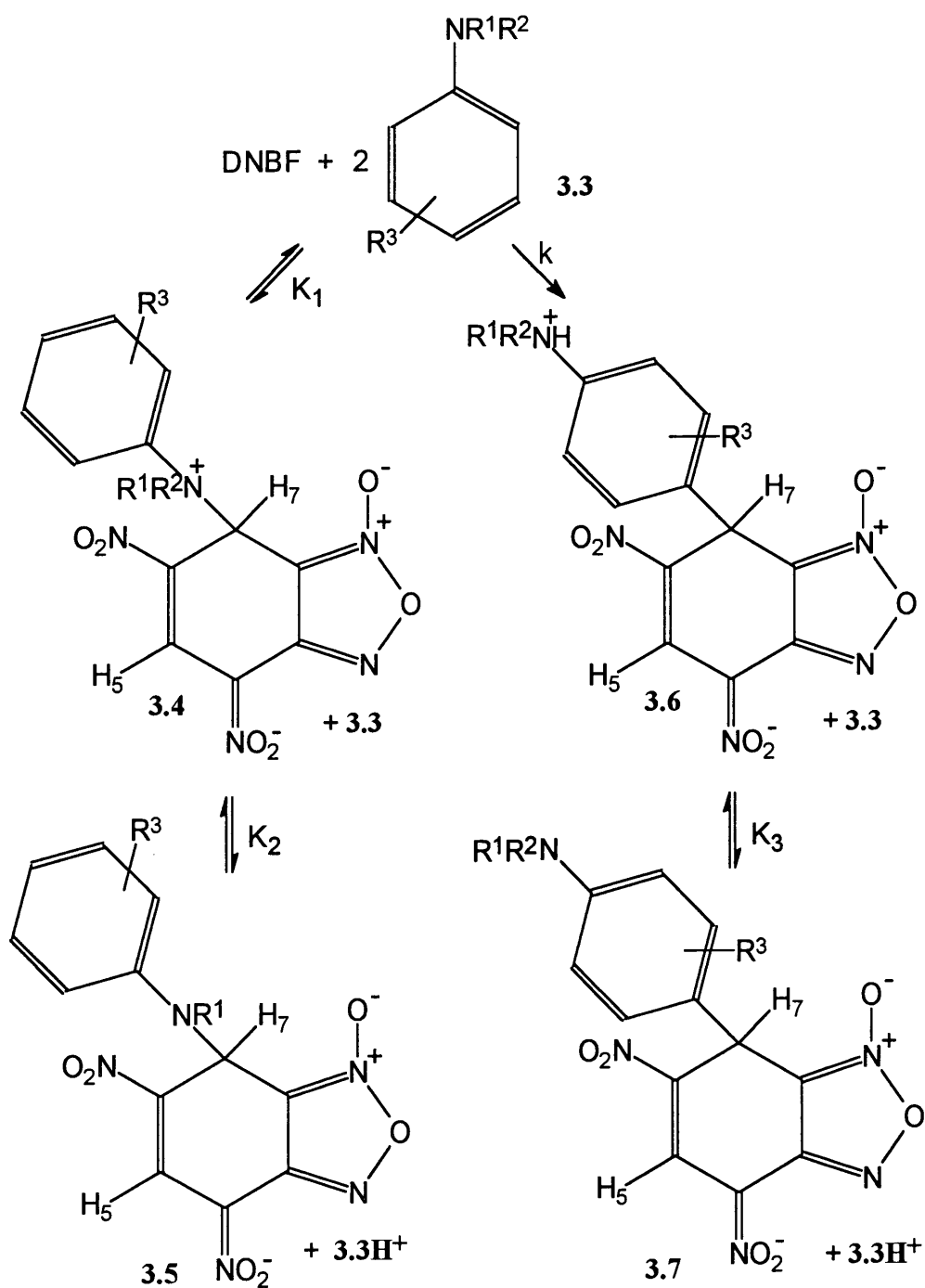
A sample of 4,6-Dinitrobenzofuroxan, **3.2**, prepared by Drost's method⁴ was available from previous work. All other reagents and solvents were the purest available commercial products.

¹H NMR spectra were recorded on a Varian Mercury 200 MHz spectrometer. UV/Visible spectra and kinetic measurements were made at 25 °C using a Perkin Elmer Lambda 2 spectrophotometer or an Applied Photophysics SX-17 MV stopped-flow spectrophotometer.

3.3 Results and Discussion

Measurements were made with aniline, **3.3a**, and the six substituted anilines, **3.3b-g**, studied in Chapter 2. The data obtained are in agreement with Scheme 3.1, where rapid formation of the nitrogen-bonded adduct, **3.5**, is followed by the slower conversion to the carbon-bonded adduct, **3.6**, which is thermodynamically more stable. In order to compare equilibrium constants calculated from NMR chemical shifts, with rate and equilibrium constants calculated from UV/Visible measurements, it was necessary to work in DMSO solution throughout.

The formation of **3.5**, the nitrogen-bonded adduct, requires a proton transfer in the second step of the reaction. Hence an adduct, **3.5** was not observed from N,N-dimethylaniline, **3.3c**. Interestingly, a nitrogen-bonded adduct was not detected from N-methylaniline, **3.3b**. This may indicate steric hindrance in the possible adduct **3.5b**.



3.3a $\text{R}^1 = \text{H}, \text{R}^2 = \text{H}, \text{R}^3 = \text{H}$

3.3b $\text{R}^1 = \text{H}, \text{R}^2 = \text{Me}, \text{R}^3 = \text{H}$

3.3c $\text{R}^1 = \text{Me}, \text{R}^2 = \text{Me}, \text{R}^3 = \text{H}$

3.3d $\text{R}^1 = \text{H}, \text{R}^2 = \text{H}, \text{R}^3 = 3\text{-Me}$

3.3e $\text{R}^1 = \text{H}, \text{R}^2 = \text{H}, \text{R}^3 = 3\text{-OMe}$

3.3f $\text{R}^1 = \text{H}, \text{R}^2 = \text{H}, \text{R}^3 = 4\text{-Me}$

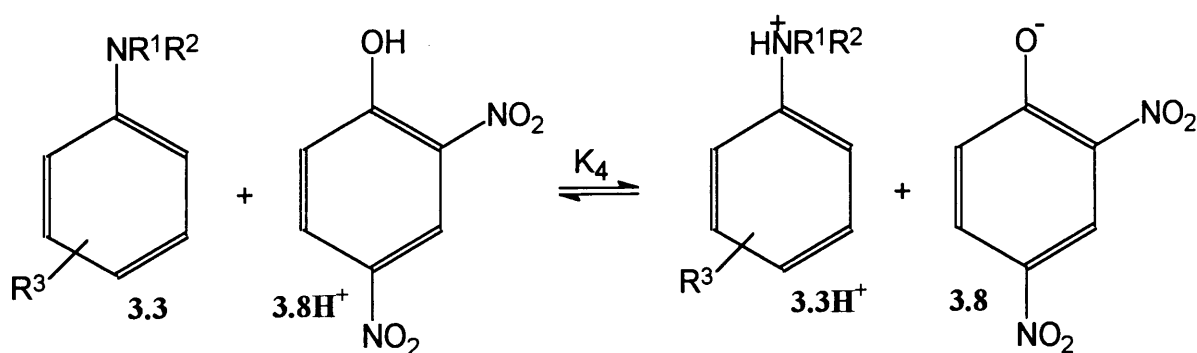
3.3g $\text{R}^1 = \text{H}, \text{R}^2 = \text{H}, \text{R}^3 = 4\text{-Cl}$

Scheme 3.1

3.3.1 Calculation of pK_a Values of Aniline Derivatives in DMSO

In order to compare the relative reactivities of the aniline derivatives in DMSO it was necessary to calculate pK_a values of the protonated forms. The value for aniline in DMSO has been measured previously, pK_a = 3.82.⁵

Aniline derivatives react with 2,4-dinitrophenol, **3.8H**⁺, according to Scheme 3.2. There is a pronounced increase in the UV/Visible absorbance measured at 430 nm on deprotonation to **3.8**, Figure 3.1. Therefore, **3.8H**⁺ can be used as an indicator for proton transfer equilibria.



Scheme 3.2

Values of the equilibrium constant, K₄, were calculated from absorbance measurements at 430 nm, according to Equation 3.1, where A₀ is the absorbance due to **3.8H**⁺, and A_∞ is the absorbance due to **3.8**. The pK_a value of the aniline, (**3.3H**⁺), was then determined from Equation 3.2, using a value of 5.12⁶ for the pK_a of **3.8H**⁺.

$$\text{Equation 3.1: } K_4 = \frac{[\mathbf{3.8}][\text{anilineH}^+]}{[\mathbf{3.8H}^+][\text{aniline}]} = \frac{(\text{Abs} - A_0)[\text{anilineH}^+]}{(A_\infty - \text{Abs})[\text{aniline}]}$$

$$\text{Equation 3.2: } \log_{10}K_4 = \text{pK}_a(\mathbf{3.3H}^+) - \text{pK}_a(\mathbf{3.8H}^+)$$

In a typical experiment, spectra were recorded using a constant concentration of **3.8H**⁺, 4 x 10⁻⁵ mol dm⁻³, in solutions buffered with the aniline derivative and its hydrochloride salt.

Generally, the salt concentration was 0.01 mol dm^{-3} , or the ionic strength maintained at 0.01 mol dm^{-3} with tetrabutylammonium chloride.

Typical spectra obtained are shown in Figure 3.1, with the absorbance due to **3.8** increasing on addition of N-methylaniline. Absorbance data is given in Tables 3.1 to 3.6.

Table 3.1: Absorbance data for 2,4-dinitrophenol ($4 \times 10^{-5} \text{ mol dm}^{-3}$) in DMSO containing **3.3b**, N-methylaniline and its hydrochloride salt at 25°C .

^a	[N-Methylaniline] / mol dm^{-3}	[N-MethylanilineH ⁺ Cl ⁻] / mol dm^{-3}	Abs (430 nm)	K_4^c
1	0.00	0.008	0.008	
2	0.10	0.008	0.068	0.0064
3	0.20	0.008	0.117	0.0062
4	0.30	0.008	0.160	0.0061
5	0.40	0.008	0.203	0.0063
6	0.50	0.008	0.248	0.0067
7	0.60	0.008	0.282	0.0068
8	0.70	0.008	0.318	0.0071
9	0.80	0.008	0.349	0.0072
	0.00 ^b	0.00	0.82	

^a Labelled spectra in Figure 3.1.

^b Made alkaline with sodium hydroxide.

^c Calculated according to Equation 3.1, $A_0 = 0.008$, $A_\infty = 0.82$.

Figure 3.1: UV/Visible spectra for the reaction of 2,4-dinitrophenol, **3.8H⁺**, (4×10^{-5} mol dm⁻³) with N-methylaniline, **3.3b**, at 25 °C.

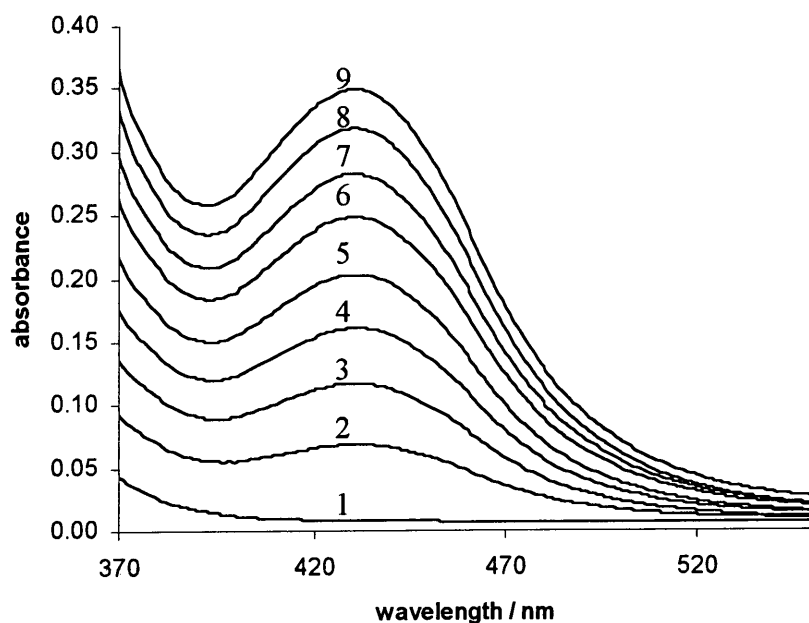


Table 3.2: Absorbance data for 2,4-dinitrophenol (4×10^{-5} mol dm⁻³) in DMSO containing **3.3c**, N,N-dimethylaniline and its hydrochloride salt at 25 °C.

[N,N-Dimethylaniline] / mol dm ⁻³	[N,N-DimethylanilineH ⁺ Cl ⁻] / mol dm ⁻³	Abs (430 nm)	K ₄ ^b
0.00	0.001	0.006	
0.10	0.001	0.230	0.0038
0.20	0.001	0.333	0.0034
0.30	0.001	0.423	0.0035
0.40	0.001	0.510	0.0041
0.50	0.001	0.545	0.0039
0.60	0.001	0.590	0.0042
0.70	0.001	0.600	0.0039
0.00 ^a	0.00	0.82	

^a Made alkaline with sodium hydroxide.

^b Calculated according to Equation 3.1, $A_0 = 0.006$, $A_\infty = 0.82$.

Table 3.3: Absorbance data for 2,4-dinitrophenol ($4 \times 10^{-5} \text{ mol dm}^{-3}$) in DMSO containing **3.3d**, 3-methylaniline and its hydrochloride salt at 25 °C.

[3-methylaniline] / mol dm^{-3}	[3-methylanilineH ⁺ Cl ⁻] / mol dm^{-3}	Abs (430 nm)	K ₄ ^b
0.00	0.01	0.014	
0.02	0.01	0.097	0.057
0.04	0.01	0.197	0.072
0.06	0.01	0.200	0.049
0.08	0.01	0.219	0.042
0.10	0.01	0.297	0.053
0.20	0.01	0.456	0.059
0.00 ^a	0.00	0.831	

^a Made alkaline with sodium hydroxide.

^b Calculated according to Equation 3.1, $A_0 = 0.014$, $A_\infty = 0.831$.

Table 3.4: Absorbance data for 2,4-dinitrophenol ($4 \times 10^{-5} \text{ mol dm}^{-3}$) in DMSO containing **3.3e**, 3-methoxyaniline and its hydrochloride salt at 25 °C.

[3-methoxyaniline] / mol dm^{-3}	[3-methoxyanilineH ⁺ Cl ⁻] / mol dm^{-3}	Abs (430 nm)	K ₄ ^b
0.00	0.01	0.016	
0.10	0.01	0.135	0.017
0.20	0.01	0.210	0.016
0.30	0.01	0.270	0.015
0.40	0.01	0.307	0.014
0.50	0.01	0.356	0.014
0.70	0.01	0.407	0.013
0.00 ^a	0.00	0.831	

^a Made alkaline with sodium hydroxide.

^b Calculated according to Equation 3.1, $A_0 = 0.016$, $A_\infty = 0.831$.

Table 3.5: Absorbance data for 2,4-dinitrophenol ($4 \times 10^{-5} \text{ mol dm}^{-3}$) in DMSO containing **3.3f**, 4-methylaniline and its hydrochloride salt at 25 °C.

[4-methylaniline] / mol dm ⁻³	[4-methylanilineH ⁺ Cl ⁻] / mol dm ⁻³	Abs (430 nm)	K ₄ ^b
0.00	0.01	0.005	
0.05	0.01	0.377	0.19
0.08	0.01	0.451	0.18
0.10	0.01	0.492	0.18
0.20	0.01	0.581	0.16
0.40	0.01	0.649	0.15
0.60	0.01	0.676	0.14
0.80	0.00	0.76	

^a Calculated according to Equation 3.1, $A_0 = 0.005$, $A_\infty = 0.76$.

Table 3.6: Absorbance data for 2,4-dinitrophenol ($4 \times 10^{-5} \text{ mol dm}^{-3}$) in DMSO containing **3.3g**, 4-chloroaniline and its hydrochloride salt at 25 °C.

[4-Chloroaniline] / mol dm ⁻³	[4-ChloroanilineH ⁺ Cl ⁻] / mol dm ⁻³	Abs (430 nm)	K ₄ ^b
0.00	0.001	0.008	
0.03	0.001	0.127	0.0056
0.05	0.001	0.182	0.0054
0.06	0.001	0.205	0.0052
0.08	0.001	0.243	0.0050
0.10	0.001	0.275	0.0048
0.20	0.001	0.340	0.0034
0.40	0.001	0.473	0.0033
0.00 ^a	0.00	0.831	

^a Made alkaline with sodium hydroxide.

^b Calculated according to Equation 3.1, $A_0 = 0.008$, $A_\infty = 0.831$.

A summary of the calculated pK_a values is given in Table 3.7. The values are absolute, in the sense that they are based on DMSO as the standard state, allowing a direct comparison with pK_a values measured in water.⁷

Table 3.7: Summary of pK_a data for anilinium ions.

Aniline	pK_a (DMSO)	pK_a (water) ^b	ΔpK_a ^c
3.3a , Aniline	3.82 ^a	4.58	0.76
3.3b , N-Methylaniline	2.94	4.85	1.91
3.3c , N,N-Dimethylaniline	2.70	5.06	2.36
3.3d , 3-Methylaniline	3.86	4.69	0.83
3.3e , 3-Methoxyaniline	3.29	4.20	0.91
3.3f , 4-Methylaniline	4.34	5.12	0.78
3.3g , 4-Chloroaniline	2.79	3.98	1.19

^a Literature value.⁵

^b Literature values.⁸

^c $\Delta pK_a = pK_a$ (water) - pK_a (DMSO)

For aniline, **3.3a**, and ring substituted anilines, **3.3d-g**, ΔpK_a is approximately 0.8, and the amines are slightly more acidic in DMSO than in water. N-methylaniline, **3.3b**, and N,N-dimethylaniline, **3.3c**, are much more acidic in DMSO than in water, with ΔpK_a 1.91 and 2.36 units respectively.

A number of factors will be involved in determining the solvent dependence of the acidities. However, DMSO is known to be an extremely good hydrogen-bond acceptor,⁹ so that solvation involving hydrogen-bonding of the NH^+ protons will be important in stabilising the acidic cation, **3.3H**⁺.^{8,5} On going from aniline, **3.3a**, to N,N-dimethylaniline, **3.3c**, the number of NH^+ protons available for hydrogen-bonding decreases, and hence the stability of the cation will also decrease. This explains the greater change in pK_a on going from water to DMSO for N,N-dimethylanilineH⁺ which has only one NH^+ proton.

3.3.2 NMR Data

^1H NMR spectra were taken of DNBF in $[\text{}^2\text{H}_6]\text{DMSO}$ solutions containing the aniline derivatives **3.3a-f**. Data are collected in Table 3.8.

Table 3.8: ^1H NMR data for adducts formed from DNBF in $[\text{}^2\text{H}_6]\text{DMSO}$.

Parent Aniline	¹ H NMR Chemical Shifts			
	Carbon-bonded adducts, 3.6			
	H ₇	H ₅	Aromatic	Other
3.3a	5.36	8.73	7.19 (d), 7.33 (d), J = 8 Hz	
3.3b	5.37	8.72	7.30 (d), 7.37 (d), J = 8.5 Hz	2.90 (NMe)
3.3c	5.39	8.74	7.40 (m)	3.12 (NMe ₂)
3.3d	5.60	8.72	7.08 (m)	2.58 (Me)
3.3e	5.56	8.66	6.89 (s), 6.87 (d), 7.34 (d), J = 7.4 Hz	3.68 (OMe)
3.3f	5.83	8.73	6.92 (s), 7.10 (d), 7.16 (d), J = 8 Hz	2.20 (Me)
	Deprotonated adducts, 3.7			
	H ₇	H ₅	Aromatic	Other
3.3a	5.14	8.70	6.53 (d), 6.90 (d)	
3.3b	5.15	8.71	6.52 (d), 6.97 (d)	2.63 (NMe)
3.3c	5.16	8.70	6.60 (d), 7.0 (d), J = 8 Hz	2.86 (NMe ₂)
3.3d	5.40	8.68	6.64 (d), 6.50 (d), J = 8 Hz	2.42 (Me)
3.3e	5.33	8.63	6.2 (m), 6.87 (d), J = 8 Hz	3.54 (OMe)
3.3f	5.56	8.71	6.54 (s), 6.60 (d), 6.76 (d)	2.04 (Me)
	Nitrogen-bonded adducts, 3.5			
	H ₇	H ₅	Aromatic ^a	Other ^a
3.3a	6.04	8.64		
3.3d	6.01	8.65		
3.3f	5.96	8.63		

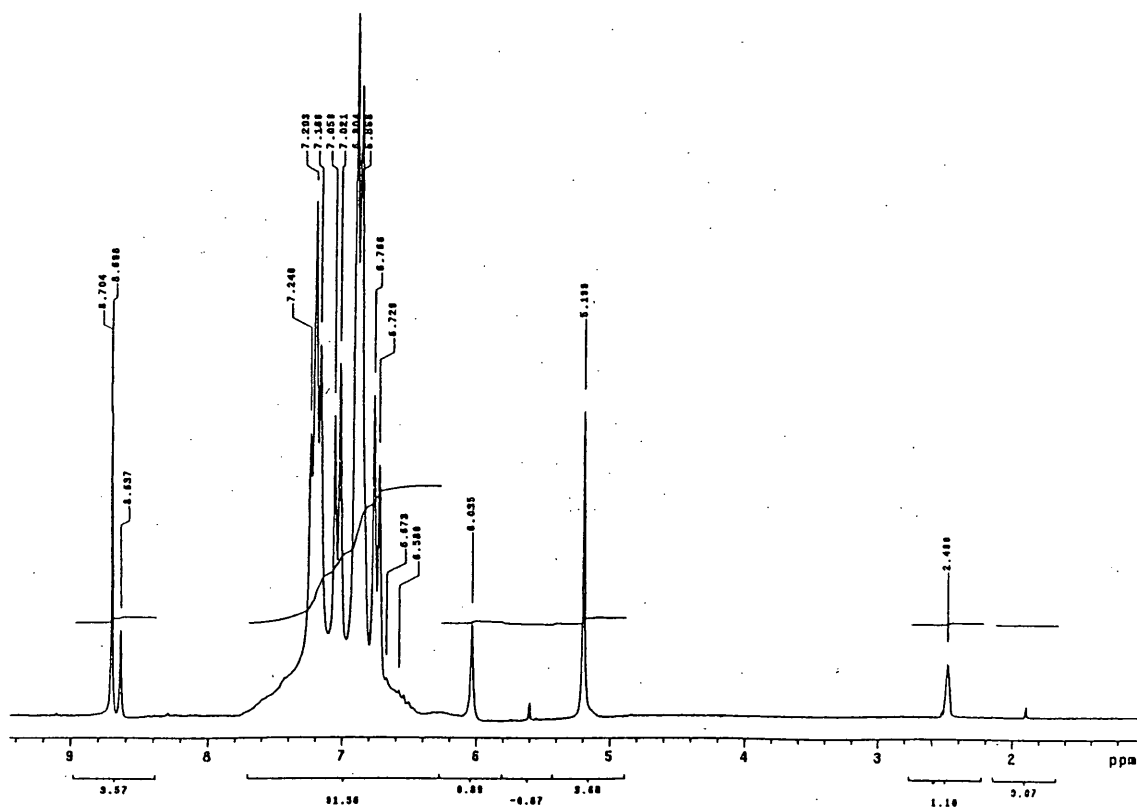
^a Shifts uncertain because of rapid chemical exchange with bulk amine.

Solutions containing one equivalent, or less of aniline gave rise to carbon-bonded adducts, **3.6**. In the presence of excess aniline derivative, the resonances due to the carbon-bonded

adduct moved to lower frequency. This change in frequency is characteristic of deprotonation, and reflects the equilibrium formation of **3.7**. The deprotonation is reversible, as the resonances returned to the positions expected for **3.6** on acidification of the solution with excess deuterium chloride.

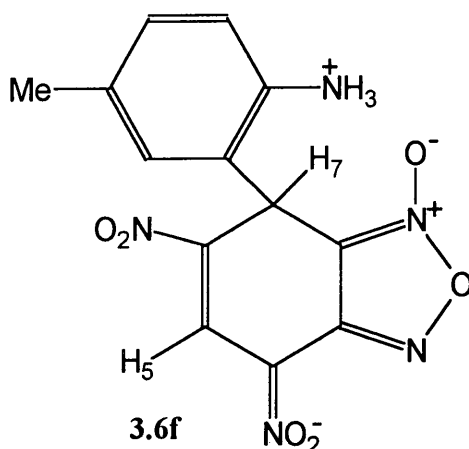
The ^1H NMR spectrum of 0.1 mol dm^{-3} DNBF in $[\text{}^2\text{H}_6]\text{DMSO}$ containing 0.13 mol dm^{-3} aniline is shown in Figure 3.2. The resonances at 6.04 and 8.64 ppm were attributed to the H_7 and H_5 protons of **3.5a**. In a typical experiment, the resonances due to **3.5a** gradually decrease in intensity with time, while the resonances due to the thermodynamically more stable carbon-adduct, **3.7a**, increase in intensity. Acidification with excess deuterium chloride led to immediate loss of the signals due to **3.5**.

Figure 3.2: ^1H NMR spectrum showing the adducts formed on reaction of 0.1 mol dm^{-3} DNBF with 0.13 mol dm^{-3} aniline in $[\text{}^2\text{H}_6]\text{DMSO}$.



The ^1H NMR spectrum of DNBF in $[\text{}^2\text{H}_6]\text{DMSO}$ containing N,N-dimethylaniline, **3.3c**, showed no evidence for the formation of **3.5c**, the nitrogen-bonded adduct. N,N-dimethylaniline contains no NH^+ hydrogens, and so the zwitterion, **3.4c**, cannot undergo deprotonation to give **3.5c**. There was also no ^1H NMR evidence for the formation of **3.5b**, from N-methylaniline, or **3.5e**, from 3-methoxyaniline. There may be some steric hindrance to formation of **3.5b**, as the N-methyl group may impede the attack of the nitrogen lone-pair electrons on DNBF.

In the reaction of DNBF with 4-methylaniline, **3.3f**, the resonances due to H_7 occurred at 5.83 ppm, at significantly higher frequency than for the adducts, **3.6**, formed from the other anilines. The preferred position for attack is at the para-carbon and as this position is blocked, reaction will occur at the ortho-carbon, to give **3.6f**. Hence the H_7 proton is in close proximity to the amino-group and also the N-oxide bond which deshields the proton from the signal and increases the resonance frequency.



3.3.2.1 Carbon-Adduct Deprotonation in the Presence of Excess Aniline

The ^1H NMR resonances due to the H_7 and H_5 protons of **3.6** move to lower frequency on addition of aniline as **3.7** is formed. ^1H NMR chemical shifts were used to calculate K_3 , the equilibrium constant for the deprotonation of **3.6** to **3.7**, Scheme 3.1, according to Equation 3.3, where δ_0 is the shift due to **3.6**, and δ_∞ is the shift due to **3.7**.

$$\text{Equation 3.3: } K_3 = \frac{[\mathbf{3.7}][\text{anilineH}^+]}{[\mathbf{3.6}][\text{aniline}]} = \frac{(\delta_0 - \delta)[\text{anilineH}^+]}{(\delta - \delta_\infty)[\text{aniline}]}$$

However, it was also necessary to calculate the concentrations of aniline and aniline hydrochloride present at equilibrium. The concentrations of the deprotonated adduct, **3.7a** and aniline hydrochloride, **3.3aH**⁺ are equal at equilibrium, as one proton from **3.6a** is transferred to aniline **3.3a**. The stoichiometric aniline concentration is given by Equation 3.4, which can be rearranged to give Equation 3.5.

$$\text{Equation 3.4: } [\text{aniline}]_{\text{stoich}} = [\text{aniline}]_{\text{free}} + [\mathbf{3.6}] + [\mathbf{3.7}] + [\text{anilineH}^+]$$

$$\text{Equation 3.5: } [\text{aniline}]_{\text{free}} = [\text{aniline}]_{\text{stoich}} - [\mathbf{3.6}] - 2[\mathbf{3.7}]$$

^1H NMR data are given in Table 3.9 for the adduct formed from aniline, **3.3a**, and DNBF. A measurement in solution made up from DNBF (0.05 mol dm⁻³), aniline (0.4 mol dm⁻³), and aniline hydrochloride (0.4 mol dm⁻³), gave a resonance due to H_7 at 5.21 ppm. The limiting values of δ_0 (5.36) and δ_∞ (5.14) gave a value for $[\mathbf{3.7a}]/[\mathbf{3.6a}]$ of 2.14, Equation 3.3. The final concentrations of **3.6** and **3.7** were then determined from this ratio and Equation 3.6.

$$\text{Equation 3.6: } [\mathbf{3.6}] + [\mathbf{3.7}] = [\text{DNBF}]_{\text{stoich}}$$

The final concentrations of aniline, 0.316 mol dm⁻³, and aniline hydrochloride, 0.434 mol dm⁻³, were then calculated using Equation 3.5, allowing the calculation, from Equation 3.3, of a value for K_3 of 3 ± 0.5 .

Table 3.9: NMR data for the reaction of DNBF with aniline, **3.3a**, in [²H₆]DMSO.

[DNBF] _{stoich} / mol dm ⁻³	[3.3a] _{stoich} / mol dm ⁻³	[3.3aH ⁺] _{stoich} / mol dm ⁻³	Chemical Shifts	
			H ₇	H ₅
0.099	0.049		5.36	8.73
0.05	0.40	0.40	5.21	8.70
0.048	0.40		5.14	8.67

The pK_a value of aniline is 3.82 in DMSO,⁵ and so the pK_a of **3.6a** was readily calculated as 3.3, according to Equation 3.7. This indicates that **3.6a** is a stronger acid, by 0.5 pK_a units, than the parent amine **3.3a**.

Equation 3.7: $\log_{10}K_3 = \text{pK}_a(\text{anilineH}^+) - \text{pK}_a(\mathbf{3.6})$

There is also evidence for the formation of **3.7b** in solutions containing N-methylaniline, Table 3.10. Again, as the excess of **3.3b** is increased, the resonances due to H₇ and the aromatic ring hydrogens move to lower frequency. There is little change in the shift of the H₅ resonance. Calculation of the [**3.7b**]/[**3.6b**] ratio using Equation 3.3, enabled the determination of the equilibrium concentrations of **3.3b** and **3.3bH**⁺, according to Equations 3.5 and 3.6. A value of K₃ was then determined from Equation 3.3. There is some variance in the calculated values, but the average K₃ value of 3.5 ± 0.5, leads to a pK_a(**3.6b**) value of 2.4. Again, the adduct, **3.6**, is a stronger acid than the parent amine.

Table 3.10: NMR data for the reaction of DNBF with N-methylaniline, **3.3b**, in $[\text{}^2\text{H}_6]\text{DMSO}$.

[DNBF] _{stoich} / mol dm ⁻³	[3.3b] _{stoich} / mol dm ⁻³	[4-Chloroaniline] _{stoich} / mol dm ⁻³	Chemical Shifts		K ₃ ^a
			H ₇	H ₅	
0.099	0.050		5.37	8.72	
0.099	0.100		5.37	8.72	
0.099	0.130		5.31	8.72	3.4
0.098	0.170		5.25	8.71	4.0
0.050	0.100		5.24	8.70	2.3
0.050	0.200		5.17	8.70	4.3
0.048	0.400		5.15	8.71	
0.099	0.099	0.10	5.26	8.71	1.0 ^b
0.099	0.099	0.20	5.21	8.71	1.6 ^b

^a Calculated from Equation 3.3.

^b Calculated from Equation 3.8.

Data are also given in Table 3.10 for experiments in which **3.6b** was formed quantitatively from equimolar amounts of **3.3b** and DNBF, before the addition of 4-chloroaniline, **3.3g**. This amine was unreactive towards DNBF on the time scale of the experiment, and deprotonated **3.6b** to yield an equilibrium mixture containing **3.6b** and **3.7b**. $K_{3,\text{Cl}}$, defined in Equation 3.8, was calculated according to the measured chemical shifts. The $K_{3,\text{Cl}}$ value of 1.3 ± 0.3 is lower than K_3 , reflecting the weaker basicity of 4-chloroaniline than of N-methylaniline.

$$\text{Equation 3.8: } K_{3,\text{Cl}} = \frac{[\text{3.7}][4\text{-chloroanilineH}^+]}{[\text{3.6}][4\text{-chloroaniline}]}$$

Data for the formation of the carbon-bonded adduct, **3.6f**, and its deprotonation in the presence of excess 4-methylaniline, **3.3f** to give **3.7f** are given in Table 3.11. A K_3 value of 11 ± 2 , was determined from Equations 3.3 and 3.5, leading to a $\text{pK}_a(\text{3.6f})$ value of 3.3.

Table 3.11: NMR data for the reaction of DNBF with 4-methylaniline, **3.3f**, in [$^2\text{H}_6$]DMSO.

[DNBF] _{stoich} / mol dm ⁻³	[3.3f] _{stoich} / mol dm ⁻³	[3.3fH ⁺] _{stoich} / mol dm ⁻³	Chemical Shifts		K ₃ ^a
			H ₇	H ₅	
0.10	0.05		5.83	8.73	
0.05	0.20 ^b	0.40 ^b	5.64	8.72	9
0.05	0.20 ^c	0.20 ^c	5.60	8.71	13
0.05	0.40		5.56	8.71	

^a Calculated from Equation 3.3, δ_0 (5.83) and δ_∞ (5.56).

^b Equilibrium concentrations calculated as 0.115 and 0.435 mol dm⁻³ respectively.

^c Equilibrium concentrations calculated as 0.108 and 0.242 mol dm⁻³ respectively.

The K₃ values measured are all greater than unity and show that the equilibrium lies on the side of the deprotonated adduct, **3.7**. This indicates that, although the DNBF moiety in **3.6** is negatively charged, it is electron withdrawing relative to hydrogen. This effect is expected to increase with increasing proximity of the DNBF moiety and the positive nitrogen centre. For the aniline, **3.6a**, and N-methylaniline, **3.6b**, derivatives where reaction occurs para to the amino function, the acid strengthening effect is 0.5 pK_a units. However, for the 4-methylaniline derivative, **3.6f**, where reaction is ortho to the amino function, the effect is approximately 1 pK_a unit.

3.3.3 Kinetic Data in DMSO

3.3.3.1 Measured in the Presence of HCl

Kinetic measurements relating to the formation of the carbon-bonded adducts were made in DMSO. The primary motivation for these measurements was to allow the calculation of values of K_N as described in Section 3.3.3.2. However, it was also of interest to compare the data with those obtained in 70/30 (v/v) DMSO/water described in Chapter 2. As before, rate constants were measured in the presence of excess hydrochloric acid. This necessitated the presence of small amounts of water, so that the solvent was in fact 99/1 (v/v) DMSO/water. The presence of acid reduced the concentration of free aniline to very low levels, and there was no evidence for the formation of nitrogen-bonded adducts, **3.5**. These conditions afforded direct conversion of DNBF to the carbon-bonded adducts, **3.6**. In calculating the rate constant k , Equation 3.9, it was necessary to allow for the formation of the DNBF.OH⁻ adduct, in equilibrium with DNBF, Equation 3.10.

$$\text{Equation 3.9: } \frac{-d[\text{DNBF}]}{dt} = k[\text{DNBF}][\text{aniline}]$$

$$\text{Equation 3.10: } K_{H_2O} = \frac{[\text{DNBF.OH}^-][\text{H}^+]}{[\text{DNBF}]}$$

The value of K_{H_2O} includes the activity of the water in the medium. Spectrophotometric measurements at 470 nm (Section 2.3.3), gave a value of 0.050 mol dm⁻³ in the medium used, containing 1% water. The second order rate constant, k , shown in Equation 3.9, is related to k_{obs} , the measured first order rate constant, by Equation 3.11, (derived in Section 2.3.4.1), where K_a is the dissociation constant of the anilinium ion.

$$\text{Equation 3.11: } k = \frac{k_{\text{obs}}(K_{H_2O} + [\text{H}^+])}{K_a[\text{anilineH}^+]}$$

Data for the reaction of DNBF with aniline, **3.3a** and the aniline derivatives **3.3b-3.3f**, are reported in Tables 3.12-3.17.

Table 3.12: Kinetic data for the reaction of DNBF^a with aniline, **3.3a**, in acidic solutions in DMSO^b to give **3.6a**.

[AnilineH ⁺ Cl ⁻] / mol dm ⁻³	[HCl] / mol dm ⁻³	10 ⁴ k _{obs} ^c / s ⁻¹	k ^d / dm ³ mol ⁻¹ s ⁻¹
0.010	0.090	0.80	7.5
0.020	0.080	2.0	8.6
0.030	0.070	3.7	9.8
0.040	0.060	4.7	8.6
0.050	0.050	6.7	8.9
0.060	0.040	8.0	8.0

^a [DNBF] = 4 x 10⁻⁵ mol dm⁻³.

^b Solvent is 99/1 (v/v) DMSO/water.

^c Colour forming reaction at 489 nm.

^d Calculated according to Equation 3.11, with K_a, 1.51 x 10⁻⁴ mol dm⁻³ and KH₂O, 0.050 mol dm⁻³.

Table 3.13: Kinetic data for the reaction of DNBF^a with N-methylaniline, **3.3b**, in acidic solutions in DMSO^b to give **3.6b**.

[N-MethylanilineH ⁺ Cl ⁻] / mol dm ⁻³	[HCl] / mol dm ⁻³	10 ⁴ k _{obs} ^c / s ⁻¹	k ^d / dm ³ mol ⁻¹ s ⁻¹
0.020	0.080	17	9.6
0.030	0.070	29	10.1
0.040	0.060	47	11.2
0.050	0.050	51	8.9
0.060	0.040	75	9.8

^a [DNBF] = 4 x 10⁻⁵ mol dm⁻³.

^b Solvent is 99/1 (v/v) DMSO/water.

^c Colour forming reaction at 494 nm.

^d Calculated according to Equation 3.11, with K_a, 1.15 x 10⁻³ mol dm⁻³ and KH₂O, 0.050 mol dm⁻³.

Table 3.14: Kinetic data for the reaction of DNBF^a with N,N-dimethylaniline, **3.3c**, in acidic solutions in DMSO^b to give **3.6c**.

[N,N-DimethylanilineH ⁺ Cl ⁻] / mol dm ⁻³	[HCl] / mol dm ⁻³	10 ⁴ k _{obs} ^c / s ⁻¹	k ^d / dm ³ mol ⁻¹ s ⁻¹
0.020	0.080	8.5	2.8
0.030	0.070	13.2	2.6
0.040	0.060	17.2	2.4
0.050	0.050	31.3	3.1
0.060	0.040	42	3.1

^a [DNBF] = 4 x 10⁻⁵ mol dm⁻³.

^b Solvent is 99/1 (v/v) DMSO/water.

^c Colour forming reaction at 486 nm.

^d Calculated according to Equation 3.11, with K_a, 2.0 x 10⁻³ mol dm⁻³ and KH₂O, 0.050 mol dm⁻³.

Table 3.15: Kinetic data for the reaction of DNBF^a with 3-methylaniline, **3.3d**, in acidic solutions in DMSO^b to give **3.6d**.

[N-MethylanilineH ⁺ Cl ⁻] / mol dm ⁻³	[HCl] / mol dm ⁻³	10 ⁴ k _{obs} ^c / s ⁻¹	k ^d / dm ³ mol ⁻¹ s ⁻¹
0.010	0.090	7.2	73
0.020	0.080	13.7	65
0.030	0.070	21.5	62
0.040	0.060	24.6	49
0.050	0.050	40.6	59
0.060	0.040	59	65

^a [DNBF] = 4 x 10⁻⁵ mol dm⁻³.

^b Solvent is 99/1 (v/v) DMSO/water.

^c Colour forming reaction at 485 nm.

^d Calculated according to Equation 3.11, with K_a, 1.38 x 10⁻⁴ mol dm⁻³ and KH₂O, 0.050 mol dm⁻³.

Table 3.16: Kinetic data for the reaction of DNBF^a with 3-methoxyaniline, **3.3e**, in acidic solutions in DMSO^b to give **3.6e**.

[3-MethoxyanilineH ⁺ Cl ⁻] / mol dm ⁻³	[HCl] / mol dm ⁻³	k _{obs} ^c / s ⁻¹	k ^d / dm ³ mol ⁻¹ s ⁻¹
0.010	0.090	0.13	3500
0.020	0.080	0.22	2800
0.030	0.070	0.42	3300
0.040	0.060	0.72	3900
0.050	0.050	1.14	4400
0.060	0.040	1.66	4800

^a [DNBF] = 2 x 10⁻⁵ mol dm⁻³.

^b Solvent is 99/1 (v/v) DMSO/water.

^c Measured by stopped-flow spectrophotometry at 494 nm.

^d Calculated according to Equation 3.11, with K_a, 5.13 x 10⁻⁴ mol dm⁻³ and KH₂O, 0.050 mol dm⁻³.

Table 3.17: Kinetic data for the reaction of DNBF^a with 4-methylaniline, **3.3f**, in acidic solutions in DMSO^b to give **3.6f**.

[N-MethylanilineH ⁺ Cl ⁻] / mol dm ⁻³	[HCl] / mol dm ⁻³	10 ⁴ k _{obs} ^c / s ⁻¹	k ^d / dm ³ mol ⁻¹ s ⁻¹
0.040	0.060	1.09	6.5
0.050	0.050	1.30	5.7
0.060	0.040	1.53	5.0

^a [DNBF] = 4 x 10⁻⁵ mol dm⁻³.

^b Solvent is 99/1 (v/v) DMSO/water.

^c Colour forming reaction at 485 nm.

^d Calculated according to Equation 3.11, with K_a, 4.6 x 10⁻⁵ mol dm⁻³ and KH₂O, 0.050 mol dm⁻³.

A summary of the second order rate constants measured in 99/1 (v/v) DMSO/water is given in Table 3.18 where values are compared with those measured in 70/30 (v/v) DMSO/water.

Table 3.18: Summary of data for the formation of carbon-bonded adducts in DMSO and DMSO-water mixtures.

Aniline	pK _a (DMSO)	k / dm ³ mol ⁻¹ s ⁻¹	
		99/1 (v/v) DMSO/water	70/30 (v/v) DMSO/water
3.3a	3.82	8.6 ± 1	4.0 ± 0.7
3.3b	2.94	10.1 ± 1	10.3 ± 0.6
3.3c	2.70	2.8 ± 0.4	6.0 ± 0.8
3.3d	3.86	62 ± 10	27 ± 1
3.3e	3.29	3800 ± 700	1300 ± 100
3.3f	4.34	5.7 ± 0.7	1.14 ± 0.03

^a Data from Chapter 2.

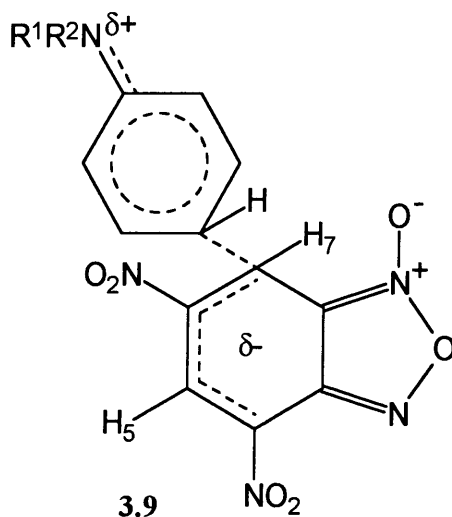
As expected, there is no correlation of the *k* values with the pK_a values measured in DMSO; the *k* values reflect reactivity at carbon atoms, while the pK_a values provide a measure of the extent of protonation at the nitrogen centre.

The substituent effects mirror those discussed in Chapter 2 for the 70/30 (v/v) DMSO/water solvent system. The derivatives **3.3d** and **3.3e**, where electron-donating groups are present at the 3-position, activate the 4-position to attack, and hence greatly increase the measured value of *k* relative to aniline. In the case of 4-methylaniline, **3.3f**, the preferred site for the electrophilic attack of DNBF is blocked, and reaction occurs at the 2-position, ortho to the amino-group, at a reduced rate relative to aniline.

The results presented in Table 3.18 allow a comparison of the solvent effect on the values of *k*. For aniline **3.3a**, and ring-substituted anilines, **3.3d-f**, the value of *k* increases by a factor of 2-3 when the solvent is changed from 70/30 (v/v) DMSO/water to 99/1 (v/v) DMSO/water. However, for N-methylaniline, **3.3b**, there is little variation in *k* for the two solvent systems, and for N,N-dimethylaniline, **3.3c**, the *k* value decreases on increasing the proportion of DMSO in the solvent.

Kinetic isotope effect studies (Section 2.3.4.2) have shown that the initial attack of DNBF is rate-limiting in the formation of **3.6**, and a transition state structure, **3.9** can be

postulated. DMSO is able to stabilise cationic nitrogen centres through hydrogen-bonding.^{8,5} For aniline, $R^1=R^2=H$, increasing the proportion of DMSO in the solvent will be expected to stabilise **3.9**, as there are two NH^+ protons to undergo hydrogen-bonding with the solvent. This solvent induced stabilisation of the transition state will diminish as the number of NH^+ protons decreases, and disappear when $R^1=R^2=Me$.



3.3.3.2 Measured in Solutions Containing Amine and Amine Hydrochloride

Kinetic measurements made in solutions containing the aniline derivative buffered with its hydrochloride salt showed two reaction processes. The first, (which was too fast to measure on the stopped-flow time scale), gave a species with an absorption maximum, λ_{max} , at 480 nm. This was attributed to the formation of the nitrogen-bonded adduct, **3.5**, in agreement with the NMR data reported in Section 3.3.2.

During the second, slower process, the absorption maximum shifted to 489 nm, corresponding to the conversion of the nitrogen-bonded adduct, **3.5**, to the thermodynamically more stable carbon-bonded adduct, **3.6**. This conversion was found to be a first order process, Figure 3.3. Increasing the proportion of aniline in the solutions decreased the observed first order rate constant, while increasing the proportion of aniline hydrochloride increased the observed first order rate constant. The measured rate constants are given in Table 3.19 for a selection of buffer systems. In all the kinetic measurements, the concentrations of the buffer components are in large excess of the concentration of DNBF.

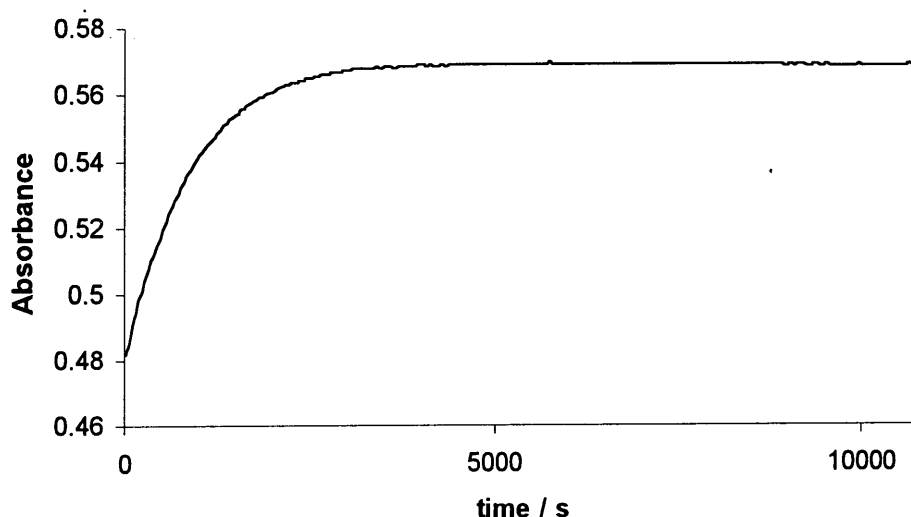
Table 3.19: Kinetic data for the conversion of the nitrogen-bonded adduct, **3.5**, to the carbon-bonded adduct, **3.6**, in DMSO.

[Aniline] / mol dm ⁻³	[AnilineH ⁺ Cl ⁻] / mol dm ⁻³	10 ⁴ k' _{obs} ^b / s ⁻¹
0.10	0.02 ^a	0.45
0.10	0.04 ^a	0.85
0.10	0.07 ^a	2.4
0.10	0.10	4.4
0.04	0.10	11.6
0.07	0.10	6.4
0.10	0.10	4.4
0.20	0.10	2.2

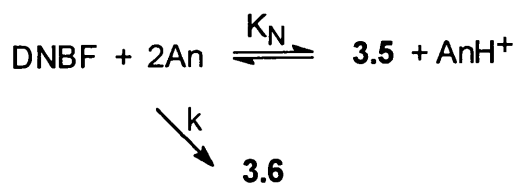
^a Ionic strength maintained at 0.1 mol dm⁻³ using tetrabutylammonium chloride.

^b Measured at 489 nm.

Figure 3.3: First order plot showing the increase in absorbance measured at 489 nm with time, corresponding to the conversion of **3.5a** to **3.6a**. DNBF, 4 x 10⁻⁵ mol dm⁻³, aniline, 0.04 mol dm⁻³; aniline hydrochloride, 0.1 mol dm⁻³.



Scheme 3.1 can be written in a simplified form to give Scheme 3.3. An expression for K_N , the equilibrium constant for nitrogen-adduct formation, is given in Equation 3.12.



Scheme 3.3

$$\text{Equation 3.12: } K_N = \frac{[\text{3.5}][\text{AnH}^+]}{[\text{DNBF}][\text{An}]^2}$$

The rate of formation of the thermodynamically more stable carbon-bonded adduct, **3.6**, from DNBF and aniline, is given by Equation 3.13.

$$\text{Equation 3.13: } \frac{d[\text{3.6}]}{dt} = k[\text{DNBF}][\text{An}]$$

The stoichiometric concentration of DNBF is given by Equation 3.14. This stoichiometric concentration is constant over time, leading to Equation 3.15.

$$\text{Equation 3.14: } [\text{3.6}] + [\text{DNBF}] + [\text{3.5}] = [\text{DNBF}]_{\text{stoich}}$$

$$\text{Equation 3.15: } \frac{d[\text{3.6}]}{dt} + \frac{d[\text{DNBF}]}{dt} + \frac{d[\text{3.5}]}{dt} = 0$$

Rearrangement of Equation 3.12 and substitution of Equations 3.12 and 3.13 into Equation 3.15, leads to Equation 3.16, and subsequently Equation 3.17, which can then be factorised to give Equation 3.18.

$$\text{Equation 3.16: } k[\text{DNBF}][\text{An}] + \frac{d}{dt} \frac{[\text{3.5}][\text{AnH}^+]}{K_N[\text{An}]^2} + \frac{d[\text{3.5}]}{dt} = 0$$

$$\text{Equation 3.17: } \frac{k[\text{3.5}][\text{AnH}^+]}{K_N[\text{An}]} + \frac{d}{dt} \frac{[\text{3.5}][\text{AnH}^+]}{K_N[\text{An}]^2} + \frac{d[\text{3.5}]}{dt} = 0$$

$$\text{Equation 3.18: } \frac{k[3.5][\text{AnH}^+]}{K_N[\text{An}]} + \frac{d[3.5]}{dt} \left(1 + \frac{[\text{AnH}^+]}{K_N[\text{An}]^2} \right) = 0$$

The rate of decomposition of the nitrogen-bonded adduct, **3.5**, is given by Equation 3.19, and substitution of this equation into Equation 3.18 gives Equation 3.20.

$$\text{Equation 3.19: } -\frac{d[3.5]}{dt} = k'_{\text{obs}}[3.5]$$

$$\text{Equation 3.20: } \frac{k[3.5][\text{AnH}^+]}{K_N[\text{An}]} - k'_{\text{obs}}[3.5] \left(1 + \frac{[\text{AnH}^+]}{K_N[\text{An}]^2} \right) = 0$$

Equation 3.20 can then be rearranged to give Equation 3.21, leading to Equation 3.22, which is then inverted to give Equation 3.23.

$$\text{Equation 3.21: } \frac{1}{k'_{\text{obs}}} = \frac{K_N[\text{An}]}{k[\text{AnH}^+]} \left(1 + \frac{[\text{AnH}^+]}{K_N[\text{An}]^2} \right)$$

$$\text{Equation 3.22: } \frac{1}{k'_{\text{obs}}} = \frac{K_N[\text{An}]^2 + [\text{AnH}^+]}{k[\text{AnH}^+][\text{An}]}$$

$$\text{Equation 3.23: } k'_{\text{obs}} = \frac{k[\text{AnH}^+][\text{An}]}{K_N[\text{An}]^2 + [\text{AnH}^+]}$$

There are two limiting cases to consider:

1) If $K_N[\text{An}]^2 \gg [\text{AnH}^+]$, Equation 3.23 reduces to Equation 3.24.

$$\text{Equation 3.24: } k'_{\text{obs}} = \frac{k[\text{AnH}^+]}{K_N[\text{An}]}$$

2) If $[\text{AnH}^+] \gg K_N[\text{An}]^2$, Equation 3.23 reduces to Equation 3.25.

$$\text{Equation 3.25: } k'_{\text{obs}} = k[\text{An}]$$

The experimental results show that k'_{obs} is proportional to $[\text{AnH}^+]$ and inversely proportional to $[\text{An}]$. This corresponds to the first limiting case above. Hence K_N is calculated from Equation 3.26.

$$\text{Equation 3.26: } K_N = \frac{k[\text{AnH}^+]}{k'_{\text{obs}}[\text{An}]}$$

Kinetic data were measured for aniline, **3.3a**, 3-methylaniline, **3.3d**, 3-methoxyaniline, **3.3e**, and 4-methylaniline, **3.3f**, Tables 3.20-3.23. As discussed previously in Section 3.3.2, N,N-dimethylaniline, **3.3c**, is not able to form a nitrogen-bonded adduct, **3.5c**, with DNBF. There was also no reaction at the nitrogen centre of N-methylaniline, **3.3b**, probably due to steric hindrance of the lone pair electrons. Therefore, it was not possible to measure K_N values for these derivatives.

Table 3.20: Kinetic data for the conversion of **3.5a** to **3.6a**.

$[\text{Aniline}]^a / \text{mol dm}^{-3}$	$10^4 k'_{\text{obs}} / \text{s}^{-1}$	$K_N^b / \text{dm}^3 \text{mol}^{-1}$
0.04	11.6	18500
0.07	6.4	19200
0.10	4.4	19500
0.20	2.2	19500

^a All solutions contain aniline hydrochloride, 0.1 mol dm^{-3} .

^b Calculated from Equation 3.26, with k , $8.6 \text{ dm}^3 \text{mol}^{-1} \text{s}^{-1}$.

Table 3.21: Kinetic data for the conversion of **3.5d** to **3.6d**.

$[\text{3-Methylaniline}]^a / \text{mol dm}^{-3}$	$10^4 k'_{\text{obs}} / \text{s}^{-1}$	$K_N^b / \text{dm}^3 \text{mol}^{-1}$
0.04	5.16	30000
0.07	2.64	33500
0.10	2.20	28000
0.20	1.10	28000

^a All solutions contain 3-methylaniline hydrochloride, 0.1 mol dm^{-3} .

^b Calculated from Equation 3.26, with k , $62 \text{ dm}^3 \text{mol}^{-1} \text{s}^{-1}$.

Table 3.22: Kinetic data for the conversion of **3.5e** to **3.6e**.

[3-Methoxyaniline] ^a / mol dm ⁻³	k' _{obs} / s ⁻¹	K _N ^b / dm ³ mol ⁻¹
0.04	2.88	3300
0.07	1.35	4000
0.10	1.14	3300
0.20	0.56	3400

^a All solutions contain 3-methoxyaniline hydrochloride, 0.1 mol dm⁻³.^b Calculated from Equation 3.26, with k, 3800 dm³ mol⁻¹ s⁻¹.Table 3.23: Kinetic data for the conversion of **3.5f** to **3.6f**.

[4-Methylaniline] ^a / mol dm ⁻³	10 ⁴ k' _{obs} / s ⁻¹	K _N ^b / dm ³ mol ⁻¹
0.04	3.4	42000
0.07	2.3	35000
0.10	1.8	32000
0.20	0.8	36000

^a All solutions contain 4-methylaniline hydrochloride, 0.1 mol dm⁻³.^b Calculated from Equation 3.26, with k, 5.7 dm³ mol⁻¹ s⁻¹.

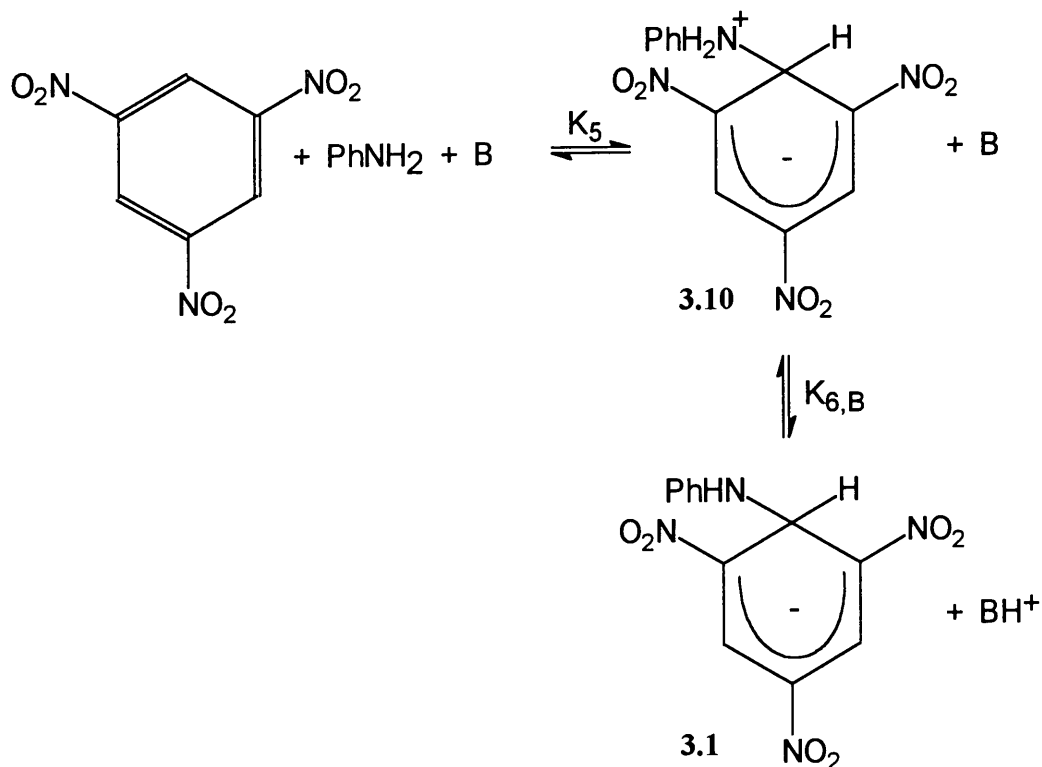
A summary of the equilibrium constants, K_N, measured for the derivatives is given in Table 3.24. There is a correlation between the K_N values, for reaction at the nitrogen centre of the anilines, and the pK_a values measured in DMSO. The highest value of K_N is found for the most basic aniline, 4-methylaniline, and the lowest value for the least basic ring-substituted derivative, 3-methoxyaniline.

Table 3.24: Summary of data for reaction of DNBF and aniline derivatives to form nitrogen-bonded adducts, **3.5**, in DMSO.

Aniline	pK _a	K _N / dm ³ mol ⁻¹
3.3a , Aniline	3.82	19000
3.3d , 3-Methylaniline	3.86	30000
3.3e , 3-Methoxyaniline	3.29	3500
3.3f , 4-Methylaniline	4.34	36000

3.4 Comparison with TNB

DNBF reacts readily with aniline at the nitrogen centre under kinetic control, to give a nitrogen-bonded adduct. This adduct then undergoes isomerism to the thermodynamically more stable carbon-bonded adduct. Trinitrobenzene, (TNB), will only react with aniline to produce the nitrogen-bonded adduct, **3.1**, in the presence of a strong base, such as Dabco which acts as a proton transfer agent, Scheme 3.4.



Scheme 3.4

The overall equilibrium constant, $K_5K_{6,\text{Dabco}}$, for the reaction in Scheme 3.4, in DMSO, with tetrabutylammonium chloride (0.1 mol dm^{-3}) has a value of $1.8 \text{ dm}^3 \text{ mol}^{-1}$.^{10,11} The pK_a values of the protonated forms of aniline and Dabco have been measured and are 3.82 and 9.06 respectively.⁵ Knowledge of these values permits calculation of a value of $1 \times 10^{-5} \text{ dm}^3 \text{ mol}^{-1}$ for $K_5K_{6,\text{An}}$ (the overall equilibrium constant in Scheme 3.4, with aniline acting as the base) according to Equation 3.27.

$$\text{Equation 3.27: } K_5K_{6,\text{An}} = K_5K_{6,\text{Dabco}} \frac{K_a(\text{DabcoH}^+)}{K_a(\text{AnH}^+)}$$

This $K_5K_{6,\text{An}}$ value can be compared with the value of $2 \times 10^4 \text{ dm}^3 \text{ mol}^{-1}$ measured for K_N , for reaction of DNBF with aniline to form the nitrogen-bonded adduct, **3.5**. The ratio $K_N/K_5K_{6,\text{An}}$ of 2×10^9 illustrates the difference in the stabilities of the adducts formed from DNBF and TNB.

Similar differences in stability have been observed for the reactions of DNBF and TNB with methoxide ions in methanol,¹² (1×10^9), and with hydroxide ions in water,¹³ (5×10^9). In these reactions, anionic adducts are formed directly. However, for aniline, nitrogen-bonded adduct formation involves formation of a zwitterion, followed by proton transfer to yield the anionic form. For DNBF, K_N is the product of the equilibrium constants K_1 and K_2 , Scheme 3.1, while for TNB the overall equilibrium constant is the product of K_5 and K_6 .

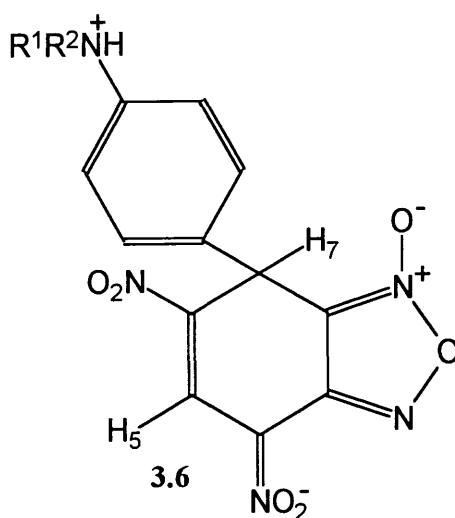
The similar stability ratios calculated for all three nucleophiles, aniline, methoxide and hydroxide, probably indicates that the major difference in the stability of adducts formed from DNBF and TNB is due to the K_1/K_5 ratio rather than the K_2/K_6 ratio. Hence the acidifying effect on the adjacent ammonium proton of the negatively charged DNBF group in **3.4** is likely to be similar to that of the negatively charged TNB group in **3.10**. This acidifying effect has a value of around 500.¹⁴

3.5 Conclusion

The results reported provide further evidence in support of the ambident reactivity of aniline in reactions with DNBF. The nitrogen-bonded adduct is formed under kinetic control, and then undergoes isomerism to give the thermodynamically more stable carbon-bonded adduct.

Equilibrium constants have been measured for the formation of the nitrogen-bonded adduct, and these correlate with the pK_a values of the anilines measured in DMSO. A comparison of the electrophilicity of DNBF with TNB led to a reactivity ratio of 2×10^9 .

The carbon-bonded adducts, **3.6**, formed from reaction of DNBF on aniline, N-methylaniline and 4-methylaniline, all have pK_a values 0.5 to 1.0 units less than the value of the parent anilinium ion in DMSO. This is a reflection of the strong electron-withdrawing capability of the negatively charged DNBF moiety relative to hydrogen. The acidifying effect will be attenuated with distance from the positive centre. Thus in the nitrogen-bonded zwitterionic adducts, **3.4**, a greater effect is observed.



3.6 References

- ¹ R. J. Spear, W. P. Norris and R. W. Read., *Tetrahedron Lett.*, 1983, **24**, 1555.
- ² M. J. Strauss, R. A. Renfrow and E. Buncel., *J. Am. Chem. Soc.*, 1983, **105**, 2473.
- ³ F. Terrier., *Spec. Pub. Soc. Chem.*, 1995, 399.
- ⁴ P. Drost., *Liebigs Ann. Chem.*, 1899, **307**, 49.
- ⁵ M. R. Crampton and I. A. Robotham., *J. Chem. Res. (S)*, 1997, 22.
- ⁶ F. G. Bordwell, J. C. Branca, D. L. Hughes and W. N. Olmstead., *J. Org. Chem.*, 1980, **45**, 3305.
- ⁷ F. G. Bordwell., *Acc. Chem. Res.*, 1988, **21**, 456.
- ⁸ K. Yates and G. Welch., *Can. J. Chem.*, 1972, **50**, 474.
- ⁹ R. W. Taft and F. G. Bordwell., *Acc. Chem. Res.*, 1988, **21**, 465.
- ¹⁰ E. Buncel, W. Eggimann and H. W. Leung., *J. Chem. Soc., Chem. Commun.*, 1977, 55.
- ¹¹ E. Buncel and W. Eggimann., *J. Am. Chem. Soc.*, 1977, **99**, 5958.
- ¹² F. Terrier, *Nucleophilic Aromatic Displacement*, VCH, New York, 1991.
- ¹³ F. Terrier., *Chem. Rev.*, 1982, **82**, 77.
- ¹⁴ M. R. Crampton and B. Gibson., *J. Chem. Soc., Perkin Trans. 2.*, 1981, 533.

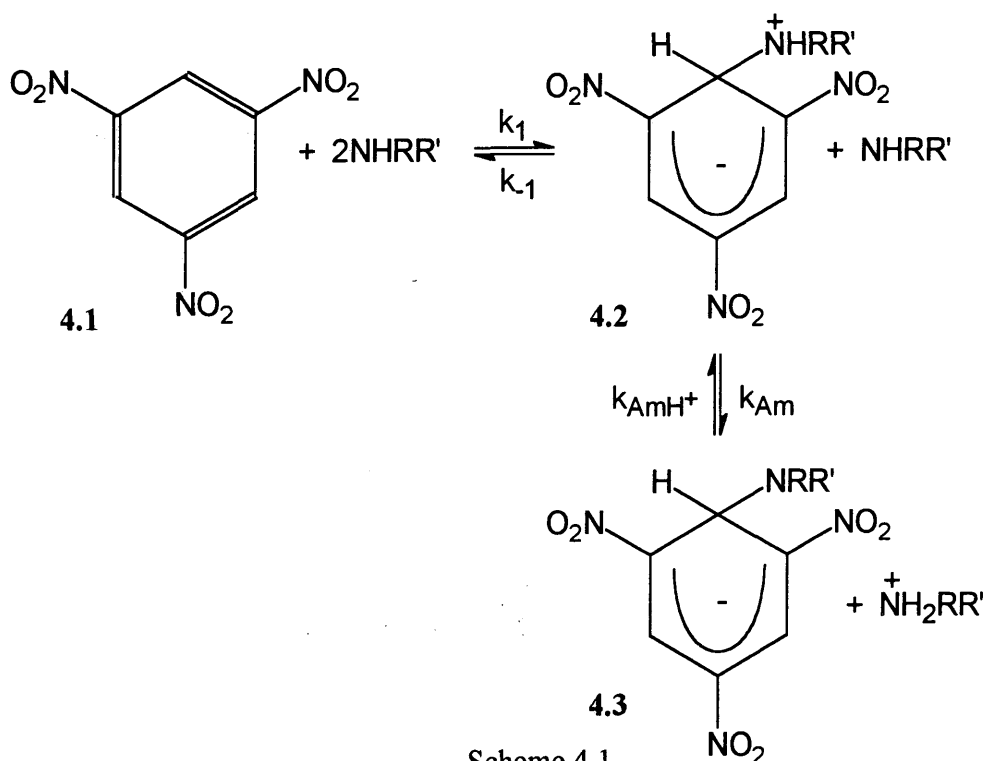
Chapter 4

The Reactions of 4-Nitrobenzofurazan and 4-Nitrobenzofuroxan with Amines in DMSO

4 The reactions of 4-Nitrobenzofurazan and 4-Nitrobenzofuroxan with Amines in DMSO

4.1 Introduction

Aliphatic amines react with aromatic substrates such as trinitrobenzene, (TNB), **4.1**, to give zwitterionic σ -adducts, **4.2**, which are subsequently deprotonated to **4.3** in the presence of excess amine, Scheme 4.1.

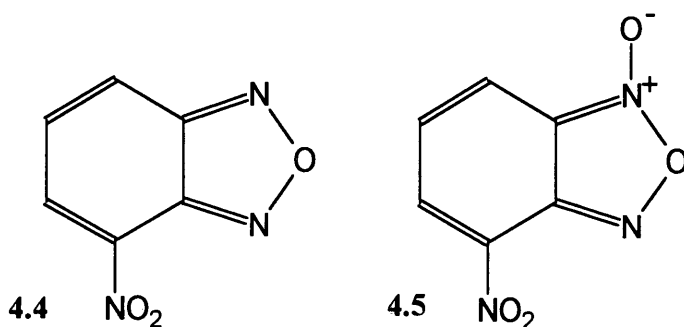


Scheme 4.1

Studies of the reaction outlined in Scheme 4.1 have shown that the proton transfer step may be rate-limiting.^{1,2,3} The measured values of k_{Am} are considerably lower than the diffusion controlled limit.⁴ For example, a value of $3 \times 10^7 \text{ dm}^3 \text{ mol}^{-1} \text{ s}^{-1}$ for k_{Am} has been measured for the reaction of **4.1** with *n*-butylamine in DMSO.² Previous studies have shown that lower values of k_{Am} are obtained with secondary amines in comparison with primary amines.⁵ This is probably due to steric hindrance at the reaction centre.

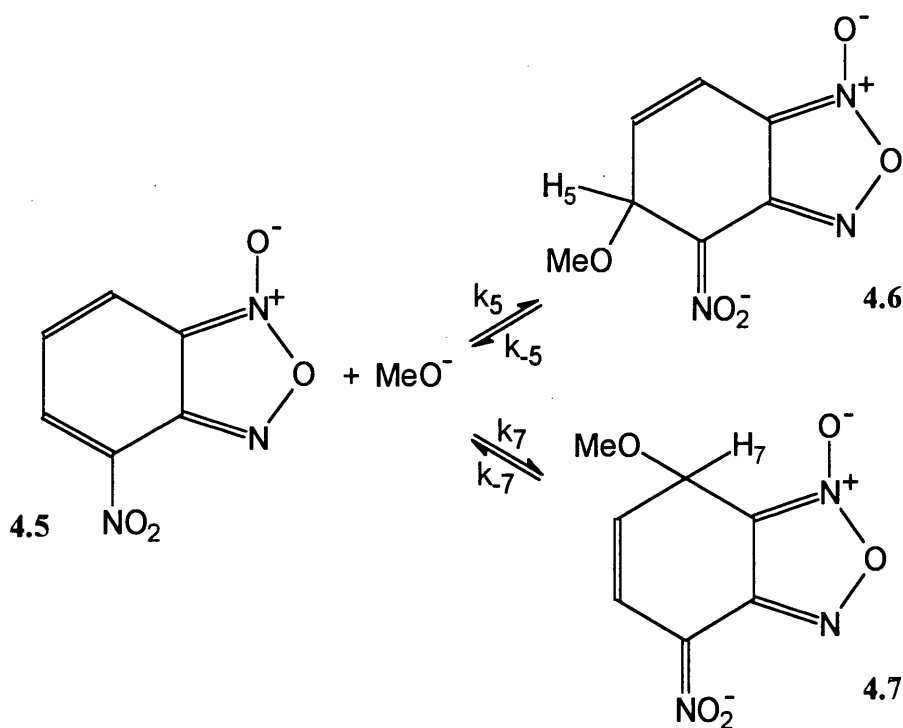
In this Chapter, 4-Nitrobenzofurazan, (NBZ) **4.4**, and 4-nitrobenzofuroxan, (NBF) **4.5**, were chosen as substrates to study σ -adduct formation in activated aromatic systems

where steric hindrance at the activated positions is less than for **4.1**. These compounds are known to react with nucleophiles to produce stable Meisenheimer complexes.⁶



The formation of an hydroxide-adduct with **4.4**, (NBZ) or **4.5**, (NBF) via competitive equilibria with adventitious water in the solvent system is not generally observed, illustrating that these electrophiles are less reactive than dinitrobenzofuroxan, (DNBF).⁷

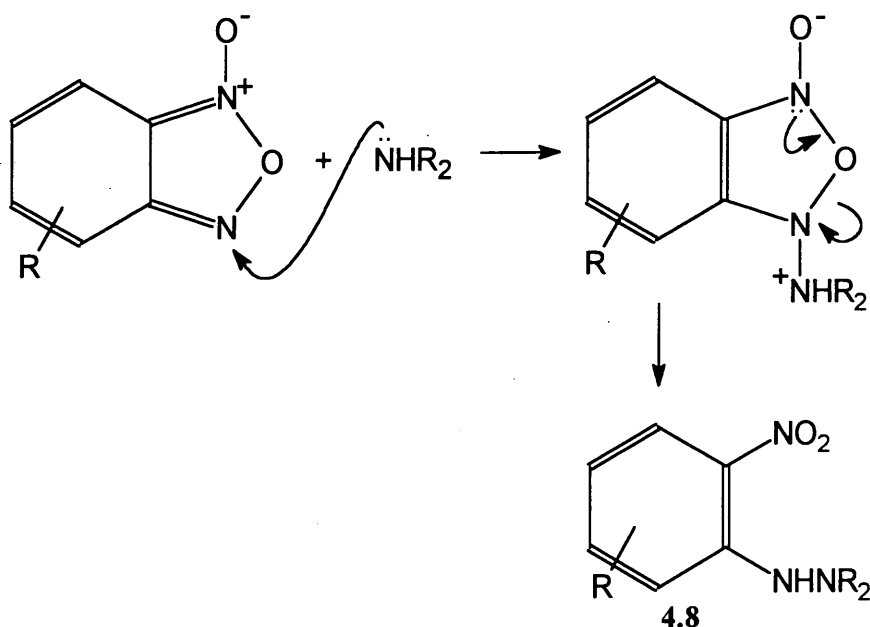
Previous workers have studied the attack of methoxide ions on **4.4**, **4.5** and their derivatives in methanol and methanol-DMSO solvents, using NMR spectroscopy^{8,9} and UV/Visible spectrophotometry.^{10,11,12,6,7,13} In reactions of methoxide with NBF, **4.5**, attack at the 5-position to give **4.6** is kinetically preferred, but the adduct, **4.7**, formed from attack at the 7-position is thermodynamically more stable,⁷ Scheme 4.2. Terrier and co-workers have determined a k_5/k_7 value of 70, and a K_7/K_5 value of 200.⁶



Scheme 4.2

The reactions of aryloxy ions with NBF, **4.5**, have also been studied.⁷ There was no evidence for attack at the 5-position, and the resulting adduct formed from attack of the oxygen centre at the 7-position was both kinetically and thermodynamically preferred. Although phenoxide derivatives are potentially ambident nucleophiles, there was no evidence for the formation of a carbon-bonded adduct.⁷

Reactions of benzofuroxan derivatives with secondary amines have been studied by Latham and co-workers.¹¹ Addition of the benzofuroxan to an excess of amine at 0 °C resulted in the opening of the furoxan ring, to yield hydrazine derivatives, Scheme 4.3.



Scheme 4.3

As the benzofuroxan was made increasingly electrophilic, (by the introduction of electron-withdrawing substituents), the reactivity with secondary amines and the tendency to give hydrazines, **4.8**, diminished. The adduct resulting from attack at the 7-position of the benzene ring was then the only observed species.¹¹

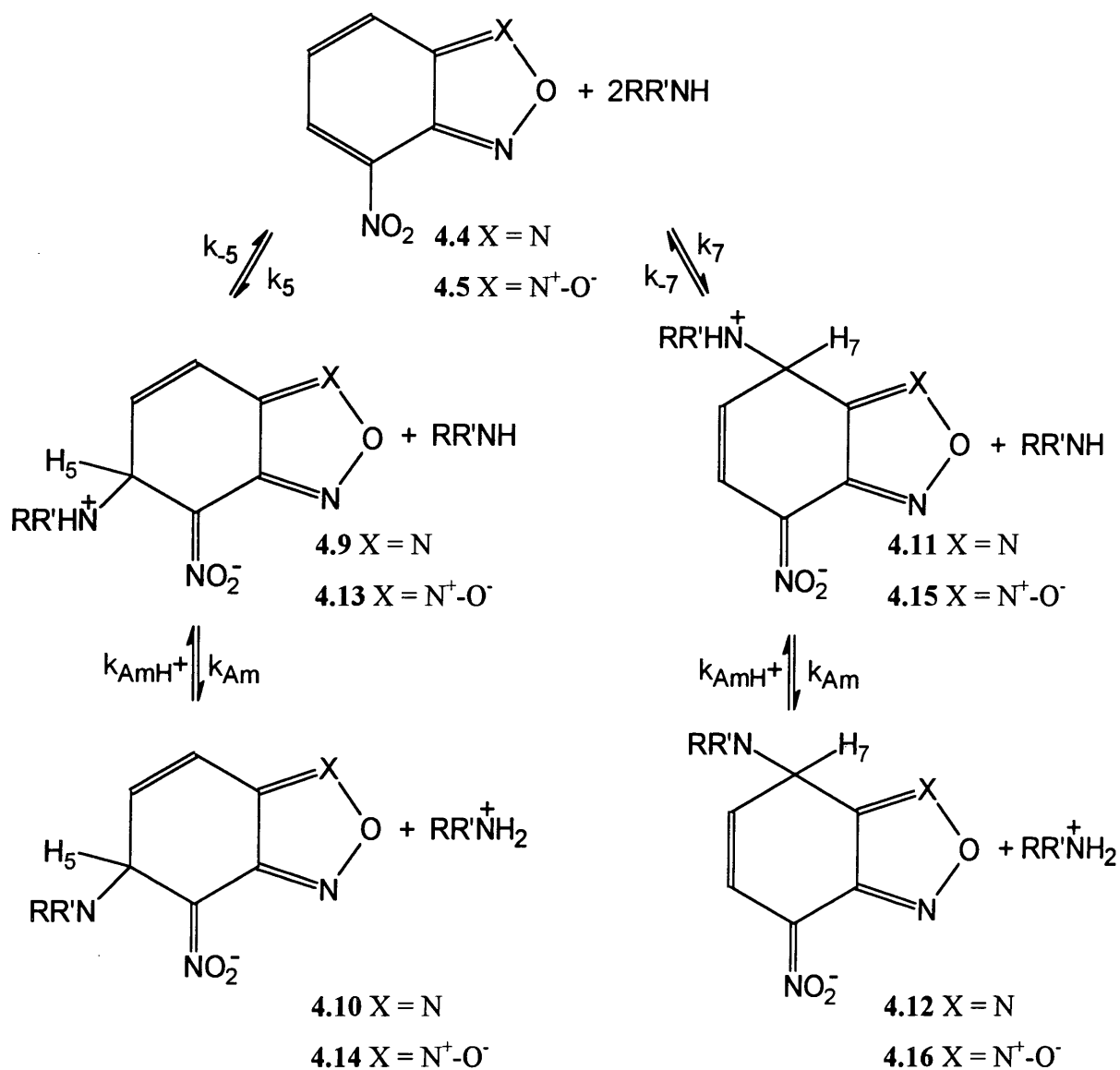
4.2 Experimental

A sample of 4-nitrobenzofuroxan, **4.5**, prepared by nitration of benzofuroxan¹⁴ was available from previous work, (mp 143 °C, literature value,¹⁴ 143 °C). 4-Nitrobenzofurazan, **4.4**, was prepared by nitration of benzofurazan using a 4:1 sulfuric:nitric acid mixture at 5 °C. The resulting pale yellow precipitate was filtered under vacuum to give **4.4** in 63% yield, (mp 91-93 °C, literature value,¹⁵ 93 °C). All amines and solvents used were the purest available commercial products. Amine salts were prepared as solutions in DMSO by accurate neutralisation of the amine with hydrochloric acid or perchloric acid as appropriate.

¹H NMR spectra were recorded on a Varian Mercury 200 MHz spectrometer. UV/Visible spectra and kinetic measurements were made at 25 °C using a Perkin Elmer Lambda 2 spectrophotometer, or an Applied Photophysics SX-17 MV stopped-flow spectrophotometer.

4.3 Results and Discussion

The reactions of 4-nitrobenzofurazan, **4.4**, and 4-nitrobenzofuroxan, **4.5**, with six aliphatic amines in DMSO are discussed. There is NMR evidence that the thermodynamically stable adducts result from reaction at the 7-position. The kinetic studies show that there are two adduct-forming reactions, and these are likely to occur according to Scheme 4.4.



RR'NH

- a Piperidine
- b Pyrrolidine
- c Morpholine
- d n-Butylamine
- e Benzylamine
- f N-Methylbenzylamine

Scheme 4.4

4.3.1 NMR Data

^1H NMR spectra of **4.4** and **4.5** in the presence of a four-fold excess of amine in $[\text{}^2\text{H}_6]$ DMSO were recorded immediately after mixing. The shifts indicate the formation of the thermodynamically stable adducts **4.12** and **4.16**, as these are similar to those measured for attack of methoxide to give 7-adducts.⁹ The data summarised in Tables 4.1 and 4.2 show that for the adducts **4.12** and **4.16**, spin-coupled resonances are observed for H_7 at approximately 4.6 ppm, for H_6 at around 5.0 ppm and for H_5 at approximately 7.0 ppm.

Figure 4.1 shows that in adducts formed from **4.4**, rotation is slow about the nitrogen to α -carbon bond in the added amine. For example, in the spectrum of the adduct **4.12f**, formed from N-methylbenzylamine, the methylene hydrogens give an AB quartet at 3.36 and 3.63 ppm, with a coupling constant, $J = 13.2$ Hz. This phenomena is also observed for adducts formed from **4.5**. For example, in **4.16e**, the adduct from NBF and benzylamine, the methylene hydrogens give an AB quartet with chemical shifts, 3.41 and 3.61 ppm and a coupling constant, $J = 13.4$ Hz. In a related manner in the piperidine adduct, **4.16a**, the two methylene groups adjacent to nitrogen give distinct multiplets at 2.2 and 2.5 ppm.

Figure 4.1: ^1H NMR spectrum of the adduct **4.12f**, formed from reaction of NBZ, **4.4**, 0.05 mol dm^{-3} with N-methylbenzylamine, 0.20 mol dm^{-3} , in $[\text{}^2\text{H}_6]$ DMSO.

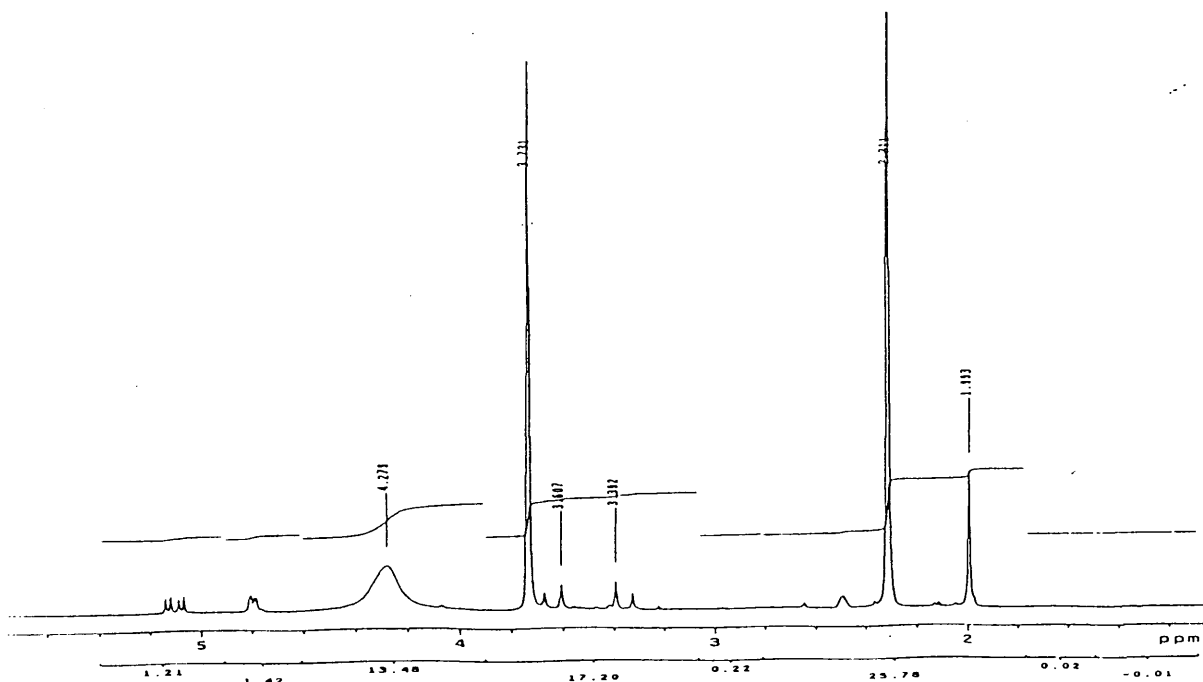


Table 4.1: ^1H NMR data^a for 4-nitrobenzofurazan, **4.4**, and adducts **4.12**, formed at the 7-position, in [$^2\text{H}_6$] DMSO.

	^1H NMR Shifts			J_{56}	J_{67}	Other ^b
	H_5	H_6	H_7			
4.4	8.68	7.84	8.59	7.3	8.8	
4.12a	7.06	5.02	4.65	10.3	4.4	2.56 (2H), 2.07 (2H), 1.30 (6H)
4.12b	7.01	5.10	4.84	10.2	4.2	2.68 (2H), 2.26 (2H), 1.6 (4H)
4.12c	7.10	5.04	4.73	10.3	4.4	3.51 (4H), 2.62 (2H), 2.12 (2H)
4.12d	6.93	5.07	4.61	10.4	4.2	2.37 (1H), 2.32 (1H), 1.35 (4H), 0.80 (3H)
4.12e	6.97	5.12	4.61	10.3	4.1	4.76 (NH), 3.82 (1H), 3.65 (1H)
4.12f	7.12	5.12	4.79	10.4	4.1	3.60 (1H), 3.40 (1H), 2.0 (NMe)

^a J values in Hz.

^b Non-equivalence is observed for hydrogen atoms on the carbon atom(s) α to nitrogen in the adducts.

Table 4.2: ^1H NMR data^a for 4-nitrobenzofuroxan, **4.5**, and adducts **4.16**, formed at the 7-position, in [$^2\text{H}_6$] DMSO.

	^1H NMR Shifts			J_{56}	J_{67}	Other ^b
	H_5	H_6	H_7			
4.5	8.61	7.53	8.13	7.3	8.9	
4.16a	6.94	4.92	4.47	10.2	4.4	2.5 (2H), 2.2 (2H), 1.3 (6H)
4.16b	6.99	5.03	4.73	10.4	4.6	2.6 (2H), 2.4 (2H), 1.6 (4H)
4.16c	7.04	5.00	4.61	10.4	4.4	3.48 (4H), 2.60 (2H), 2.35 (2H)
4.16d	6.93	4.94	4.62	10.4	4.4	2.35 (1H), 2.15 (1H), 1.40 (4H), 0.82 (3H)
4.16e	6.99	5.00	4.71	10.2	4.2	4.95 (NH), 3.61 (1H), 3.41 (1H)
4.16f	7.09	5.14	4.73	10.4	4.4	3.59 (2H), 2.05 (NMe)

^a J values in Hz.

^b Non-equivalence is observed for hydrogen atoms on the carbon atom(s) α to nitrogen in the adducts.

Table 4.3 gives the ^1H NMR chemical shifts for methoxide adducts formed from reaction of NBZ, 4.4, and NBF, 4.5.⁹ Comparison with this data shows that the spectra obtained are not compatible with the formation of 4.10 or 4.14, where H_6 is expected to be considerably less shielded than is observed in Tables 4.1 and 4.2.

Table 4.3: ^1H NMR data for methoxide adducts⁹ formed from NBZ, 4.4, and NBF, 4.5.

Compound	Temperature / °C	^1H NMR Shifts				
		H_5	H_6	H_7	J_{56}	J_{67}
4.4 ^a	+37	8.70	7.88	8.60	7.2	9.0
4.4 (5-adduct) ^b	-20	5.50	6.53	7.02	5.0	10.0
4.4 (7-adduct) ^b	-20	7.17	5.29	5.37	10.0	4.4
4.5 ^a	+37	8.62	7.55	8.12	7.2	9.0
4.6 ^b	-20	5.47	6.38	6.65	5.0	10.0
4.7 ^b	-20	7.17	5.23	5.33	10.3	4.4

^a Measured in [$^2\text{H}_6$]DMSO.

^b Measured in 30/70 (v/v) [$^2\text{H}_3$]MeOH/[$^2\text{H}_6$]DMSO.

The NMR spectra show that the initial formation of σ -adducts is followed by slow, irreversible decomposition reactions which were not investigated.

4.3.2 Kinetic Data

All kinetic measurements were made by stopped-flow spectrophotometry and generally showed two rate processes associated with σ -adduct formation. These two processes may be attributed to the rapid formation of the 5-adducts, **4.10** or **4.14**, followed by slower formation of the thermodynamically more stable 7-adducts, **4.12** or **4.16**. The UV absorption maxima of **4.4** and **4.5** are 324 nm and 414 nm respectively. Data for the parent electrophiles and adducts formed are given in Table 4.4.

Table 4.4: Absorbance data for adduct^a formation in DMSO.

	$\lambda_{\text{max}} / \text{nm}$	Absorbance	$\epsilon / \text{dm}^3 \text{mol}^{-1} \text{cm}^{-1}$
4.4	324	0.29	7×10^3
4.12	344 (shoulder at 380)	0.60	1.5×10^4
4.5	414	0.32	8×10^3
4.16	350 (shoulder at 400)	0.60	1.5×10^4

^a Substrate concentration, $4 \times 10^{-5} \text{ mol dm}^{-3}$.

Therefore, for reactions involving NBZ, **4.4**, kinetic measurements were made at 344 nm, while for NBF, **4.5**, measurements were made at 350 nm.

In general, reactions were carried out in solutions of the amine, buffered with the hydrochloride or perchlorate salt. The buffer solutions were in large excess over the substrate concentration to ensure first order conditions. For reactions with amines in the absence of added amine salts, a sufficient excess of amine was used to ensure >95% conversion to adducts at equilibrium.

The zwitterionic species, **4.9** and **4.13**, were treated as steady state intermediates, leading to the general rate expression for reaction at the 5-position to give **4.10** and **4.14**, Equation 4.1.

$$\text{Equation 4.1: } k_{\text{fast}} = \frac{k_5 k_{\text{Am}} [\text{Am}]^2 + k_{-5} k_{\text{AmH}^+} [\text{AmH}^+]}{k_{-5} + k_{\text{Am}} [\text{Am}]}$$

The full derivation of this equation can be found in Section 8.2. Equation 4.1 may be simplified by considering two limiting cases:

1) If proton transfer from the zwitterions, **4.9** and **4.13** is slow compared to reversal to reactants, $k_{-5} \gg k_{\text{Am}} [\text{Am}]$, and Equation 4.1 reduces to Equation 4.2.

$$\text{Equation 4.2: } k_{\text{fast}} = \frac{k_5 k_{\text{Am}} [\text{Am}]^2}{k_{-5}} + k_{\text{AmH}^+} [\text{AmH}^+]$$

2) If proton transfer from the zwitterions, **4.9** and **4.13** is rapid compared to reversal to reactants, $k_{\text{Am}} [\text{Am}] \gg k_{-5}$, and Equation 4.1 reduces to Equation 4.3.

$$\text{Equation 4.3: } k_{\text{fast}} = k_5 [\text{Am}] + \frac{k_{-5} k_{\text{AmH}^+} [\text{AmH}^+]}{k_{\text{Am}} [\text{Am}]}$$

The overall equilibrium constant for formation of the 5-adduct is defined in Equation 4.4, for the reaction of **4.4** with amine.

$$\text{Equation 4.4: } K_{\text{C},5} = \frac{[\text{4.10}][\text{AmH}^+]}{[\text{4.4}][\text{Am}]^2} = \frac{k_5 k_{\text{Am}}}{k_{-5} k_{\text{AmH}^+}}$$

In most cases, values of k_{fast} were high, and close to the limit of detection by the stopped-flow method. Also, particularly in the presence of amine salts, amplitudes were low. Therefore, only limited measurements of k_{fast} were possible.

The rate expression for the formation of 7-adducts, **4.12** and **4.16**, from **4.4** and **4.5** respectively, is given by Equation 4.5.

$$\text{Equation 4.5: } k_{\text{slow}} = \frac{k_7 k_{\text{Am}} [\text{Am}]^2}{k_{-7} + k_{\text{Am}} [\text{Am}]} + \frac{k_{-7} k_{\text{AmH}^+} [\text{AmH}^+]}{k_{-7} + k_{\text{Am}} [\text{Am}]}$$

However, the equilibration of the 7-adducts with the substrates occurs in the presence of the initially formed 5-adducts, and so the term for the forward reaction in Equation 4.5 must be modified to give Equation 4.6.

$$\text{Equation 4.6: } k_{\text{slow}} = \frac{k_7 k_{\text{Am}} [\text{Am}]^2}{(k_{-7} + k_{\text{Am}} [\text{Am}]) \left(1 + \frac{K_{\text{C},s} [\text{Am}]^2}{[\text{AmH}^+]} \right)} + \frac{k_{-7} k_{\text{AmH}^+} [\text{AmH}^+]}{k_{-7} + k_{\text{Am}} [\text{Am}]}$$

If proton transfer from the zwitterions, **4.11** or **4.15** is slow, corresponding to the condition, $k_{-7} \gg k_{\text{Am}} [\text{Am}]$, Equation 4.6 reduces to Equation 4.7.

$$\text{Equation 4.7: } k_{\text{slow}} = \frac{k_7 k_{\text{Am}} [\text{Am}]^2}{k_{-7} \left(1 + \frac{K_{\text{C},s} [\text{Am}]^2}{[\text{AmH}^+]} \right)} + k_{\text{AmH}^+} [\text{AmH}^+]$$

If proton transfer from the zwitterions, **4.11** or **4.15** is rapid, corresponding to the condition, $k_{\text{Am}} [\text{Am}] \gg k_{-7}$, Equation 4.6 reduces to Equation 4.8.

$$\text{Equation 4.8: } k_{\text{slow}} = \frac{k_7 [\text{Am}]}{\left(1 + \frac{K_{\text{C},s} [\text{Am}]^2}{[\text{AmH}^+]} \right)} + \frac{k_{-7} k_{\text{AmH}^+} [\text{AmH}^+]}{k_{\text{Am}} [\text{Am}]}$$

The overall equilibrium constant for the formation of the 7-adduct is defined in Equation 4.9, for reaction of **4.4** with amine.

$$\text{Equation 4.9: } K_{\text{C},7} = \frac{[\text{4.12}][\text{AmH}^+]}{[\text{4.4}][\text{Am}]^2} = \frac{k_7 k_{\text{Am}}}{k_{-7} k_{\text{AmH}^+}}$$

In general, for a given amine, the rate constants, k_{Am} and k_{AmH^+} will have different values for formation of the 5- and 7-adducts.

In order to obtain the maximum kinetic information it was necessary to make rate measurements at different concentrations of amine salt. Measurements were made at low,

$\leq 0.01 \text{ mol dm}^{-3}$, salt concentration, and also at higher, 0.10 mol dm^{-3} concentrations using perchlorate and/or hydrochloride salts.

Previous workers have obtained evidence for the association of chloride ions with substituted ammonium ions, to yield complexes $\text{RR}'\text{NH}_2^+ \cdots \text{Cl}^-$, in which the activities of the ammonium ions are reduced.^{16,17} The expected effect of a 0.1 mol dm^{-3} chloride concentration^{18,17,5} is to increase values of $K_{C,5}$ and $K_{C,7}$ by a factor of 2. The main effect on rate constants is expected to be an approximate two-fold lowering of the k_{AmH^+} values.

4.3.2.1 Reactions of Piperidine

Data are reported in Tables 4.5 and 4.6 for the reactions of **4.4**, (NBZ) and **4.5**, (NBF) with piperidine. The formation of the 5-adducts **4.10** and **4.14** was studied in the absence of piperidine salt. As there was no salt present, the reverse reaction made a negligible contribution to the rate expression defined in Equation 4.1, and Equation 4.10 was found to give a better fit for the data, where $K_5 = k_5/k_{-5}$.

$$\text{Equation 4.10: } k_{\text{fast}} = \frac{K_5 k_{\text{Am}} [\text{Am}]^2}{1 + \frac{k_{\text{Am}} [\text{Am}]}{k_{-5}}}$$

Values of $K_5 k_{\text{Am}}$, $3.6 \times 10^7 \text{ dm}^6 \text{ mol}^{-2} \text{ s}^{-1}$ and k_{Am}/k_{-5} , $560 \text{ dm}^3 \text{ mol}^{-1}$ for the reaction with **4.4**, gave a k_5 value of $6.4 \times 10^4 \text{ dm}^3 \text{ mol}^{-1} \text{ s}^{-1}$, Table 4.5. The corresponding values for reaction with **4.5**, $K_5 k_{\text{Am}}$, $1.7 \times 10^7 \text{ dm}^6 \text{ mol}^{-2} \text{ s}^{-1}$ and k_{Am}/k_{-5} , $100 \text{ dm}^3 \text{ mol}^{-1}$, led to a value of $1.7 \times 10^5 \text{ dm}^3 \text{ mol}^{-1} \text{ s}^{-1}$ for k_5 , Table 4.6.

It was found that values of k_{slow} , measured in the presence of piperidine salt were correlated by Equation 4.8. This allowed the calculation of values for $K_{C,5}$. The values obtained at low salt concentration are $5.8 \text{ dm}^3 \text{ mol}^{-1}$ for reaction with NBZ and $27 \text{ dm}^3 \text{ mol}^{-1}$ for reaction with NBF. These values enabled calculation of k_{AmH^+} values of $6.2 \times 10^6 \text{ dm}^3 \text{ mol}^{-1} \text{ s}^{-1}$ and $6.3 \times 10^5 \text{ dm}^3 \text{ mol}^{-1} \text{ s}^{-1}$ respectively, according to Equation 4.4.

The rate data for the slow reaction give a much better fit with Equation 4.8 than with Equation 4.7. This indicates that proton transfer from the zwitterionic intermediates, **4.11** and **4.15** is rapid, and $k_{\text{Am}}[\text{Am}] \gg k_{-7}$. The observed and calculated rate constants for the reaction with NBZ, **4.4**, are shown graphically in Figure 4.2.

Values of $K_{C,7}$ for the reaction of **4.4** with piperidine in the presence of 0.001 and 0.01 mol dm^{-3} piperidine perchlorate, were obtained from combination of the respective k_7 and $k_{-7}k_{\text{AmH}^+}/k_{\text{Am}}$ values according to Equation 4.9. The values were found to increase with increasing piperidine perchlorate, and were 4500 and 11300 $\text{dm}^3 \text{ mol}^{-1}$ in 0.001 and 0.01 mol dm^{-3} amine salt.

Similar treatment of the data for reaction of **4.5** at $0.005 \text{ mol dm}^{-3}$ salt concentration, gave a value for $K_{C,7}$ of $(1.8 \pm 0.4) \times 10^4 \text{ dm}^3 \text{ mol}^{-1}$. With 0.1 mol dm^{-3} piperidine hydrochloride, formation of **4.14** was sufficiently inhibited that Equation 4.8 reduced to Equation 4.11.

$$\text{Equation 4.11: } k_{\text{slow}} = k_7[\text{Am}] + \frac{k_{-7}k_{\text{AmH}^+}[\text{AmH}^+]}{k_{\text{Am}}[\text{Am}]}$$

The values for k_7 $2600 \pm 200 \text{ dm}^3 \text{ mol}^{-1} \text{ s}^{-1}$ and $k_{-7}k_{\text{AmH}^+}/k_{\text{Am}}$ $0.07 \pm 0.01 \text{ s}^{-1}$ led to a value for $K_{C,7}$ of $(3.7 \pm 0.5) \times 10^4 \text{ dm}^3 \text{ mol}^{-1}$.

Data are also given in Table 4.6 for the reaction of NBF and piperidine, in solutions containing a range of piperidine hydrochloride concentrations, where the ionic strength is maintained using tetra-*n*-butylammonium chloride. This data enabled a study of the variation of $k_{\text{AmH}^+}k_{-7}/k_{\text{Am}}$ with piperidine hydrochloride concentration, using Equation 4.11.

Figure 4.2: The observed (■) and calculated (-) rate constants for the reaction of NBZ, **4.4**, with piperidine (in the presence of $0.001 \text{ mol dm}^{-3}$ piperidine perchlorate) in DMSO.

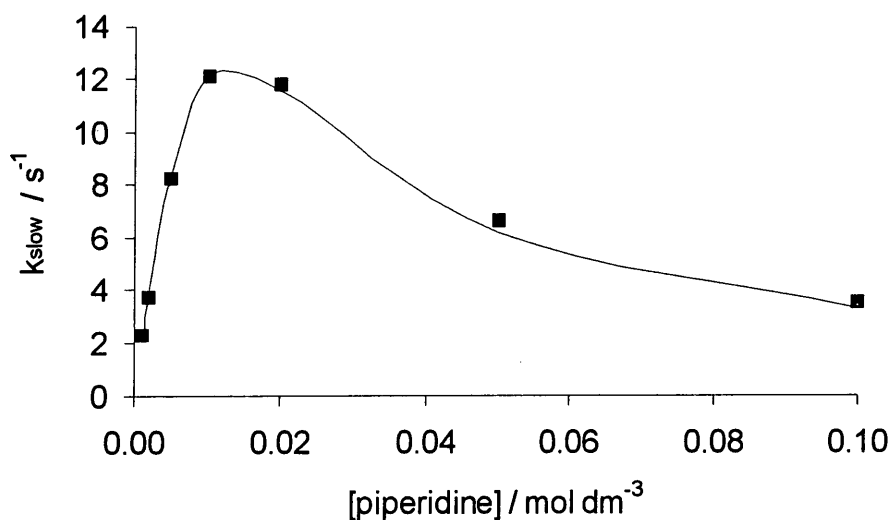


Table 4.5: Kinetic data for the reaction of **4.4**^a with piperidine, in DMSO at 25 °C.

[Piperidine] / mol dm ⁻³	[PiperidineH ⁺ ClO ₄ ⁻] / mol dm ⁻³	k _{fast} / s ⁻¹	k _{calc} ^b / s ⁻¹	k _{slow} / s ⁻¹	k _{calc} ^c / s ⁻¹
0.001	0	23	23		
0.002	0	72	68		
0.005	0	225	236		
0.01	0	543	543		
0.001	0.001			2.3	2.3
0.002	0.001			3.7	3.9
0.005	0.001			8.2	8.4
0.01	0.001			12.1	12.2
0.02	0.001			11.8	11.6
0.05	0.001			6.6	6.2
0.10	0.001			3.5	3.3
0.001	0.01			3.4	3.4
0.002	0.01			4.4	4.4
0.005	0.01			9.3	9.2
0.01	0.01			17.7	17.0
0.02	0.01			28.1	27.3
0.05	0.01			29.7	29.8
0.10	0.01			19.8	19.8

^a concentration of **4.4**, 4×10^{-5} mol dm⁻³.

^b Calculated from Equation 4.10 with K_5k_{Am} , 3.6×10^7 dm⁶ mol⁻² s⁻¹, and k_{Am}/k_{-5} , 560 dm³ mol⁻¹.

^c Calculated from Equation 4.8, with k_7 , 1900 dm³ mol⁻¹ s⁻¹, $K_{C,5}$, 5.8 dm³ mol⁻¹ and $k_7k_{AmH^+}/k_{Am}$, 0.42 s⁻¹, for 0.001 mol dm⁻³ salt concentration, and with k_7 , 1800 dm³ mol⁻¹ s⁻¹, $K_{C,5}$, 8.1 dm³ mol⁻¹ and $k_7k_{AmH^+}/k_{Am}$, 0.16 s⁻¹, for 0.01 mol dm⁻³ salt concentration.

Table 4.6: Kinetic data for the reaction of **4.5**^a with piperidine, in DMSO at 25 °C.

[Piperidine] / mol dm ⁻³	[PiperidineH ⁺ Cl ⁻] / mol dm ⁻³	$k_{\text{fast}}^b / \text{s}^{-1}$	$k_{\text{calc}}^c / \text{s}^{-1}$	$k_{\text{slow}} / \text{s}^{-1}$	$k_{\text{calc}}^d / \text{s}^{-1}$
0.002	0	62	57		
0.004	0	200	190		
0.006	0	380	380		
0.008	0	620	600		
0.010	0	800	850		
0.001	0.1			9.8	9.6
0.002	0.1			9.1	8.7
0.004	0.1			12.1	12.1
0.007	0.1			19.4	19.2
0.010	0.1			26.6	26.7
0.001	0.06 ^e			5.7	5.8
0.001	0.04 ^e			4.3	5.2
0.001	0.02 ^e			3.1	4.0
0.002	0.02 ^e			5.5	5.9
0.001	0.06			8.0	
0.001	0.04			6.7	
0.001	0.02			5.2	
0.002	0.02			6.6	
0.002	0.005			6.0	6.1
0.003	0.005			8.6	8.6
0.004	0.005			11.1	10.9
0.006	0.005			14.4	14.5
0.008	0.005			17.1	17.1
0.010	0.005			18.9	18.9

^a concentration of **4.5**, 2×10^{-5} mol dm⁻³.

^b Where no value is given, rate constants were too high for measurement.

^c Calculated from Equation 4.10 with $K_5 k_{\text{Am}}$, 1.7×10^7 dm⁶ mol⁻² s⁻¹, and k_{Am}/k_{-5} , 100 dm³ mol⁻¹.

^d Calculated from Equations 4.8, with k_7 , $2900 \pm 300 \text{ dm}^3 \text{ mol}^{-1} \text{ s}^{-1}$, $K_{C,5}$, $27 \pm 5 \text{ dm}^3 \text{ mol}^{-1}$ and $k_7 k_{AmH^+}/k_{Am}$, 0.16 s^{-1} , for $0.005 \text{ mol dm}^{-3}$ salt concentration, and 4.11 with k_7 , $2600 \pm 200 \text{ dm}^3 \text{ mol}^{-1} \text{ s}^{-1}$, and $k_7 k_{AmH^+}/k_{Am}$, $0.07 \pm 0.01 \text{ s}^{-1}$, for 0.10 mol dm^{-3} salt concentration

^e Salt concentration maintained at 0.10 mol dm^{-3} using tetra-*n*-butylammonium chloride.

4.3.2.2 Reactions of Pyrrolidine

Two processes were observed for the reaction of **4.4**, (NBZ), with pyrrolidine. The fast reaction was generally inconveniently rapid for measurement, so that only limited data could be obtained. The values in Table 4.7 show that in the absence of piperidine perchlorate, k_{fast} increases in an approximately linear way with increasing amine concentration. Hence Equation 4.12 applies and leads to a value of $2 \times 10^5 \text{ dm}^3 \text{ mol}^{-1} \text{ s}^{-1}$ for k_5 .

Equation 4.12: $k_{\text{fast}} = k_5[\text{Am}]$

Data for the slower reaction are also in Table 4.7. The values of k_{slow} , measured in 0.001 and 0.01 mol dm^{-3} amine salt, go through a maximum with increasing pyrrolidine concentration, as predicted by Equation 4.8. Combination of the k_7 and $k_7 k_{\text{AmH}^+}/k_{\text{Am}}$ values according to Equation 4.9, gave $K_{\text{C},7}$ values of $10700 \text{ dm}^3 \text{ mol}^{-1}$ for solutions containing 0.001 mol dm^{-3} pyrrolidine perchlorate. As the salt concentration was increased to 0.01 mol dm^{-3} , the $K_{\text{C},7}$ value increased to $13000 \text{ dm}^3 \text{ mol}^{-1}$.

Table 4.7: Kinetic data for the reaction of **4.4**^a with pyrrolidine, in DMSO at 25 °C.

[Pyrrolidine] / mol dm ⁻³	[PyrrolidineH ⁺ ClO ₄ ⁻] / mol dm ⁻³	k _{fast} ^b / s ⁻¹	k _{slow} / s ⁻¹	k _{calc} ^c / s ⁻¹
0.001	0	251	1.9	
0.002	0	456	2.7	
0.005	0	937	2.3	
0.01	0		1.4	
0.02	0		0.8	
0.05	0		0.4	
0.10	0		0.2	
0.001	0.001		3.1	3.3
0.002	0.001		5.6	5.9
0.005	0.001		11.6	11.8
0.01	0.001		14.3	14.3
0.02	0.001		11.1	11.1
0.05	0.001		5.3	5.3
0.10	0.001		2.7	2.7
0.001	0.01		5.3	5.3
0.002	0.01		6.5	7.1
0.005	0.01		14.2	14.8
0.01	0.01		25.5	25.8
0.02	0.01		35.6	35.6
0.05	0.01		28.5	28.3
0.10	0.01		16.0	16.5

^a concentration of **4.4**, 4×10^{-5} mol dm⁻³.

^b k₅ calculated as 2×10^5 dm³ mol⁻¹ s⁻¹, from k_{fast}/[pyrrolidine].

^c Calculated from Equation 4.8, with k₇, 3000 dm³ mol⁻¹ s⁻¹, K_{C,5}, 11 dm³ mol⁻¹ and k₋₇k_{AmH⁺}/k_{Am}, 0.28 s⁻¹, for 0.001 mol dm⁻³ salt concentration, and with k₇, 3000 dm³ mol⁻¹ s⁻¹, K_{C,5}, 17 dm³ mol⁻¹ and k₋₇k_{AmH⁺}/k_{Am}, 0.23 s⁻¹, for 0.01 mol dm⁻³ salt concentration.

4.3.2.3 Reactions of Morpholine

Morpholine is the weakest of the six amines studied (pK_a , 9.15 in DMSO¹⁹) and the presence of $0.001 \text{ mol dm}^{-3}$ amine salt was sufficient to inhibit the formation of the adducts **4.10** and **4.14**. Values of k_{slow} gave a good fit with Equation 4.11. With both substrates it is possible to set a limit, $K_{C,5} < 1$, for the value of the equilibrium constant for reaction at the 5-position.

For **4.4**, (NBZ), $K_{C,7}$ values calculated from the k_7 and $k_7 k_{\text{AmH}^+}/k_{\text{Am}}$ values appending Table 4.8, were 150 and $130 \text{ dm}^3 \text{ mol}^{-1}$ in 0.001 and 0.01 mol dm^{-3} morpholine perchlorate respectively. For **4.5**, (NBF), the slow process was studied in 0.001 and 0.1 mol dm^{-3} morpholine hydrochloride, Table 4.9. In solutions containing 0.1 mol dm^{-3} amine salt it was possible to determine a $K_{C,7}$ value of $550 \text{ dm}^3 \text{ mol}^{-1}$ from the k_7 and $k_7 k_{\text{AmH}^+}/k_{\text{Am}}$ values, according to Equation 4.9. The results are shown graphically in Figure 4.3. In the presence of $0.001 \text{ mol dm}^{-3}$ morpholine hydrochloride, the final term in Equation 4.11 is negligible, and a linear dependence of k_{slow} on amine concentration was observed, Table 4.9, with a k_7 value of $250 \pm 30 \text{ dm}^3 \text{ mol}^{-1} \text{ s}^{-1}$.

Figure 4.3: The observed (■) and calculated (—) rate constants for the reaction of NBF, **4.5**, with morpholine (in the presence of 0.1 mol dm^{-3} morpholine hydrochloride) in DMSO.

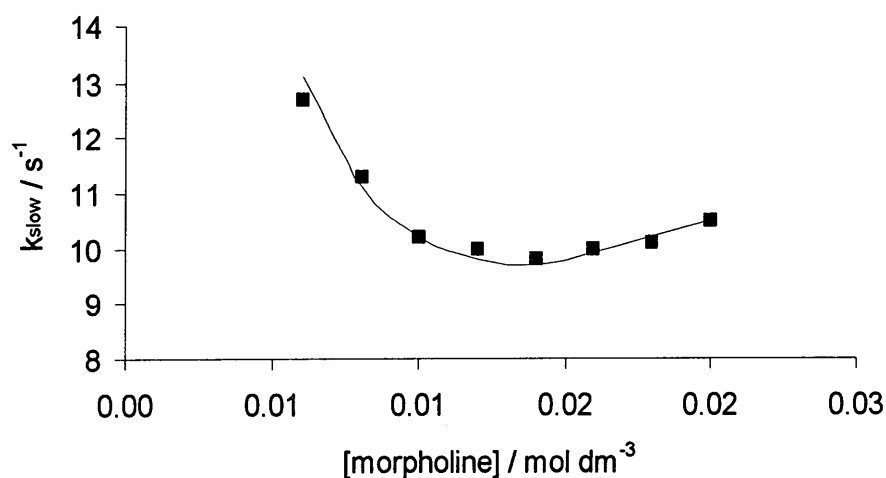


Table 4.8: Kinetic data for the reaction of **4.4**^a with morpholine, in DMSO at 25 °C.

[Morpholine] / mol dm ⁻³	[MorpholineH ⁺ ClO ₄ ⁻] / mol dm ⁻³	k _{slow} / s ⁻¹	k _{calc} ^b / s ⁻¹
0.005	0.001	1.6	1.6
0.008	0.001	2.2	2.3
0.01	0.001	2.7	2.7
0.02	0.001	5.1	5.0
0.05	0.001	10.3	10.3
0.08	0.001	12.5	12.5
0.10	0.001	12.8	12.8
0.005	0.01	4.5	4.7
0.008	0.01	4.1	4.1
0.01	0.01	4.2	4.1
0.02	0.01	5.9	5.6
0.05	0.01	12.0	12.0
0.08	0.01	19.3	19.0
0.10	0.01	23.0	23.5

^a concentration of **4.4**, 4×10^{-5} mol dm⁻³.

^b Calculated from Equation 4.11, with k_7 , 260 dm³ mol⁻¹ s⁻¹, and $k_7k_{AmH^+}/k_{Am}$, 1.7 s⁻¹, for 0.001 mol dm⁻³ salt concentration, and with k_7 , 230 dm³ mol⁻¹ s⁻¹, and $k_7k_{AmH^+}/k_{Am}$, 1.8 s⁻¹, for 0.01 mol dm⁻³ salt concentration.

Table 4.9: Kinetic data for the reaction of **4.5**^a with morpholine, in DMSO at 25 °C.

[Morpholine] / mol dm ⁻³	[MorpholineH ⁺ Cl ⁻] / mol dm ⁻³	k _{slow} / s ⁻¹	k _{calc} ^b / s ⁻¹
0.006	0.10	12.7	13.1
0.008	0.10	11.3	11.1
0.010	0.10	10.2	10.2
0.012	0.10	10.0	9.8
0.014	0.10	9.8	9.7
0.016	0.10	10.0	9.9
0.018	0.10	10.1	10.2
0.020	0.10	10.5	10.5
0.006	0.001	1.47	1.5
0.010	0.001	2.42	2.5
0.014	0.001	3.44	3.5
0.018	0.001	4.40	4.5
0.020	0.001	4.96	5.0

^a concentration of **4.5**, 2×10^{-5} mol dm⁻³.

^b Calculated from Equation 4.11, with k_7 , 250 ± 30 dm³ mol⁻¹ s⁻¹, and $k_7k_{AmH^+}/k_{Am}$, 0 s⁻¹, for 0.001 mol dm⁻³ salt concentration, and with k_7 , 360 ± 60 dm³ mol⁻¹ s⁻¹, and $k_7k_{AmH^+}/k_{Am}$, 0.66 ± 0.06 s⁻¹, for 0.10 mol dm⁻³ salt concentration.

4.3.2.4 Reactions of n-Butylamine

It was possible to measure two rate processes for the reactions of both **4.4**, (NBZ) and **4.5**, (NBF) with n-butylamine. Analysis of the data in Tables 4.10 and 4.11 indicates that the proton transfer equilibria between zwitterionic intermediates and anionic adducts are rapid. The data for the initial, fast process were fitted to Equation 4.3. For the reaction of **4.4** measurements were made with either no added salt, or with $1 \times 10^{-3} \text{ mol dm}^{-3}$ salt. One set of parameters was found to fit the data adequately. Use of Equation 4.4 gave a value for $K_{C,5}$ of $23 \text{ dm}^3 \text{ mol}^{-1}$. For **4.5** where measurements were also made at $1 \times 10^{-2} \text{ mol dm}^{-3}$ salt concentration, it was found that significantly better fits for the rate data were obtained using two sets of values. These differ only slightly and give $K_{C,5}$ values of 108 and $110 \text{ dm}^3 \text{ mol}^{-1}$ for n-butylamine hydrochloride concentrations 0.001 and 0.01 mol dm^{-3} respectively.

Equation 4.8 was used to correlate the data for the slow process. A $K_{C,5}$ value of $19 \text{ dm}^3 \text{ mol}^{-1}$ was determined for the reaction of **4.4** with n-butylamine, and compares well with the value of $23 \text{ dm}^3 \text{ mol}^{-1}$ previously determined from the data for the fast process. Combination of the k_7 and $k_{-7}k_{AmH^+}/k_{Am}$ values according to Equation 4.9, led to $K_{C,7}$ values of 1020 and $1800 \text{ dm}^3 \text{ mol}^{-1}$ in 0.001 and 0.01 mol dm^{-3} n-butylamine perchlorate solutions:

For the reaction of **4.5** with n-butylamine, a $K_{C,5}$ value of $91 \text{ dm}^3 \text{ mol}^{-1}$ was determined in 0.01 mol dm^{-3} n-butylamine hydrochloride, according to Equation 4.8. This compares favourably with the previously calculated value of $110 \text{ dm}^3 \text{ mol}^{-1}$ at this salt concentration. The $K_{C,7}$ values according to Equation 4.9 are 5800 and $13000 \text{ dm}^3 \text{ mol}^{-1}$ in 0.01 and 0.10 mol dm^{-3} n-butylamine hydrochloride.

The $K_{C,5}$ and $K_{C,7}$ values increase with increasing salt concentration for both substrates.

Table 4.10: Kinetic data for the reaction of **4.4**^a with n-butylamine, in DMSO at 25 °C.

[n-butylamine] / mol dm ⁻³	[n-butylamineH ⁺ ClO ₄ ⁻] / mol dm ⁻³	k _{fast} / s ⁻¹	k _{calc} ^b / s ⁻¹	k _{slow} / s ⁻¹	k _{calc} ^c / s ⁻¹
0.005	0	78	70		
0.01	0	146	140		
0.02	0	265	280		
0.001	0.001			0.101	0.101
0.002	0.001			0.122	0.120
0.005	0.001	185	190	0.183	0.183
0.01	0.001	201	200	0.175	0.181
0.02	0.001	313	310	0.121	0.121
0.05	0.001			0.056	0.053
0.10	0.001			0.027	0.027
0.001	0.01			0.38	0.38
0.002	0.01			0.28	0.27
0.005	0.01			0.34	0.31
0.01	0.01			0.44	0.44
0.02	0.01			0.49	0.49
0.05	0.01			0.30	0.30
0.10	0.01			0.15	0.17

^a concentration of **4.4**, 4×10^{-5} mol dm⁻³.

^b Calculated from Equation 4.3 with k_5 , 1.4×10^4 dm³ mol⁻¹ s⁻¹, and $k_{-5}k_{AmH^+}/k_{Am}$, 600 s⁻¹.

^c Calculated from Equation 4.8, with k_7 , 51 dm³ mol⁻¹ s⁻¹, $K_{C,5}$, 19 dm³ mol⁻¹ and $k_{-7}k_{AmH^+}/k_{Am}$, 0.05 s⁻¹, for 0.001 mol dm⁻³ salt concentration, and with k_7 , 54 dm³ mol⁻¹ s⁻¹, $K_{C,5}$, 32 dm³ mol⁻¹ and $k_{-7}k_{AmH^+}/k_{Am}$, 0.03 s⁻¹, for 0.01 mol dm⁻³ salt concentration.

Table 4.11: Kinetic data for the reaction of **4.5**^a with n-butylamine, in DMSO at 25 °C.

[n-butylamine] / mol dm ⁻³	[n-butylamineH ⁺ Cl ⁻] / mol dm ⁻³	k _{fast} / s ⁻¹	k _{calc} ^b / s ⁻¹	k _{slow} / s ⁻¹	k _{calc} ^c / s ⁻¹
0.004	0.001	118	114		
0.006	0.001	136	136		
0.008	0.001	164	165		
0.010	0.001	195	198		
0.002	0.01			0.39	0.41
0.004	0.01			0.59	0.57
0.006	0.01	340	340	0.75	0.70
0.008	0.01	280	310	0.77	0.77
0.010	0.01	300	300	0.78	0.79
0.020	0.01	460	390	0.64	0.64
0.040	0.01	740	660	0.38	0.38
0.050	0.01	810	810	0.33	0.31
0.002	0.10			0.67	0.67
0.003	0.10			0.61	0.63
0.004	0.10			0.66	0.67
0.006	0.10			0.83	0.79
0.008	0.10			0.98	0.92
0.010	0.10			1.09	1.04
0.012	0.10			1.13	1.14
0.014	0.10			1.17	1.21
0.016	0.10			1.22	1.26

^a concentration of **4.5**, 2×10^{-5} mol dm⁻³.

^b Calculated from Equation 4.3 with k_5 , 1.8×10^4 dm³ mol⁻¹ s⁻¹, and $k_{-5}k_{\text{AmH}^+}/k_{\text{Am}}$, 166 s⁻¹, for 0.001 mol dm⁻³ salt concentration, and with k_5 , 1.6×10^4 dm³ mol⁻¹ s⁻¹, and $k_{-5}k_{\text{AmH}^+}/k_{\text{Am}}$, 145 s⁻¹, for 0.01 mol dm⁻³ salt concentration.

^c Calculated from Equation 4.8, with k_7 , 146 dm³ mol⁻¹ s⁻¹, $K_{\text{C},5}$, 91 dm³ mol⁻¹ and $k_{-7}k_{\text{AmH}^+}/k_{\text{Am}}$, 0.025 s⁻¹, for 0.01 mol dm⁻³ salt concentration, and with k_7 , 115 dm³ mol⁻¹ s⁻¹, $K_{\text{C},5}$, 205 dm³ mol⁻¹ and $k_{-7}k_{\text{AmH}^+}/k_{\text{Am}}$, 0.0088 s⁻¹, for 0.10 mol dm⁻³ salt concentration.

4.3.2.5 Reactions of Benzylamine

Data are given in Table 4.12 for the reaction of NBZ, **4.4**, with benzylamine in DMSO. A fast reaction, corresponding to the formation of **4.10** was observed in a limited number of cases. At amine concentrations $< 0.02 \text{ mol dm}^{-3}$, the amplitude of the process was too small for measurements to be made. The data were fitted according to Equation 4.3, and indicate that proton transfer is rapid in the equilibration of **4.9** and **4.10**. Combination of the k_5 and $k_5 k_{\text{AmH}^+}/k_{\text{Am}}$ values led to a $K_{\text{C},5}$ value of $1.9 \text{ dm}^3 \text{ mol}^{-1}$, according to Equation 4.4.

Data for the slow reaction gave a good fit with Equation 4.8, and combination of the k_7 and $k_7 k_{\text{AmH}^+}/k_{\text{Am}}$ values, according to Equation 4.9, gave $K_{\text{C},7}$ values of 87 and $100 \text{ dm}^3 \text{ mol}^{-1}$ in $0.001 \text{ mol dm}^{-3}$ and 0.01 mol dm^{-3} benzylamine perchlorate solutions. This further illustrates the effect of the salt concentration on the measured equilibrium constants.

$K_{\text{C},5}$ values calculated from data for the slow reaction according to Equation 4.8 and from combination of rate constants determined from the data for the fast process are $1.3 \text{ dm}^3 \text{ mol}^{-1}$ and $1.9 \text{ dm}^3 \text{ mol}^{-1}$ respectively in solutions containing $0.001 \text{ mol dm}^{-3}$ benzylamine perchlorate.

Table 4.12: Kinetic data for the reaction of 4.4^a with benzylamine, in DMSO at 25 °C.

[Benzylamine] / mol dm ⁻³	[BenzylamineH ⁺ ClO ₄ ⁻] / mol dm ⁻³	$k_{\text{fast}} / \text{s}^{-1}$	$k_{\text{calc}}^{\text{b}} / \text{s}^{-1}$	$k_{\text{slow}} / \text{s}^{-1}$	$k_{\text{calc}}^{\text{c}} / \text{s}^{-1}$
0.001	0.001			0.20	0.20
0.002	0.001			0.13	0.12
0.005	0.001			0.12	0.11
0.01	0.001			0.16	0.16
0.02	0.001	155	158	0.22	0.22
0.05	0.001	208	206	0.19	0.19
0.10	0.001	373	358	0.12	0.11
0.001	0.01			1.53	1.53
0.002	0.01			0.81	0.79
0.005	0.01			0.39	0.38
0.01	0.01			0.29	0.30
0.02	0.01			0.35	0.35
0.05	0.01			0.52	0.55
0.10	0.01			0.57	0.57

^a concentration of 4.4, $4 \times 10^{-5} \text{ mol dm}^{-3}$.

^b Calculated from Equation 4.3 with k_5 , $3.4 \times 10^3 \text{ dm}^3 \text{ mol}^{-1} \text{ s}^{-1}$, and $k_{-5}k_{\text{AmH}^+}/k_{\text{Am}}$, $1.8 \times 10^3 \text{ s}^{-1}$.

^c Calculated from Equation 4.8, with k_7 , $16 \text{ dm}^3 \text{ mol}^{-1} \text{ s}^{-1}$, $K_{\text{C},5}$, $1.30 \text{ dm}^3 \text{ mol}^{-1}$ and $k_{-7}k_{\text{AmH}^+}/k_{\text{Am}}$, 0.18 s^{-1} , for $0.001 \text{ mol dm}^{-3}$ salt concentration, and with k_7 , $14.8 \text{ dm}^3 \text{ mol}^{-1} \text{ s}^{-1}$, $K_{\text{C},5}$, $1.9 \text{ dm}^3 \text{ mol}^{-1}$ and $k_{-7}k_{\text{AmH}^+}/k_{\text{Am}}$, 0.15 s^{-1} , for 0.01 mol dm^{-3} salt concentration.

4.3.2.6 Reactions of N-Methylbenzylamine

Data are reported in Table 4.13 for the reaction of N-methylbenzylamine with NBZ, **4.4**, to produce **4.12**. The data indicate that proton transfer from **4.11** to give **4.12** is partially rate-limiting, and a good correlation was obtained from Equation 4.13, derived from Equation 4.6, where $K_7 = k_7/k_{-7}$.

$$\text{Equation 4.13: } k_{\text{slow}} = \frac{K_7 k_{\text{Am}} [\text{Am}]^2}{\left(1 + \frac{k_{\text{Am}} [\text{Am}]}{k_{-7}}\right) \left(1 + \frac{K_{\text{C},5} [\text{Am}]^2}{[\text{AmH}^+]}\right)} + \frac{k_{\text{AmH}^+} [\text{AmH}^+]}{1 + \frac{k_{\text{Am}} [\text{Am}]}{k_{-7}}}$$

Combination of the values for $K_7 k_{\text{Am}}$ and k_{Am}/k_{-7} quoted in Table 4.13 gave near constant values for k_7 of $195 \text{ dm}^3 \text{ mol}^{-1} \text{ s}^{-1}$ for solutions containing 0.001 to 0.10 mol dm^{-3} N-methylbenzylamine perchlorate. Equation 4.9 could then be used to calculate a value for $K_{\text{C},7}$. This equilibrium constant was found to increase with increasing concentration of amine perchlorate, and values are 42, 57 and $138 \text{ dm}^3 \text{ mol}^{-1}$ in solutions containing 0.001, 0.01 and 0.10 mol dm^{-3} N-methylbenzylamine perchlorate respectively. These increases are expected, since the reaction results in the formation of ionic products from neutral reagents. It is interesting that values of $K_7 k_{\text{Am}}$ and k_{Am}/k_{-7} show little dependence on salt concentration. The main change is the decrease in value of k_{AmH^+} reflecting the stabilisation of the products at higher ionic strength.

Values of $K_{\text{C},5}$ are also found to increase with increasing salt concentration. The values are relatively small, $\leq 0.1 \text{ mol dm}^{-3}$. Hence it was not possible to make kinetic measurements relating to formation of the 5-adduct.

Table 4.13: Kinetic data for the reaction of **4.4**^a with N-methylbenzylamine, in DMSO at 25 °C.

[N-Methylbenzylamine] / mol dm ⁻³	[N-MethylbenzylamineH ⁺ ClO ₄ ⁻] / mol dm ⁻³	k _{slow} / s ⁻¹	k _{calc} ^b / s ⁻¹
0.001	0.001	0.58	0.57
0.002	0.001	0.55	0.56
0.005	0.001	0.78	0.75
0.01	0.001	1.4	1.4
0.02	0.001	3.0	3.0
0.05	0.001	7.5	7.6
0.10	0.001	12.0	12.0
0.001	0.01	4.1	3.9
0.002	0.01	3.6	3.6
0.005	0.01	2.9	3.0
0.01	0.01	2.9	3.0
0.02	0.01	3.9	4.0
0.05	0.01	8.7	8.7
0.10	0.01	16.9	16.8
0.006	0.1	10.8	10.7
0.008	0.1	9.9	9.7
0.010	0.1	9.0	9.0
0.012	0.1	8.5	8.5
0.015	0.1	8.0	8.1
0.02	0.1	7.7	7.9
0.04	0.1	9.4	9.5
0.07	0.1	14.3	14.0
0.10	0.1	19.7	19.2
0.15	0.1	28.1	28.1
0.20	0.1	34.3	36.8

^a concentration of **4.4**, 4×10^{-5} mol dm⁻³.

^b Calculated according to Equation 4.13, with values of K_7k_{Am} , 2.5×10^4 dm⁶ mol⁻² s⁻¹, k_{Am}/k_{-7} , 128 dm³ mol⁻¹, $K_{C,5}$, 0.05 dm³ mol⁻¹ and k_{AmH^+} , 600 dm³ mol⁻¹ s⁻¹, in 0.001 mol

dm⁻³ amine salt, with values of K_7k_{Am} , 2.5×10^4 dm⁶ mol⁻² s⁻¹, k_{Am}/k_{-7} , 131 dm³ mol⁻¹, $K_{C,5}$, 0.06 dm³ mol⁻¹ and k_{AmH^+} , 440 dm³ mol⁻¹ s⁻¹, in 0.01 mol dm⁻³ amine salt, with values of K_7k_{Am} , 2.5×10^4 dm⁶ mol⁻² s⁻¹, k_{Am}/k_{-7} , 128 dm³ mol⁻¹, $K_{C,5}$, 0.10 dm³ mol⁻¹ and k_{AmH^+} , 180 dm³ mol⁻¹ s⁻¹, in 0.10 mol dm⁻³ amine salt.

Rate and equilibrium data are available for the reaction of the amines a-e with trinitrobenzene (TNB), **4.1**, in DMSO.^{2,17,20} In order to compare the data measured for NBZ, **4.4**, and NBF, **4.5**, in these systems with data for TNB, it was necessary to study the reaction of TNB with N-methylbenzylamine. Data are given in Table 4.14.

Table 4.14: Kinetic data for the reaction of TNB^a, **4.1**, with N-methylbenzylamine in DMSO at 25 °C.

[N-Methylbenzylamine] / mol dm ⁻³	[N-MethylbenzylamineH ⁺ ClO ₄ ⁻] / mol dm ⁻³	k_{obs} / s ⁻¹	k_{calc} / s ⁻¹
0.005	0	0.016	0.012
0.008	0	0.033	0.032
0.01	0	0.050	0.050
0.005	0.01	0.42	0.44
0.008	0.01	0.46	0.46
0.01	0.01	0.47	0.47
0.02	0.01	0.63	0.62
0.05	0.01	1.66	1.66
0.08	0.01	3.63	3.59
0.10	0.01	5.38	5.38

^a [TNB], 4×10^{-5} mol dm⁻³.

^b Calculated according to Equation 4.15, with k_1k_{Am}/k_{-1} , 495 dm⁶ mol⁻² s⁻¹ and k_{AmH^+} , 42 s⁻¹.

The reaction of N-methylbenzylamine with TNB proceeds according to Scheme 4.1. The observed first order rate constant is the sum of the terms for the forward and reverse reactions according to Equation 4.14.

$$\text{Equation 4.14: } k_{\text{obs}} = \frac{k_1 k_{\text{Am}} [\text{Am}]^2}{k_{-1} + k_{\text{Am}} [\text{Am}]} + \frac{k_{-1} k_{\text{AmH}^+} [\text{AmH}^+]}{k_{-1} + k_{\text{Am}} [\text{Am}]}$$

Previous workers have found that when reaction involves secondary amines, proton transfer from the zwitterionic intermediate **4.2**, is rate-limiting, corresponding to the condition, $k_{-1} \gg k_{\text{Am}} [\text{Am}]$, and hence Equation 4.14 reduces to Equation 4.15.

$$\text{Equation 4.15: } k_{\text{obs}} = \frac{k_1 k_{\text{Am}} [\text{Am}]^2}{k_{-1}} + k_{\text{AmH}^+} [\text{AmH}^+]$$

Kinetic measurements were made at 448 nm, (the absorption maximum for the adducts formed) in DMSO at 25 °C. The observed first order rate constants measured in the presence of 0.01 mol dm⁻³ N-methylbenzylamine perchlorate were fitted to Equation 4.15, and a $K_{\text{C},1}$ value of 11.7 dm³ mol⁻¹ was determined according to Equation 4.16.

$$\text{Equation 4.16: } K_{\text{C},1} = \frac{k_1 k_{\text{Am}}}{k_{-1} k_{\text{AmH}^+}}$$

4.4 Comparison of 4-Nitrobenzofurazan, (NBZ) and 4-Nitrobenzofuroxan, (NBF)

A summary of the results measured in DMSO is given in Table 4.15.

Table 4.15: Summary of data measured in DMSO at 25 °C.

	Piperidine	Pyrrolidine	Morpholine	n-Butylamine	Benzylamine	N-Methyl benzylamine
pK_a^a	10.85	11.06	9.15	11.12	10.16	9.30 ^b
Reaction with 4.4 ^c						
$k_5 / \text{dm}^3 \text{mol}^{-1} \text{s}^{-1}$	6.4×10^4 ^d	2×10^5 ^e		1.4×10^4 ^f	3.4×10^3 ^g	
$(k_5 k_{\text{AmH}^+} / k_{\text{Am}})$ $/ \text{s}^{-1}$	7800			600 ^f	1.8×10^3 ^g	
$K_{C,5} / \text{dm}^3 \text{mol}^{-1}$	8.1	17		23 ^f	1.9 ^g	0.06
k_{AmH^+} $/ \text{dm}^3 \text{mol}^{-1} \text{s}^{-1}$	6.2×10^6					
$k_7 / \text{dm}^3 \text{mol}^{-1} \text{s}^{-1}$	1800	3000	230	54	14.8	191
$(k_7 k_{\text{AmH}^+} / k_{\text{Am}})$ $/ \text{s}^{-1}$	0.16	0.23	1.8	0.03	0.15	3.4
$K_{C,7} / \text{dm}^3 \text{mol}^{-1}$	11300	13000	130	1800	100	57
k_{AmH^+} $/ \text{dm}^3 \text{mol}^{-1} \text{s}^{-1}$						440
Reaction with 4.5 ^{c,j}						
$k_5 / \text{dm}^3 \text{mol}^{-1} \text{s}^{-1}$	1.7×10^5			1.6×10^4		
$(k_5 k_{\text{AmH}^+} / k_{\text{Am}})$ $/ \text{s}^{-1}$	6.3×10^3			145		
$K_{C,5} / \text{dm}^3 \text{mol}^{-1}$	27	52	<1	110	4.1	<1
k_{AmH^+} $/ \text{dm}^3 \text{mol}^{-1} \text{s}^{-1}$	6.3×10^5					
$k_7 / \text{dm}^3 \text{mol}^{-1} \text{s}^{-1}$	2600	5300	300 ⁱ	146	40	340
$(k_7 k_{\text{AmH}^+} / k_{\text{Am}})$ $/ \text{s}^{-1}$	0.07	0.36	1.1 ⁱ	0.025	0.13	6.8
$K_{C,7} / \text{dm}^3 \text{mol}^{-1}$	3.7×10^4	1.5×10^4	280 ⁱ	5800	300	50
k_{AmH^+} $/ \text{dm}^3 \text{mol}^{-1} \text{s}^{-1}$						170

^a Literature values for corresponding ammonium ions.¹⁹

^b Calculated from absorbance measurements with 2,4-dinitrophenol indicator.

^c Values at 0.01 mol dm⁻³ salt concentration.

^d Calculated according to Equation 4.10, in the absence of amine salt.

^e Calculated from $k_{\text{fast}}/[\text{amine}]$ ratios, in the absence of amine salt.

^f Calculated both in the presence of $0.001 \text{ mol dm}^{-3}$ amine salt and in the absence of amine salt.

^g Calculated in the presence of $0.001 \text{ mol dm}^{-3}$ amine salt.

^h Calculated according to Equation 4.13.

ⁱ Values for 0.01 mol dm^{-3} salt concentration estimated from known values in 0.001 and 0.10 mol dm^{-3} .

^j Values for the reaction of **4.5** with pyrrolidine, benzylamine and N-methylbenzylamine, were measured by a project student, Miss J. Delaney, and are included for comparison.

The relative stabilities of the 5- and 7-adducts formed from reaction of the amines with **4.4** and **4.5** are shown in Table 4.16. The data show, in agreement with NMR results, that the 7-adducts are considerably more thermodynamically stable than the isomeric 5-adducts. The actual value of the $K_{C,7}/K_{C,5}$ ratio shown in Table 4.16, depends slightly on the nature of the amine. For the two primary amines studied, the ratio is approximately 60, for adducts formed from **4.4** and **4.5**. The $K_{C,7}/K_{C,5}$ ratio increases markedly for the secondary amines, and is as high as 1390 for the reaction of piperidine with NBZ, **4.4**. The increase in the $K_{C,7}/K_{C,5}$ ratio on going from primary to secondary amines, may be due to unfavourable steric interactions with the ortho nitro-group in the 5-adducts formed on addition of the bulkier secondary amines. Also for secondary amines, the decrease in value of the $K_{C,7}/K_{C,5}$ ratio on going from NBZ to NBF may indicate some small unfavourable steric interaction with the N-oxide function.

Nevertheless, the 5-adducts are formed more rapidly than the 7-adducts, and for some amines, the kinetics of the faster reaction were too fast for measurement by the stopped-flow method. The k_5/k_7 ratio is approximately 100, for those amines where the formation of the 5-adduct could be measured satisfactorily. Where measurable, the value of $k_5 k_{\text{AmH}^+}/k_{\text{Am}}$ is approximately 10^4 times larger than the value of $k_7 k_{\text{AmH}^+}/k_{\text{Am}}$ for the corresponding amine. The value of $k_{\text{Am}}/k_{\text{AmH}^+}$ which reflects the acidity of the adduct relative to that of the parent ammonium ion, will not be expected to vary greatly with the position of attack. Hence the data suggest that $k_5 \gg k_7$.

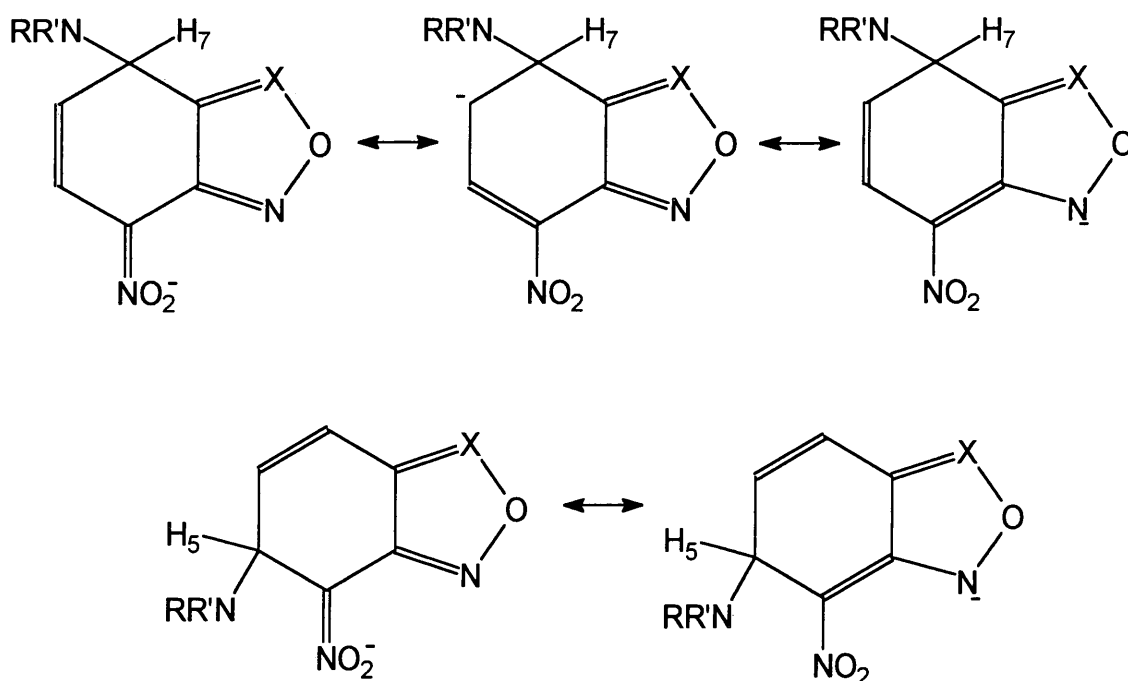
Table 4.16: The relative stability of adducts formed from NBZ, 4.4 and NBF, 4.5 in DMSO.

Amine	pK _a ^a	K _{C,5} (NBF/NBZ)	K _{C,7} (NBF/NBZ)	K _{C,7} /K _{C,5} (NBF)	K _{C,7} /K _{C,5} (NBZ)
Piperidine	10.85	3.3	1.6	670	1390
Pyrrolidine	11.06	3.0	1.2	290	750
Morpholine	9.15		2.2	>280	
n-Butylamine	11.12	4.8	3.2	53	78
Benzylamine	10.16	2.2	3.0	73	53
N-Methylbenzylamine	9.30 ^b		0.9	>50	950

^a Literature values for corresponding ammonium ions.¹⁹

^b Calculated from absorbance measurements with 2,4-dinitrophenol indicator.

A consideration of the resonance forms available for charge delocalisation in the adducts is shown in Scheme 4.5. It shows that there is a greater possibility of charge delocalisation in the 7-adducts. This will result in a greater stability, coupled with a higher kinetic barrier to formation, as predicted by Bernasconi.^{21,22,23}



Scheme 4.5

For the cyclic, secondary amines, morpholine, piperidine and pyrrolidine, there is a good correlation of the values of $K_{C,5}$ and $K_{C,7}$ with basicity, as measured by the pK_a value in DMSO. Morpholine is the least basic of these three amines, and the $K_{C,5}$ and $K_{C,7}$ values are considerably lower than those measured for pyrrolidine and piperidine. Similarly, the nucleophilicity, as measured by k_7 , follows the same pattern.

The secondary amines exhibit much larger k_7 values than the primary amines. It is not possible to correlate these values with the pK_a values of the amines in DMSO, as k_7 is a measure of nucleophilic attack at a carbon atom, while the pK_a values refer to equilibrium protonation of the nitrogen centre. For example, the value of k_7 for reaction of both substrates with pyrrolidine, is larger by a factor of around 40 than that for reaction with *n*-butylamine, an amine with a similar pK_a value. Likewise, the k_7 value for *N*-methylbenzylamine is approximately ten times greater than that for benzylamine, despite the higher proton basicity of the latter.

It is known that primary ammonium ions are particularly well stabilised in DMSO by hydrogen bonding of the NH^+ protons to the solvent. Such stabilisation may be less effective in the transition state for nucleophilic attack, where charge development is only partial. Thus the primary amines show lower nucleophilicity than expected from their basicities.

The relative stabilities of the 5- and 7-adducts of NBZ and NBF are compared in Table 4.16. The $K_{C,5}$ values are not well defined for morpholine or *N*-methylbenzylamine, due to the low basicities of these amines. $K_{C,5}(NBF)/K_{C,5}(NBZ)$ ratios are approximately 3.0 for the other amines, illustrating the slightly greater stability of the NBF-adducts compared to the NBZ-adducts.

$K_{C,7}(NBF)/K_{C,7}(NBZ)$ ratios are also around 3.0 for *n*-butylamine and benzylamine. There is very little steric hindrance to attack at this position for these amines, and the difference in the $K_{C,7}$ values is due to the greater electron-withdrawing power of the furoxan ring. The remaining amines have lower $K_{C,7}(NBF)/K_{C,7}(NBZ)$ ratios and this may be due to steric factors. As the amine becomes increasingly bulky, there may be hindrance to attack at the 7-position from the N^+-O^- bond in the furoxan ring. There may also be steric

hindrance to proton transfer as another amine molecule approaches. This effect may counteract the increased electron-withdrawing power of the furoxan ring, and $K_{C,7}(\text{NBF})/K_{C,7}(\text{NBZ})$ ratios tend to 1.0 for sterically hindered secondary amines.

4.5 Comparison with Trinitrobenzene (TNB)

A summary of the data measured for the reaction of TNB, **4.1**, with amines in DMSO is given for comparison in Table 4.17. The relative stabilities of these adducts are compared with those formed from NBZ and NBF in Table 4.18. The data in Table 4.18 show that adducts formed from NBZ or NBF at the 7-position are more stable than adducts formed from reaction at an unsubstituted position of TNB; the $K_{C,7}/K_{C,1}$ ratios are between 1.0 and 8.6. This indicates the greater ability of NBZ and NBF to delocalise negative charge and hence stabilise σ -adducts. Despite the higher thermodynamic stabilities of adducts formed from NBZ and NBF, the values of k_7 for nucleophilic attack are considerably lower than values of k_1 for reaction with TNB. This may be a consequence of the possible extensive charge delocalisation in the benzofurazan and benzofuroxan systems, which leads to higher intrinsic barriers to reaction.

Table 4.17: Summary of data measured for the reaction of amines with TNB in DMSO.

	Piperidine	Pyrrolidine	Morpholine	n-Butylamine	Benzylamine	N-Methyl benzylamine
pK_a^a	10.85	11.06	9.15	11.12	10.16	9.30 ^b
Reaction with 4.1 ^{a, b}						
$k_1 / \text{dm}^3 \text{mol}^{-1} \text{s}^{-1}$	$>2 \times 10^5$	7.5×10^5	>100	4.5×10^4	1.3×10^4	$>1 \times 10^3$
$(k_1 k_{\text{AmH}^+}/k_{\text{Am}}) / \text{s}^{-1}$	>100	210	>2.5	45	120	>100
$K_{C,1} / \text{dm}^3 \text{mol}^{-1}$	2.1×10^3	3.5×10^3	34	1×10^3	105	11.7
$k_{\text{AmH}^+} / \text{dm}^3 \text{mol}^{-1} \text{s}^{-1}$	280	3×10^3	250	6×10^4	1.5×10^4	42

^a Refer to Scheme 4.1, $K_{C,1} = k_1 k_{\text{Am}}/k_{-1} k_{\text{AmH}^+}$. Literature values measured in 0.1 mol dm^{-3} amine salt.^{2,17,20}

^b Values for the reaction of N-methylbenzylamine with TNB reported in Section 4.3.2.6.

Table 4.18: The relative stability of adducts formed from NBZ, NBF and TNB in DMSO.

Amine	k_1/k_7 (TNB/NBZ)	k_1/k_7 (TNB/NBF)	$K_{C,7}/K_{C,1}$ (NBZ/TNB)	$K_{C,7}/K_{C,1}$ (NBF/TNB)
Piperidine	110	70	5.4	8.6
Pyrrolidine	250	140	3.7	4.3
Morpholine			3.8	8.2
n-Butylamine	830	310	1.8	5.8
Benzylamine	880	325	1.0	2.9
N-Methylbenzylamine			4.9	4.3

For reaction of TNB with amines, proton transfer from the zwitterionic intermediate is generally rate-limiting for secondary amines, and may be partially rate-limiting with primary amines.² However, when NBF and NBZ react with amines, nucleophilic attack, the k_7 step, is rate-determining in the forward direction. The only exception is in the reaction with the sterically hindered amine, N-methylbenzylamine, where proton transfer becomes partially rate-determining.

Proton transfers from zwitterions to amines are thermodynamically favourable processes. Nevertheless, the values of k_{Am} for reaction with TNB are considerably below the diffusion limit. For example, k_{Am} has the value $5 \times 10^4 \text{ dm}^3 \text{ mol}^{-1} \text{ s}^{-1}$ for the reaction involving piperidine.² This may be due to steric hindrance to proton transfer between the zwitterion and the amine.

In the reactions with piperidine to give **4.10** and **4.14**, the adducts at the 5-position, it is possible to directly compare values of rate constants for proton transfer in the nitrobenzofurazan system with the TNB system. Here k_{AmH^+} has a value of $6.3 \times 10^5 \text{ dm}^3 \text{ mol}^{-1} \text{ s}^{-1}$ for the NBF adduct, $6.2 \times 10^6 \text{ dm}^3 \text{ mol}^{-1} \text{ s}^{-1}$ for the NBZ adduct, and $280 \text{ dm}^3 \text{ mol}^{-1} \text{ s}^{-1}$ for the adduct formed from TNB. Although these values refer to proton transfers from piperidinium ions to the anionic adducts, they will largely reflect the steric situation at the reaction centre. This illustrates that there is much less steric hindrance to proton transfer in reactions involving NBZ and NBF, than for TNB, where reaction occurs ortho to two nitro-groups. Further evidence comes from a comparison of the $k_7 k_{AmH^+}/k_{Am}$

values with $k_{-1}k_{\text{AmH}^+}/k_{\text{Am}}$. The values for the parameter for reaction at the 7-positions of NBZ and NBF are considerably lower than that for reaction with TNB. This indicates that the values of k_{-7} are likely to be considerably lower than the values of k_{-1} .

The differences in the rate constants for the individual reaction steps may be used to explain the observed difference in the rate-determining step between reactions involving NBZ and NBF with those involving TNB. This is likely to be a consequence of higher rate constants for proton transfer with NBZ and NBF, and also a reduction in the value of k_{-7} relative to k_{-1} . Hence the condition $k_{\text{Am}}[\text{Am}] > k_{-7}$ is more likely to apply.

In the reactions of NBZ and NBF with N-methylbenzylamine, large steric effects are likely due to the bulky nature of the secondary amine. Hence values of k_{Am} and k_{AmH^+} will be reduced, leading to partially rate-limiting proton transfer in the formation of both the 5-adduct and the 7-adduct.

4.6 Conclusion

A study of σ -adduct formation in reactions of NBZ and NBF with amine nucleophiles has highlighted important differences in the rate-determining step, in comparison with reactions involving the benchmark electrophile, TNB. For NBZ and NBF, steric effects are less pronounced and proton transfer from the zwitterionic intermediates is rapid. The only exception occurs for N-methylbenzylamine, where the proton transfer step is partially rate-limiting. In reactions with TNB, the proton transfer step is generally rate-limiting.

The investigation has also provided evidence for the initial, rapid formation of adducts at the 5-position of NBZ and NBF, followed by slower isomerisation to the thermodynamically more stable 7-adducts.

4.7 References

- ¹ C. F. Bernasconi, M. C. Muller and P. Schmid., *J. Org. Chem.*, 1979, **44**, 3189.
- ² M. R. Crampton and B. Gibson., *J. Chem. Soc., Perkin Trans. 2.*, 1981, 533.
- ³ E. Buncl and W. Eggimann., *J. Am. Chem. Soc.*, 1977, **99**, 5958.
- ⁴ R. A. Chamberlin, M. R. Crampton and I. A. Robotham., *J. Phys. Org. Chem.*, 1996, **9**, 152.
- ⁵ M. R. Crampton, P. J. Routledge and P. Golding., *J. Chem. Soc., Perkin Trans. 2.*, 1984, 329.

-
- ⁶ F. Terrier, A-P. Chatrousse and F. Millot., *J. Org. Chem.*, 1980, **45**, 2666.
⁷ R. A. Manderville and E. Buncel., *J. Chem. Soc., Perkin Trans. 2.*, 1993, 1887.
⁸ E. Buncel, N. Chuaqui-Offermans, B. K. Hunter and A. R. Norris., *Can. J. Chem.*, 1977, **55**, 2852.
⁹ F. Terrier, F. Millot, A-P. Chatrousse, M-J. Pouet and M-P. Simonnin., *Org. Mag. Res.*, 1976, **8**, 56.
¹⁰ L. Di Nunno, S. Florio and P. E. Todesco., *J. Chem. Soc., Perkin Trans. 2.*, 1975, 1469.
¹¹ D. W. S. Latham, O. Meth-Cohn and H. Suschitzky., *J. Chem. Soc., Perkin Trans. 1.*, 1976, 2216.
¹² E. Buncel, N. Chuaqui-Offermans and A. R. Norris., *J. Chem. Soc., Perkin Trans. 1.*, 1977, 415.
¹³ G. Ah-Kow., *C. R. Hebd Seances., Acad. Sci. Ser. C.*, 1978, 231.
¹⁴ P. Drost., *Justus Liebigs Ann. Chem.*, 1899, **307**, 49.
¹⁵ P. B. Ghosh and M. W. Whitehouse., *J. Med. Chem.*, 1968, **11**, 305.
¹⁶ E. Buncel and W. Eggimann., *J. Chem. Soc., Perkin Trans. 2.*, 1978, 673.
¹⁷ M. R. Crampton and C. Greenhalgh., *J. Chem. Soc., Perkin Trans. 2.*, 1983, 1175.
¹⁸ M. R. Crampton and P. J. Routledge., *J. Chem. Soc., Perkin Trans. 2.*, 1984, 573.
¹⁹ M. R. Crampton and I. A. Robotham., *J. Chem. Res. (S)*, 1997, 22.
²⁰ R. A. Chamberlin, M. R. Crampton and I. A. Robotham., *J. Phys. Org. Chem.*, 1996, **9**, 152.
²¹ C. F. Bernasconi., *Pure Appl. Chem.*, 1982, 2335.
²² C. F. Bernasconi., *Acc. Chem. Res.*, 1987, **20**, 301.
²³ C. F. Bernasconi., *Adv. Phys. Org. Chem.*, 1992, **27**, 119.

Chapter 5

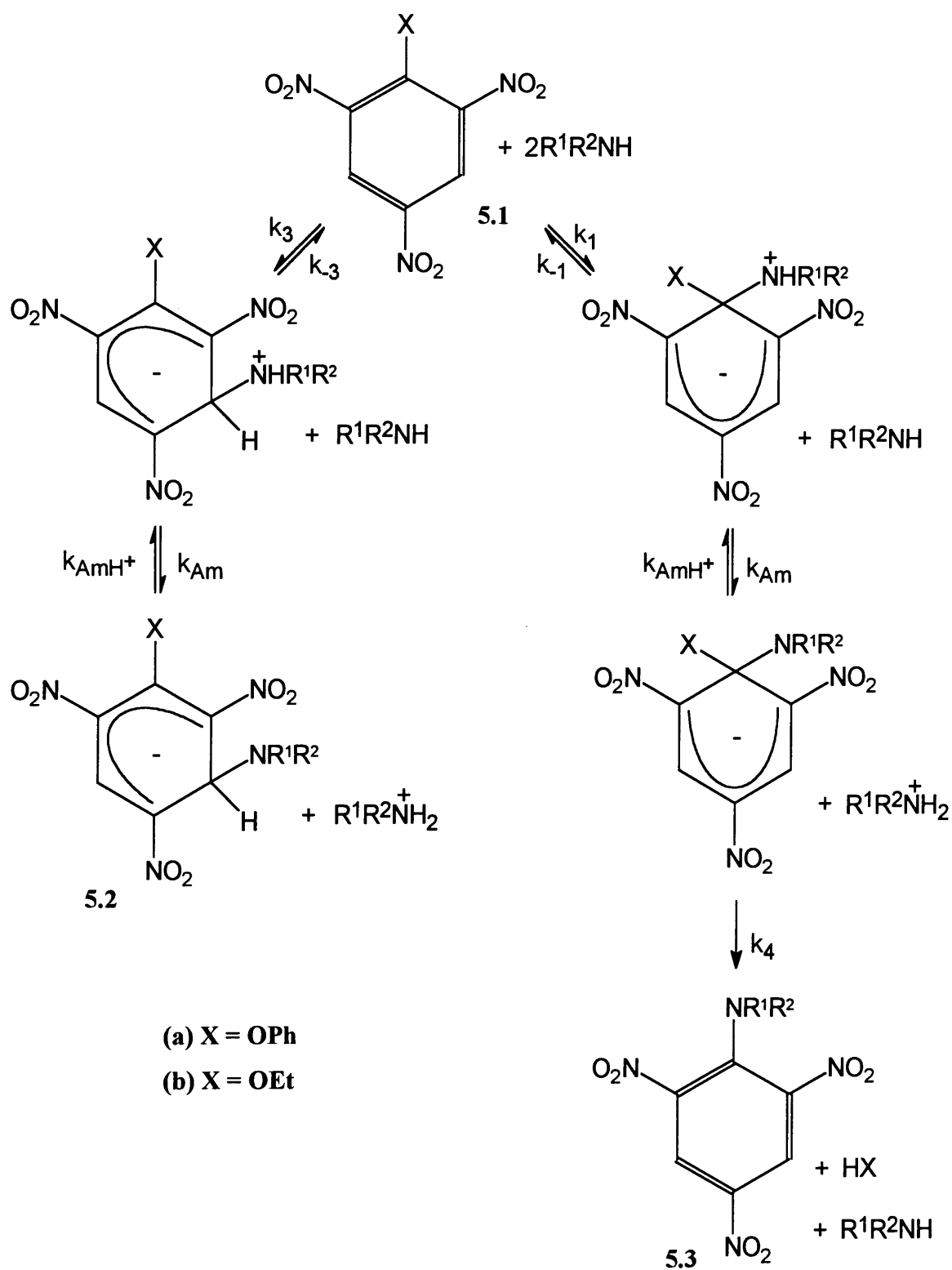
The Reactions of 4-Nitro-7-X-Benzofurazans with Amines in DMSO

5 The Reactions of 4-Nitro-7-X-Benzofurazans with Amines in DMSO

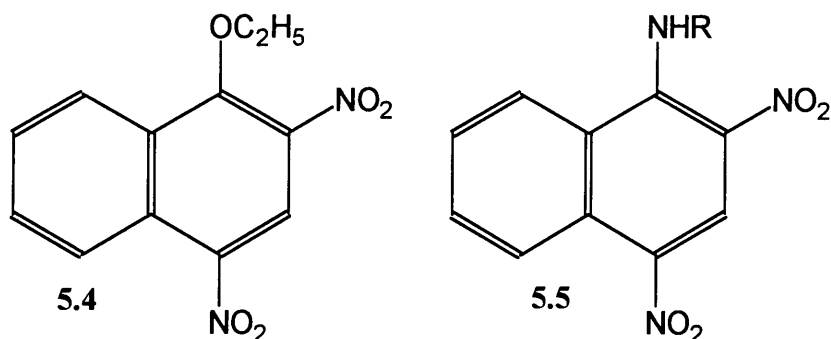
5.1 Introduction

The general pattern of regioselectivity in the reaction of nucleophiles with 1-X-2,4,6-trinitrobenzenes, **5.1**,^{1,2} has been considered to be the formation of a kinetically preferred 1,3-adduct that isomerises to a more thermodynamically stable 1,1-adduct. For example, the reaction of **5.1** with aliphatic amines in DMSO occurs in two stages. A rapid reaction is observed, corresponding to the formation of the 3-adduct, **5.2**, while a second, much slower reaction results in the substitution of the leaving group, X, to yield **5.3**.^{3,4}

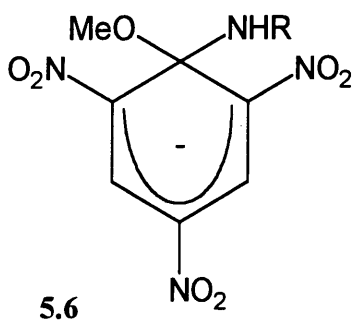
Scheme 5.1 was found to accurately represent the reaction mechanism in reactions of trinitrobenzene derivatives, in accordance with the earlier work of Orvik and Bunnett, who found that 2,4-dinitro-1-naphthyl ethyl ether, **5.4**, reacted with amines in DMSO to yield the substitution product, **5.5**.⁵



Scheme 5.1



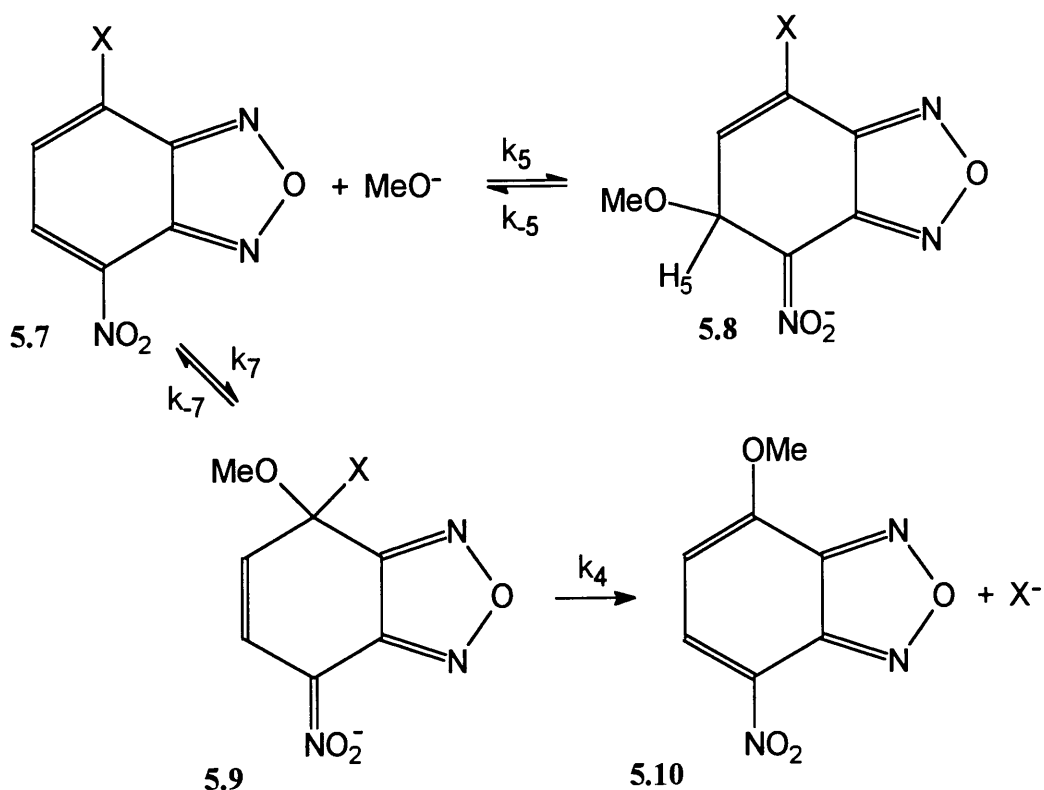
Adducts, **5.6**, have been observed as transient intermediates during reactions of 2,4,6-trinitroanisole (**5.1**, X = OMe) with primary aliphatic amines using NMR spectroscopy.^{6,7} When the reaction involves secondary amines, the adducts may have long lifetimes, and in some cases, do not yield the expected substitution products.^{6,8}



Di Nunno and co-workers have studied the reaction of 4-nitro-7-X-benzofurazans, **5.7**, with methoxide in methanol, Scheme 5.2. The methoxide initially attacks the electrophile at the 5-position to give **5.8**, before a slow isomerism to yield the thermodynamically more stable 7-adduct, **5.9**, followed by substitution of X to give **5.10**. The factor mainly responsible for the lower nucleophilic reactivity of C-X than C-H was assumed to be the higher repulsive interaction between X and the nucleophile in the transition state, rather than the loss of resonance stabilisation.⁹

The reactions of five aliphatic amines with 4-nitro-7-X-benzofurazans have been studied, where X is chloride, methoxide or phenoxide. The aims of the work were twofold. First, to compare the reactions of the amines with those of 1-X-2,4,6-trinitrobenzenes, **5.1**, in which the substitution reaction occurs at a sterically hindered position, with an analogous substitution at a less hindered site. Second, to compare the directing and leaving group

effects of the X-substituents, and to provide further insight as to the relative nucleophilic reactivity of the amines.



Scheme 5.2

5.2 Experimental

4-nitro-7-chlorobenzofurazan, **5.7i** ($\text{X} = \text{Cl}$), was the purest commercial sample available. A sample of 4-nitro-7-methoxybenzofurazan, **5.7ii** ($\text{X} = \text{OMe}$), was prepared from a 1:1 mixture of **5.7i** and sodium methoxide in methanol. The solution was heated at 40 °C for one hour. The resulting precipitate was filtered under vacuum, and dried in air, giving **5.7ii** in 65% yield (mp 113 °C, literature value,⁹ 115 °C).

4-nitro-7-phenoxybenzofurazan, **5.7iii** ($\text{X} = \text{OPh}$), was prepared by the addition of a fifty-fold excess of phenol (0.05 moles) in sodium hydroxide (5×10^{-3} moles) to 4-nitro-7-chlorobenzofurazan, **5.7i**, (1×10^{-3} moles) in sufficient water to give a homogeneous solution. After heating at 40 °C for one hour, the solution was quenched with distilled

water, and the resulting precipitate filtered under vacuum, giving **5.7iii** in 24% yield (mp 117 °C, literature value,¹⁰ 121 °C).

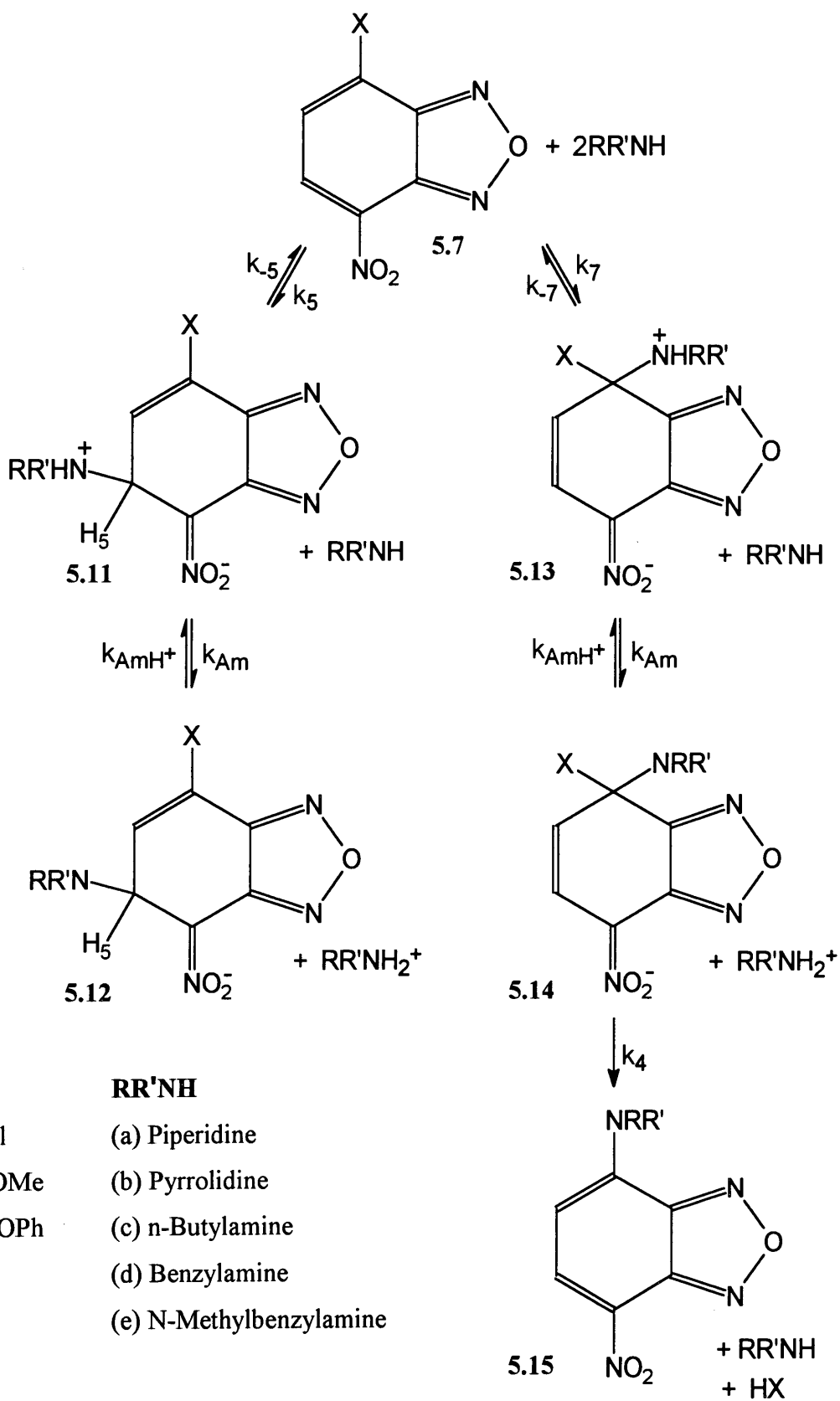
The substitution products, **5.15**, were prepared by the addition of a four-fold excess of amine to 4-nitro-7-chlorobenzofurazan, **5.7i**, in DMSO. The solution was left to react at room temperature for up to six hours (depending on the reactivity of the amine), before being quenched with ice-cold distilled water and the resulting precipitate filtered under vacuum. The ¹H NMR spectra of the resulting adducts were identical to the spectra gained when **5.7i** was reacted with a four-fold excess of the amine in [²H₆]DMSO.

All amines and solvents used were the purest available commercial products. Amine salts were prepared as solutions in DMSO by accurate neutralisation of the amines with perchloric acid.

¹H NMR spectra were recorded in [²H₆]DMSO with a Varian Mercury 200 MHz spectrometer. UV/Visible spectra were recorded at 25 °C with a Perkin-Elmer Lambda 2 spectrophotometer, while kinetic measurements were made at 25 °C using an Applied Photophysics SX-17 MV stopped-flow spectrophotometer.

5.3 Results and Discussion

In view of the previously studied reaction of 4-nitrobenzofurazan, **5.7** (X = H), with amines in DMSO, (Chapter 4), and the reactions outlined in Schemes 5.1 and 5.2, the reactions of the 7-derivatives studied were assumed to occur via an analogous pathway, according to Scheme 5.3.



Scheme 5.3

5.3.1 NMR Data

The ^1H NMR chemical shifts and coupling constants for the three substrates, **5.7i-iii**, and the substitution products, **5.15a-e**, are given in Table 5.1.

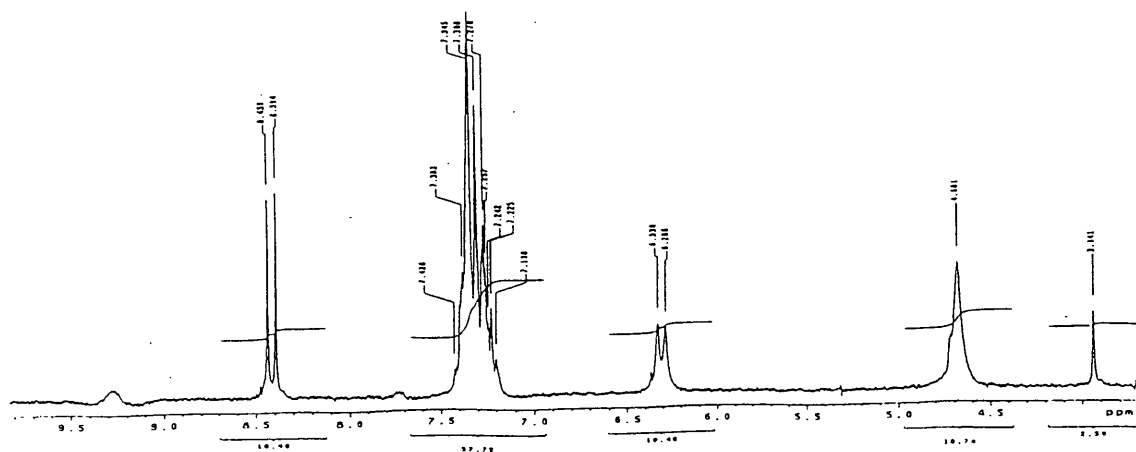
Table 5.1: ^1H NMR data for substrates, **5.7**, and adducts, **5.15**, formed in $[\text{}^2\text{H}_6]\text{DMSO}$.

	Chemical Shift			Other
	H_5	H_6	J_{56}^a	
5.7i	8.67	8.01	8.0	
5.7ii	8.75	7.06	8.2	4.20 (OMe)
5.7iii	8.64	6.67	8.4	7.50 (OPh)
5.15a	8.42	6.63	9.4	4.13 (4H), 1.73 (6H)
5.15b	8.46	6.27	9.2	4.19 (2H), 3.69 (2H), 2.08(4H)
5.15c	8.49	6.39	9.0	3.41 (2H), 1.61 (2H), 1.33 (2H), 0.87 (3H)
5.15d	8.42	6.31	9.0	7.1-7.5 (C_6H_5), 4.68 (CH_2), 7.3 (NH)
5.15e	8.50	6.47	9.0	7.1-7.5 (C_6H_5), 5.33 (CH_2), 3.55 (CH_3)

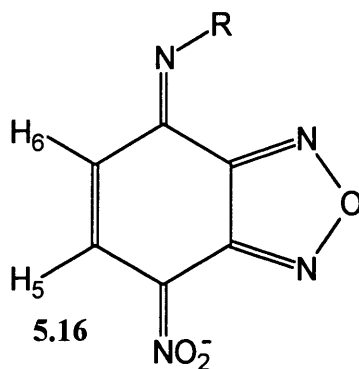
^a Coupling constant in Hz.

A sample NMR spectrum is shown in Figure 5.1 for the substitution product, **5.15d**, formed from the addition of a four-fold excess of benzylamine to 4-nitro-7-chlorobenzofurazan, **5.7i**, in DMSO.

Figure 5.1: ^1H NMR spectrum of the substitution product **5.15d** in $[\text{}^2\text{H}_6]\text{DMSO}$.



For reactions involving the primary amines, butylamine and benzylamine, the product, **5.15**, may be deprotonated at the nitrogen centre in the presence of excess amine to give **5.16**.



The H₅ and H₆ resonances move to lower frequency on deprotonation. This is a reflection of the change in the nature of the bond between the carbons bearing H₅ and H₆. The chemical shifts measured in [²H₆]DMSO for the deprotonation of **5.15c** in the presence of excess butylamine are given in Table 5.2.

Table 5.2: ¹H NMR evidence for the equilibrium deprotonation of **5.15c** in the presence of excess butylamine in [²H₆]DMSO.

[5.15c] / mol dm ⁻³	[butylamine] / mol dm ⁻³	Chemical Shift	
		H ₅	H ₆
0.01	0	8.49	6.39
0.01	0.01	8.07	6.14
0.01	0.02	7.86	6.04
0.01	0.04	7.77	5.97

5.3.2 Kinetic Data

Table 5.3 contains data concerning the substrates, **5.7i-iii**, 5-adducts, **5.12**, and substitution products, **5.15**, formed from the amines in DMSO.

Table 5.3: UV/Visible absorbance data for substrates^a and adducts formed in DMSO.

	$\lambda_{\text{max}} / \text{nm}$	$\epsilon / \text{dm}^3 \text{mol}^{-1} \text{cm}^{-1}$
Substrates		
5.7i	342	6250
5.7ii	380	7500
5.7iii	380	11250
5-adducts		
5.12ia	355	8000
5.12ib	356	13750
5.12ic	353	15000
5.12id	364	14500
5.12iia	353	8750
5.12iib	356	100000
5.12iic	350	7500
5.12iiia	353	10000
5.12iiib	356	10000
5.12iiic	352	12500
5.12iiid	362	10000
Substitution products		
5.15a	499	25000
5.15b	494	30000
5.15c^b	480	18000
5.15d	474	22000
5.15e	489	27500

^a Substrate concentration, $4 \times 10^{-5} \text{mol dm}^{-3}$.

^b Substrate concentration, $6 \times 10^{-5} \text{mol dm}^{-3}$.

All kinetic measurements were made at 25 °C in solutions of the amine buffered with its perchlorate salt. The buffer component concentrations were all in large excess of the substrate to ensure first order conditions. For measurements in the absence of amine salt, the amine concentration was sufficient to give >95% conversion to adducts at equilibrium. Kinetic measurements were generally made at the absorption maximum for the adducts or substitution products, λ_{max} , unless a significant overlap of the spectra for substrate and adduct caused low amplitudes, in which case, measurements were made at an alternative wavelength, usually the isosbestic point.

There were three observable reaction steps, which were easily distinguished and separate in time. The first, was a rapid, colour forming reaction which could be followed at around 360 nm, corresponding to the formation of the 5-adduct, **5.12**. The second, slower reaction, was attributed to the formation of the thermodynamically more stable 7-adduct, **5.14**, in equilibrium with the kinetically preferred adduct at the 5-position. Finally, a third reaction was observed, where expulsion of the leaving group, X, occurred to give the substitution product, **5.15**. The reaction to form the 7-adduct was only observed in a limited number of cases, as leaving group expulsion was generally rapid.

The rate constant for the fast process, k_{fast} , is made up of the terms for the forward and reverse rate constants according to the steady state principle, Equation 5.1, (for a full derivation of the steady state principle see Section 8.2).

$$\text{Equation 5.1: } k_{\text{fast}} = \frac{k_5 k_{\text{Am}} [\text{Am}]^2}{k_{-5} + k_{\text{Am}} [\text{Am}]} + \frac{k_{-5} k_{\text{AmH}^+} [\text{AmH}^+]}{k_{-5} + k_{\text{Am}} [\text{Am}]}$$

Equation 5.1 may be simplified by considering the limiting cases:

1) Proton transfer from the zwitterionic intermediate, **5.11**, to the amine is slow compared to reversal to reactants, and the condition $k_{-5} \gg k_{\text{Am}} [\text{Am}]$, leads to Equation 5.2.

$$\text{Equation 5.2: } k_{\text{fast}} = \frac{k_5 k_{\text{Am}} [\text{Am}]^2}{k_{-5}} + k_{\text{AmH}^+} [\text{AmH}^+]$$

2) Proton transfer from the zwitterionic intermediate, **5.11**, to the amine is rapid compared to reversal to reactants, and the condition $k_{Am}[Am] \gg k_{-5}$ leads to Equation 5.3.

$$\text{Equation 5.3: } k_{fast} = k_5[Am] + \frac{k_{-5}k_{AmH^+}[AmH^+]}{k_{Am}[Am]}$$

An equilibrium constant for formation of the 5-adduct, $K_{C,5}$, may be defined by Equation 5.4.

$$\text{Equation 5.4: } K_{C,5} = \frac{[5.12][AmH^+]}{[5.7][Am]^2} = \frac{k_5k_{Am}}{k_{-5}k_{AmH^+}}$$

The rate constant for the slow process, the rate-limiting formation of the thermodynamically more stable 7-adduct, is given by Equation 5.5. However, the 7-adduct is in equilibrium with the initially formed 5-adduct, and Equation 5.5 must be modified to take account of the proportion of **5.12** in equilibrium with the 7-adduct, **5.14**, Equation 5.6.

$$\text{Equation 5.5: } k_{slow} = \frac{k_7k_{Am}[Am]^2}{k_{-7} + k_{Am}[Am]} + \frac{k_{-7}k_{AmH^+}[AmH^+]}{k_{-7} + k_{Am}[Am]}$$

$$\text{Equation 5.6: } k_{slow} = \frac{k_7k_{Am}[Am]^2}{(k_{-7} + k_{Am}[Am])\left(1 + \frac{K_{C,5}[Am]^2}{[AmH^+]}\right)} + \frac{k_{-7}k_{AmH^+}[AmH^+]}{k_{-7} + k_{Am}[Am]}$$

Again, there are two limiting cases to consider:

1) Proton transfer from the zwitterionic intermediate, **5.13**, to the amine is slow compared to reversal to reactants, and the condition $k_{-7} \gg k_{Am}[Am]$, leads to Equation 5.7.

$$\text{Equation 5.7: } k_{slow} = \frac{k_7k_{Am}[Am]^2}{k_{-7}\left(1 + \frac{K_{C,5}[Am]^2}{[AmH^+]}\right)} + k_{AmH^+}[AmH^+]$$

2) Proton transfer from the zwitterionic intermediate, **5.13**, to the amine is rapid compared to reversal to reactants, and the condition $k_{Am}[Am] \gg k_{-7}$ leads to Equation 5.8.

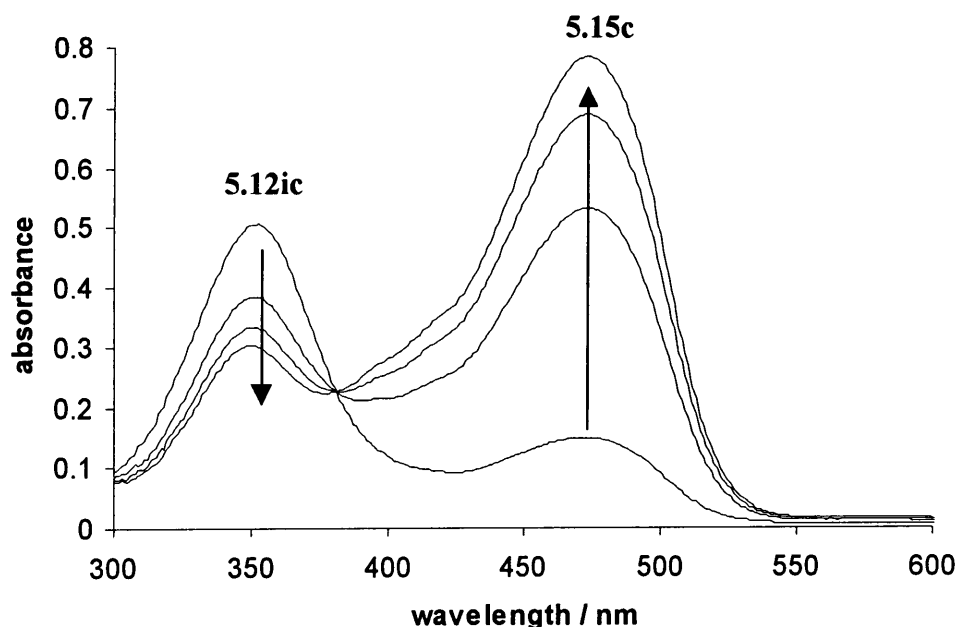
$$\text{Equation 5.8: } k_{\text{slow}} = \frac{k_7[Am]}{\left(1 + \frac{K_{C,5}[Am]^2}{[AmH^+]}\right)} + \frac{k_{-7}k_{AmH^+}[AmH^+]}{k_{Am}[Am]}$$

An equilibrium constant, $K_{C,7}$, for formation of the 7-adduct, is defined in Equation 5.9.

$$\text{Equation 5.9: } K_{C,7} = \frac{[5.14][AmH^+]}{[5.7][Am]^2} = \frac{k_7k_{Am}}{k_{-7}k_{AmH^+}}$$

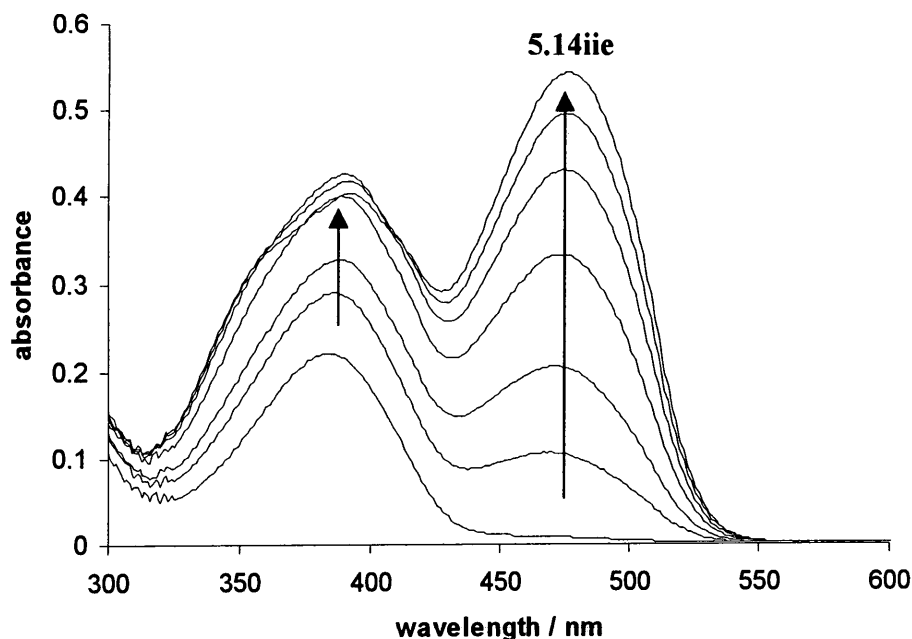
In most cases, the reaction to give the 7-adduct was rate limiting on the substitution pathway, and the expulsion of the leaving group was rapid. This led to clean spectra over time, with clear isosbestic points, giving no evidence for the build up of the intermediate 7-adduct, **5.14**. For example, the UV/Visible spectra gained over time during the reaction of 0.01 mol dm^{-3} butylamine with $4 \times 10^{-5} \text{ mol dm}^{-3}$, 4-nitro-7-chlorobenzofurazan, **5.7i**, in the presence of 0.01 mol dm^{-3} butylamine perchlorate are shown in Figure 5.2. The absorbance at 360 nm, due to the 5-adduct, **5.12ic** decreases over time, with the concurrent increase in the absorbance at 473 nm, due to the formation of the substitution product, **5.15c**, where expulsion of the chloro-group was rapid.

Figure 5.2: UV/Visible spectra measured over time for the reaction of 4-nitro-7-chlorobenzofurazan, **5.7i**, with n-butylamine in the presence of n-butylamine perchlorate in DMSO at 25 °C.



However, in some cases, the UV/Visible spectra obtained over time on addition of amine to substrate showed evidence for the build-up of the 7-adduct on the substitution pathway, suggesting that the departure of the leaving group was rate-limiting. For example, the spectra over time due to the attack of 0.01 mol dm^{-3} , N-methylbenzylamine on $4 \times 10^{-5} \text{ mol dm}^{-3}$, 4-nitro-7-methoxybenzofurazan, lacked an isosbestic point, and showed evidence for the build-up of the 7-adduct, **5.14iie** on the substitution pathway, Figure 5.3. Spectra obtained with several amines indicated that 7-adducts with structure **5.14** showed absorbances in the range 380-450 nm, although precise absorption maxima could not be measured.

Figure 5.3: UV/Visible spectra measured over time, for the reaction of N-methylbenzylamine with 4-nitro-7-methoxybenzofurazan in DMSO at 25 °C. The reaction was complete after 30 minutes.



The rate expression for the formation of the substitution product is defined in Equation 5.10, assuming that the departure of the leaving group is rate-limiting.

$$\text{Equation 5.10: } \frac{d[5.15]}{dt} = k_4[\text{AmH}^+][5.14]$$

At equilibrium, the sum of the concentrations of the substrate, adducts and substitution product is constant, according to Equation 5.11, which can be differentiated with respect to time, to give Equation 5.12.

$$\text{Equation 5.11: } [5.7] + [5.12] + [5.14] + [5.15] = \text{constant}$$

$$\text{Equation 5.12: } \frac{d[5.7]}{dt} + \frac{d[5.12]}{dt} + \frac{d[5.14]}{dt} + \frac{d[5.15]}{dt} = 0$$

The expression for the equilibrium constant, $K_{C,7}$, given in Equation 4.9, may be rearranged to give an expression for the concentration of the substrate, **5.7**, at equilibrium, Equation 5.13.

$$\text{Equation 5.13: } [\mathbf{5.7}] = \frac{[\mathbf{5.14}][\text{AmH}^+]}{K_{C,7}[\text{Am}]^2}$$

The ratio of the equilibrium constants, $K_{C,5}$ and $K_{C,7}$, may be used to define the concentration of the 5-adduct, **5.12**, at equilibrium in terms of the concentration of the 7-adduct, **5.14**, Equation 5.14.

$$\text{Equation 5.14: } [\mathbf{5.12}] = \frac{K_{C,5}}{K_{C,7}}[\mathbf{5.14}]$$

Equation 5.12 may then be re-written as Equation 5.15, by making the relevant substitutions.

$$\text{Equation 5.15: } \frac{d[\mathbf{5.14}]}{dt} \frac{[\text{AmH}^+]}{K_{C,7}[\text{Am}]^2} + \frac{d[\mathbf{5.14}]}{dt} \frac{K_{C,5}}{K_{C,7}} + \frac{d[\mathbf{5.14}]}{dt} + k_4[\text{AmH}^+][\mathbf{5.14}] = 0$$

Equation 5.15 can then be factorised to give Equation 5.16.

$$\text{Equation 5.16: } \frac{d[\mathbf{5.14}]}{dt} \left(\frac{[\text{AmH}^+]}{K_{C,7}[\text{Am}]^2} + \frac{K_{C,5}}{K_{C,7}} + 1 \right) + k_4[\text{AmH}^+][\mathbf{5.14}] = 0$$

The rate of decomposition of the 7-adduct, **5.14**, is directly proportional to the rate of formation of the substitution product, **5.15**, according to Equation 5.17, where k_{sub} is the observed first order rate constant.

$$\text{Equation 5.17: } -\frac{d[\mathbf{5.14}]}{dt} = k_{\text{sub}}[\mathbf{5.14}]$$

Therefore, Equation 5.16 may be re-written as Equation 5.18.

$$\text{Equation 5.18: } k_{\text{sub}} \left(\frac{[\text{AmH}^+]}{K_{\text{C},7}[\text{Am}]^2} + \frac{K_{\text{C},5}}{K_{\text{C},7}} + 1 \right) = k_4[\text{AmH}^+]$$

Multiplying all the terms in Equation 5.18 by $K_{\text{C},7}[\text{Am}]^2$, leads to Equation 5.19, which can be rearranged to give Equation 5.20.

$$\text{Equation 5.19: } k_{\text{sub}}([\text{AmH}^+] + K_{\text{C},5}[\text{Am}]^2 + K_{\text{C},7}[\text{Am}]^2) = k_4 K_{\text{C},7}[\text{AmH}^+][\text{Am}]^2$$

$$\text{Equation 5.20: } k_{\text{sub}} = \frac{k_4 K_{\text{C},7}[\text{AmH}^+][\text{Am}]^2}{[\text{AmH}^+] + (K_{\text{C},5} + K_{\text{C},7})[\text{Am}]^2}$$

5.3.2.1 Reactions of Piperidine

Data for the reaction of piperidine with 4-nitro-7-chlorobenzofurazan, **4.7i**, are given in Table 5.4. The formation of the 5-adduct, **5.12ia**, was measured at 370 nm in the absence of amine salt. Data were fitted to Equation 5.1 to yield k_5 , $1.5 \times 10^5 \text{ dm}^3 \text{ mol}^{-1} \text{ s}^{-1}$ and k_{Am}/k_{-5} , $480 \text{ dm}^3 \text{ mol}^{-1}$. There was no evidence for contribution from the reverse reaction in the absence of amine salt. The formation of the 7-adduct was rate-limiting in the reaction to give **5.15ia**, measured at 499 nm in the presence of $0.010 \text{ mol dm}^{-3}$ piperidine perchlorate and hydrochloride. The $K_{\text{C},5}$ values shown appending Table 5.4, illustrate the effect of chloride in stabilising the adducts formed, as $K_{\text{C},5}$ increases on going from perchlorate to hydrochloride solutions. Data for the slow reaction to produce **5.15ia** were fitted according to Equation 5.8 for both amine salts. Again, there was no contribution from the reverse reaction, even in the presence of $0.010 \text{ mol dm}^{-3}$ amine salt.

Combination of the terms for the fast reaction, together with the $K_{\text{C},5}$ value of $233 \text{ dm}^3 \text{ mol}^{-1}$ measured in piperidine perchlorate according to Equation 5.4, gave a k_{AmH^+} value of $3.1 \times 10^5 \text{ dm}^3 \text{ mol}^{-1} \text{ s}^{-1}$ for proton transfer from the 5-adduct, **5.12ia** to piperidine.

In the reaction of piperidine with 4-nitro-7-methoxybenzofurazan, **5.7ii**, two rate processes were observed, Table 5.5. Here measurements relating to formation of the 5-adduct **5.12iia** were not possible; at low amine concentrations the amplitude of this process was very small, while at high amine concentrations the process was too rapid for measurement. The first measurable process gave rise to increased absorbance at 415 nm and is attributed to the formation of the 7-adduct, **5.14iia**. Data gave a good fit with Equation 5.8, with $K_{\text{C},5} = 0$, indicating that in the formation of the 7-adduct the proton transfer equilibrium is rapid. Combination of the values obtained for k_7 and $k_{-7}k_{\text{AmH}^+}/k_{\text{Am}}$ according to Equation 5.9 led to a value for $K_{\text{C},7}$ of $24 \text{ dm}^3 \text{ mol}^{-1}$. The second observable process leading to the substitution product, **5.15a**, was measured at 499 nm, and data were fitted according to Equation 5.20. They lead to a value for k_4 of $39 \pm 4 \text{ dm}^3 \text{ mol}^{-1} \text{ s}^{-1}$.

In the reaction of piperidine with 4-nitro-7-phenoxybenzofurazan, **5.7iia**, only one rate process was observed giving rise to the substitution product **5.15a**. Results measured at 499 nm are in Table 5.6. Data give a good fit with Equation 5.6, corresponding to rate-

limiting formation of the 7-adduct followed by rapid expulsion of phenoxide, an excellent leaving group. At high amine concentrations the condition $k_{Am}[Am] \gg k_7$ applies, so that Equation 5.8 was applicable.

Table 5.4: Kinetic data for the reaction of **5.7i**^a with piperidine in DMSO at 25 °C.

[Piperidine] / mol dm ⁻³	[PiperidineH ⁺ Cl ⁻] / mol dm ⁻³	[PiperidineH ⁺ ClO ₄ ⁻] / mol dm ⁻³	k_{fast}^b / s ⁻¹	k_{calc}^c / s ⁻¹	k_{slow}^d / s ⁻¹	k_{calc}^e / s ⁻¹
0.001	0	0	49	49		
0.002	0	0	133	147		
0.003	0	0	266	266		
0.004	0	0	422	395		
0.005	0	0	577	529		
0.001	0.010	0			0.18	0.19
0.002	0.010	0			0.34	0.34
0.005	0.010	0			0.55	0.55
0.01	0.010	0			0.50	0.48
0.02	0.010	0			0.28	0.29
0.001	0	0.010			0.15	0.15
0.002	0	0.010			0.29	0.28
0.005	0	0.010			0.49	0.49
0.01	0	0.010			0.47	0.47
0.02	0	0.010			0.30	0.30

^a substrate concentration, 4×10^{-5} mol dm⁻³.

^b Data measured at 370 nm.

^c Calculated according to Equation 5.1, with values of k_5 , 1.5×10^5 dm³ mol⁻¹ s⁻¹ and k_{Am}/k_5 , 480 dm³ mol⁻¹.

^d Data measured at 499 nm.

^e Calculated from Equation 5.8, with values of k_7 , 192 dm³ mol⁻¹ s⁻¹ and $K_{C,5}$, 300 dm³ mol⁻¹ for reaction in piperidine hydrochloride, and of k_7 , 155 dm³ mol⁻¹ s⁻¹ and $K_{C,5}$, 233 dm³ mol⁻¹ for reaction in piperidine perchlorate.

Table 5.5: Kinetic data for the reaction of **5.7ii**^a with piperidine in DMSO at 25 °C.

[Piperidine] / mol dm ⁻³	[PiperidineH ⁺ ClO ₄] / mol dm ⁻³	k _{slow} ^b / s ⁻¹	k _{calc} ^c / s ⁻¹	k _{sub} ^d / s ⁻¹	k _{calc} ^e / s ⁻¹
0.05	0.005	2.40	2.45		
0.05	0.01	2.64	2.64	0.39 ^f	
0.05	0.02	3.01	3.01		
0.10	0.01	5.36	4.72	0.39 ^f	
0.20	0.01	9.17	9.17	0.38 ^f	
0.001	0.01			0.0011	0.0010
0.002	0.01			0.0038	0.0040
0.005	0.01			0.024	0.024
0.007	0.01			0.043	0.044
0.01	0.01			0.083	0.082
0.04	0.01			0.34	0.36
0.05	0.01			0.39	0.39
0.06	0.01			0.39	0.41
0.002	0.10			0.008	0.006
0.005	0.10			0.038	0.037
0.007	0.10			0.071	0.069
0.01	0.10			0.13	0.14
0.04	0.10			0.79	0.85
0.05	0.10			1.45	1.45
0.08	0.10			1.94	1.92
0.10	0.01 ^g			0.32	0.26
0.10	0.02 ^g			0.60	0.52
0.10	0.04 ^g			1.09	1.03
0.10	0.06 ^g			1.52	1.55
0.10	0.08 ^g			1.87	2.07

^a substrate concentration, 4×10^{-5} mol dm⁻³.

^b Data measured at 415 nm.

^c Calculated according to Equation 5.8, with values of k_7 , 45 dm³ mol⁻¹ s⁻¹ and $k_7k_{AmH^+}/k_{Am}$, 1.9 s⁻¹.

^d Data measured at 499 nm.

^e Calculated from Equation 5.20, with values of $k_4K_{C,7}$, $1 \times 10^3 \text{ dm}^6 \text{ mol}^{-2} \text{ s}^{-1}$ and $(K_{C,7} + K_{C,5})$, $22 \text{ dm}^3 \text{ mol}^{-1}$ in $0.010 \text{ mol dm}^{-3}$ piperidine perchlorate, and $k_4K_{C,7}$, $1.45 \times 10^3 \text{ dm}^6 \text{ mol}^{-2} \text{ s}^{-1}$ and $(K_{C,7} + K_{C,5})$, $60 \text{ dm}^3 \text{ mol}^{-1}$ in 0.10 mol dm^{-3} piperidine perchlorate.

^f Data measured at 415 nm, the condition $K_{C,7}[\text{Am}]^2 \gg [\text{AmH}^+]$, led to $k_{\text{slow}} = k_4[\text{AmH}^+]$, and a k_4 value of $39 \text{ dm}^3 \text{ mol}^{-1} \text{ s}^{-1}$.

^g Ionic strength maintained at 0.10 mol dm^{-3} using tetrapropylammonium perchlorate.

Table 5.6: Kinetic data for the reaction of **5.7iii**^a with piperidine in DMSO at 25 °C.

[Piperidine] / mol dm ⁻³	[PiperidineH ⁺ ClO ₄ ⁻] / mol dm ⁻³	k_{slow}^b / s ⁻¹	k_{calc}^c / s ⁻¹
0.002	0.001	0.031	0.032
0.004	0.001	0.089	0.090
0.006	0.001	0.16	0.16
0.008	0.001	0.23	0.22
0.010	0.001	0.29	0.29
0.005	0.010	0.13	0.13
0.007	0.010	0.21	0.20
0.010	0.010	0.33	0.31
0.04	0.010	1.13	1.14
0.07	0.010	1.32	1.32
0.10	0.010	1.26	1.23
0.01	0.10	0.39	0.43
0.02	0.10	0.84	0.85
0.04	0.10	1.55	1.55
0.06	0.10	2.12	2.03
0.08	0.10	2.31	2.30
0.10	0.10	2.40	2.42

^a substrate concentration, 4×10^{-3} mol dm⁻³.

^b Data measured at 499 nm.

^c Calculated from Equation 5.6, with values of k_7 , 42 dm³ mol⁻¹ s⁻¹, k_{Am}/k_7 , 300 dm³ mol⁻¹ and $K_{\text{C},5}$, 1.1 dm³ mol⁻¹ in 0.001 mol dm⁻³ piperidine perchlorate, and k_7 , 42 dm³ mol⁻¹ s⁻¹, k_{Am}/k_7 , 300 dm³ mol⁻¹ and $K_{\text{C},5}$, 2.3 dm³ mol⁻¹ in 0.010 mol dm⁻³ piperidine perchlorate. For solutions containing 0.10 mol dm⁻³ amine salt, data were fitted to Equation 5.8, with values of k_7 , 44 dm³ mol⁻¹ s⁻¹ and $K_{\text{C},5}$, 8.1 dm³ mol⁻¹.

5.3.2.2 Reactions of Pyrrolidine

Data for the reaction of pyrrolidine with 4-nitro-7-chlorobenzofurazan, **5.7i**, are given in Table 5.7. The initial rapid reaction to give the 5-adduct, **5.12ib**, was inconveniently rapid for measurement in all but a few cases, and a k_5 value of $3 \times 10^5 \text{ dm}^3 \text{ mol}^{-1} \text{ s}^{-1}$ was calculated from $k_{\text{fast}}/[\text{pyrrolidine}]$, according to Equation 5.3 in the absence of amine salt. The slower reaction, measured at 495 nm corresponded to the rate-limiting formation of the 7-adduct, **5.14ib**, and the data were fitted according to Equation 5.8. This illustrates that proton transfer from **5.13ib** is rapid, and there is a negligible contribution from the reverse reaction.

Only one process was observed in the reaction of pyrrolidine with 4-nitro-7-methoxybenzofurazan, **5.7ii**, corresponding to rate-limiting 7-adduct formation, Table 5.8. The data were fitted according to Equation 5.6 and indicate that proton transfer is partially rate-limiting in the formation of **5.14iib**, and that there is a negligible contribution to the rate constant from the reverse reaction. There is a rapid pre-equilibrium with the initially formed 5-adduct (the formation of which was too fast to measure in this case), and Equation 5.6 includes the term for the equilibrium constant $K_{\text{C},5}$.

Two processes were observed for the reaction of pyrrolidine with the phenoxy-derivative, **5.7iii** in DMSO, Table 5.9. The data for the fast process, measured at 350 nm, were fitted according to Equation 5.1. No contribution from the reverse reaction was observed as the data were measured in the absence of amine salt. Equation 5.6 was used to fit the data for the slow process. There was no contribution from the reverse reaction, even in $0.010 \text{ mol dm}^{-3}$ pyrrolidine perchlorate, and proton transfer from **5.14iiib** to pyrrolidine was partially rate-limiting.

Table 5.7: Kinetic data for the reaction of **5.7i**^a with pyrrolidine in DMSO at 25 °C.

[Pyrrolidine] / mol dm ⁻³	[PyrrolidineH ⁺ ClO ₄ ⁻] mol dm ⁻³	k_{fast} ^b / s ⁻¹	k_{slow} ^c / s ⁻¹	k_{calc} ^d / s ⁻¹
0.001	0	290		
0.002	0	600		
0.003	0	910		
0.001	0.010		0.16	0.17
0.004	0.010		0.43	0.43
0.007	0.010		0.43	0.42
0.010	0.010		0.37	0.35
0.04	0.010		0.11	0.11
0.06	0.010		0.071	0.072
0.08	0.010		0.053	0.054
0.10	0.010		0.042	0.044

^a substrate concentration, 4×10^{-5} mol dm⁻³.

^b Data measured at 360 nm, k_5 value of 3×10^5 dm³ mol⁻¹ s⁻¹ calculated from $k_{\text{fast}}/[\text{pyrrolidine}]$.

^c Data measured at 495 nm.

^d Calculated according to Equation 5.8, with values of k_7 , 180 dm³ mol⁻¹ s⁻¹ and $K_{C,5}$, 410 dm³ mol⁻¹.

Table 5.8: Kinetic data for the reaction of **5.7ii**^a with pyrrolidine in DMSO at 25 °C.

[Pyrrolidine] / mol dm ⁻³	[PyrrolidineH ⁺ ClO ₄ ⁻] mol dm ⁻³	k_{slow}^b / s ⁻¹	k_{calc}^c / s ⁻¹
0.001	0.001	0.053	0.046
0.004	0.001	0.38	0.36
0.007	0.001	0.76	0.72
0.010	0.001	1.15	1.10
0.04	0.001	3.49	3.50
0.06	0.001	3.86	3.87
0.08	0.001	3.76	3.76
0.10	0.001	3.52	3.48
0.001	0.010	0.045	0.045
0.004	0.010	0.36	0.36
0.007	0.010	0.74	0.73
0.010	0.010	1.16	1.11
0.04	0.010	4.74	4.78
0.06	0.010	6.75	6.75
0.08	0.010	8.23	8.23
0.10	0.010	9.23	9.23

^a substrate concentration, 4×10^{-5} mol dm⁻³.

^b Data measured at 495 nm.

^c Calculated from Equation 5.6, with values of k_7 , 131 dm³ mol⁻¹ s⁻¹, k_{Am}/k_7 , 540 dm³ mol⁻¹ and $K_{\text{C},5}$, 0.27 dm³ mol⁻¹ in 0.001 mol dm⁻³ piperidine perchlorate, and k_7 , 134 dm³ mol⁻¹ s⁻¹, k_{Am}/k_7 , 500 dm³ mol⁻¹ and $K_{\text{C},5}$, 0.42 dm³ mol⁻¹ in 0.010 mol dm⁻³ piperidine perchlorate.

Table 5.9: Kinetic data for the reaction of **5.7iii**^a with pyrrolidine in DMSO at 25 °C.

[Pyrrolidine] / mol dm ⁻³	[PyrrolidineH ⁺ ClO ₄ ⁻] / mol dm ⁻³	k _{fast} ^b / s ⁻¹	k _{calc} ^c / s ⁻¹	k _{slow} ^d / s ⁻¹	k _{calc} ^e / s ⁻¹
0.003	0	407	416		
0.004	0	565	565		
0.001	0.001			0.060	0.061
0.002	0.001			0.14	0.14
0.003	0.001			0.22	0.22
0.004	0.001			0.30	0.30
0.005	0.001			0.38	0.37
0.006	0.001			0.43	0.44
0.001	0.010			0.057	0.055
0.004	0.010			0.28	0.28
0.007	0.010			0.51	0.50
0.010	0.010			0.71	0.71
0.04	0.010			1.66	1.68
0.06	0.010			1.60	1.60
0.08	0.010			1.43	1.42
0.10	0.010			1.24	1.24

^a substrate concentration, 4×10^{-5} mol dm⁻³.

^b Data measured at 350 nm.

^c Calculated according to Equation 5.1, with k_5 , 1.5×10^5 dm³ mol⁻¹ s⁻¹ and k_{Am}/k_{-5} , 4000 dm³ mol⁻¹.

^d Data measured at 495 nm.

^e Calculated from Equation 5.6, with values of k_7 , 85 dm³ mol⁻¹ s⁻¹, k_{Am}/k_{-7} , 2600 dm³ mol⁻¹ and $K_{C,5}$, 2.8 dm³ mol⁻¹ in 0.001 mol dm⁻³ piperidine perchlorate, and k_7 , 78 dm³ mol⁻¹ s⁻¹, k_{Am}/k_{-7} , 2300 dm³ mol⁻¹ and $K_{C,5}$, 5.3 dm³ mol⁻¹ in 0.010 mol dm⁻³ piperidine perchlorate.

5.3.2.3 Reactions of n-Butylamine

Data for the reaction of n-butylamine with the chloro-derivative, **5.7i**, are given in Table 5.10. Two rate processes were observed, which corresponded to the rapid formation of the 5-adduct, **5.12ic**, followed by the rate-limiting formation of the 7-adduct, **5.14ic**, before rapid expulsion of chloride, to give **5.15c**. The fast reaction was measured at 380 nm in the presence of 0.001 mol dm⁻³ butylamine perchlorate. Data were fitted according to Equation 5.3, showing that the initial attack of butylamine at the 5-position is rate-limiting. Combination of the k_5 and $k_{-5}k_{\text{AmH}^+}/k_{\text{Am}}$ values appearing in Table 5.9 gave a $K_{\text{C},5}$ value of 430 dm³ mol⁻¹ according to Equation 5.4. The rate-limiting formation of **5.14ic** was measured at 473 nm. There was no evidence for a contribution from the reverse reaction, and data were fitted accordingly to Equation 5.8. The $K_{\text{C},5}$ value of 450 dm³ mol⁻¹ calculated from the data for the slow reaction compares favourably with the value of 430 dm³ mol⁻¹ calculated from Equation 5.3.

The reactions of butylamine with both the methoxy- and phenoxy-derivatives showed similar features. The fast reaction was measured at 350 nm and combination of the k_5 and $k_{-5}k_{\text{AmH}^+}/k_{\text{Am}}$ values according to Equation 5.4, led to $K_{\text{C},5}$ values of 0.60 and 5.5 dm³ mol⁻¹ for the methoxy- and phenoxy-derivatives respectively. The slow reaction corresponded to the rate-limiting formation of the 7-adducts **5.14iic** and **5.14iiic**, followed by rapid expulsion of the leaving group. The data were successfully fitted to Equation 5.8, indicating that the proton transfer step was rapid, with a negligible contribution from the reverse reaction. Hence in both cases the formation of the zwitterionic intermediate was rate-limiting.

Table 5.10: Kinetic data for the reaction of **5.7i**^a with n-butylamine in DMSO at 25 °C.

[n-Butylamine] / mol dm ⁻³	[n-ButylamineH ⁺ ClO ₄ ⁻] / mol dm ⁻³	k _{fast} ^b / s ⁻¹	k _{calc} ^c / s ⁻¹	k _{slow} ^d / s ⁻¹	k _{calc} ^e / s ⁻¹
0.001	0.001	150	150		
0.002	0.001	145	143		
0.003	0.001	169	170		
0.004	0.001	204	206		
0.006	0.001	288	288		
0.008	0.001	373	373		
0.010	0.001	480	461		
0.001	0.010			0.0046	0.0046
0.002	0.010			0.0082	0.0082
0.005	0.010			0.011	0.011
0.008	0.010			0.0094	0.0099
0.02	0.010			0.0053	0.0051
0.03	0.010			0.0035	0.0035
0.04	0.010			0.0026	0.0026
0.05	0.010			0.0021	0.0021
0.06	0.010			0.0019	0.0018
0.08	0.010			0.0014	0.0013
0.10	0.010			0.0013	0.0011

^a substrate concentration, 4×10^{-5} mol dm⁻³.

^b Data measured at 380 nm.

^c Calculated according to Equation 5.3, with values of k_5 , 4.5×10^4 dm³ mol⁻¹ s⁻¹ and $k_{-5}k_{AmH^+}/k_{Am}$, 105 s⁻¹.

^d Data measured at 473 nm.

^e Calculated according to Equation 5.8, with values of k_7 , 4.8 dm³ mol⁻¹ s⁻¹ and $K_{C,5}$, 450 dm³ mol⁻¹.

Table 5.11: Kinetic data for the reaction of **5.7ii**^a with n-butylamine in DMSO at 25 °C.

[n-Butylamine] / mol dm ⁻³	[n-ButylamineH ⁺ ClO ₄ ⁻] / mol dm ⁻³	k _{fast} ^b / s ⁻¹	k _{calc} ^c s ⁻¹	k _{slow} ^d s ⁻¹	k _{calc} ^e s ⁻¹
0.001	0.001			0.011	0.011
0.005	0.001			0.056	0.056
0.010	0.001			0.11	0.11
0.04	0.001	332	332	0.26	0.26
0.05	0.001	342	339		
0.07	0.001	382	382	0.24	0.24
0.08	0.001	411	411		
0.10	0.001	463	475	0.21	0.20
0.001	0.010			0.011	0.011
0.002	0.010			0.025	0.022
0.003	0.010			0.032	0.034
0.004	0.010			0.046	0.045
0.005	0.010			0.050	0.056
0.006	0.010			0.060	0.067
0.007	0.010			0.080	0.078
0.010	0.010			0.12	0.11
0.04	0.010			0.40	0.41
0.07	0.010			0.59	0.59
0.10	0.010			0.66	0.67

^a substrate concentration, 4×10^{-5} mol dm⁻³.

^b Data measured at 350 nm.

^c Calculated according to Equation 5.3, with values of k_5 , 4100 dm³ mol⁻¹ s⁻¹ and $k_{-5}k_{AmH^+}/k_{Am}$, 6800 s⁻¹.

^d Data measured at 473 nm.

^e Calculated according to Equation 5.8, with values of k_7 , 11.4 dm³ mol⁻¹ s⁻¹ and $K_{C,5}$, 0.46 dm³ mol⁻¹, in 0.001 mol dm⁻³ n-butylamine perchlorate, and k_7 , 11.2 dm³ mol⁻¹ s⁻¹ and $K_{C,5}$, 0.67 dm³ mol⁻¹, in 0.010 mol dm⁻³ n-butylamine perchlorate.

Table 5.12: Kinetic data for the reaction of 5.7iii^a with n-butylamine in DMSO at 25 °C.

[n-Butylamine] / mol dm ⁻³	[n-ButylamineH ⁺ ClO ₄ ⁻] / mol dm ⁻³	k _{fast} ^b / s ⁻¹	k _{calc} ^c / s ⁻¹	k _{slow} ^d / s ⁻¹	k _{calc} ^e / s ⁻¹
0.010	0.001	236	235		
0.015	0.001	223	225		
0.02	0.001	240	240		
0.025	0.001	266	266		
0.03	0.001	298	297		
0.04	0.001	368	366		
0.05	0.001	440	440		
0.001	0.010			0.0042	0.0041
0.002	0.010			0.0081	0.0082
0.003	0.010			0.012	0.012
0.004	0.010			0.016	0.016
0.005	0.010			0.020	0.020
0.006	0.010			0.024	0.024
0.007	0.010			0.028	0.028
0.010	0.010			0.038	0.038
0.04	0.010			0.071	0.072
0.07	0.010			0.059	0.059
0.10	0.010			0.046	0.046

^a substrate concentration, 4×10^{-3} mol dm⁻³.

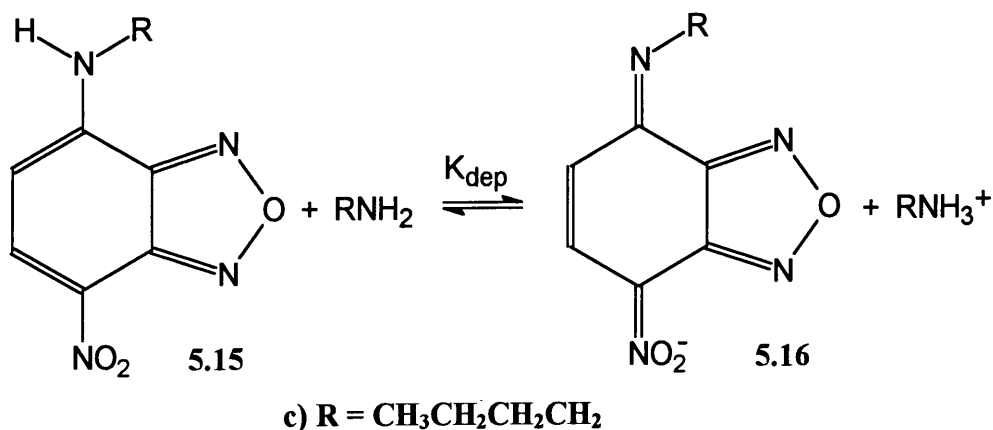
^b Data measured at 350 nm.

^c Calculated according to Equation 5.3, with values of k_5 , 8200 dm³ mol⁻¹ s⁻¹ and $k_5 k_{AmH^+} / k_{Am}$, 1500 s⁻¹.

^d Data measured at 473 nm.

^e Calculated according to Equation 5.8, with values of k_7 , 4.1 dm³ mol⁻¹ s⁻¹ and $K_{C,5}$, 8 dm³ mol⁻¹.

It was possible to study the equilibrium deprotonation of the adduct, **5.15c** in the presence of excess butylamine to give **5.16c** according to Scheme 5.4.



Scheme 5.4

The equilibrium constant, K_{dep} , defined in Scheme 5.4, is given by Equation 5.21.

$$\text{Equation 5.21: } K_{\text{dep}} = \frac{[\mathbf{5.16}][\text{RNH}_3^+]}{[\mathbf{5.15}][\text{RNH}_2]}$$

The UV/Visible absorption maximum of **5.15c** is 480 nm in the presence of 0.010 mol dm⁻³ butylamine perchlorate. The spectrum changes on addition of excess butylamine, with λ_{max} , 414 nm and 449 nm for **5.16c**, Figure 5.4. The relative proportions of **5.15c** and **5.16c** were found from absorbance measurements, according to Equation 5.22, where A_{∞} is the absorbance due to **5.15c**, and A_0 is the absorbance due to **5.16c**.

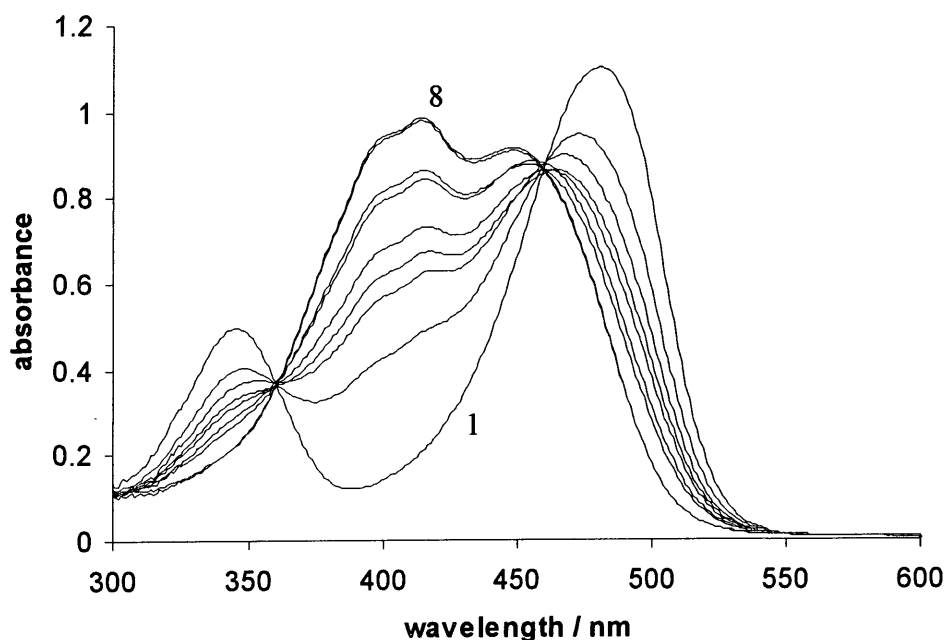
$$\text{Equation 5.22: } K_{\text{dep}} = \frac{(A_{\infty} - \text{Abs})[\text{RNH}_3^+]}{(\text{Abs} - A_0)[\text{RNH}_2]}$$

Absorbance data is given in Table 5.13. K_{dep} was calculated from absorbance measurements at 414 nm and 480 nm, according to Equation 5.22. An average K_{dep} value of 0.53 ± 0.05 , was determined from the twelve measured values.

Table 5.13: Absorbance data for the equilibrium deprotonation of **5.15c** to give **5.16c**.

Spectrum	[Butylamine] / mol dm ⁻³	[ButylamineH ⁺ ClO ₄ ⁻] / mol dm ⁻³	Abs at K _{dep}		Abs at K _{dep}	
			414 nm		480 nm	
1	0	0.010	0.206		1.10	
2	0.01	0.010	0.486	0.56	0.918	0.50
3	0.02	0.010	0.624	0.58	0.830	0.49
4	0.03	0.010	0.671	0.49	0.765	0.53
5	0.04	0.010	0.731	0.52	0.733	0.52
6	0.06	0.010	0.792	0.51	0.688	0.52
7	0.07	0.010	0.844	0.65	0.681	0.48
8	0.10	0	0.985		0.555	

Figure 5.4: UV/Visible spectra showing the equilibrium deprotonation of **5.15c**, 6×10^{-5} mol dm⁻³, in the presence of excess n-butylamine to give **5.16c**. Spectra are labelled according to Table 5.13.



5.3.2.4 Reactions of Benzylamine

Data for the reaction of benzylamine with 4-nitro-7-chlorobenzofurazan, **5.7i**, are given in Table 5.14. Two reaction processes were observed. The first was fitted to Equation 5.3, and corresponded to rate-limiting attack of benzylamine to give the 5-adduct, **5.12id**. Combination of the k_5 and $k_{-5}k_{\text{AmH}^+}/k_{\text{Am}}$ values according to Equation 5.4, led to a $K_{\text{C},5}$ value of $31 \text{ dm}^3 \text{ mol}^{-1}$. The slow process corresponded to rate-limiting formation of the 7-adduct, **5.14id**, followed by rapid expulsion of the chloro-group to yield **5.15d**. The data fitted well to Equation 5.8, and there was no evidence for a substantial contribution from the reverse reaction, in solutions containing $0.010 \text{ mol dm}^{-3}$ benzylamine perchlorate.

There was no direct kinetic evidence for the formation of the 5-adduct, **5.12iid**, in the reaction of benzylamine with 4-nitro-7-methoxybenzofurazan, **5.7ii**. Data for the slow process are given in Table 5.15, and were fitted to Equation 5.8 with no appreciable contribution from the reverse reaction. However, Equation 5.8 does include a term to account for the formation of the 7-adduct in the presence of the initially formed 5-adduct. The results in solutions containing $0.001 \text{ mol dm}^{-3}$ benzylamine perchlorate require a value for $K_{\text{C},5}$ of $0.035 \text{ dm}^3 \text{ mol}^{-1}$. The presence of 0.01 mol dm^{-3} benzylamine perchlorate was sufficient to inhibit formation of the 5-adduct.

The reaction of benzylamine with the phenoxy-derivative, **5.7iii**, occurred in two measurable stages. A fast, colour forming reaction was measured at 350 nm, and the data obtained were fitted to Equation 5.3, illustrating that the attack of benzylamine was rate-limiting in the formation of the 5-adduct, **5.12iiid**. Combination of the k_5 and $k_{-5}k_{\text{AmH}^+}/k_{\text{Am}}$ values according to Equation 5.4, led to a $K_{\text{C},5}$ value of $0.47 \text{ dm}^3 \text{ mol}^{-1}$. The data for the slow reaction were fitted to Equation 5.8, and show that the formation of the 7-adduct is rate-limiting in the substitution process, and that there is a negligible contribution to the reaction rate constant, k_{slow} , from the reverse reaction.

Table 5.14: Kinetic data for the reaction of 5.7i^a with benzylamine in DMSO at 25 °C.

[Benzylamine] / mol dm ⁻³	[BenzylamineH ⁺ ClO ₄ ⁻] / mol dm ⁻³	k _{fast} ^b / s ⁻¹	k _{calc} ^c / s ⁻¹	k _{slow} ^d / s ⁻¹	k _{calc} ^e / s ⁻¹
0.002	0.001	266	258		
0.003	0.001	178	196		
0.004	0.001	172	172		
0.006	0.001	159	163		
0.008	0.001	171	172		
0.010	0.001	186	190		
0.006	0.010			0.0071	0.0070
0.008	0.010			0.0086	0.0087
0.010	0.010			0.0097	0.0098
0.04	0.010			0.0081	0.0081
0.06	0.010			0.0059	0.0059
0.08	0.010			0.0046	0.0046
0.10	0.010			0.0036	0.0037

^a substrate concentration, 4×10^{-5} mol dm⁻³.

^b Data measured at 350 nm.

^c Calculated according to Equation 5.3, with values of k_5 , 1.44×10^4 dm³ mol⁻¹ s⁻¹ and $k_{-5}k_{AmH^+}/k_{Am}$, 460 s⁻¹.

^d Data measured at 474 nm.

^e Calculated according to Equation 5.8, with values of k_7 , 1.32 dm³ mol⁻¹ s⁻¹ and $K_{C,5}$, 34.4 dm³ mol⁻¹.

Table 5.15: Kinetic data for the reaction of **5.7ii**^a with benzylamine in DMSO at 25 °C.

[Benzylamine] / mol dm ⁻³	[BenzylamineH ⁺ ClO ₄ ⁻] / mol dm ⁻³	k _{slow} ^b / s ⁻¹	k _{calc} ^c / s ⁻¹
0.01	0.001	0.030	0.030
0.05	0.001	0.14	0.14
0.08	0.001	0.20	0.20
0.11	0.001	0.23	0.23
0.14	0.001	0.25	0.25
0.17	0.001	0.25	0.25
0.20	0.001	0.25	0.25
0.001	0.010	0.0023	0.0030
0.002	0.010	0.0052	0.0059
0.004	0.010	0.012	0.012
0.006	0.010	0.018	0.018
0.008	0.010	0.024	0.024
0.010	0.010	0.030	0.030
0.04	0.010	0.12	0.12
0.06	0.010	0.18	0.18
0.08	0.010	0.24	0.24
0.10	0.010	0.30	0.30

^a substrate concentration, 4×10^{-5} mol dm⁻³.

^b Data measured at 474 nm.

^c Calculated according to Equation 5.8, with values of k_7 , 3 dm³ mol⁻¹ s⁻¹ and $K_{C,5}$, 0.035 dm³ mol⁻¹ in 0.001 mol dm⁻³ benzylamine perchlorate, and k_7 , 3 dm³ mol⁻¹ s⁻¹ and $K_{C,5}$, 0 dm³ mol⁻¹ in 0.01 mol dm⁻³ benzylamine perchlorate.

Table 5.16: Kinetic data for the reaction of **5.7iii**^a with benzylamine in DMSO at 25 °C.

[Benzylamine] / mol dm ⁻³	[BenzylamineH ⁺ ClO ₄ ⁻] / mol dm ⁻³	k _{fast} ^b / s ⁻¹	k _{calc} ^c / s ⁻¹	k _{slow} ^d / s ⁻¹	k _{calc} ^e / s ⁻¹
0.03	0.001	241	242		
0.04	0.001	227	223		
0.05	0.001	226	221		
0.06	0.001	228	228		
0.08	0.001	252	254		
0.10	0.001	289	289		
0.006	0.002			0.0064	0.0060
0.008	0.002			0.0084	0.0080
0.010	0.002			0.010	0.010
0.02	0.002			0.019	0.019
0.05	0.002			0.033	0.034
0.08	0.002			0.036	0.036
0.10	0.002			0.035	0.035
0.006	0.010			0.0064	0.0057
0.008	0.010			0.0086	0.0075
0.010	0.010			0.010	0.0094
0.04	0.010			0.036	0.036
0.06	0.010			0.049	0.050
0.08	0.010			0.060	0.060
0.10	0.010			0.068	0.068

^a substrate concentration, 4×10^{-5} mol dm⁻³.

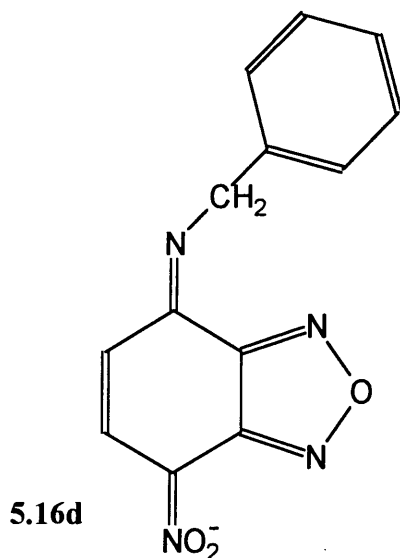
^b Data measured at 350 nm.

^c Calculated according to Equation 5.3, with values of k_5 , 2.4×10^3 dm³ mol⁻¹ s⁻¹ and $k_{-5}k_{AmH^+}/k_{Am}$, 5.1×10^3 s⁻¹.

^d Data measured at 474 nm.

^e Calculated according to Equation 5.8, with values of k_7 , 1 dm³ mol⁻¹ s⁻¹ and $K_{C,5}$, 0.38 dm³ mol⁻¹ in 0.002 mol dm⁻³ benzylamine perchlorate, and k_7 , 1 dm³ mol⁻¹ s⁻¹ and $K_{C,5}$, 0.40 dm³ mol⁻¹ in 0.010 mol dm⁻³ benzylamine perchlorate.

Absorbance measurements again proved useful for the study of the equilibrium deprotonation of **5.15d** in the presence of excess benzylamine to give **5.16d**, Table 5.17.

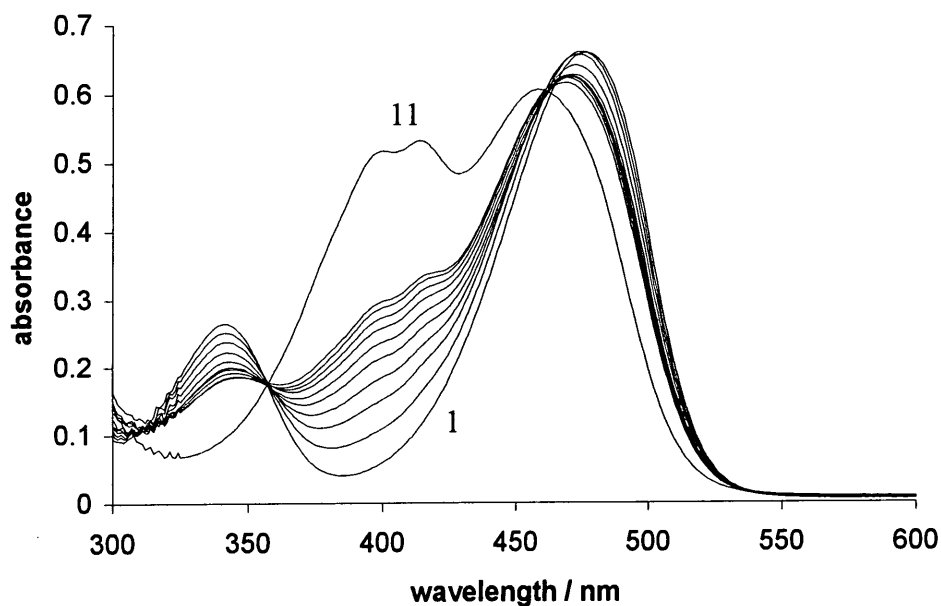


The UV/Visible spectrum of **5.15d** in the presence of $0.010 \text{ mol dm}^{-3}$ benzylamine perchlorate has λ_{max} 474 nm. In the presence of excess benzylamine ionisation occurred to give **5.16d** with λ_{max} 414 nm and 460 nm, as shown in Figure 5.5. The equilibrium constant for the formation of **5.16d**, K_{dep} , was conveniently calculated from absorbance measurements at 414 nm according to Equation 5.22. An average K_{dep} value of 0.130 ± 0.001 , was calculated from the individual values given in Table 5.17.

Table 5.17: Absorbance data for the equilibrium deprotonation of **5.15d** to give **5.16d**.

Spectrum	[Benzylamine] / mol dm ⁻³	[BenzylamineH ⁺ ClO ₄ ⁻] / mol dm ⁻³	Abs at 414 nm	K _{dep}
1	0	0.01	0.112	
2	0.01	0.01	0.161	0.130
3	0.02	0.01	0.200	0.132
4	0.03	0.01	0.229	0.129
5	0.04	0.01	0.256	0.130
6	0.05	0.01	0.277	0.129
7	0.06	0.01	0.297	0.131
8	0.07	0.01	0.312	0.129
9	0.08	0.01	0.325	0.128
10	0.09	0.01	0.333	0.123
11	0.10	0	0.532	

Figure 5.5: UV/Visible spectra for the equilibrium deprotonation of **5.15d** in the presence of excess benzylamine to give **5.16d**. Spectra are labelled according to Table 5.17.



5.3.2.5 Reactions of N-Methylbenzylamine

Two time-separated processes were measured for the reaction of N-methylbenzylamine with the chloro-derivative, **5.7i**, Table 5.18. The fast reaction was fitted to Equation 5.1 and corresponded to the formation of the 5-adduct, **5.12ie**, where proton transfer from the zwitterion **5.11ie**, was partially rate-limiting. A k_5 value of $1.8 \times 10^4 \text{ dm}^3 \text{ mol}^{-1} \text{ s}^{-1}$ was calculated from combination of the $K_5 k_{\text{Am}}$ and k_{Am}/k_{-5} values, where $K_5 = k_5/k_{-5}$. The equilibrium constant, $K_{\text{C},5}$, $2 \text{ dm}^3 \text{ mol}^{-1}$, was calculated from the $K_5 k_{\text{Am}}$ and k_{AmH^+} values according to Equation 5.4. Data for the slow process were fitted to Equation 5.8, corresponding to rate-limiting formation of the 7-adduct, **5.14ie**, on the substitution pathway. The two processes correlated extremely well, as both gave a $K_{\text{C},5}$ value of $2 \text{ dm}^3 \text{ mol}^{-1}$.

Table 5.19 contains data for the reaction of N-methylbenzylamine with the methoxy-derivative, **5.7ii**. Only one process was observed, corresponding to the rate-limiting formation of the 7-adduct, **5.14iie** on the substitution pathway. The data were fitted according to Equation 5.6, and show that proton transfer is partially rate-limiting in the formation of the 7-adduct. The $K_7 k_{\text{Am}}$ and k_{Am}/k_{-7} values yield a k_7 value of $2.5 \text{ dm}^3 \text{ mol}^{-1} \text{ s}^{-1}$. A $K_{\text{C},5}$ value, $0.004 \text{ dm}^3 \text{ mol}^{-1}$, was determined from Equation 5.6, but is quite low, indicating the low thermodynamic stability of the 5-adduct.

Similarly, the data for reaction of N-methylbenzylamine with 4-nitro-7-phenoxybenzofurazan, **5.7iii**, were fitted to Equation 5.6. There was no kinetic evidence for an initial, rapid reaction to give the 5-adduct, **5.12iiie**, although a $K_{\text{C},5}$ value of $0.01 \text{ dm}^3 \text{ mol}^{-1}$ was obtained from the data for the slow reaction. Combination of the $K_7 k_{\text{Am}}$ and k_{Am}/k_{-7} values gave a k_7 value of $1.6 \text{ dm}^3 \text{ mol}^{-1} \text{ s}^{-1}$ according to the relationship, $K_7 = k_7/k_{-7}$.

Table 5.18: Kinetic data for the reaction of **5.7i**^a with N-methylbenzylamine in DMSO at 25 °C.

[N-methylbenzylamine] / mol dm ⁻³	[N-methylbenzylamineH ⁺ ClO ₄ ⁻] / mol dm ⁻³	k _{fast} ^b / s ⁻¹	k _{calc} ^c / s ⁻¹	k _{slow} ^d / s ⁻¹	k _{calc} ^e / s ⁻¹
0.01	0	26	20		
0.02	0	72	71		
0.03	0	148	146		
0.04	0	247	240		
0.05	0	347	344		
0.01	0.001	112	118		
0.02	0.001	182	160		
0.03	0.001	255	230		
0.04	0.001	290	310		
0.06	0.001	480	520		
0.08	0.001	620	770		
0.001	0.010			0.0087	0.0070
0.002	0.010			0.014	0.014
0.004	0.010			0.029	0.028
0.006	0.010			0.044	0.042
0.008	0.010			0.057	0.055
0.010	0.010			0.068	0.069
0.04	0.010			0.21	0.21
0.06	0.010			0.24	0.24
0.08	0.010			0.25	0.25
0.10	0.010			0.24	0.23

^a substrate concentration, 4×10^{-5} mol dm⁻³.

^b Data measured at 350 nm.

^c Calculated according to Equation 5.1, with values of K_5k_{Am} , 2.2×10^5 dm⁶ mol⁻² s⁻¹ and k_{AmH^+} , 1.1×10^5 dm³ mol⁻¹ s⁻¹ and k_{Am}/k_{-5} , 12 dm³ mol⁻¹.

^d Data measured at 488 nm.

^e Calculated according to Equation 5.8, with values of k_7 , 7 dm³ mol⁻¹ s⁻¹ and $K_{C,5}$, 2 dm³ mol⁻¹.

Table 5.19: Kinetic data for the reaction of **5.7ii**^a with N-methylbenzylamine in DMSO at 25 °C.

[N-methylbenzylamine] / mol dm ⁻³	[N-methylbenzylamineH ⁺ ClO ₄ ⁻] / mol dm ⁻³	k _{slow} ^b / s ⁻¹	k _{calc} ^c / s ⁻¹
0.01	0.001	0.00030	0.00025
0.02	0.001	0.0010	0.0010
0.03	0.001	0.0022	0.0022
0.04	0.001	0.0038	0.0039
0.05	0.001	0.0056	0.0059
0.06	0.001	0.0082	0.0084
0.10	0.001	0.021	0.022
0.15	0.001	0.043	0.045
0.2	0.001	0.070	0.072
0.25	0.001	0.096	0.10
0.3	0.001	0.13	0.13
0.4	0.001	0.17	0.17
0.01	0.001	0.00029	0.00025
0.02	0.010	0.00095	0.0010
0.03	0.010	0.0023	0.0022
0.04	0.010	0.0039	0.0039
0.05	0.010	0.0061	0.0060
0.07	0.010	0.012	0.012
0.10	0.010	0.023	0.023
0.15	0.010	0.047	0.049
0.2	0.010	0.079	0.083
0.25	0.010	0.12	0.12
0.3	0.010	0.16	0.17
0.4	0.010	0.26	0.27
0.5	0.010	0.36	0.37

^a substrate concentration, 4×10^{-5} mol dm⁻³.

^b Data measured at 488 nm.

^c Calculated according to Equation 5.6, with values of K_7k_{Am} , $2.5 \text{ dm}^6 \text{ mol}^{-2} \text{ s}^{-1}$ and k_{Am}/k_7 , $1 \text{ dm}^3 \text{ mol}^{-1}$ and $K_{C,5}$, $0.004 \text{ dm}^3 \text{ mol}^{-1}$.

Table 5.20: Kinetic data for the reaction of **5.7iii**^a with N-methylbenzylamine in DMSO at 25 °C.

[N-methylbenzylamine] / mol dm ⁻³	[N-methylbenzylamineH ⁺ ClO ₄] / mol dm ⁻³	k_{slow}^b / s ⁻¹	k_{calc}^c / s ⁻¹
0.006	0.01	0.00075	0.00070
0.008	0.01	0.0012	0.0012
0.010	0.01	0.0018	0.0018
0.04	0.01	0.020	0.022
0.06	0.01	0.040	0.042
0.08	0.01	0.066	0.066
0.10	0.01	0.090	0.090
0.15	0.01	0.16	0.16
0.2	0.01	0.23	0.22
0.25	0.01	0.30	0.29
0.3	0.01	0.37	0.35
0.4	0.01	0.48	0.47
0.5	0.01	0.55	0.56

^a substrate concentration, $4 \times 10^{-5} \text{ mol dm}^{-3}$.

^b Data measured at 488 nm.

^c Calculated according to Equation 5.6, with values of K_7k_{Am} , $21 \text{ dm}^6 \text{ mol}^{-2} \text{ s}^{-1}$ and k_{Am}/k_7 , $13 \text{ dm}^3 \text{ mol}^{-1}$ and $K_{C,5}$, $0.01 \text{ dm}^3 \text{ mol}^{-1}$.

5.4 Comparisons

It was found that values of rate and equilibrium constants showed some variation, depending on the ionic strength of the solution used. In particular, values for the equilibrium constant, $K_{C,5}$ were found to increase with increasing ionic strength, as expected for a reaction producing ionic products from neutral reagents. In the comparisons described here results are given for solutions containing 0.01 mol dm^{-3} of the amine perchlorate.

Data for the reaction of 4-nitro-7-chlorobenzofurazan, **5.7i**, with the five aliphatic amines are given in Table 5.21. A 5-adduct, **5.12i**, was observed in all cases, and the rate constant k_5 , shows that the formation was extremely rapid. For the two primary amines, butylamine and benzylamine, and the smaller of the three secondary amines, pyrrolidine, the initial attack was rate-limiting in the formation of **5.12i**. However, for the two bulkier secondary amines, piperidine and N-methylbenzylamine, proton transfer from the zwitterion, **5.11i**, became partially rate-limiting in the formation of **5.12i**.

This is probably due to steric hindrance to proton transfer at the amine centre, due to the bulky nature of the secondary amines. There is a good correlation between the $K_{C,5}$ values obtained for the formation of **5.12i** with the pK_a values of the amines in DMSO. Hence the adduct formed from reaction of butylamine ($pK_a = 11.12$ in DMSO) has the greatest $K_{C,5}$ value, while the adduct **5.12ie**, formed from N-methylbenzylamine has the lowest $K_{C,5}$ value ($pK_a = 9.30$ in DMSO).

There is no correlation for the k_5 or k_7 values with the pK_a values measured in DMSO, as the pK_a is a measure of the extent of protonation at the nitrogen centre, whereas the k_5 and k_7 values measure nucleophilicity at a carbon centre.

Table 5.21: Summary of data for the reaction of 4-nitro-7-chlorobenzofurazan, **5.7i**, with amines in DMSO.

	Piperidine	Pyrrolidine	Butylamine	Benzylamine	N-Methylbenzylamine
pK _a	10.85	11.06	11.12	10.16	9.30
k ₅ / dm ³ mol ⁻¹ s ⁻¹	1.5 x 10 ⁵	3 x 10 ⁵	4.5 x 10 ⁴	1.44 x 10 ⁴	1.8 x 10 ⁴
(k _{Am} /k ₅) / dm ³ mol ⁻¹	480				12
(k ₅ k _{AmH⁺} /k _{Am}) / s ⁻¹	650		105	460	9.2 x 10 ³
k _{AmH⁺} / s ⁻¹	3.1 x 10 ⁵				1.1 x 10 ⁵
K _{C,5} / dm ³ mol ⁻¹	233	410	430	31	2
k ₇ / dm ³ mol ⁻¹ s ⁻¹	155	180	4.8	1.32	7

The rate and equilibrium constants measured for the reaction of 4-nitro-7-methoxybenzofurazan, **5.7ii**, with the amines in DMSO are given in Table 5.22. In most cases, the reaction to produce the 5-adduct, **5.12ii**, was inconveniently rapid for measurement at amine concentrations where appreciable adduct formation occurred. However, a measure of the stability of these adducts could be gained from the data for the slow reaction. Nevertheless, it was possible to study the rapid formation of the adduct **5.12iic**, during the reaction of **5.7ii** with butylamine. The initial attack of the amine was rate-limiting. There was no evidence for the formation of the 5-adduct, **5.12iia**, from either a measurable fast process, or the data for the substitution process. The stability of the 5-adducts, **5.12ii**, are again reflected by the pK_a values of the amines in DMSO.

Data for the slow process to give the substitution product, **5.15**, reveal a variety of rate-limiting steps in the reaction, depending on the nature of the amine. For the primary amines, n-butylamine and benzylamine, the attack of the amine at the 7-position is rate-limiting, and the formation of the 7-adduct, **5.14ii**, is followed by the rapid expulsion of the methoxy-leaving group to give **5.15**. In the reaction of **5.7ii** with pyrrolidine and N-methylbenzylamine, proton transfer is partially rate-limiting in the formation of **5.14ii**, and this is again followed by rapid departure of the methoxy-leaving group to give **5.15**.

However, in the reaction of **5.7ii** with piperidine, the expulsion of the methoxy-group becomes rate-limiting, and there is an observed build-up of the 7-adduct, **5.14ii**, in the UV/Visible spectra measured over time.

Table 5.22: Summary of data for the reaction of 4-nitro-7-methoxybenzofurazan, **5.7ii**, with amines in DMSO.

	Piperidine	Pyrrolidine	Butylamine	Benzylamine	N-Methylbenzylamine
pK_a	10.85	11.06	11.12	10.16	9.30
$k_5 / \text{dm}^3 \text{mol}^{-1} \text{s}^{-1}$			4100		
$(k_5 k_{AmH^+} / k_{Am}) / \text{s}^{-1}$			6800		
$K_{C,5} / \text{dm}^3 \text{mol}^{-1}$		0.42	0.63	0.04	0.004
$k_7 / \text{dm}^3 \text{mol}^{-1} \text{s}^{-1}$	45	134	11.2	3	2.5
$(k_{Am} / k_7) / \text{dm}^3 \text{mol}^{-1}$		500			1
$(k_7 k_{AmH^+} / k_{Am}) / \text{s}^{-1}$	1.9				
$K_{C,7} / \text{dm}^3 \text{mol}^{-1}$	24				
$k_4 K_{C,7} / \text{dm}^6 \text{mol}^{-2} \text{s}^{-1}$	1×10^3				
$k_4 / \text{dm}^3 \text{mol}^{-1} \text{s}^{-1}$	39				

Table 5.23 contains a summary of the reactions involving 4-nitro-7-phenoxybenzofurazan, **5.7iii**. A fast process, corresponding to the formation of the 5-adduct, **5.12iii**, was observed for butylamine, benzylamine and pyrrolidine, although there was evidence for the formation of **5.12iii** for all the amines, from the data for the slow process. For butylamine and benzylamine, rate-limiting attack of the amine at the 5-position was observed, while for pyrrolidine, the proton transfer from **5.11iiib**, was partially rate-limiting in the formation of **5.12iiib**.

There is a correlation between the $K_{C,5}$ values and the pK_a values of the amines in DMSO, as the most basic amine, n-butylamine, gave the most stable 5-adduct, while the least basic, N-methylbenzylamine, produced the least stable 5-adduct.

The rate-limiting step of the slow process to form the 7-adduct, **5.14iii**, was dependent on the nature of the amine. For the primary amines, n-butylamine and benzylamine, the initial attack of the amine was rate-limiting, whereas proton transfer from **5.13iii** became partially rate-limiting for reactions involving the secondary amines.

Table 5.23: Summary of data for the reaction of 4-nitro-7-phenoxybenzofurazan, **5.7iii**, with amines in DMSO.

	Piperidine	Pyrrolidine	Butylamine	Benzylamine	N-Methylbenzylamine
pK _a	10.85	11.06	11.12	10.16	9.30
k ₅ / dm ³ mol ⁻¹ s ⁻¹		1.5 x 10 ⁵	8200	2.4 x 10 ³	
(k _{Am} /k ₅) / dm ³ mol ⁻¹		4000			
(k ₅ k _{AmH⁺} /k _{Am}) / s ⁻¹			1500	5.1 x 10 ³	
K _{C,5} / dm ³ mol ⁻¹ k _{AmH⁺} / s ⁻¹	2.3	5.3	8	0.40	0.01
k ₇ / dm ³ mol ⁻¹ s ⁻¹	42	78	4.1	1.0	1.6
(k _{Am} /k ₇) / dm ³ mol ⁻¹	300	2300			13

5.4.1 The Directing Effects and Leaving Group Abilities of the X-Substituents

The study has allowed a direct comparison of the relative directing and leaving group abilities of the three X-substituents. The relative leaving group ability is $\text{Cl}^- > \text{PhO}^- > \text{MeO}^-$, and this is reflected by the variation in the rate-limiting step and the measured rate constants. The relative nucleophilicities and basicities of the amines, and the stabilities of the adducts formed are compared in Table 5.24.

Table 5.24: A comparison of the relative reactivities of the amines towards the substrates and the 5-adduct stability.

Amine	pK _a	$k_7(\text{Cl})/$ $k_7(\text{OMe})$	$k_7(\text{Cl})/$ $k_7(\text{OPh})$	$k_7(\text{OMe})/$ $k_7(\text{OPh})$	$K_{\text{C},5}(\text{Cl})/$ $K_{\text{C},5}(\text{OMe})$	$K_{\text{C},5}(\text{Cl})/$ $K_{\text{C},5}(\text{OPh})$
Piperidine	10.85	3.4	3.7	1.1		100
Pyrrolidine	11.06	1.3	2.3	1.7	980	77
Butylamine	11.12	0.4	1.2	2.7	680	54
Benzylamine	10.16	0.4	1.3	3.0	780	78
N-Methylbenzylamine	9.30	2.8	4.4	1.6	500	200

The k_7 values for reaction at the 7-position of **5.7i** are one to four times greater than for reaction at the 7-positions of **5.7ii** or **5.7iii**, for attack of secondary amines. The ratio is smaller for the reaction of primary amines where the $k_7(\text{Cl})/k_7(\text{OMe})$ ratio is less than one.

This trend is reversed for reactions involving **5.7ii** and **5.7iii**. For primary amines the $k_7(\text{OMe})/k_7(\text{OPh})$ ratio is around 3.0. However, for secondary amines, $k_7(\text{OMe})/k_7(\text{OPh})$ decreases to around 1.0. The results may indicate small steric effects between the group at the 7-position and the entering amine which increase in the order $\text{Cl} < \text{OMe} < \text{OPh}$ and primary amine < secondary amine.

The Hammett values of the three substituents are given in Table 5.25. The positive σ_{meta} values illustrate that the 7-substituents exert an electron-withdrawing effect at the 5-position giving increased stabilisation to the 5-adducts formed. The chloro-substituent exhibits the greater meta-directing ability relative to phenoxide and methoxide. Hence the

5-position of 4-nitro-7-chlorobenzofurazan is more susceptible to nucleophilic attack, and greater values of k_5 and $K_{C,5}$ were measured in comparison with the methoxy-derivative, **5.7ii**, or the phenoxy-derivative, **5.7iii**.

Table 5.25: Hammett σ_{meta} values for the 7-substituents.

	X	σ_{meta}
5.7i	Cl	0.37
5.7ii	OMe	0.08
5.7iii	OPh	0.25

The rate of removal of phenoxide is rapid relative to that of methoxide, and this may be due to the resonance stabilisation afforded by the delocalisation of electrons into the aromatic ring, as in Figure 5.6.

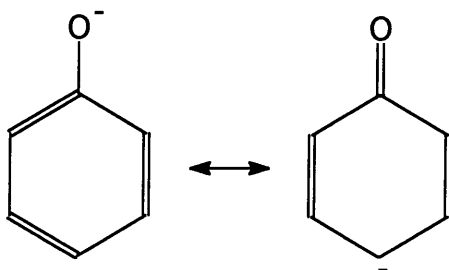
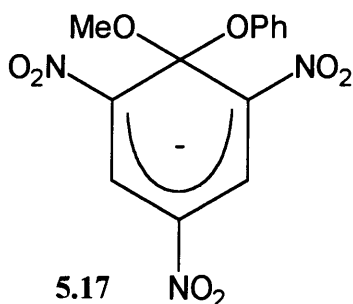


Figure 5.6

The different leaving group abilities of alkoxide and phenoxide ions have been studied by Bernasconi and co-workers.¹¹ Phenoxide ion departure from **5.17** is 10^6 times faster than methoxide ion departure.



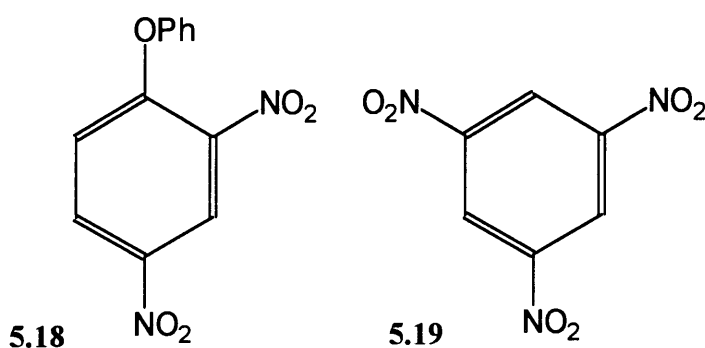
Methoxide ($\text{p}K_{\text{a}} = 29.0$) is a stronger base in DMSO than phenoxide ($\text{p}K_{\text{a}} = 18.0$),^{12,2} and this may enhance the stability of the 7-adducts, **5.14ii**, relative to the substitution product,

5.15. This, together with the decrease in leaving group ability, leads to a build-up of the 7-adduct in the UV/Visible absorbance spectra.

5.4.2 Reactivity of Piperidine and Pyrrolidine

Piperidine and pyrrolidine are very similar in properties such as their pK_a values in DMSO,¹³ and electron delocalisation ability towards unsaturated systems.¹⁴ Piperidine has a greater steric requirement relative to pyrrolidine, with the lone pair electrons being shielded. This is due to the conformation of the six-membered ring, in relation to that of the five-membered ring of pyrrolidine.¹⁵ For these stereoelectronic reasons, reactions which involve possible rate-limiting expulsion of the leaving group are very much more rapid when pyrrolidine is the nucleophile than piperidine.³ For example, in the reaction of 1-ethoxy-2,4-dinitronaphthalene with amines in DMSO, product formation was found to be approximately 10^4 times faster with pyrrolidine than with piperidine.¹⁵

However, for reactions where leaving group expulsion is not rate-limiting, the reactivities of pyrrolidine and piperidine are quite similar. Thus Bunnett and co-workers studied the reactions of **5.18** and **5.19** with piperidine and pyrrolidine, and found that the rate of reaction of pyrrolidine was greater by a factor of 1.5 for **5.18**, and by 2.5 for **5.19**.^{16,15}



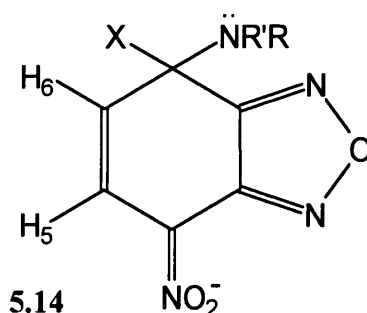
Pyrrolidine is more reactive than piperidine towards all three derivatives studied in the present work. A comparison of the relative rate and equilibrium constants is given in Table 5.26. The k_7 ratio is greater for the methoxy-derivative, where leaving group departure may be rate-limiting. Where measurable, the $K_{C,5}$ ratio is around 2.0. The two amines have similar pK_a values in DMSO, and the difference in the stability of the 5-adducts, **5.12ii**, is probably due to the steric hindrance of the lone pair electrons on piperidine. The

bulkier amine may also exert a steric effect, whereby the nitro-group is displaced from the ring-plane, and the resonance delocalisation available decreases.

Table 5.26: Reactivity of piperidine vs pyrrolidine.

Substrate	$k_5(\text{pyrrolidine})/$ $k_5(\text{piperidine})$	$K_{C,5}(\text{pyrrolidine})/$ $K_{C,5}(\text{piperidine})$	$k_7(\text{pyrrolidine})/$ $k_7(\text{piperidine})$
5.7i	2	1.8	1.2
5.7ii			3.0
5.7iii		2.3	1.8

A major difference between the reactions of **5.7ii** with piperidine and pyrrolidine is that only in the reaction with the former amine is the intermediate in the reaction pathway observable. The unshared electron pair on the nitrogen atom in **5.14** probably plays a role in the expulsion of the leaving group.¹⁵ This implies that the unshared electron pair must be anti-periplanar with respect to the rupturing C-X bond in the transition state. The evidence indicates that this conformation is much more difficult to achieve for piperidine than pyrrolidine.¹⁵



5.4.3 Reactivity of Primary and Secondary Amines

Butylamine is the only amine for which reaction to produce a 5-adduct was observed for all three substrates. Equilibrium constants for the formation of **5.12i-iii**, with butylamine are given in Table 5.27, together with Hammett σ_{meta} values for the 7-substituents. There is a definite correlation between the electron-withdrawing capabilities of the 7-substituents and the stability of the adducts formed.

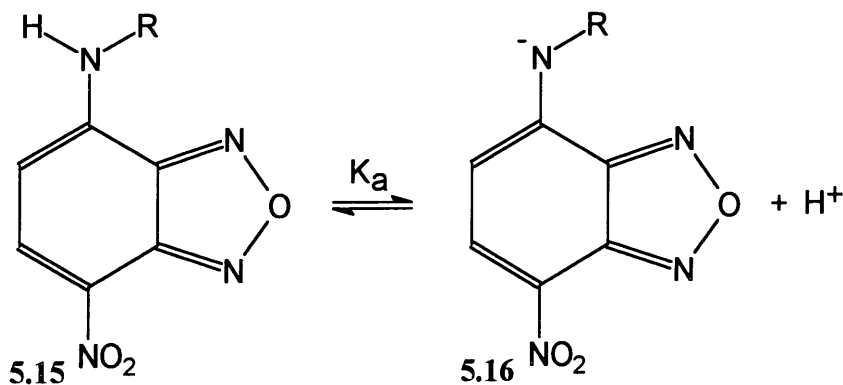
Table 5.27: Comparison of the stability of the 5-adducts, **5.12i-iii**, formed from addition of butylamine.

	X	$K_{C,5} / \text{dm}^3 \text{mol}^{-1}$	σ_{meta}
5.7i	Cl	430	0.37
5.7ii	OMe	0.63	0.08
5.7iii	OPh	8	0.25

The formation of the substitution product, **5.15**, is the final stage in the reaction of the substrates with secondary amines. However, **5.15**, formed from reaction of the substrates with primary amines may undergo deprotonation to **5.16**, Scheme 5.4. It is worth noting that this deprotonation does not affect the kinetics of the reaction studied, since it is a rapid equilibrium occurring after the rate-determining step. The equilibrium constant for deprotonation, K_{dep} , has been determined as 0.53 ± 0.05 for butylamine, and 0.130 ± 0.001 for benzylamine, Table 5.28. These K_{dep} values may be used to calculate the pK_a value of the substitution product, **5.15**, defined in Scheme 5.5, according to Equations 5.23 and 5.24.

Table 5.28: Summary of the K_{dep} values calculated for the equilibrium deprotonation of **5.15** to **5.16** in the presence of excess amine.

	pK_a	K_{dep}	pK_{dep}
Butylamine	11.12	0.53 ± 0.05	0.28
Benzylamine	10.16	0.130 ± 0.001	0.89



Scheme 5.5

$$\text{Equation 5.23: } K_{\text{dep}} = \frac{K_{\text{a}}(\mathbf{5.15})}{K_{\text{a}}(\text{parent amine})}$$

$$\text{Equation 5.24: } \text{p}K_{\text{a}}(\mathbf{5.15}) = \text{p}K_{\text{dep}} + \text{p}K_{\text{a}}(\text{parent amine})$$

Therefore, the $\text{p}K_{\text{a}}$ values of the substitution products, **5.15c** and **5.15d** are 11.40 and 11.05 units respectively. The neutral compounds, **5.15c** and **5.15d** are therefore only slightly less acidic than the ammonium ions formed from the corresponding parent amines.

N-methylbenzylamine ($\text{p}K_{\text{a}} = 9.30$) is less basic than benzylamine ($\text{p}K_{\text{a}} = 10.16$), but the nucleophilicity of this amine, as measured by the k_7 and k_5 values, appears greater than the less sterically hindered benzylamine. It is possible that the N-methyl group may inductively donate electrons to the nitrogen centre, hence increasing the nucleophilic reactivity. However, steric considerations would suggest that the bulkier, secondary amine display lower reactivity than the primary amine. A comparison of the $K_{\text{c},5}$ values shows that the 5-adducts, **5.12i-iii**, formed from benzylamine are more stable than those formed from N-methylbenzylamine, and here, there is a correlation with the basicity of the amine. This is probably due to the much greater values of k_5 for the reaction with N-methylbenzylamine, due to steric congestion in the zwitterions, **5.11i-iii**,³ and the greater leaving group ability of N-methylbenzylamine relative to benzylamine.¹⁷

This reflects the general phenomenon observed in this work, that, relative to primary amines, the secondary amines have unusually high nucleophilicities. This is likely to be due to the ability of the solvent, DMSO, to effectively stabilise ammonium ions through hydrogen bonding interactions. Primary ammonium ions, having three NH-hydrogens, will be more stabilised than secondary ammonium ions. Hence the proton acidities of the primary amines are reduced relative to the secondary amines. This leads to apparently low proton basicities for the secondary amines. However, when nucleophilic attack occurs at a ring carbon atom, only partial charge development occurs at nitrogen. Hence the high reactivity of the secondary amines. Primary amines have high proton basicities, but relatively low nucleophilicities, as charge development is only partial in the transition state.

The rate-limiting step of the reaction is dependent on the nature of the amine. In general, attack of the amine is rate-limiting for reactions involving primary amines, whereas proton-transfer becomes partially rate-limiting for reactions involving secondary amines.

5.4.4 Amine Attack at Substituted vs Unsubstituted Positions

Comparison of the data in Tables 5.21-5.23 show that for substrates **5.7i-iii**, values of k_5 are, for a given amine, larger than the values of k_7 , by a factor of around 10^3 . Hence there is a kinetic preference for attack at the 5-position. For reaction to produce the 5-adducts, **5.12i-iii**, the reaction occurs in each case at an unsubstituted ring position. Therefore, steric factors at the reaction centre should be the same for all three substrates.

A summary of the rate and equilibrium constants measured for the reaction of the five amines with 4-nitrobenzofurazan, **5.7** ($X = H$), is given in Table 5.29. The data are taken from Chapter 4.

Table 5.29: Summary of data for the reaction of 4-nitrobenzofurazan with amines in DMSO at 25 °C.

	Piperidine	Pyrrolidine	Butylamine	Benzylamine	N-Methylbenzylamine
pK_a	10.85	11.06	11.12	10.16	9.30
$k_5 / \text{dm}^3 \text{mol}^{-1} \text{s}^{-1}$	6.4×10^4	2×10^5	1.4×10^4	3.4×10^3	
$(k_5 k_{\text{AmH}^+} / k_{\text{Am}})$ $/ \text{s}^{-1}$	7800		600	1.8×10^3	
$K_{C,5} / \text{dm}^3 \text{mol}^{-1}$	8.13	17.3	23	1.9	0.06
k_{AmH^+} $/ \text{dm}^3 \text{mol}^{-1} \text{s}^{-1}$	6.2×10^6				
$k_7 / \text{dm}^3 \text{mol}^{-1} \text{s}^{-1}$	1800	3000	54	14.8	191
$(k_7 k_{\text{AmH}^+} / k_{\text{Am}})$ $/ \text{s}^{-1}$	0.16	0.23	0.03	0.15	3.4
$K_{C,7} / \text{dm}^3 \text{mol}^{-1}$	11300	13000	1800	100	57
k_{AmH^+} $/ \text{dm}^3 \text{mol}^{-1} \text{s}^{-1}$					440

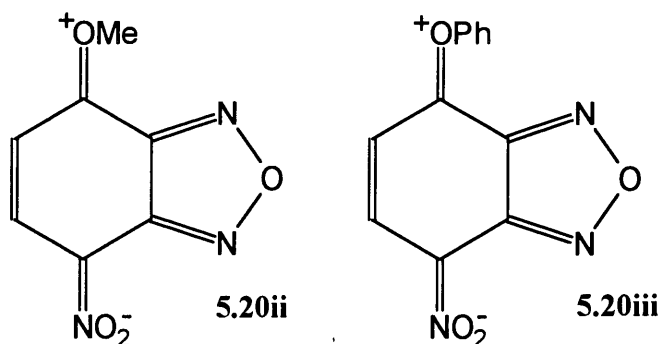
The relative stabilities of the 5-adducts, **5.12i-iii**, are compared to those formed from 4-nitrobenzofurazan, (X = H), in Table 5.30. The k_7 values are also compared for reaction at a substituted position, (substrates **5.7i-iii**) with those measured at the unsubstituted 7-position of 4-nitrobenzofurazan.

Table 5.30: Comparison of the rate and equilibrium parameters for substrates **5.7i-iii** with **5.7**, (X = H).

	Piperidine	Pyrrolidine	Butylamine	Benzylamine	N-Methylbenzylamine
$K_{C,5}(H)/$ $K_{C,5}(Cl)$	0.03	0.04	0.05	0.06	0.03
$k_7(H)/k_7(Cl)$	11.6	16.7	11.3	11.2	27.3
$K_{C,5}(H)/$ $K_{C,5}(OMe)$		41	37	48	15
$k_7(H)/k_7(OMe)$	40	22	5	5	76
$K_{C,5}(H)/$ $K_{C,5}(OPh)$	3.5	3.3	2.9	4.8	6
$k_7(H)/k_7(OPh)$	43	38	13	15	120

The ratio of the $K_{C,5}$ values measured for 4-nitrobenzofurazan and the chloro-derivative are all approximately 0.04. This illustrates the greater meta-directing ability of the chloro-substituent relative to hydrogen. The greater electron-withdrawing power of this substituent leads to a 25-fold increase in the stability of the 5-adduct, **5.12i** over **5.12,H**.

Nevertheless, it is noteworthy that the $K_{C,5}(H)/K_{C,5}(OMe)$ and $K_{C,5}(H)/K_{C,5}(OPh)$ ratios are greater than unity. The σ_{meta} values for the methoxy and phenoxy groups are positive, hence they are expected to have an adduct-stabilising effect at the 5-position. The fact that this is not observed experimentally is likely to derive from the possibility of conjugation in the substrates as shown in structures **5.20ii** and **5.20iii**. This will stabilise the reactant molecules, but will be lost on adduct formation, hence explaining the reduced stabilities of the 5-adducts from **5.7ii** and **5.7iii**.



The $k_7(\text{H})/k_7(\text{X})$ values are all greater than 1. This is likely to reflect the repulsion between the entering and leaving groups in 7-substituted benzofurazans. The ratios are generally larger for the secondary than for the primary amines, reflecting the greater steric requirements of the secondary amines when attacking a substituted position. This effect is maximised with N-methylbenzylamine.

5.5 Conclusion

The study has enabled several comparisons to be drawn and has highlighted important correlations and trends within the amine series. Reaction to produce an adduct at the 5-position is kinetically preferred, but these adducts are not inherently stable, and undergo isomerism to yield the thermodynamically more stable 7-adducts. In most cases, this isomerism is followed by the rapid expulsion of the 7-substituent, to yield the substitution product, and the formation of the 7-adduct is rate-limiting on the reaction pathway. However, for reaction of the amines with the methoxy-derivative, the removal of the methoxy-group becomes rate-limiting for reaction with piperidine, and there is an observed build-up of the 7-adduct.

In general, the attack of the amine to yield the 5- or 7-adduct is rate-limiting for reaction with primary amines, whereas proton transfer from the zwitterion becomes partially rate-limiting for reactions involving secondary amines.

The equilibrium constant for the formation of the 5-adduct, $K_{\text{C},5}$, has been shown to correlate with the pK_a value of the ammonium ions in DMSO, and also with the σ_{meta} values of the 7-substituents, which exert an electron-withdrawing effect at the 5-position.

A pK_a value of the substitution product formed from reaction with primary amines has been estimated. The substitution product is slightly less acidic than the parent ammonium ion, and so the deprotonation equilibrium lies on the side of the substitution product with values of $K_{dep} < 1$.

5.6 References

- ¹ E. Bunce, M. R. Crampton, M. J. Strauss and F. Terrier. Electron Deficient Aromatic- and Heteroaromatic-Base Interactions. The Chemistry of Anionic Sigma Complexes. Elsevier. Amsterdam 1984.
- ² E. Bunce, J. M. Dust, A. Jonczyk, R. A. Manderville and I. Onyido., *J. Am. Chem. Soc.*, 1992, **114**, 5610.
- ³ R. A. Chamberlin and M. R. Crampton., *J. Chem. Soc., Perkin Trans. 2.*, 1995, 1831.
- ⁴ M. R. Crampton and P. J. Routledge., *J. Chem. Soc., Perkin Trans. 2.*, 1984, 573.
- ⁵ J. A. Orvik and J. F. Bunnett., *J. Am. Chem. Soc.*, 1970, **92**, 2417.
- ⁶ C. A. Fyfe, S. W. H. Damji and A. Koll., *J. Am. Chem. Soc.*, 1979, **101**, 951.
- ⁷ J. F. McGarrity, J. Prodoliet and T. Smyth., *Org. Mag. Res.*, 1981, **17**, 59.
- ⁸ S. Sekiguchi, T. Itagaki, T. Hirose, K. Matsui and K. Sekine., *Tetrahedron.*, 1973, **29**, 3527.
- ⁹ L. DiNunno, S. Florio and P. E. Todesco., *J. Chem. Soc., Perkin Trans. 2.*, 1975, 1469.
- ¹⁰ S. Uchiyama, T. Santa, T. Fukushima, H. Homma and K. Imai., *J. Chem. Soc., Perkin Trans. 2.*, 1998, 2165.
- ¹¹ C. F. Bernasconi and M. C. Muller., *J. Am. Chem. Soc.*, 1978, **100**, 5536.
- ¹² F. G. Bordwell., *Acc. Chem. Res.*, 1988, **21**, 456.
- ¹³ M. R. Crampton and I. A. Robotham., *J. Chem. Res. (S)*., 1997, 22.
- ¹⁴ W. Schwotzer and W. von Philipsborn., *Helv. Chim. Acta.*, 1977, **60**, 1501.
- ¹⁵ J. F. Bunnett, S. Sekiguchi and L. A. Smith., *J. Am. Chem. Soc.*, 1981, **103**, 4865.
- ¹⁶ J. F. Bunnett and A. V. Cartano., *J. Am. Chem. Soc.*, 1981, **103**, 4861.
- ¹⁷ C. F. Bernasconi, M. C. Muller and P. Schmid., *J. Org. Chem.*, 1979, **44**, 3189.

Chapter 6

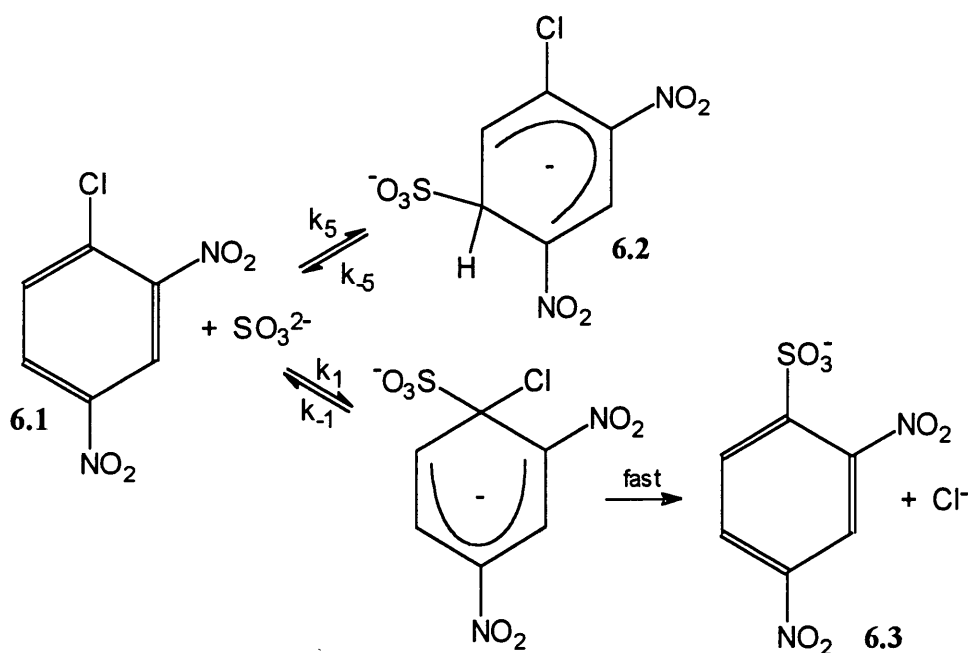
Kinetic and Equilibrium Studies of the Reactions of 4-Nitrobenzofurazan and some Derivatives, with Sulfite Ions in Water

6 Kinetic and Equilibrium Studies of the Reactions of 4-Nitrobenzofurazan, and some Derivatives, with Sulfite Ions in Water

6.1 Introduction

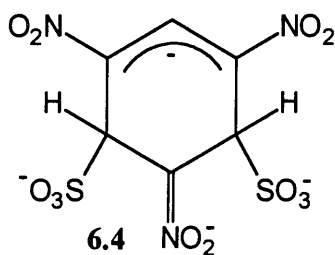
The sulfite ion, (SO_3^{2-}) is a highly reactive nucleophile, which does not exhibit ambident reactivity with electrophilic carbon, where attack is always by the sulfur atom.¹ This is in agreement with the concept of hard and soft acids and bases, according to Pearson.² It is well known, that in nucleophilic substitution reactions, sulfur bases are considerably more reactive than oxygen bases.³

Sulfite readily forms σ -adducts by reaction as a sulfur nucleophile with electron-deficient aromatics.^{4,5} Several studies have been reported involving σ -adduct formation and nucleophilic substitution, resulting from the reaction of sulfite with dinitro-⁶ and trinitrobenzene^{7,1,8} derivatives. For example, two processes were observed in the reaction of 1-chloro-2,4-dinitrobenzene, **6.1**, with sulfite ions in DMSO-water solvent systems, Scheme 6.1.⁶ The first corresponded to sulfite attack at C5 to give **6.2**, which was characterised by a rapid increase in absorbance at 540 nm. The band at 540 nm slowly decreased in intensity during the second process, to give a new absorption maximum at 340 nm, which was attributed to **6.3**, the substitution product.

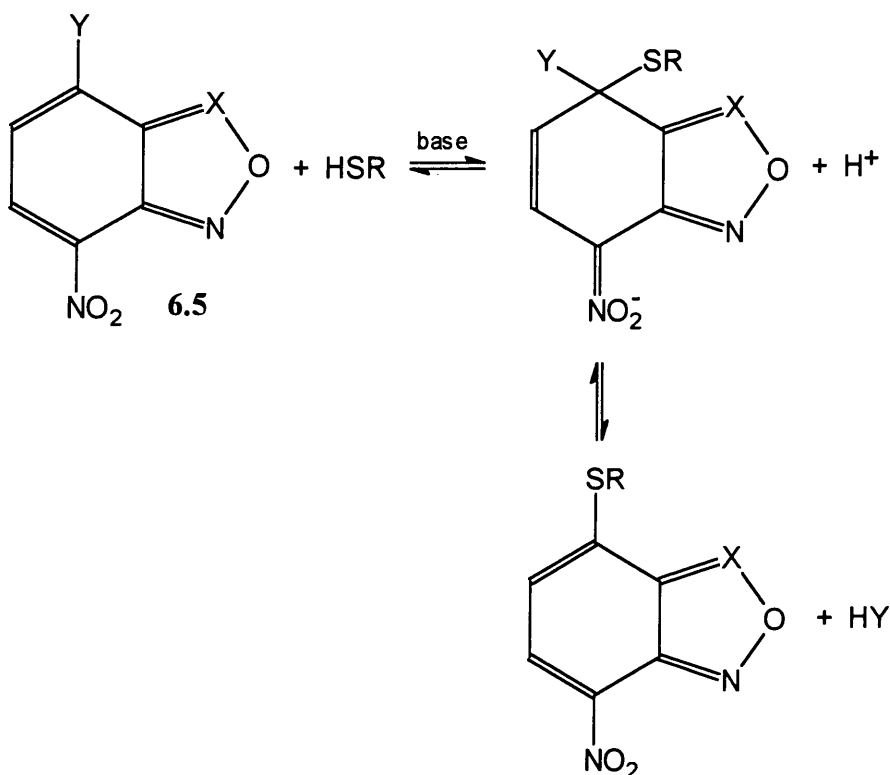


Scheme 6.1

In solutions containing a high concentration of sulfite ions, di-adducts, **6.4**, are readily observed during reaction with trinitrobenzene derivatives.^{7,8} These di-adducts may be characterised using UV/Visible absorbance measurements, or NMR chemical shifts.



In this work, the reactions of sulfite with some 4-nitrobenzofurazan derivatives have been studied, in order to further investigate the electrophilic reactivity of these compounds in comparison with trinitrobenzene. The derivatives, **6.5**, have been previously shown to act as *in vitro* inhibitors of nucleic acid and protein biosynthesis in animal cells,^{9,10} which is likely to involve σ -adduct formation with sulfur nucleophiles, Scheme 6.2.^{11,10}



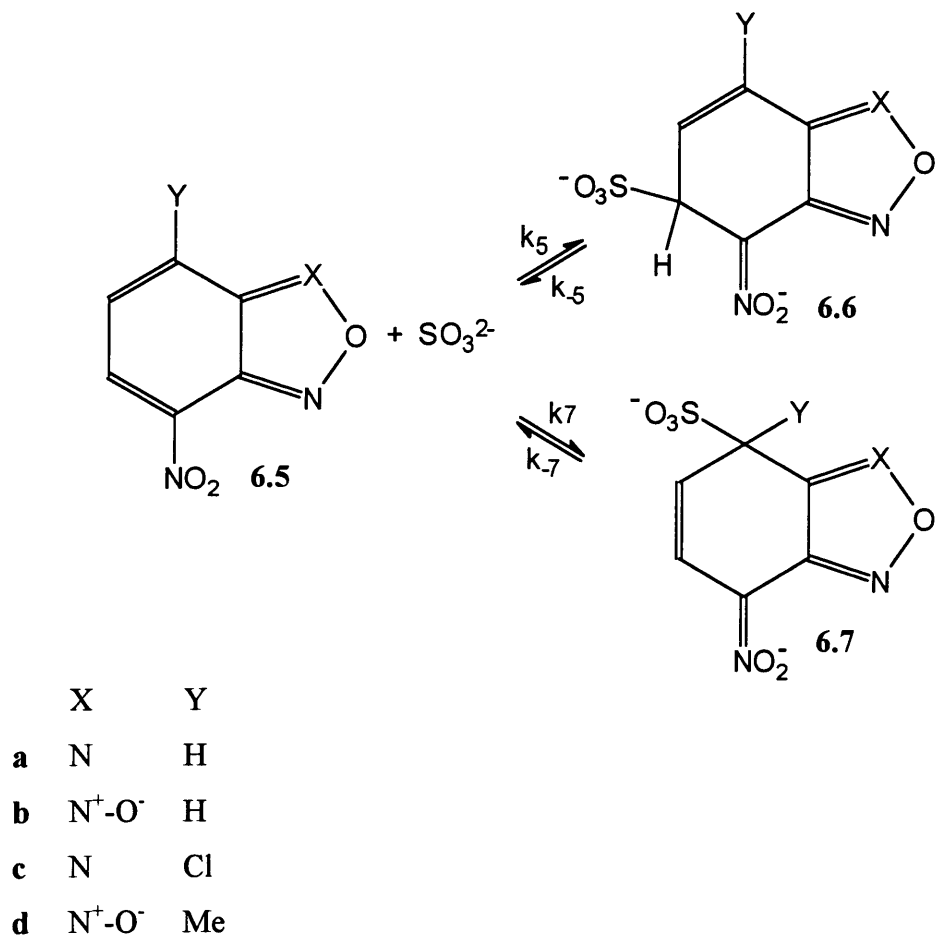
6.2 Experimental

A sample of 4-nitrobenzofurazan, **6.5a** (mp 92-94 °C, literature value⁹ 93 °C), was prepared by nitration of benzofurazan (Lancaster, 97%) with a 4:1 sulfuric:nitric acid mixture. 4-nitrobenzofuroxan, **6.5b** (mp 143 °C, literature value¹² 143 °C), was available from previous work. 4-nitro-7-chlorobenzofurazan, **6.5c**, was available from Aldrich, (98%, mp 97-99 °C). 4-nitro-7-methylbenzofuroxan, **6.5d**, (mp 166 °C, literature value¹³ 168 °C) was prepared by nitration of 5-methylbenzofuroxan (Lancaster, 97%) with fuming nitric acid to yield a mixture of **6.5d**, and the 4-nitro-5-methyl-derivative. This mixture was subsequently dissolved in acetic acid and heated for four hours at 110 °C. The acid layer was left to evaporate overnight in a fumes cupboard, and the resulting product, **6.5d**, was characterised by ¹H NMR. All other reagents and buffer components used were the purest available commercial products.

UV/Visible spectra were recorded using a Perkin-Elmer Lambda 2 spectrophotometer, while kinetic measurements were made at 25 °C using an Applied Photophysics SX-17 MV stopped-flow spectrophotometer. ¹H NMR spectra were recorded in D₂O and D₂O/[²H₆]DMSO mixtures, with a Varian Mercury 200 MHz spectrometer, or a Varian VXR 400 MHz spectrometer.

6.3 Results and Discussion

As all the derivatives studied contained only one nitro-group, di-adduct formation was not expected and the reaction was assumed to follow Scheme 6.3.



Scheme 6.3

6.3.1 NMR Data

The substrates, **6.5a-d**, were found to have poor solubility in D₂O, and for this reason, ¹H NMR spectra were recorded in 80/20 (v/v) D₂O/[²H₆]DMSO solvent. Data for the substrates and σ-adducts formed are summarised in Table 6.1.

Table 6.1: ¹H NMR data for parent molecules, **6.5**, and sulfite adducts, **6.6** and **6.7**, in 80/20 (v/v) D₂O/[²H₆]DMSO.

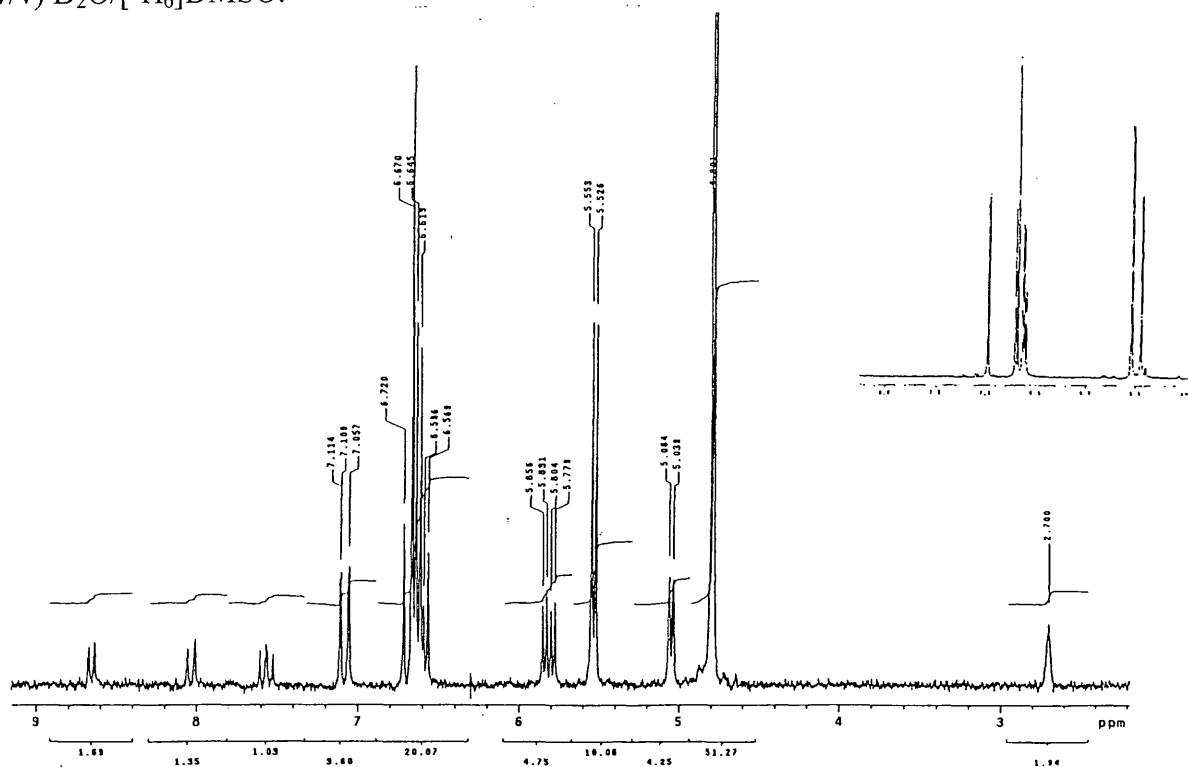
	¹ H NMR Shifts				J ₅₆ ^a	J ₆₇ ^a
	H ₅	H ₆	H ₇	Me		
Parent molecules						
6.5a	8.72	7.84	8.48		7.2	8.8
6.5b	8.65	7.57	8.04		7.2	9.2
6.5c	8.70	7.92			7.8	
6.5d	8.50	7.27		2.61	7.6	
5-adducts						
6.6a	5.54	6.72	7.04		5.8	9.8
6.6b	5.54	6.61	6.69		5.4	9.8
6.6c	5.61	6.82			6.2	
6.6d	5.40	6.22		2.23	6.2	
7-adducts						
6.7a	7.13	5.92	5.31		10.6	4.6
6.7b	7.08	5.82	5.04		10.4	5.0
6.7d	6.99	5.61		1.89	10.3	

^a J values in Hz

The reaction of **6.5** with sulfite occurred rapidly to give a spectrum characteristic of the formation of **6.6**. The chemical shift of H₆ in the ¹H NMR spectrum was around 6.6 ppm, thereby discounting the possible formation of the 7-adduct, **6.7**, which would be expected to give a much lower chemical shift value for H₆ (approximately 5.8 ppm).^{14,15}

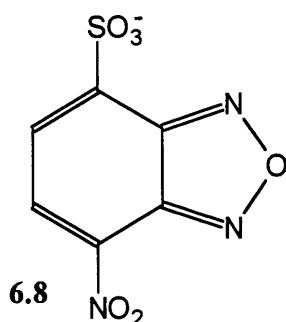
The spectrum of 4-nitrobenzofuroxan, **6.5b**, in the presence of sulfite indicated the initial attack at the 5-position, to give **6.6b**, with peaks of lower intensity indicating some isomerisation to the thermodynamically more stable 7-adduct, **6.7b**. The reaction was followed over several days in order to study the complete conversion to the 7-adduct, in accordance with Scheme 6.3. Figure 6.1 shows the spectrum obtained immediately on mixing an equimolar solution of 4-nitrobenzofuroxan, **6.5b**, and sulfite, with peaks due to the substrate, **6.5b**, (at 8.65, 8.04 and 7.57 ppm) the 5-adduct, **6.6b**, (at 6.69, 6.61 and 5.54 ppm) and the 7-adduct, **6.7b**, (at 7.08, 5.82 and 5.04 ppm). The H₆ and H₇ resonances in the 5-adduct overlapped to produce a multiplet, and so the spectrum was also recorded using a 400 MHz spectrometer in order to improve the resolution of the peaks, Figure 6.1 (inset).

Figure 6.1: ¹H NMR spectrum of the substrate, **6.5b**, and adducts **6.6b** and **6.7b**, formed immediately on mixing an equimolar solution of 4-nitrobenzofuroxan and sulfite in 80/20 (v/v) D₂O/[²H₆]DMSO.



In the presence of one equivalent of sulfite, there was little decomposition of the 7-adduct over a period of two days. However, in the presence of excess sulfite, irreversible decomposition of the 7-adduct, **6.7b**, occurred, to yield products which were not identified.

The isomerisation of the 5-adduct to the thermodynamically more stable 7-adduct was also followed for substrates, **6.5a** and **6.5d**. In the case of 4-nitro-7-chlorobenzofurazan, **6.5c**, there was no detectable change in the spectrum after 24 hours. Isomerism to the 7-adduct, would, in this case, lead to the rapid expulsion of the chloro-group to yield the substitution product, **6.8**. However, in the presence of excess sulfite, formation of **6.6c**, was followed by irreversible decomposition to give unidentified products.



The rate constant for the isomerisation of the 5-adduct, **6.6**, to the thermodynamically more stable 7-adduct, **6.7**, k_{isom} , was calculated from the integrated intensities of the resonances due to the isomeric adducts. Experimentally, the rate of decomposition of the 5-adduct, **6.6**, is proportional to the rate of formation of the 7-adduct, **6.7**, Equation 6.1.

$$\text{Equation 6.1: } k_{\text{isom}} = -\frac{d[\mathbf{6.6}]}{dt} = \frac{d[\mathbf{6.7}]}{dt}$$

The isomerism is a first order process, and the isomerisation rate constant, k_{isom} , can be calculated from Equation 6.2, where (a-x) is the relative concentration of **6.6**.

$$\text{Equation 6.2: } k_{\text{isom}} = \frac{1}{t} \ln \left(\frac{a}{a-x} \right)$$

Data for the isomerisation process are given in Tables 6.2-6.4, for the reaction of **6.5a**, **6.5b** and **6.5d**, with sulfite in 80/20 (v/v) D₂O/[²H₆]DMSO. The solutions were maintained at a constant temperature of 25 °C in between recording the spectra, using a thermostatted water bath, as variations in temperature (especially overnight) would have adversely affected the kinetics.

For the reaction with 4-nitrobenzofurazan, **6.5a**, a value for k_{isom} of $(5.7 \pm 0.5) \times 10^{-6} \text{ s}^{-1}$ was calculated corresponding to the isomerisation of the 5-adduct, **6.6a**, to the 7-adduct, **6.7a**, Table 6.2. However, the data given in Table 6.3, concerning the reaction of 4-nitrobenzofuroxan, **6.5b**, in the presence of sulfite, yield a k_{isom} value of $(5.7 \pm 0.5) \times 10^{-4} \text{ s}^{-1}$. This value is one hundred times greater than the corresponding value for **6.5a**.

Table 6.2: Kinetics of isomerisation^a of **6.6a** to **6.7a**, calculated from ^1H NMR measurements in 80/20 (v/v) $\text{D}_2\text{O}/[^2\text{H}_6]\text{DMSO}$ at 25 °C.

10^{-4} Time / s	Relative concentrations ^b		$10^6 k_{\text{isom}}^c / \text{s}^{-1}$
	6.6a	6.7a	
0	100	0	
1.08	94	6	5.7
1.86	90	10	5.7
8.73	63	37	5.3
17.5	36	64	5.8
18.2	32	68	6.1
19.2	32	68	5.9
26.0	24	76	5.5

^a Measured using **6.5a**, $0.020 \text{ mol dm}^{-3}$, and sodium sulfite, $0.018 \text{ mol dm}^{-3}$.

^b Calculated from integration of the resonance intensities.

^c Calculated according to Equation 6.2, where (a-x) is the relative concentration of **6.6a**.

Table 6.3: Kinetics of isomerisation^a of **6.6b** to **6.7b**, calculated from ¹H NMR measurements in 80/20 (v/v) D₂O/[²H₆]DMSO at 25 °C.

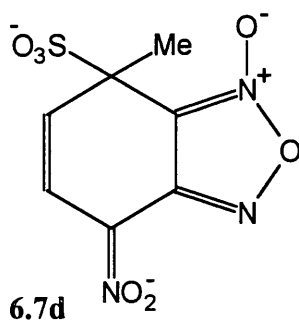
10 ⁻² Time / s	Relative concentrations ^b		10 ⁴ k _{isom} ^c / s ⁻¹
	6.6b	6.7b	
0	100	0	
6.0	73	27	5.2
9.0	56	44	6.4
24	24	76	5.9
28	19	81	5.9
47	10	90	4.9

^a Measured using **6.5b**, 0.020 mol dm⁻³, and sodium sulfite, 0.018 mol dm⁻³.

^b Calculated from integration of the resonance intensities.

^c Calculated according to Equation 6.2, where (a-x) is the relative concentration of **6.6b**.

For reactions involving furoxan-derivatives, there is another possible isomerisation pathway available, due to an intramolecular rearrangement of the furoxan ring, known as a Boulton-Katritzky rearrangement, Scheme 6.4.^{13,16,17,18} In order to establish whether this intramolecular mechanism was responsible for the 100-fold difference in the k_{isom} values of 4-nitrobenzofuroxan, **6.5b**, and 4-nitrobenzofurazan, **6.5a**, the reaction of 4-nitro-7-methylbenzofuroxan, **6.5d**, was studied, Table 6.4. The ¹H NMR coupling constant, (J₅₆ = 10.4 Hz) confirmed that intermolecular isomerism to yield the 7-adduct, **6.7d**, had occurred over time, with a k_{isom} value of (8.5 ± 0.3) × 10⁻⁶ s⁻¹.



There was no evidence for the formation of **6.9d**, the product of the possible Boulton-Katritzky rearrangement, according to Scheme 6.4, where the J_{AB} value would have been significantly lower than for **6.7d**.

Table 6.4: Kinetics of isomerisation^a of **6.6d** to **6.7d**, calculated from ¹H NMR measurements in 80/20 (v/v) D₂O/[²H₆]DMSO at 25 °C.

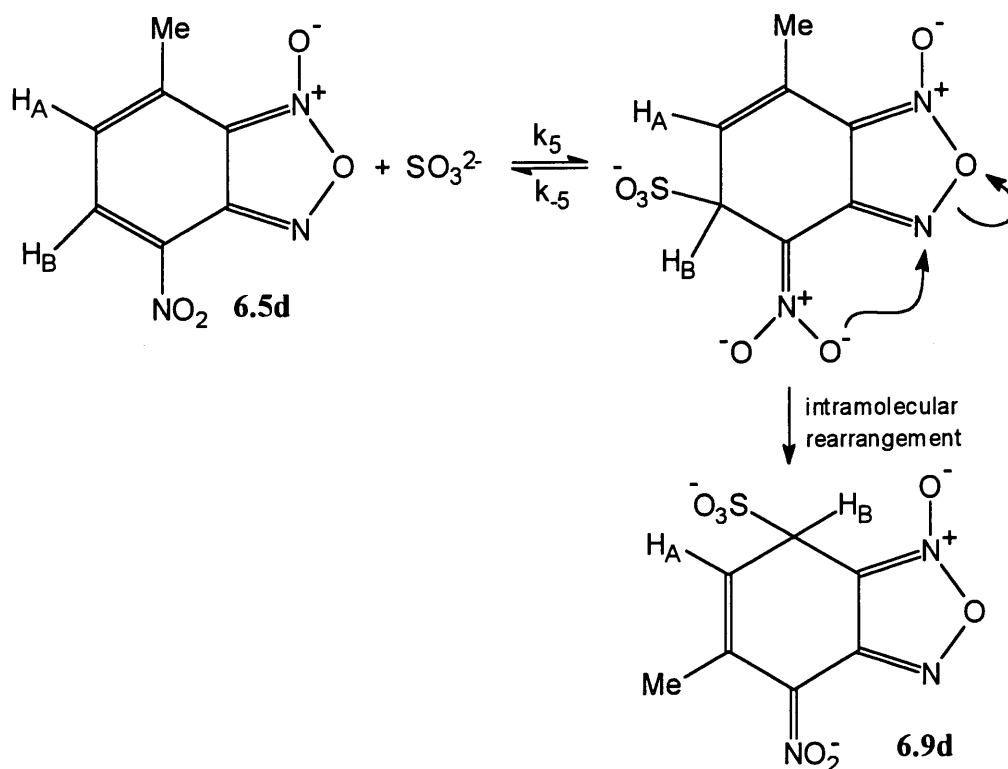
10 ⁻⁴ Time / s	Relative concentrations ^b		10 ⁶ k _{isom} ^c / s ⁻¹
	6.6d	6.7d	
0	100	0	
1.1	74	26	27
2.5	67	33	16
8.8	47	53	8.6 ^d
9.9	42	58	8.8 ^d
11	41	59	8.1 ^d

^a Measured using **6.5d**, 0.020 mol dm⁻³, and sodium sulfite, 0.018 mol dm⁻³.

^b Calculated from integration of the resonance intensities.

^c Calculated according to Equation 6.2, where (a-x) is the relative concentration of **6.6d**.

^d Values used to calculate k_{isom}.



Scheme 6.4

6.3.2 Kinetic Data

UV/Visible data detailing the absorption maxima of the substrates, **6.5a-d**, and sulfite adducts, **6.6a-d**, are given in Table 6.5. In a typical experiment, absorbance measurements were made with a constant concentration, ($4 \times 10^{-5} \text{ mol dm}^{-3}$) of the substrates **6.5a-d**, in solutions of sodium sulfite. In view of the NMR data, the adducts, which were observed to form rapidly at 327 nm on addition of sulfite were considered to be the 5-adducts, **6.6a-d**.

Table 6.5: UV/Visible absorbance data for parent molecules, **6.5**, and sulfite adducts, **6.6** in water.

	$\lambda_{\text{max}} / \text{nm}$	$\epsilon / \text{dm}^3 \text{mol}^{-1} \text{cm}^{-1}$
Parent Molecules		
6.5a	327	5900
6.5b	397	6000
6.5c	343	9800
6.5d	412	5400
5-adducts		
6.6a	327	8500
6.6b	327	9800
6.6c	327	11600
6.6d	322	6500

For kinetic measurements, the sulfite concentration was in large excess over the substrate concentration, or was maintained constant in buffered solutions. The ionic strength was maintained at $I (= 0.5 \sum c_i z_i^2) = 0.03 \text{ mol dm}^{-3}$, using sodium sulfate as the compensating electrolyte. Under these conditions, first order traces were observed, and the observed first order rate constant, k_{obs} , is related to the sulfite concentration by Equation 6.3.

Equation 6.3: $k_{\text{obs}} = k_5[\text{SO}_3^{2-}]_{\text{free}} + k_{-5}$

6.3.2.1 Reaction of 4-Nitrobenzofurazan

The reaction of 4-nitrobenzofurazan, **6.5a**, with sulfite was studied at 327 nm in aqueous solution. Data are reported in Table 6.6. A linear plot according to Equation 6.3, gave a k_5 value of $(2.8 \pm 0.3) \times 10^4 \text{ dm}^3 \text{ mol}^{-1} \text{ s}^{-1}$ for sulfite concentrations 0.001 to 0.01 mol dm^{-3} . The intercept was too small to allow the accurate determination of a value for k_5 .

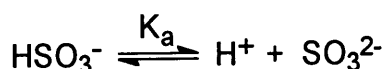
Table 6.6: Kinetic data for the reaction of **6.5a**^a with sodium sulfite in water at 25 °C.

$[\text{SO}_3^{2-}]^b / \text{mol dm}^{-3}$	$k_{\text{obs}} / \text{s}^{-1}$
0.001	18
0.002	45
0.004	103
0.006	161
0.008	215
0.010	280

^a Substrate concentration, $4 \times 10^{-5} \text{ mol dm}^{-3}$.

^b Ionic strength maintained, $I = 0.03 \text{ mol dm}^{-3}$, using sodium sulfate as the compensating electrolyte.

In order to reduce the concentration of free sulfite ions in solution, measurements were made in acidic buffers. Here, the sulfite ions are in equilibrium with hydrogen sulfite ions according to Scheme 6.5, where K_a is the acid dissociation constant.



Scheme 6.5

The stoichiometric concentration of sulfite ions is related to the concentration of free sulfite and hydrogen sulfite ions in solution by Equation 6.4.

$$\text{Equation 6.4: } [\text{SO}_3^{2-}]_{\text{stoich}} = [\text{SO}_3^{2-}]_{\text{free}} + [\text{HSO}_3^-]$$

The acid dissociation constant K_a , may be defined according to Equation 6.5.

$$\text{Equation 6.5: } K_a = \frac{[H^+][SO_3^{2-}]_{\text{free}}}{[HSO_3^-]}$$

Rearrangement of Equation 6.5 and substitution into Equation 6.4, leads to Equation 6.6, where the stoichiometric concentration of sulfite ions is related only to the concentration of free sulfite ions.

$$\text{Equation 6.6: } [SO_3^{2-}]_{\text{stoich}} = [SO_3^{2-}]_{\text{free}} + \frac{[H^+][SO_3^{2-}]_{\text{free}}}{K_a}$$

Equation 6.6 may then be factorised to give Equation 6.7.

$$\text{Equation 6.7: } [SO_3^{2-}]_{\text{stoich}} = [SO_3^{2-}]_{\text{free}} \left(1 + \frac{[H^+]}{K_a} \right)$$

The general expressions for the pH and pK_a of the solution and acid species are given in Equations 6.8 and 6.9 respectively.

$$\text{Equation 6.8: } pH = -\log_{10}[H^+]$$

$$\text{Equation 6.9: } pK_a = -\log_{10}K_a$$

Therefore, Equation 6.7 can be written as Equation 6.10. This uses a value of 7.05 for the pK_a of the hydrogen sulfite ion, which is appropriate for the ionic strength of the solutions.^{19,20}

$$\text{Equation 6.10: } [SO_3^{2-}]_{\text{stoich}} = [SO_3^{2-}]_{\text{free}} \left(1 + \frac{10^{-pH}}{10^{-7.05}} \right)$$

Equation 6.10 can be rearranged to give an expression for the concentration of the free sulfite ions in terms of the stoichiometric concentration, the acid dissociation constant for the hydrogen sulfite ion and the pH of the solution, Equation 6.11.

$$\text{Equation 6.11: } [\text{SO}_3^{2-}]_{\text{free}} = \frac{[\text{SO}_3^{2-}]_{\text{stoich}}}{\left(1 + \frac{10^{-\text{pH}}}{10^{-7.05}}\right)}$$

Reactions were carried out in aqueous solutions buffered at pH 4. The data reported in Table 6.7 were fitted to Equation 6.3 and gave a k_5 value of $(3.3 \pm 0.3) \times 10^4 \text{ dm}^3 \text{ mol}^{-1} \text{ s}^{-1}$ and a k_{-5} value of $(0.020 \pm 0.004) \text{ s}^{-1}$. Combination of these values led to a K_5 value of $1.65 \times 10^6 \text{ dm}^3 \text{ mol}^{-1}$, where $K_5 = k_5/k_{-5}$.

On completion of the colour forming reaction, the absorbance at 327 nm was recorded, Table 6.7. The equilibrium constant, K_5 was calculated from Equation 6.12, where A_0 is the absorbance due to **6.5**, and A_∞ is the absorbance due to **6.6**.

$$\text{Equation 6.12: } K_5 = \frac{[\text{6.6}]}{[\text{6.5}][\text{SO}_3^{2-}]_{\text{free}}} = \frac{(\text{Abs} - A_0)}{(A_\infty - \text{Abs})[\text{SO}_3^{2-}]_{\text{free}}}$$

The K_5 value of $(1.78 \pm 0.22) \times 10^6 \text{ dm}^3 \text{ mol}^{-1}$ calculated from absorbance measurements, is in good agreement with the value obtained from kinetic data.

The similarity of the values obtained for k_5 in the buffered and unbuffered solutions, indicates that sulfite, rather than hydrogen sulfite, is the effective nucleophile.

Table 6.7: Kinetic and equilibrium data for the reaction of **6.5a**^a with sulfite ions in water at 25 °C and pH 4^b.

$10^6 [\text{SO}_3^{2-}]_{\text{free}}^c$ / mol dm ⁻³	$k_{\text{obs}} / \text{s}^{-1}$	$k_{\text{calc}}^d / \text{s}^{-1}$	Abs ^e at 327 nm	$10^6 K_5^f$ / dm ³ mol ⁻¹
0			0.250	
0.74	0.042	0.044	0.326	2.0
1.70	0.065	0.076	0.342	1.5
2.73	0.102	0.110	0.354	1.7
4.28	0.16	0.16	0.361	1.6
6.00	0.22	0.22	0.367	2.0
7.90	0.30	0.28	0.369	1.9
9.90	0.33	0.35	0.372	
12.4	0.43	0.43	0.372	
15.3	0.53	0.52	0.372	
18.6	0.64	0.63	0.373	

^a Substrate concentration, 4×10^{-5} mol dm⁻³.

^b Acetate buffers.

^c Calculated according to Equation 6.11.

^d Calculated from Equation 6.3, with k_5 , 3.3×10^4 dm³ mol⁻¹ s⁻¹ and k_{-5} , 0.020 s⁻¹.

^e Absorbance at completion of 5-adduct formation.

^f Calculated according to Equation 6.12, with A_0 , 0.250 and A_∞ , 0.377.

Rate measurements were also made in unbuffered water/DMSO solvents, in order to establish the effect of the solvent composition on the value of k_5 , Table 6.8. The data obtained led to linear plots of the observed first order rate constant versus the concentration of free sulfite ions, according to Equation 6.3. Determination of the gradients of these plots led to k_5 values of 4.4×10^4 dm³ mol⁻¹ s⁻¹ and 8.8×10^4 dm³ mol⁻¹ s⁻¹ in 80/20 and 60/40 (v/v) water/DMSO respectively.

Therefore, as the proportion of DMSO in the solvent was increased, the k_5 value also increased. DMSO is known to stabilise 1:1 σ -adducts,⁵ and to destabilise sulfite ions,^{5,21}

and so the formation of the 5-adduct, **6.6a**, will be favoured in solvents with a higher DMSO content.

However, previous workers have proposed that the transition state for σ -adduct formation is “reactant-like” for reactions with sulfite.⁸ If this is the case, the transition state occurs early in the reaction, there is little bonding, and any solvent effects observed are mainly expressed in the rate constant for the reverse reaction, k_{-5} . It is therefore difficult to fully assess the effect of the solvent composition on the stability of the 5-adduct, **6.6a**, without knowledge of the k_{-5} or K_5 values.

Table 6.8: Kinetic data for the reaction of **6.5a**, with sulfite ions in water/DMSO mixtures at 25 °C.

(v/v) H ₂ O/DMSO	$10^{-4} k_5 / \text{dm}^3 \text{mol}^{-1} \text{s}^{-1}$
100/0	2.8 ± 0.3
80/20	4.4
60/40	8.8

6.3.2.2 Reaction of 4-Nitrobenzofuroxan

Data for the reaction of 4-nitrobenzofuroxan, **6.5b**, with sulfite in aqueous solution are reported in Table 6.9. A linear plot according to Equation 6.3 gave a k_5 value of $6.0 \times 10^4 \text{ dm}^3 \text{ mol}^{-1} \text{ s}^{-1}$.

Table 6.9: Kinetic data for the reaction of **6.5b**^a with sodium sulfite in water at 25 °C.

$[\text{SO}_3^{2-}]^b / \text{mol dm}^{-3}$	$k_{\text{obs}} / \text{s}^{-1}$
0.001	21
0.002	67
0.004	197
0.006	324
0.008	438
0.010	547

^a Substrate concentration, $4 \times 10^{-5} \text{ mol dm}^{-3}$.

^b Ionic strength maintained, $I = 0.03 \text{ mol dm}^{-3}$, using sodium sulfate as the compensating electrolyte.

The intercept was again too small to give an accurate value of k_5 , and reactions were carried out in solutions buffered at pH 4. The kinetic data, reported in Table 6.10, gave a good fit with Equation 6.3, and led to a k_5 value of $(6.5 \pm 0.5) \times 10^4 \text{ dm}^3 \text{ mol}^{-1} \text{ s}^{-1}$. However, the value of k_5 obtained had a large associated error, $0.003 \pm 0.01 \text{ s}^{-1}$. A value of $(5.1 \pm 0.5) \times 10^6 \text{ dm}^3 \text{ mol}^{-1}$ for K_5 was obtained from absorbance measurements. Hence it is possible to calculate a value for k_5 ($=k_5/K_5$) of $0.013 \pm 0.002 \text{ s}^{-1}$.

Table 6.10: Kinetic and equilibrium data for the reaction of **6.5b**^a with sulfite ions in water at 25 °C and pH 4^b.

$10^6 [\text{SO}_3^{2-}]_{\text{free}}^{\text{c}}$ / mol dm ⁻³	$k_{\text{obs}} / \text{s}^{-1}$	$k_{\text{calc}}^{\text{d}} / \text{s}^{-1}$	Abs ^e at 327 nm	$10^{-6} K_5^{\text{f}}$ / dm ³ mol ⁻¹
0			0.060	
0.81	0.038	0.056	0.340	5.8
1.74	0.100	0.116	0.367	5.4
3.07	0.175	0.203	0.377	4.5
4.28	0.274	0.281	0.383	4.5
6.00	0.41	0.39	0.386	
8.08	0.54	0.53	0.387	
10.3	0.65	0.67	0.387	
12.7	0.77	0.83	0.387	
17.1	1.1	1.1	0.388	
20.4	1.4	1.3	0.388	

^a Substrate concentration, 4×10^{-3} mol dm⁻³.

^b Acetate buffers.

^c Calculated according to Equation 6.11.

^d Calculated from Equation 6.3, with k_5 , 6.5×10^4 dm³ mol⁻¹ s⁻¹ and k_{-5} , 0.003 s⁻¹.

^e Absorbance at completion of 5-adduct formation.

^f Calculated according to Equation 6.12, with A_0 , 0.060 and A_{∞} , 0.40.

Reactions were also carried out in buffer solutions in the range pH 5 to pH 8. The results given in Table 6.11 illustrate that the value of k_5 is independent of the pH of the solution. Therefore, sulfite was considered the active nucleophile, as in the reaction of **6.5a**.

Table 6.11: Kinetic data for reaction of **6.5b**^a with sulfite ions in buffered solutions at 25 °C in water.

pH ^b	Range of [SO ₃ ²⁻] _{free} / mol dm ⁻³	10 ⁻⁴ k ₅ / dm ³ mol ⁻¹ s ⁻¹
8	(1-10) x 10 ⁻³	6.1
7	(1-6) x 10 ⁻³	6.8
6	(1-20) x 10 ⁻⁴	7.4
5	(4-80) x 10 ⁻⁶	6.8
4	(1-20) x 10 ⁻⁶	6.5

^a Substrate concentration, 4 x 10⁻⁵ mol dm⁻³.

^b Phosphate buffers, pH 6-8, acetate buffers, pH 4-5.

6.3.2.3 Reaction of 4-Nitro-7-chlorobenzofurazan

Data for the reaction of 4-nitro-7-chlorobenzofurazan, **6.5c**, with sulfite in aqueous solution (reported in Table 6.12) gave a linear plot in accordance with Equation 6.3. A k_5 value of $7.5 \times 10^4 \text{ dm}^3 \text{ mol}^{-1} \text{ s}^{-1}$ was obtained from the gradient.

Table 6.12: Kinetic data for the reaction of **6.5c**^a with sodium sulfite in water at 25 °C.

$[\text{SO}_3^{2-}]^b / \text{mol dm}^{-3}$	$k_{\text{obs}} / \text{s}^{-1}$
0.001	34
0.002	85
0.004	250
0.006	440
0.008	560
0.010	680

^a Substrate concentration, $4 \times 10^{-3} \text{ mol dm}^{-3}$.

^b Ionic strength maintained, $I = 0.03 \text{ mol dm}^{-3}$, using sodium sulfate as the compensating electrolyte.

Reactions were carried out at pH 4, in order to reduce the concentration of free sulfite ions and hence enable the determination of k_5 . Data are reported in Table 6.13, and were fitted according to Equation 6.3 with k_5 , $(8.5 \pm 1) \times 10^4 \text{ dm}^3 \text{ mol}^{-1} \text{ s}^{-1}$ and k_{-5} , $(0.020 \pm 0.005) \text{ s}^{-1}$. Combination of these values led to a $K_5 (= k_5/k_{-5})$ value of $(4.2 \pm 1) \times 10^6 \text{ dm}^3 \text{ mol}^{-1}$, which is in good agreement with the value of $(4.2 \pm 0.6) \times 10^6 \text{ dm}^3 \text{ mol}^{-1}$ calculated from absorbance measurements.

Table 6.13: Kinetic and equilibrium data for the reaction of **6.5c**^a with sulfite ions in water at 25 °C and pH 4^b.

$10^6 [\text{SO}_3^{2-}]_{\text{free}}^{\text{c}}$ / mol dm ⁻³	$k_{\text{obs}} / \text{s}^{-1}$	$k_{\text{calc}}^{\text{d}} / \text{s}^{-1}$	Abs ^e at 327 nm	$10^{-6} K_5^{\text{f}}$ / dm ³ mol ⁻¹
0			0.270	
0.65	0.064	0.074	0.366	4.6
1.59	0.151	0.156	0.379	3.6
2.80	0.253	0.258	0.386	3.5
4.09	0.39	0.37	0.392	5.0
5.87	0.58	0.52	0.395	
7.54	0.68	0.66	0.395	
9.65	0.83	0.84	0.395	
12.1	1.0	1.0	0.395	
15.3	1.3	1.3	0.396	

^a Substrate concentration, 4×10^{-5} mol dm⁻³.

^b Acetate buffers.

^c Calculated according to Equation 6.11.

^d Calculated from Equation 6.3, with k_5 , 8.5×10^4 dm³ mol⁻¹ s⁻¹ and k_{-5} , 0.020 s⁻¹.

^e Absorbance at completion of 5-adduct formation.

^f Calculated according to Equation 6.12, with A_0 , 0.270 and A_{∞} , 0.398.

6.3.2.4 Reaction of 4-Nitro-7-methylbenzofuroxan

A linear plot was obtained from the data for the reaction of 4-nitro-7-methylbenzofuroxan with sulfite, in the concentration range 0.001 to 0.01 mol dm⁻³, Table 6.14. A k_5 value of 2×10^4 dm³ mol⁻¹ s⁻¹ was obtained from the gradient, but again, the intercept was too small to allow an accurate determination of k_{-5} .

Table 6.14: Kinetic data for the reaction of **6.5d**^a with sodium sulfite in water at 25 °C.

[SO ₃ ²⁻] ^b / mol dm ⁻³	k_{obs} / s ⁻¹
0.001	16
0.002	34
0.004	76
0.006	122
0.008	163
0.010	216

^a Substrate concentration, 4×10^{-3} mol dm⁻³.

^b Ionic strength maintained, $I = 0.03$ mol dm⁻³, using sodium sulfate as the compensating electrolyte.

Kinetic and absorbance data obtained in solutions buffered at pH 4 are reported in Table 6.15. The kinetic data were fitted according to Equation 6.3, and yield values of k_5 , 3.2×10^4 dm³ mol⁻¹ s⁻¹ and k_{-5} , 0.017 s⁻¹. Combination of these values led to a K_5 value of 1.9×10^6 dm³ mol⁻¹, which is comparable with the value of $(1.8 \pm 0.3) \times 10^6$ dm³ mol⁻¹ calculated from absorbance measurements.

Table 6.15: Kinetic and equilibrium data for the reaction of **6.5d**^a with sulfite ions in water at 25 °C and pH 4^b.

$10^6 [\text{SO}_3^{2-}]_{\text{free}}^c$ / mol dm ⁻³	$k_{\text{obs}} / \text{s}^{-1}$	$k_{\text{calc}}^d / \text{s}^{-1}$	Abs ^e at 327 nm	$10^{-6} K_s^f$ / dm ³ mol ⁻¹
0			0.080	
0.81	0.043	0.043	0.154	1.48
1.91	0.077	0.078	0.184	1.97
3.00	0.112	0.112	0.192	2.07
4.48	0.168	0.159	0.200	
6.43	0.22	0.22	0.204	
8.08	0.27	0.27	0.205	
10.3	0.34	0.34	0.208	
15.8	0.52	0.52	0.208	

^a Substrate concentration, 4×10^{-5} mol dm⁻³.

^b Acetate buffers.

^c Calculated according to Equation 6.11.

^d Calculated from Equation 6.3, with k_s , 3.17×10^4 dm³ mol⁻¹ s⁻¹ and k_{-s} , 0.017 s⁻¹.

^e Absorbance at completion of 5-adduct formation.

^f Calculated according to Equation 6.12, with A_0 , 0.080 and A_∞ , 0.208.

6.4 Comparisons

A summary of the rate and equilibrium constants measured for σ -adduct formation in water is given in Table 6.16. The results are compared with data for the reaction of 1,3,5-trinitrobenzene, TNB, with sulfite in water to give **6.10**.

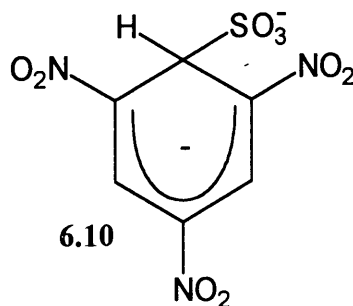


Table 6.16: Summary of rate and equilibrium data in water at 25 °C.

	6.5a	6.5b	6.5c	6.5d	TNB ^c
$k_5 / \text{dm}^3 \text{mol}^{-1} \text{s}^{-1}$	3.3×10^4	6.5×10^4	8.5×10^4	3.2×10^4	3.5×10^4
k_5 / s^{-1}	0.020	0.013	0.020	0.017	125
$K_5 / \text{dm}^3 \text{mol}^{-1}$	1.65×10^6	5.1×10^6	4.2×10^6	1.9×10^6	290
$k_{\text{isom}}^a / \text{s}^{-1}$	5.7×10^{-6}	5.7×10^{-4}		8.5×10^{-6}	
$k_7^{a,b} / \text{dm}^3 \text{mol}^{-1} \text{s}^{-1}$	(9.4)	(2900)		(16)	

^a Values in 80/20 (v/v) D₂O/[²H₆]DMSO.

^b Calculated as $k_7 = K_5 k_{\text{isom}}$.

^c Literature values¹ for reaction at unsubstituted ring position of 1,3,5-trinitrobenzene. Data have not been statistically corrected.

A comparison of the K_5 values illustrates the difference in stability of the 5-adducts, **6.6a-d**, formed from **6.5a-d**, with the σ -adduct, **6.10**, formed from TNB. This 10^4 -fold difference is noteworthy, as the difference in the stability of σ -adducts formed from attack of methoxide on these substrates in methanol is approximately 10-fold. For example, for reaction with methoxide, values corresponding to K_5 are $163 \text{ dm}^3 \text{mol}^{-1}$ for 4-nitrobenzofurazan,²² **6.5a**, and $22.3 \text{ dm}^3 \text{mol}^{-1}$ for TNB.²³

This difference in stability may be attributed to the solvation effects experienced by the σ -adducts. Experiments were carried out in water, which is known to solvate localised

negative charges very effectively.^{7,21} For the 5-adducts, **6.6a-d**, the negative charge is localised on the sulfite and nitro-groups, leading to stabilisation by water. However, in the adduct, **6.10**, formed from sulfite attack on TNB, the negative charge is delocalised about the ring and the three nitro-groups. This leads to poorer solvation and hence the adduct, **6.10**, is less stable than the 5-adducts, **6.6a-d**.

The main factor responsible for lower stability of the adduct, **6.10**, in comparison with the 5-adducts, **6.6a-d**, is probably the large difference in the value of the rate constant for the reverse reaction, k_{-5} . The k_5 values show little variation with the nature of the substrate, and reinforce the idea that the transition state for sulfite attack is "reactant-like".⁸

The data in Table 6.16 show that the value of K_5 for formation of **6.5b** is approximately three times higher than the corresponding value for formation of **6.5a**. This may be attributed to the greater electron withdrawing ability of the furoxan ring compared to the furazan ring. Similar differences in stability have been observed for methoxide adducts,²² and also for the amine adducts reported in Chapter 4. The electron withdrawing effect of the 7-chloro substituent in **6.5c** results in enhanced stability for the adduct **6.6c** compared with **6.6a**. Similarly, the reduction in stability of **6.6d** relative to **6.6b** may be attributed to the electron releasing effect of the 7-methyl group.

Data are also given in Table 6.16 for the observed rate constant for isomerisation from the 5-adducts, **6.6**, to the 7-adducts, **6.7**. This isomerisation was very slow, and in some cases occurred over several days.

Using the nomenclature of Scheme 6.3, the velocity of the isomerisation may be expressed by Equation 6.13.

$$\text{Equation 6.13: } \text{vel} = \frac{d[\mathbf{6.7}]}{dt} = -\frac{d[\mathbf{6.6}]}{dt} = k_{-5}[\mathbf{6.6}] \frac{k_7[\mathbf{6.5}][\text{SO}_3^{2-}]}{k_7[\mathbf{6.5}][\text{SO}_3^{2-}] + k_5[\mathbf{6.5}][\text{SO}_3^{2-}]}$$

Here the velocity of isomerisation is written as the rate of dissociation of the initially formed 5-adduct, **6.6**, multiplied by the fractionation between the 7-adduct and the 5-

adduct. Since $k_5 \gg k_7$, Equation 6.13 reduces to Equation 6.14, and the first order rate constant for the isomerisation is given by Equation 6.15.

$$\text{Equation 6.14: } -\frac{d[6.6]}{dt} = k_{-5}[6.6]\frac{k_7}{k_5}$$

$$\text{Equation 6.15: } k_{\text{isom}} = \frac{k_{-5}k_7}{k_5} = \frac{k_7}{K_5}$$

Therefore, estimated values of k_7 , the rate constant for formation of the 7-adducts, **6.7**, from sulfite attack on the substrates, **6.5**, were calculated from the values of the isomerisation rate constant, k_{isom} , and the equilibrium constant for the formation of the 5-adduct, K_5 . The values serve for a direct comparison of these substrates, but are not absolute, as the k_{isom} values were calculated from data measured in 80/20 (v/v) D₂O/[²H₆]DMSO, while the K_5 values were measured in water.

The k_7 values calculated for the formation of **6.7a** and **6.7d**, are much lower than the value for formation of **6.7b**. There is a possibility that the 5-adduct, **6.6b**, may undergo an intramolecular Boulton-Katritzky rearrangement to give **6.7b**, and this may account for the difference in the k_7 values. The 5-adduct, **6.6a**, is unable to undergo rearrangement to the 7-adduct via this intramolecular pathway, as there is no N-oxide bond to facilitate the mechanism. However, **6.6d** does contain an N-oxide bond, and rearrangement via the Boulton-Katritzky mechanism to give **6.7d** is also possible. Nevertheless, the NMR results show that the product of the isomerisation is **6.7d**, rather than **6.9d**, indicating an intermolecular mechanism. The k_7 value for the formation of **6.7d** is 180 times lower than that for the formation of **6.7b**, and this is likely to be due to steric hindrance from the methyl-group to attack at the 7-position.

6.5 Conclusion

In the reaction of the nitrobenzofurazan derivatives, **6.5a-d**, with sulfite, σ -adducts were observed to form rapidly in aqueous solution, where sulfite attack occurred at the 5-

position. The stability of the 5-adducts was remarkably high in comparison with the corresponding σ -adducts formed from attack of sulfite on TNB.

The 5-adducts eventually undergo isomerisation to the thermodynamically more stable 7-adducts, except in the reaction with 4-nitro-7-chlorobenzofurazan, where attack at the 7-position would lead to the nucleophilic substitution of the chloro-group to give the substitution product, **6.8**.

The mechanism of this isomerism was investigated and was found to occur via an intermolecular rearrangement, and not according to the intramolecular Boulton-Katritzky rearrangement.

6.6 References

- ¹ C. F. Bernasconi and R. G. Bergstrom., *J. Am. Chem. Soc.*, 1973, **95**, 3603.
- ² R. G. Pearson., *Surv. Progr. Chem.*, 1969, **5**, 1.
- ³ F. Terrier., *Chem. Rev.*, 1982, **82**, 77.
- ⁴ E. Buncel, M. R. Crampton, M. J. Strauss and F. Terrier., "Electron-Deficient Aromatic- and Heteroaromatic-Base Interactions". Elsevier, Amsterdam, 1984.
- ⁵ F. Terrier. "Nucleophilic Aromatic Displacement". VCH, New York, 1991.
- ⁶ M. R. Crampton and C. Greenhalgh., *J. Chem. Soc., Perkin Trans. 2.*, 1985, 599.
- ⁷ M. R. Crampton., *J. Chem. Soc. B.*, 1967, 1341.
- ⁸ M. R. Crampton and M. J. Willison., *J. Chem. Soc., Perkin Trans. 2.*, 1976, 160.
- ⁹ P. B. Ghosh and M. W. Whitehouse., *J. Med. Chem.*, 1968, **11**, 305.
- ¹⁰ M. W. Whitehouse and P. B. Ghosh., *Biochem. Pharmacol.*, 1968, **17**, 158.
- ¹¹ M. J. Strauss, A. DeFusco and F. Terrier., *Tetrahedron Lett.*, 1981, **22**, 1945.
- ¹² P. Drost., *Justus Liebigs Ann. Chem.*, 1899, **307**, 49.
- ¹³ A. J. Boulton and A. R. Katritzky., *Revue de Chimie (Romania)*., 1962, **7**, 691.
- ¹⁴ F. Terrier, F. Millot, A-P. Chatrousse, M-J. Pouet and M-P. Simonnin., *Org. Mag. Res.*, 1976, **8**, 56.
- ¹⁵ E. Buncel, N. Chuaqui-Offermans, B. K. Hunter and A. R. Norris., *Can. J. Chem.*, 1977, **55**, 2852.
- ¹⁶ A. J. Boulton and A. R. Katritzky., *Proc. Chem. Soc.*, 1962, 257.
- ¹⁷ A. J. Boulton, P. B. Ghosh and A. R. Katritzky., *Angew. Chem.*, 1964, **3**, 693.
- ¹⁸ P. B. Ghosh., *J. Chem. Soc. (B)*., 1968, 334.
- ¹⁹ H. V. Tartar and H. H. Garretson., *J. Am. Chem. Soc.*, 1941, **63**, 808.
- ²⁰ L. G. Sillen and A. E. Martell., *Chem. Soc. Sp. Publ.* 17, 1964, Table 55.
- ²¹ M. R. Crampton and M. A. El Ghariani., *J. Chem. Soc. (B)*., 1971, 1043.
- ²² F. Terrier, A-P. Chatrousse and F. Millot., *J. Org. Chem.*, 1980, **45**, 2666.
- ²³ C. F. Bernasconi., *J. Am. Chem. Soc.*, 1970, **92**, 4682.

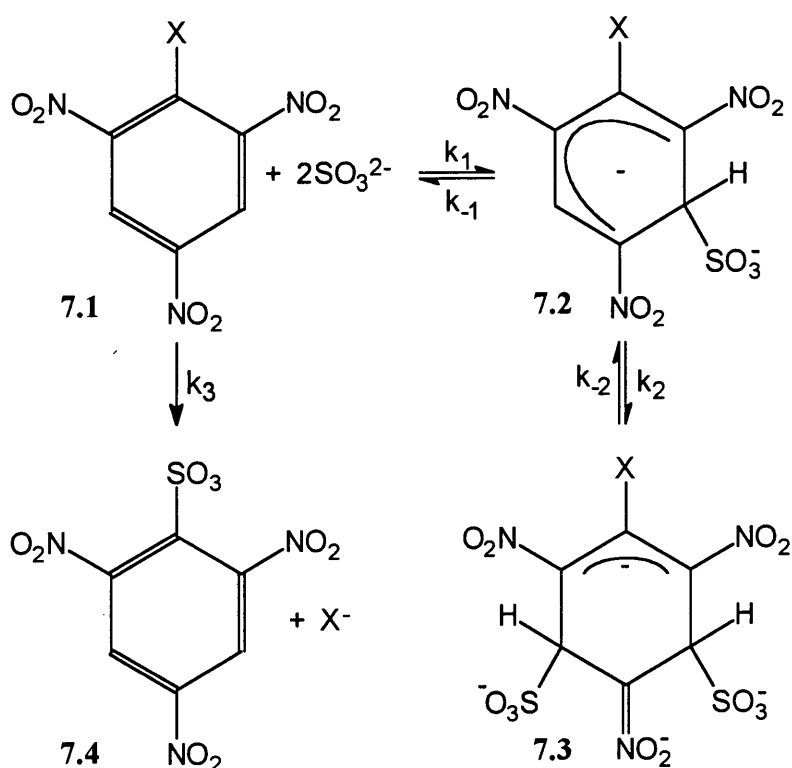
Chapter 7

Reactions of 4,6-Dinitrobenzofuroxan with Sulfite in Aqueous Solution

7 Reactions of 4,6-Dinitrobenzofuroxan with Sulfite in Aqueous Solution

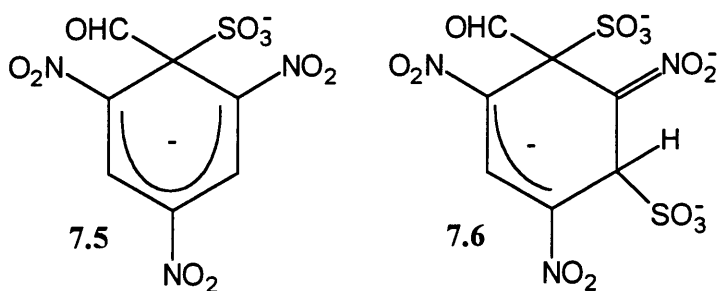
7.1 Introduction

The reaction of sulfite at an unsubstituted position of 1-X-2,4,6-trinitrobenzenes, **7.1**, has been found to yield adducts **7.2** and **7.3**, with 1:1, or 1:2, stoichiometry.^{1,2,3,4} When X is a good leaving group, such as a halide or phenoxide, the reaction may eventually yield the substitution product, **7.4**, a derivative of benzene sulfonic acid, Scheme 7.1.^{5,6} When X is a poor leaving group, such as hydrogen, complexes **7.2** and **7.3** are time stable, and the substitution product, **7.4**, is not observed.¹

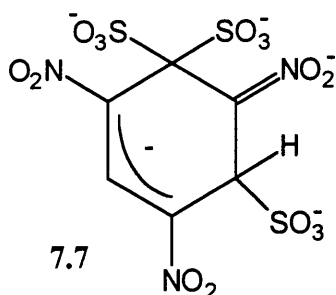


Scheme 7.1

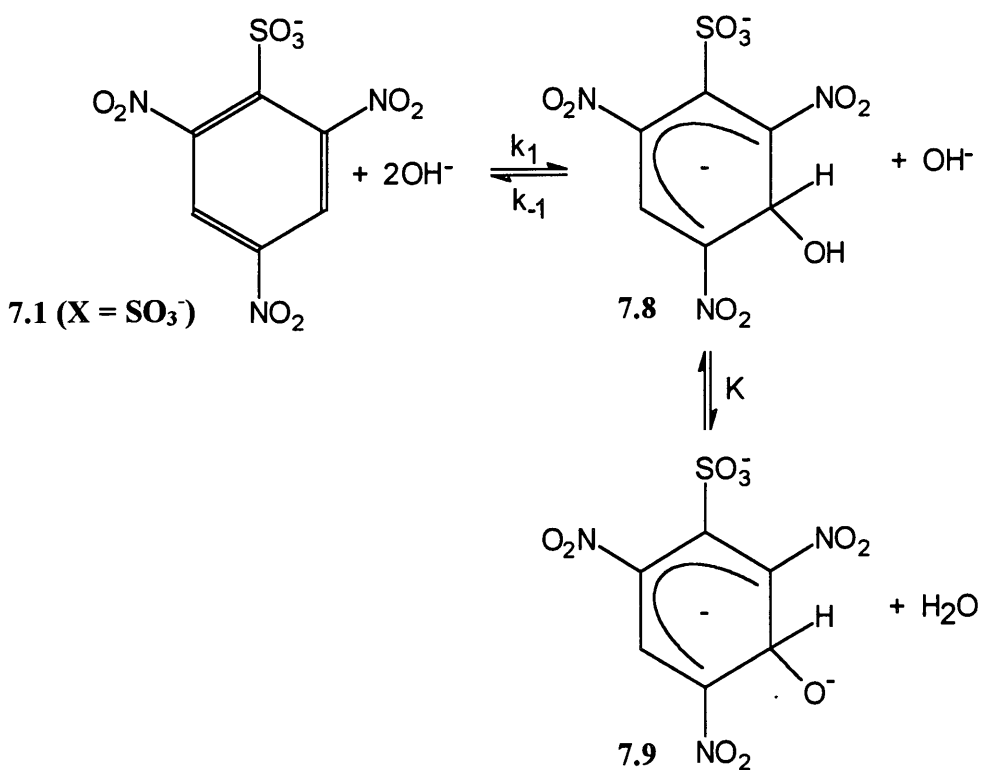
For reactions of sulfite with **7.1**, ($\text{X} \neq \text{H}$), there has generally been little evidence for 1:1 or 1:2 σ -complexes containing the sulfite ion bonded at the 1-position.³ However, Norris and Marendic have shown that σ -adducts, **7.5** and **7.6** are formed from the reaction of 2,4,6-trinitrobenzaldehyde, **7.1** ($\text{X} = \text{CHO}$), with sulfite.⁷



The reactions of 2,4,6-trinitrobenzenesulfonate, 7.1 ($X = \text{SO}_3^-$), with sulfite and hydroxide ions have been studied.¹ In the reaction with sulfite ions, 1:1 and 1:2 adducts, 7.2 and 7.3, were observed. There was no evidence for attack at the 1-position to give the di-adduct, 7.7.¹



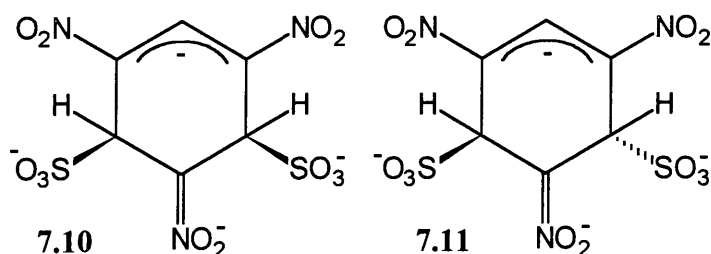
Reaction with hydroxide ions gave an adduct at the 3-position, 7.8, followed by a rapid equilibrium involving proton transfer from the adduct to a second hydroxide ion, to yield 7.9, according to Scheme 7.2.¹



Scheme 7.2

The 1:1 adducts formed from sulfite attack on nitro-aromatic substrates, have much higher stabilities than the analogous 1:1 hydroxide complexes.⁸ For example, the ratio $K_1(\text{SO}_3^{2-})/K_1(\text{OH}^-)$ is approximately 80 for 1:1 adducts, 7.8,¹ showing that the carbon basicity of the sulfite ion is generally greater than that of the hydroxide ion for attack on the parent nitro-aromatics.

The 1:2 complexes formed from attack of sulfite on trinitrobenzene, 7.1 ($X = \text{H}$), were found to occur in two isomeric forms. Evidence for the formation of the cis and trans complexes, 7.10 and 7.11, has come from both UV/Visible spectrophotometry,⁹ and ^1H NMR spectroscopy.^{10,11}

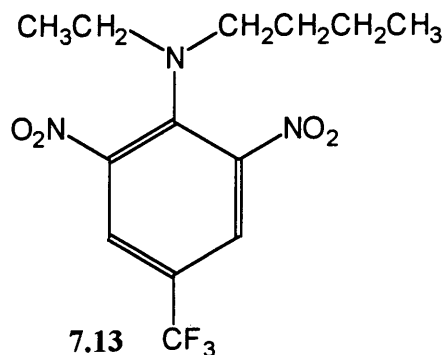
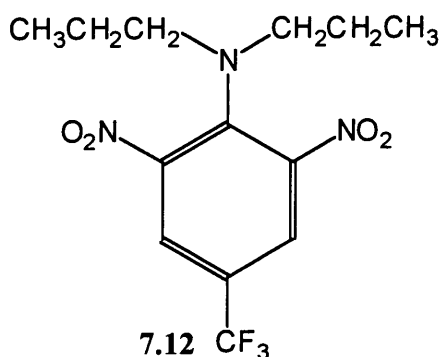


A kinetic study of the reaction of trinitrobenzene (TNB), with sulfite ions separated the formation of the cis and trans isomers.⁹ There were three observable kinetic processes, sufficiently separated in time to allow the evaluation of each. These processes corresponded to formation of the 1:1 adduct and the two isomeric 1:2 adducts. Kinetic analysis allowed the determination of rate constants for the forward and reverse reactions.

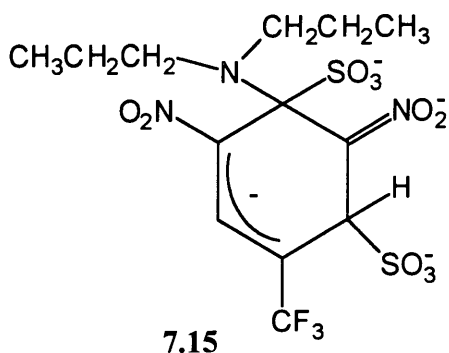
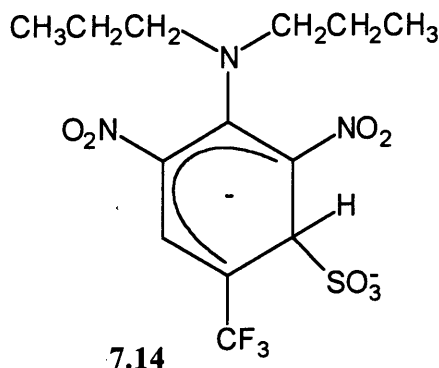
Strauss and Taylor produced a resolved ^1H NMR spectrum for the 1:2 adduct formed from attack of sulfite on TNB in D_2O . Two sets of peaks were obtained, which were attributed to the formation of cis and trans isomers.¹⁰

Crampton and Willison also used ^1H NMR spectroscopy to prove the formation of cis and trans isomers, by performing experiments at low temperatures. At $5\text{ }^\circ\text{C}$, two sets of sharp resonances were observed, each in a 1:2 ratio, indicating one hydrogen situated at an sp^2 carbon centre, and two hydrogens at an sp^3 carbon centre. On warming to $30\text{ }^\circ\text{C}$, one set of resonances remained sharp, while the other set were observed to broaden considerably.¹¹ It was suggested that the resonance broadening was due to the molecule “flipping” between the two equivalent cis conformations as the temperature was increased.

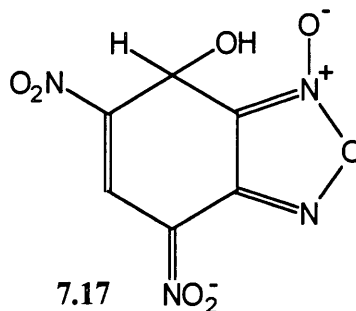
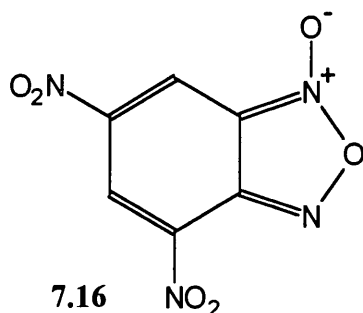
Recently, Annandale and co-workers have studied the reactions of OD^- and SO_3^{2-} nucleophiles with trifluralin, **7.12** and benefin, **7.13** in D_2O , using ^1H NMR spectroscopy.¹²



These compounds are herbicides, generally used in the control of most grasses and broad-leaved weeds. The mode of action has been suggested to involve the formation of σ -adducts with nucleophiles in plant cells. In the presence of sulfite, a 1:1 adduct, **7.14**, was formed at the 3-position of trifluralin. However, with time, new resonances were observed in the ^1H NMR spectrum, which were attributed to the formation of cis and trans isomers of **7.15**.¹²



In the present chapter, results are reported for the reactions of 4,6-dinitrobenzofuroxan (DNBF), **7.16**, and the hydroxide derivative, **7.17**, with sulfite in aqueous solution.



DNBF is a powerful electrophile, forming σ -adducts with weak nucleophiles such as aniline in the absence of an external base.¹³ The presence of two nitro-groups and the high electrophilic character of DNBF, **7.16**, would suggest that di-adducts may form on addition of sulfite, as negative charge is readily delocalised by the nitro-groups and the benzofuroxan moiety. The reactions were investigated with the aim of providing evidence for the formation of cis and trans isomers, and to determine the stability of the adducts in comparison with those formed from trinitrobenzene, **7.1**.

7.2 Experimental

4,6-Dinitrobenzofuroxan, **7.16**, prepared by Drost's method,¹⁴ (mp 172 °C, literature value¹⁴ 172-174 °C) was available from previous work. All other reagents, solvents and buffer components were the purest available commercial products.

¹H NMR spectra were recorded in D₂O/[²H₆]DMSO mixtures using a Varian Mercury 200 MHz spectrometer, or a Varian VXR 400 MHz spectrometer. UV/Visible spectra were recorded using a Perkin-Elmer Lambda 2 spectrophotometer, while kinetic measurements and rapid spectral changes over time were recorded at 25 °C, using an Applied Photophysics SX-17 MV stopped-flow spectrophotometer fitted with a PD.1 Photodiode Array accessory.

7.3 Results and Discussion

7.3.1 NMR Data

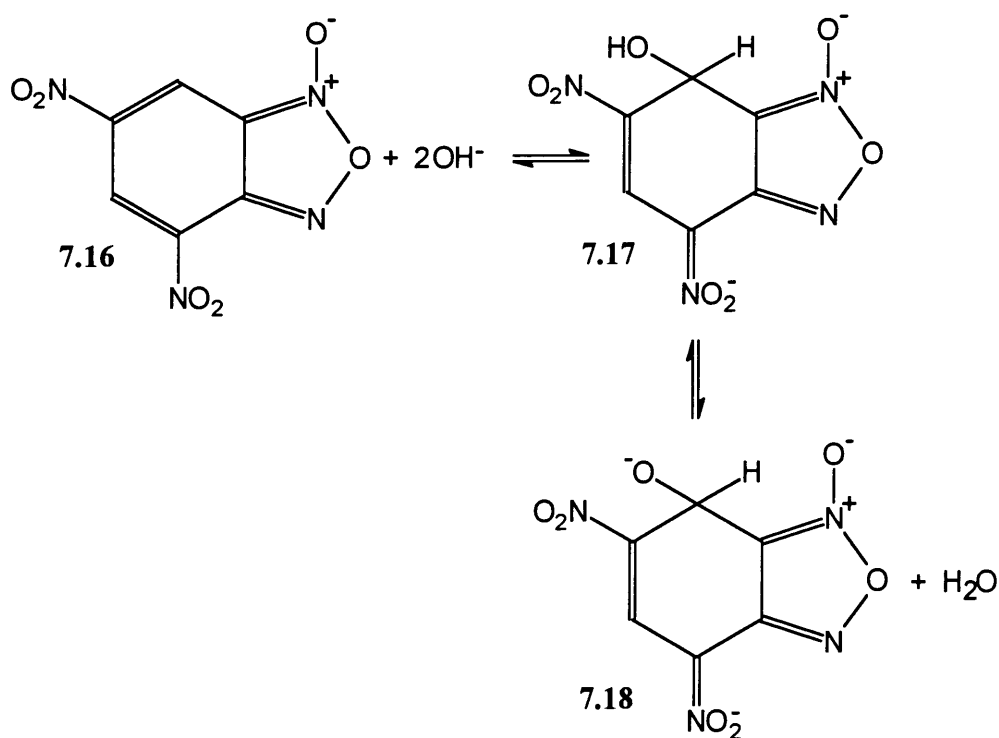
4,6-Dinitrobenzofuroxan, **7.16**, was found to be insoluble in D₂O, and for this reason, ¹H NMR spectra were recorded in D₂O/[²H₆]DMSO mixtures. The ¹H NMR data for DNBF, **7.16**, and σ -adducts formed are given in Table 7.1. DMSO is known to stabilise 1:1 σ -adducts,⁸ while 1:2 σ -adducts are generally destabilised.¹⁵ Therefore, it was necessary to reduce the proportion of DMSO in the solvent in order to study the formation of di-adducts.

Table 7.1: ¹H NMR data measured in D₂O/[²H₆]DMSO mixtures at 25 °C

D ₂ O/[² H ₆]DMSO ^a		Chemical Shift / ppm		Features
		H ₅	H ₇	
7.16	90/10	8.85	9.03	
7.17	80/20	8.75	6.12	
7.18	80/20	8.71	6.09	
7.19	75/25	6.41	5.90	
7.20	80/20	8.74	5.84	
7.21	90/10	6.44	5.80	sharp
7.22	90/10	6.18	5.65	broad

^a Ratio by volume

DNBF, **7.16**, will readily react with hydroxide ions in solution, and has enough electrophilic character to be able to abstract an hydroxide ion from water to give **7.17**. In the presence of excess hydroxide, ionisation to give the dianionic adduct, **7.18**, is expected, according to Scheme 7.3.¹⁶ Evidence for this ionisation was obtained from ¹H NMR data, Table 7.1, where the H₅ and H₇ resonances shifted to lower frequency on deprotonation to **7.18**, in the presence of excess hydroxide.



The hydroxide adduct, **7.17**, was prepared in 50/50 (v/v) $\text{D}_2\text{O}/[^2\text{H}_6]\text{DMSO}$. One equivalent of sulfite in D_2O was added to the solution, to give the adduct, **7.19**, in 75/25 (v/v) $\text{D}_2\text{O}/[^2\text{H}_6]\text{DMSO}$, Figure 7.1. Chemical shifts are reported in Table 7.1. Only one set of peaks were observed in the ^1H NMR spectrum, and no evidence for trans-cis isomerism was obtained.

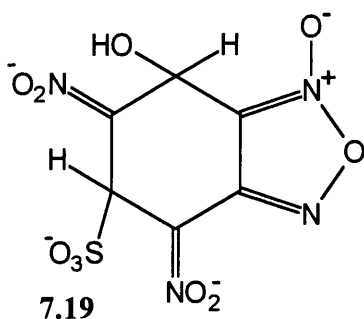
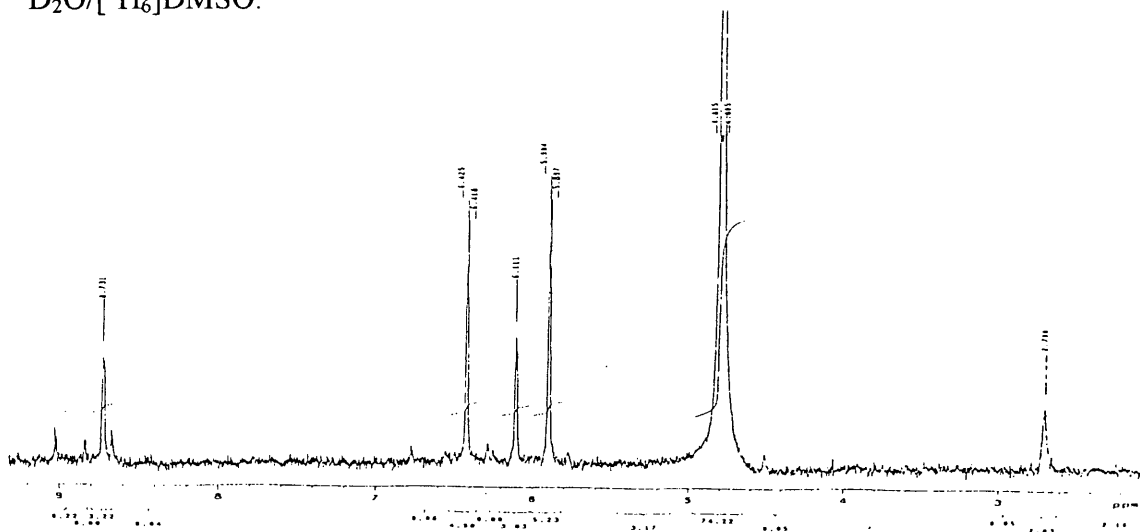
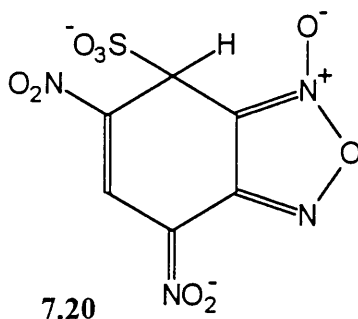


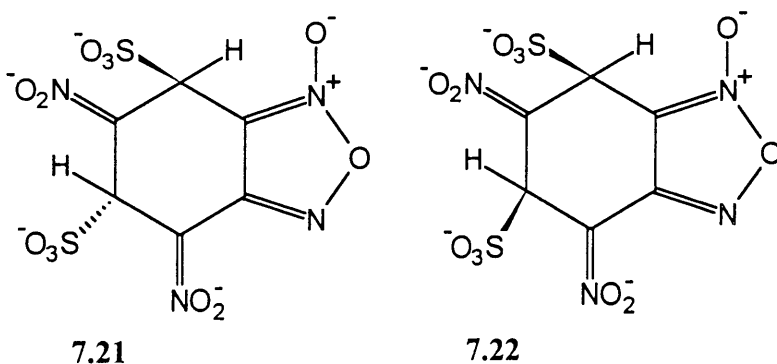
Figure 7.1: ^1H NMR spectrum of the adducts, 7.17 and 7.19, in 75/25 (v/v) $\text{D}_2\text{O}/[^2\text{H}_6]\text{DMSO}$.



An equimolar solution of DNBF and sulfite in 80/20 (v/v) $\text{D}_2\text{O}/[^2\text{H}_6]\text{DMSO}$ gave a spectrum with two resonances, which were attributed to the formation of a 1:1 σ -adduct, 7.20. Data are given in Table 7.1.



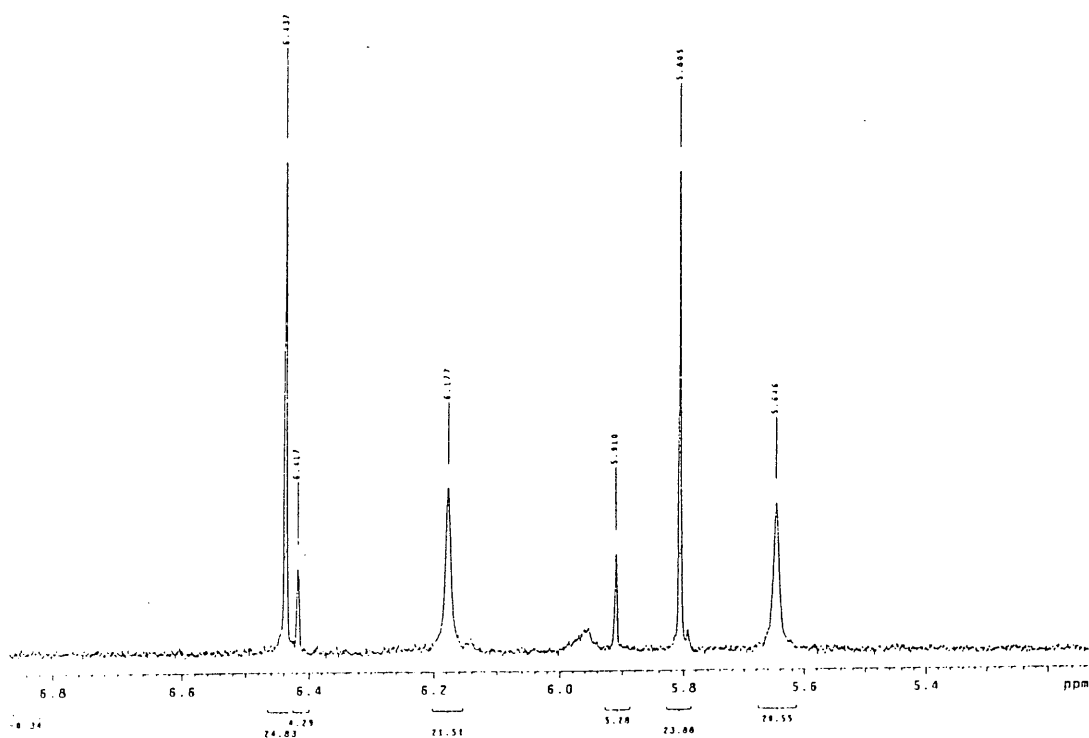
^1H NMR spectra of solutions which contained a high excess of sulfite were recorded, in order to obtain data for di-adduct formation. Two sets of peaks were recorded which indicated the formation of isomeric trans and cis σ -adducts, 7.21 and 7.22, Table 7.1.



The two sets of peaks were easily distinguished as one set was very sharp, while the other set was broad, Figure 7.2. In the trans-complex, repulsion between the NO_2^- and

SO_3^- groups will probably result in a near planar molecule, giving sharp ^1H NMR resonances. However, the cis-complex will prefer to exist in one of two possible conformations in order to minimise electrostatic repulsions. If the two conformations are in dynamic equilibrium, then “flipping” from one form to another will result in considerable line broadening in the NMR spectrum, as observed in similar TNB-sulfite systems.¹¹

Figure 7.2: ^1H NMR spectrum illustrating the adducts formed from reaction of DNBF, 7.16, with a 10-fold excess of sulfite in 90/10 (v/v) $\text{D}_2\text{O}/[^2\text{H}_6]\text{DMSO}$ at 25 °C.



7.3.2 Kinetic and Equilibrium Studies

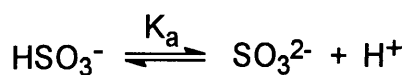
All kinetic measurements were made in aqueous solution at 25 °C with the concentration of free sulfite ions in large excess over DNBf to ensure first order conditions. The absorption maxima of the adducts formed are given in Table 7.2, together with the extinction coefficients measured in aqueous solution.

Table 7.2: UV/Visible absorbance data measured in water at 25 °C.

	$\lambda_{\text{max}} / \text{nm}$	$\epsilon / \text{dm}^3 \text{mol}^{-1} \text{cm}^{-1}$
7.16	418	8200
7.17	465	22000
7.19	333	3100
7.20	476	22000
7.21/7.22	340	8300
7.23	330	4500

7.3.2.1 Formation of a 1:1 DNBf:Sulfite Adduct

Kinetic data were measured at 476 nm, the absorption maximum for the 1:1 σ -adduct, **7.20**, in acid solutions buffered at pH 4.5. It was necessary to study the formation of **7.20** in acid buffers in order to decrease the concentration of free sulfite ions in solution, and hence decrease the rate of σ -adduct formation, to allow measurement of rate constants. Formation of **7.17** will also be inhibited in the presence of acid, and reactions will predominantly involve free DNBf. There will be an equilibrium in acidic solution between sulfite and hydrogen sulfite ions according to Scheme 7.4, where K_a is the acid dissociation constant of hydrogen sulfite.

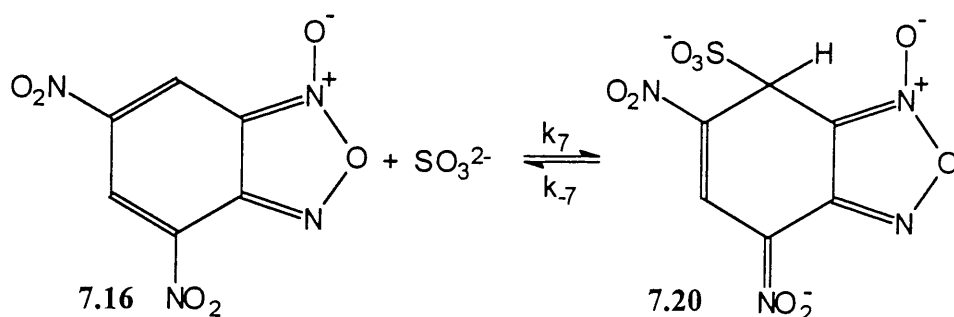


Scheme 7.4

The concentration of free sulfite ions in solution is related to the stoichiometric concentration by Equation 7.1, (derived in Chapter 6) which uses a $\text{p}K_a$ value of 7.05, appropriate for the ionic strength of the solutions.^{17,18}

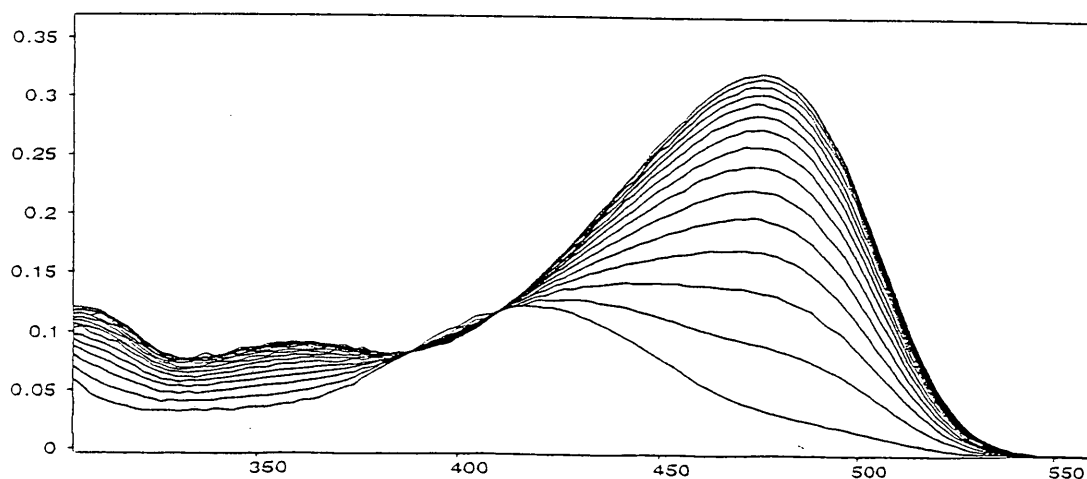
$$\text{Equation 7.1: } [\text{SO}_3^{2-}]_{\text{free}} = \frac{[\text{SO}_3^{2-}]_{\text{stoich}}}{\left(1 + \frac{10^{-\text{pH}}}{10^{-7.05}}\right)}$$

The formation of the 1:1 σ -adduct, **7.20**, Scheme 7.5, was characterised by a rapid increase in absorbance at 476 nm, Figure 7.3.



Scheme 7.5

Figure 7.3: UV/Visible spectra recorded over time, for the formation of **7.20** at pH 5. Spectra were taken at 0.02 second intervals for 0.30 seconds.



Data are reported in Table 7.3 for the reaction at pH 4.5. The data were fitted according to Equation 7.2, using a k_7 value of $(2.3 \pm 0.2) \times 10^7 \text{ dm}^3 \text{ mol}^{-1} \text{ s}^{-1}$. The value of k_7 was too large to enable an accurate determination of k_{-7} .

$$\text{Equation 7.2: } k_{\text{obs}} = k_7[\text{SO}_3^{2-}] + k_{-7}$$

Table 7.3: Kinetic data for the formation of **7.20**, in buffered solution, pH 4.5, at 25 °C.

$10^6 [\text{SO}_3^{2-}]_{\text{free}} / \text{mol dm}^{-3}$	$k_{\text{obs}}^{\text{a}} / \text{s}^{-1}$	$k_{\text{calc}}^{\text{b}} / \text{s}^{-1}$
2.8	65	65
5.6	124	130
11	254	255
17	400	395

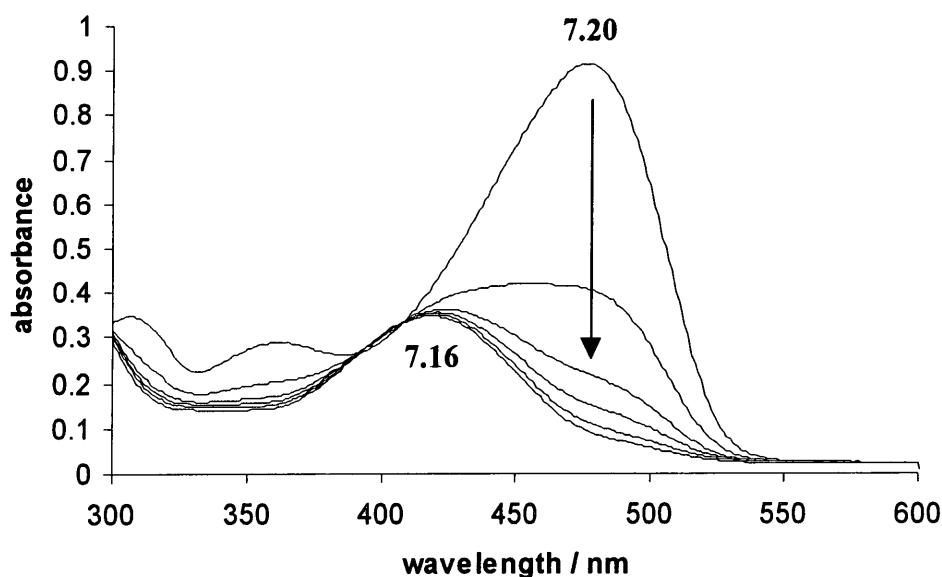
^a Data measured at 476 nm.

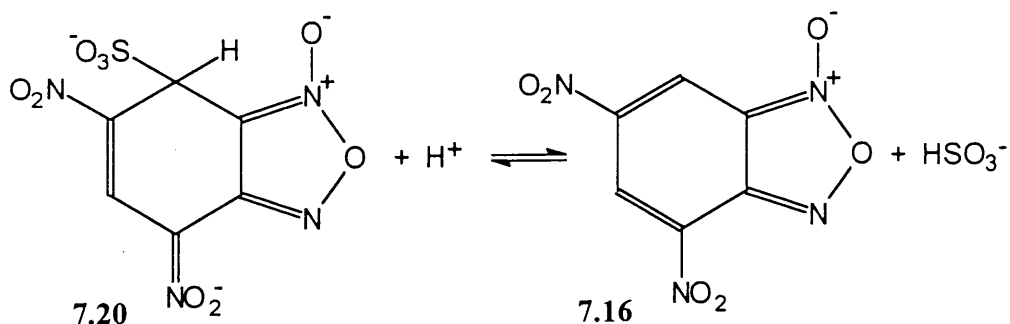
^b Calculated from Equation 7.2, with a k_7 value of $(2.3 \pm 0.2) \times 10^7 \text{ dm}^3 \text{ mol}^{-1} \text{ s}^{-1}$, and $k_{-7} \approx 0$.

7.3.2.2 Reactions of the 1:1 DNBF:Sulfite Adduct with Protons and Hydroxide Ions

A sample of the 1:1 DNBF:sulfite adduct, **7.20**, was prepared in deuteriated solvents and a ^1H NMR spectrum taken to ensure its formation. Reaction with 1.5 mol dm^{-3} hydrochloric acid led to a decrease in intensity of the absorbance due to **7.20** at 476 nm, Figure 7.4. At the end-point of the reaction, the absorption maximum had moved to 418 nm, indicating the formation of **7.16**, after 15 hours, according to Scheme 7.6.

Figure 7.4: Reaction of the 1:1 DNBF:sulfite adduct, $4 \times 10^{-5} \text{ mol dm}^{-3}$, with 1.5 mol dm^{-3} hydrochloric acid. Spectra were taken immediately after mixing, and after 30 min, 60 min, 90 min, 5 hours, and 15 hours.



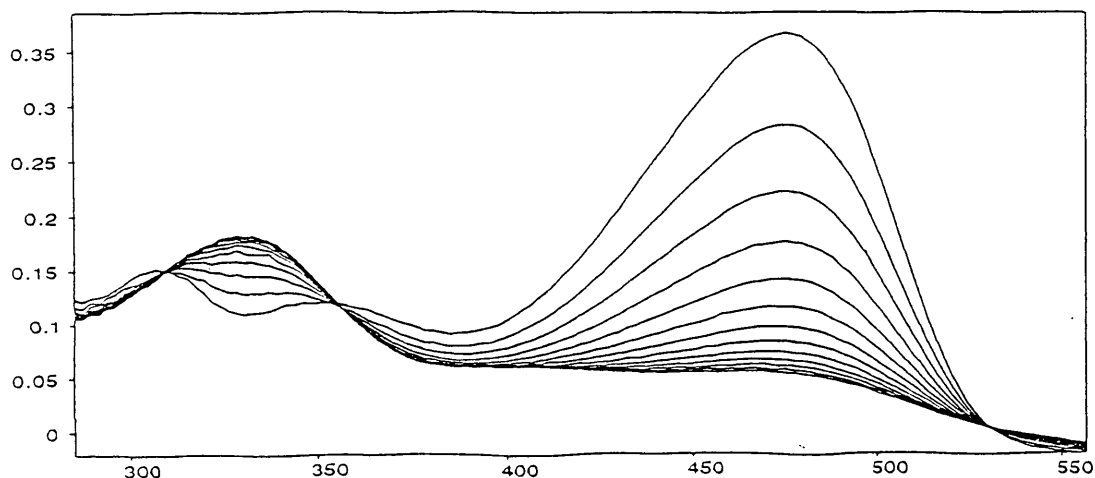


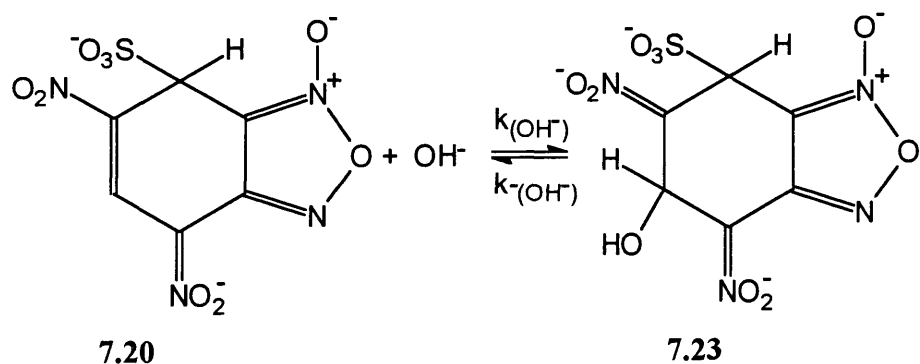
Scheme 7.6

The reaction was carried out with acid concentrations in the range 0.5 to 2.0 mol dm⁻³, and the rate of decomposition of the adduct measured. A non-linear dependence of the observed first order rate constant on the acid concentration was observed, and the role of the proton was assumed to involve “mopping up” the free sulfite. Hence, the adduct formation was reversible, but only under stringent conditions, using high concentrations of acid to afford the expulsion of sulfite. Quantitative measurements of the reaction of 7.16 with sulfite in strongly acidic solutions are reported in Section 7.3.2.5.

In order to study the reaction of the 1:1 DNBF:sulfite adduct, 7.20, with hydroxide ions, a sample of 7.20 was prepared in deuteriated solvents, before dilution with water. The adduct was then reacted with hydroxide ions in the concentration range 0.004 to 0.10 mol dm⁻³. The reaction gave rise to a rapid decrease in intensity at the absorption maximum due to 7.20, ($\lambda_{\text{max}} = 476$ nm), with a concomitant increase in intensity at 330 nm, Figure 7.5. This increase was attributed to the formation of 7.23, according to Scheme 7.7.

Figure 7.5: Reaction of 7.20, 4×10^{-5} mol dm⁻³ with hydroxide, 0.10 mol dm⁻³ in water at 25 °C. Spectra recorded at 0.4 second intervals for 5.0 seconds.





Scheme 7.7

The first order rate constant, k_{obs} , obtained from data for the colour fading reaction at 476 nm, corresponded to the rate of consumption of 7.20. Data are reported in Table 7.4, and gave a linear plot according to Equation 7.3, with values of $k_{(\text{OH}^-)}$, $7.0 \text{ dm}^3 \text{ mol}^{-1} \text{ s}^{-1}$ and $k_{-(\text{OH}^-)}$, 0.022 s^{-1} . Combination of these values gave a $K_{(\text{OH}^-)}$ ($= k_{(\text{OH}^-)}/k_{-(\text{OH}^-)}$) value of $320 \text{ dm}^3 \text{ mol}^{-1}$.

Equation 7.3: $k_{\text{obs}} = k_{(\text{OH}^-)}[\text{OH}^-] + k_{-(\text{OH}^-)}$

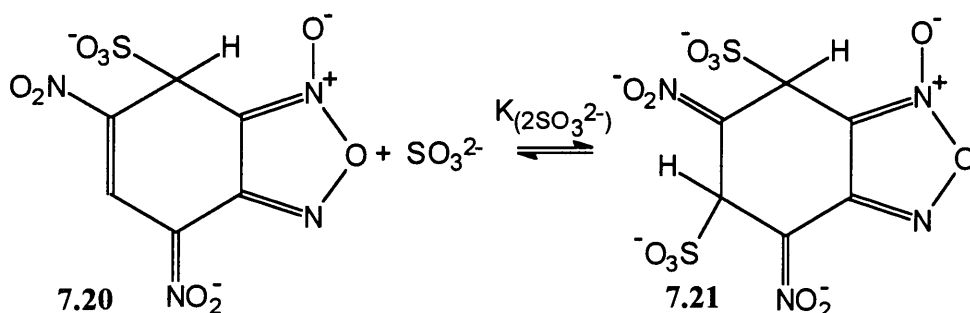
Table 7.4: Kinetic data for the reaction of 7.20, $4 \times 10^{-5} \text{ mol dm}^{-3}$, with hydroxide ions in water at 25 °C.

$[\text{OH}^-] / \text{mol dm}^{-3}$	$k_{\text{obs}} / \text{s}^{-1}$	A_{∞}
0.004	0.041	
0.006	0.063	
0.008	0.080	
0.01	0.088	0.027
0.02	0.17	0.033
0.03	0.26	0.037
0.04	0.29	0.042
0.07	0.48	0.048
0.10	0.73	0.048

^a Colour fading reaction measured at 476 nm.

7.3.2.3 Formation of a 1:2 DNBF:Sulfite Adduct

As the concentration of sulfite was increased, di-adducts, **7.21**, were observed according to Scheme 7.8. The absorption maxima of the di-adducts occurred at 340 nm. There is no possible charge delocalisation in the di-adduct, and so any absorbance will be due to the negatively charged nitro-groups.



Scheme 7.8

The equilibrium constant for di-adduct formation, $K(2\text{SO}_3^{2-})$, $15.4 \pm 1.7 \text{ dm}^3 \text{ mol}^{-1}$, was calculated from absorbance measurements at 476 nm, according to Equation 7.4, where A_0 is the absorbance due to the 1:1 adduct, **7.20**, and A_∞ is the absorbance due to the 1:2 adduct, **7.21**. Data are given in Table 7.5, and correspond to the spectra shown in Figure 7.6.

$$\text{Equation 7.4: } K(2\text{SO}_3^{2-}) = \frac{[\text{7.21}]}{[\text{7.20}][\text{SO}_3^{2-}]_{\text{free}}} = \frac{(A_0 - \text{Abs})}{(\text{Abs} - A_\infty)[\text{SO}_3^{2-}]_{\text{free}}}$$

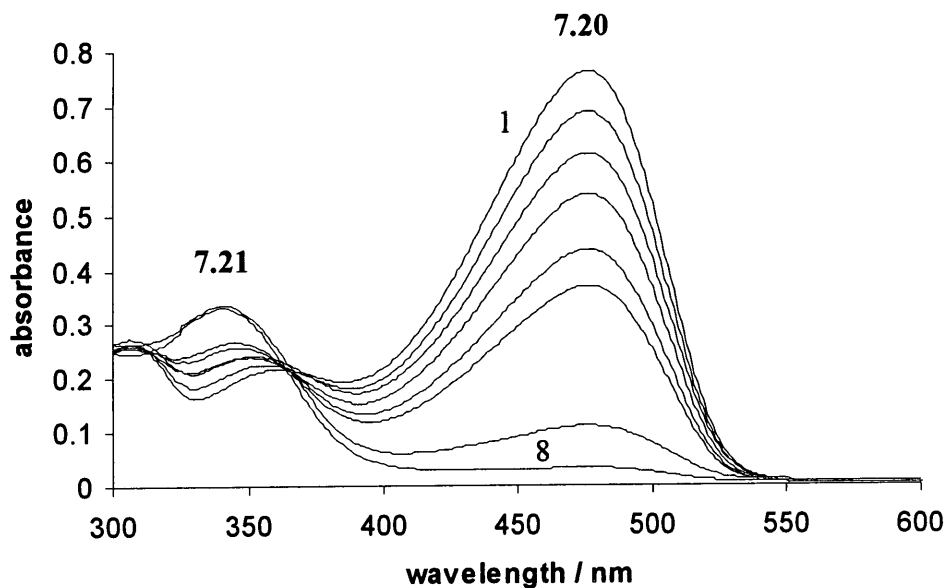
Table 7.5: Absorbance data for the formation of the di-adduct, ^a **7.21** at 25 °C.

Spectrum	$[\text{SO}_3^{2-}] / \text{mol dm}^{-3}$	Absorbance at 476 nm	$K(2\text{SO}_3^{2-})^b / \text{dm}^3 \text{ mol}^{-1}$
1	0.0008	0.764	
2	0.008	0.688	14.4
3	0.017	0.612	15.5
4	0.026	0.537	17.3
5	0.05	0.436	16.3
6	0.07	0.370	16.7
	0.09	0.347	14.8
7	0.2	0.110	
8	0.4	0.033	

^a $I (=0.5\sum c_i z_i^2) = 0.30 \text{ mol dm}^{-3}$. The ionic strength was maintained with sodium sulfate for sulfite concentrations $< 0.10 \text{ mol dm}^{-3}$.

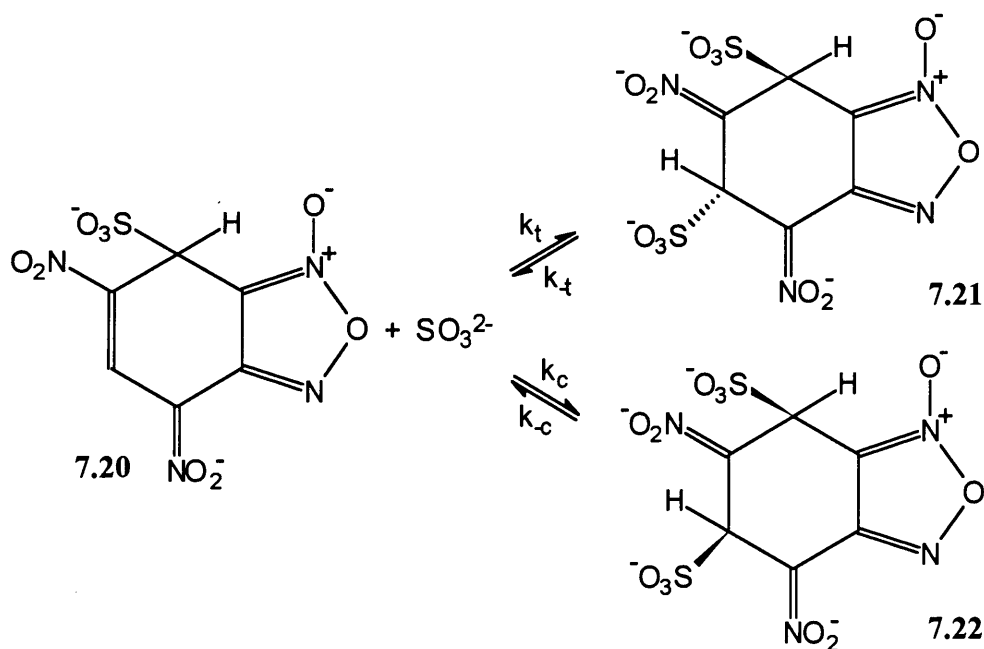
^b Calculated from Equation 7.4, with A_0 , 0.764 and A_∞ , 0.033.

Figure 7.6: Spectral changes on formation of the di-adduct, **7.21**, at 25 °C.



The reversibility of this reaction was studied by pre-forming the di-adduct, **7.21**, in sulfite solution, ($\lambda_{\text{max}} = 340 \text{ nm}$), and then diluting the solution with water to give the adduct **7.20**, ($\lambda_{\text{max}} = 476 \text{ nm}$). This proved that the pre-formed di-adduct could be reverted to the mono-adduct by reducing the concentration of free sulfite ions in the solution.

A kinetic study of the colour fading process at 476 nm, gave two time-separated reactions. The first will correspond to the rapid formation of the di-adduct, **7.21**, followed by a second, slower reaction to yield the isomeric form, **7.22**. In accordance with the earlier work of Bernasconi and Bergstrom,⁹ the initial rapid decrease in intensity at 476 nm was attributed to the formation of the trans-isomer. The second, slower, colour fading reaction was attributed to the isomerisation of the trans-form, **7.21**, to the cis-isomer, **7.22**, according to Scheme 7.9.



Scheme 7.9

The results in Table 7.5 show that 1:2 adducts have little absorbance at 476 nm. Hence, a K_T ($=k_t/k_t$) value was calculated according to Equation 7.5, where A_0 is the absorbance due to **7.20**, and A_F is the absorbance at the end of the fast, colour fading reaction.

$$\text{Equation 7.5: } K_T = \frac{[\text{7.21}]}{[\text{7.20}][\text{SO}_3^{2-}]} = \frac{(A_0 - A_F)}{(A_F - 0)[\text{SO}_3^{2-}]}$$

The equilibrium conversion of **7.20** to the isomeric di-adducts, **7.21** and **7.22**, was calculated according to Equation 7.6, where A_0 is the absorbance due to **7.20**, and A_S is the absorbance at the end of the slow, or colour fading reaction.

$$\text{Equation 7.6: } K_T + K_C = \frac{[\text{7.21}] + [\text{7.22}]}{[\text{7.20}][\text{SO}_3^{2-}]} = \frac{(A_0 - A_S)}{(A_S - 0)[\text{SO}_3^{2-}]}$$

A value of K_C was then determined according to Equation 7.7.

$$\text{Equation 7.7: } K_C = (K_T + K_C) - K_T$$

Absorbance data are reported in Table 7.6, for the isomerisation process at constant ionic strength, $I = 0.30 \text{ mol dm}^{-3}$, and in Table 7.7 for the reaction at constant ionic strength, $I = 0.49 \text{ mol dm}^{-3}$, and with pH maintained at 6.9.

Table 7.6: Absorbance data for the isomerisation process at 25 °C.

$[\text{SO}_3^{2-}] / \text{mol dm}^{-3}$	A_0^a	A_F^a	A_S^a	$K_T^b /$ mol dm^{-3}	$(K_T + K_C)^c /$ mol dm^{-3}
0.035	0.36	0.256	0.218	11.6	18.6
0.045	0.36	0.238	0.197	11.4	18.4
0.055	0.36	0.220	0.178	11.6	18.6
0.075	0.36	0.192	0.149	11.7	18.9
0.095	0.36	0.170	0.129	11.8	19.1

^a Absorbance values measured at 476 nm, $I = 0.30 \text{ mol dm}^{-3}$. A_0 is the absorbance due to **7.20**, A_F is the absorbance at the end of the fast, colour fading reaction and A_S is the absorbance at the end of the slow, colour fading reaction.

^b Calculated according to Equation 7.5.

^c Calculated according to Equation 7.6.

Table 7.7: Absorbance data for the isomerisation process at 25 °C.

$[\text{SO}_3^{2-}] / \text{mol dm}^{-3}$	A_0^a	A_F^a	A_S^a	$K_T^b /$ mol dm^{-3}	$(K_T + K_C)^c /$ mol dm^{-3}
0.035	0.385	0.275	0.222	11.4	21.0
0.055	0.385	0.228	0.165	12.5	24.2
0.075	0.385	0.190	0.130	13.7	26.2
0.095	0.385	0.170	0.115	13.3	24.7

^a Absorbance values measured at 476 nm, $I = 0.49 \text{ mol dm}^{-3}$, pH 6.9. A_0 is the absorbance due to **7.20**, A_F is the absorbance at the end of the fast, colour fading reaction and A_S is the absorbance at the end of the slow, colour fading reaction.

^b Calculated according to Equation 7.5.

^c Calculated according to Equation 7.6.

The data in Table 7.6 ($I = 0.30 \text{ mol dm}^{-3}$), gave a K_T value of $11.6 \pm 0.7 \text{ dm}^3 \text{ mol}^{-1}$ and a $K_T + K_C$ value of $18.7 \pm 0.9 \text{ dm}^3 \text{ mol}^{-1}$. Combination of these values according to Equation 7.7, led to a K_C value of $7.1 \pm 0.1 \text{ dm}^3 \text{ mol}^{-1}$. The data in Table 7.7 ($I = 0.49 \text{ mol dm}^{-3}$, pH 6.9), gave a K_T value of $12.7 \pm 1.2 \text{ dm}^3 \text{ mol}^{-1}$, and a $K_T + K_C$ value of $24.0 \pm 2.2 \text{ dm}^3 \text{ mol}^{-1}$. Combination of these values according to Equation 7.7, gave a K_C value of $11.3 \pm 1.1 \text{ dm}^3 \text{ mol}^{-1}$. The calculated equilibrium constants were greater in

solutions of higher ionic strength, as expected for the formation of multi-charged adducts.⁸

Kinetic data for the fast and slow colour fading processes are reported in Table 7.8. A plot of k_{fast} versus sulfite ion concentration was linear according to Equation 7.8, with a positive intercept, illustrating that the formation of the trans-complex was reversible. Values of k_t , $172 \pm 14 \text{ dm}^3 \text{ mol}^{-1} \text{ s}^{-1}$ and k_{-t} , $16.2 \pm 0.9 \text{ s}^{-1}$ were calculated from the gradient and intercept respectively. Combination of these values led to a $K_T (=k_t/k_{-t})$ value of $10.6 \pm 0.6 \text{ dm}^3 \text{ mol}^{-1}$.

Equation 7.8: $k_{fast} = k_t[\text{SO}_3^{2-}] + k_{-t}$

Table 7.8: Kinetic data for the isomerisation process at 25 °C.

$[\text{SO}_3^{2-}] / \text{mol dm}^{-3}$	$k_{fast}^a / \text{s}^{-1}$	$k_{slow}^a / \text{s}^{-1}$
0.015		0.065
0.035	22.2	0.074
0.055	25.4	0.080
0.075	29.9	0.088
0.095	32.3	0.088

^a Colour fading reaction measured at 476 nm, $I = 0.49 \text{ mol dm}^{-3}$ and pH 6.9.

Kinetic data for the slow process were also obtained at a constant ionic strength, $I = 0.30 \text{ mol dm}^{-3}$, using sodium sulfate as the compensating electrolyte. The rate constants for the slow process to give the cis-isomer can be defined in terms of the individual forward and reverse rate constants in Scheme 7.9, according to Equation 7.9.

Equation 7.9: $k_{slow} = k_f + k_r$

However, the cis-isomer is in equilibrium with the 1:1 adduct, and the trans-isomer, and so Equation 7.9 must account for these equilibria, leading to Equation 7.10. Under the experimental conditions used, $K_7[\text{SO}_3^{2-}] \gg 1$, and $K_T[\text{SO}_3^{2-}] \geq 1$, and Equation 7.10 reduced to Equation 7.11. Data are reported in Table 7.9.

Equation 7.10: $k_{slow} = \frac{k_c K_7 [\text{SO}_3^{2-}]^2}{(1 + K_7 [\text{SO}_3^{2-}]) (1 + K_T [\text{SO}_3^{2-}])} + k_{-c}$

Equation 7.11:
$$k_{\text{slow}} = \frac{k_c[\text{SO}_3^{2-}]}{1 + K_T[\text{SO}_3^{2-}]} + k_{-c}$$

Table 7.9: Kinetic data for the isomerisation of 7.21 to 7.22 at 25 °C.

$[\text{SO}_3^{2-}] / \text{mol dm}^{-3}$	$k_{\text{slow}}^a / \text{s}^{-1}$	$k_{\text{calc}}^b / \text{s}^{-1}$
0.015	0.064	0.064
0.025	0.067	0.067
0.035	0.068	0.069
0.045	0.073	0.071
0.075	0.076	0.076
0.095	0.078	0.078

^a Slow, colour fading reaction measured at 476 nm, $I = 0.30 \text{ mol dm}^{-3}$.

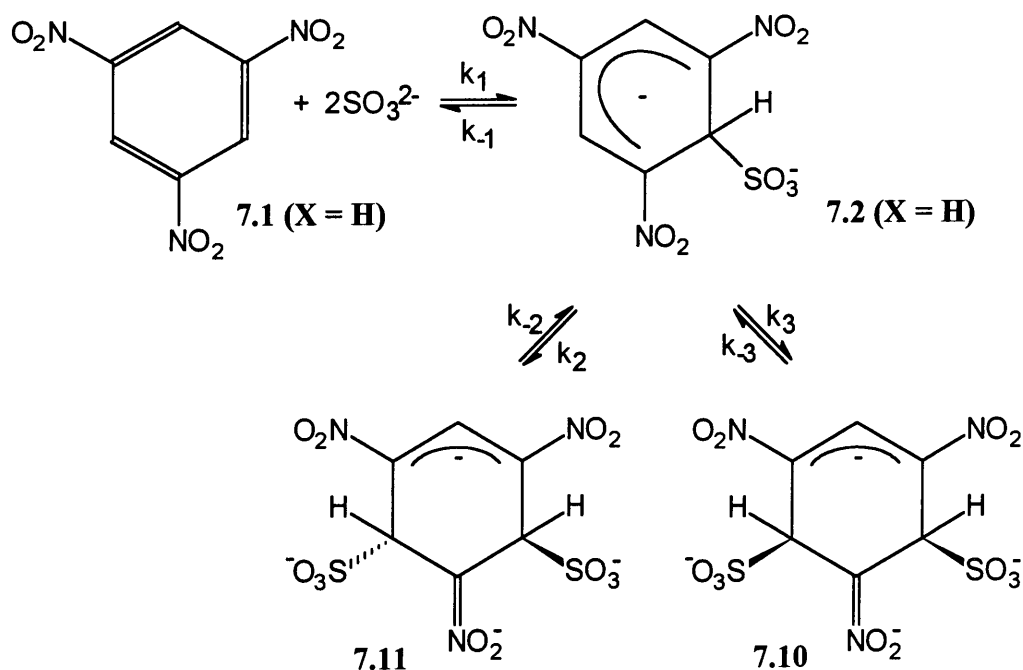
^b Calculated according to Equation 7.11, with k_c , $0.44 \pm 0.04 \text{ dm}^3 \text{ mol}^{-1} \text{ s}^{-1}$, k_{-c} , $0.06 \pm 0.006 \text{ s}^{-1}$, and K_T , $11.6 \pm 1.0 \text{ dm}^3 \text{ mol}^{-1}$.

Combination of the forward and reverse rate constants led to a $K_C (= k_c/k_{-c})$ value of $7.3 \text{ dm}^3 \text{ mol}^{-1}$. A summary of the rate and equilibrium constants measured is given in Table 7.10.

Table 7.10: Summary of the rate and equilibrium constants measured at 25 °C.

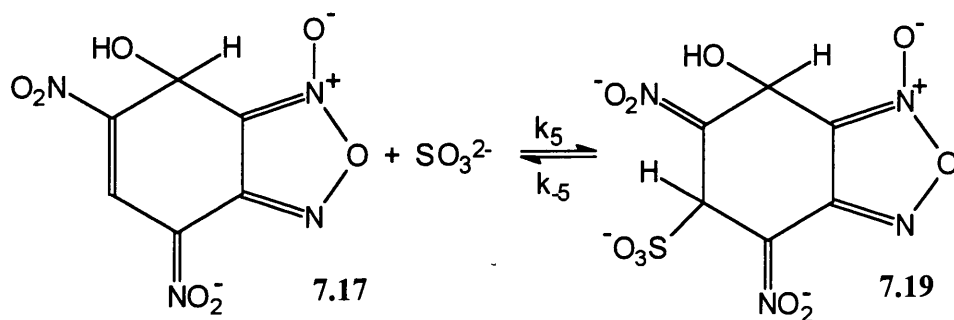
$K_T /$ $\text{dm}^3 \text{ mol}^{-1}$	$K_C /$ $\text{dm}^3 \text{ mol}^{-1}$	$k_t /$ $\text{dm}^3 \text{ mol}^{-1} \text{ s}^{-1}$	k_t / s^{-1}	$k_c /$ $\text{dm}^3 \text{ mol}^{-1} \text{ s}^{-1}$	k_{-c} / s^{-1}
11.6 ± 0.7	7.1 ± 0.1	172 ± 14	16.2 ± 0.9	0.44 ± 0.04	0.06 ± 0.006

The rate and equilibrium constants given in Table 7.10 illustrate that the stabilities of the cis- and trans-isomers are approximately the same ($K_T \approx K_C$), but the complexes have very different rates of formation and decomposition, with $k_t/k_c = 390$ and $k_t/k_{-c} = 270$. This is similar to the situation found in the formation of the trans- and cis-isomers from sulfite attack on TNB, 7.1 ($X = \text{H}$), according to Scheme 7.10, where $K_2/K_3 = 1.01$, $k_2/k_3 = 163$, and $k_2/k_{-3} = 161$.⁹



7.3.2.4 Reaction of the 1:1 DNBF:Hydroxide Adduct with Sulfite

In aqueous solution, DNBF, **7.16**, is able to abstract an hydroxide ion from water to give **7.17**. Experiments were carried out in solutions buffered at pH 7.5, to ensure that most of the DNBF was present in the hydroxide-adduct form. Reaction with sulfite ions produced the di-adduct, **7.19**, according to Scheme 7.11.



The formation of the di-adduct, **7.19**, was studied spectrophotometrically by following the decrease in the intensity of the absorption maximum due to **7.17**, ($\lambda_{\text{max}} = 465 \text{ nm}$), or the increase in intensity of the absorption maximum due to **7.19**, ($\lambda_{\text{max}} = 333 \text{ nm}$).

Kinetic data are reported in Table 7.11 for the formation of **7.19**, using sulfite / hydrogen sulfite as an internal buffer, (pH = 7.5), and sodium sulfate as the

compensating electrolyte, ($I = 0.75 \text{ mol dm}^{-3}$). A plot of the observed first order rate constant, k_{obs} , versus the concentration of free sulfite ions was linear, with a positive intercept, indicating the reversibility of the reaction according to Equation 7.12, with k_5 , $1600 \text{ dm}^3 \text{ mol}^{-1} \text{ s}^{-1}$ and k_{-5} , $(2 \pm 1) \text{ s}^{-1}$. Combination of these values gave a K_5 ($= k_5/k_{-5}$) value of $800 \text{ dm}^3 \text{ mol}^{-1}$.

Equation 7.12: $k_{\text{obs}} = k_5[\text{SO}_3^{2-}] + k_{-5}$

Table 7.11: Kinetic data^a for the formation of 7.19 at 25 °C.

[SO ₃ ²⁻] / mol dm ⁻³	k _{obs} / s ⁻¹		Abs at 465 nm	K ₅ ^b
	(465 nm)	(333 nm)		
0.0040	6.9	6.4	0.114	
0.0080	15	14	0.103	
0.020	34	33	0.089	865
0.028	48	45	0.085	758
0.040	67	66	0.079	795
0.060	97	91	0.074	890

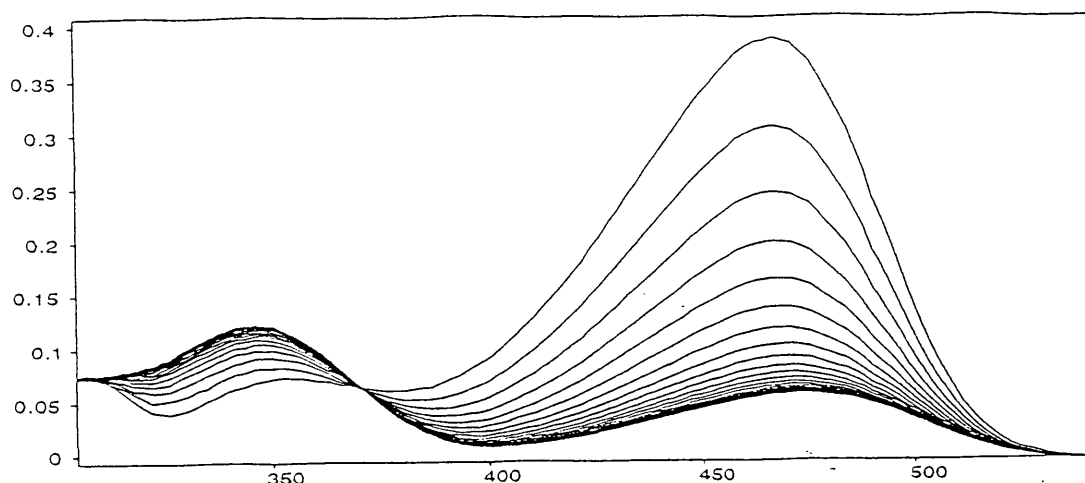
^a $I = 0.75 \text{ mol dm}^{-3}$, pH 7.5.

^b Calculated according to Equation 7.13, with $A_0 = 0.480$, and $A_\infty = 0.066$.

The equilibrium constant for formation of 7.19, K_5 was also calculated from absorbance values measured at 465 nm, according to Equation 7.13. The change in the UV/Visible spectra of 7.17, on addition of sulfite ions is shown in Figure 7.7. The data, reported in Table 7.11, gave an average K_5 value of $830 \pm 50 \text{ dm}^3 \text{ mol}^{-1}$. Using this value for K_5 and the known value for k_5 leads to a value for k_{-5} ($=k_5/K_5$) of $(1.9 \pm 0.2) \text{ s}^{-1}$. This is more precise than that obtained from the plot according to Equation 7.12.

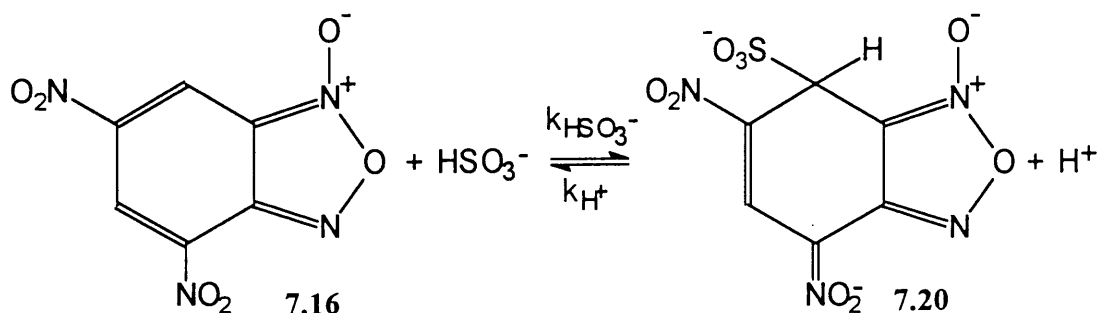
Equation 7.13:
$$K_5 = \frac{[\text{7.19}]}{[\text{7.17}][\text{SO}_3^{2-}]} = \frac{(A_0 - \text{Abs})}{(\text{Abs} - A_\infty)[\text{SO}_3^{2-}]}$$

Figure 7.7: Spectral changes with time on addition of $0.0040 \text{ mol dm}^{-3}$ sulfite to $4 \times 10^{-5} \text{ mol dm}^{-3}$ **7.17**, at 25°C . Spectra taken at 0.04 second intervals for 1.0 seconds.



7.3.2.5 Reaction of DNBF with the Hydrogen Sulfite Ion

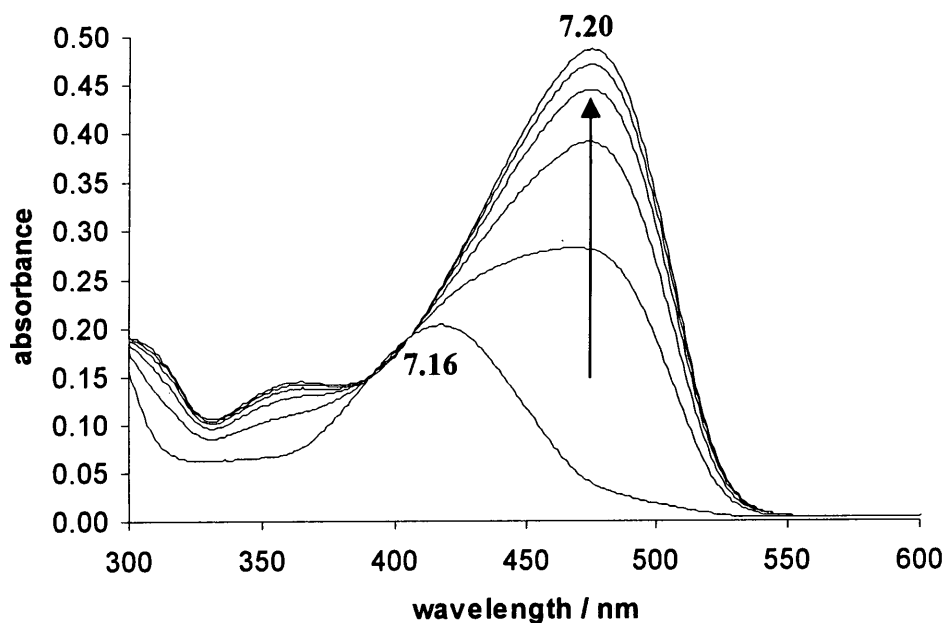
Reactions were carried out with DNBF, **7.16**, in acid solution of very high concentration, ($\geq 0.5 \text{ mol dm}^{-3}$) and with very low concentrations of sulfite ions ($1-4 \times 10^{-4} \text{ mol dm}^{-3}$). Here, the sulfite ions were largely protonated and the reaction observed was that of DNBF with hydrogen sulfite, according to Scheme 7.12.



Scheme 7.12

UV/Visible spectral changes over time illustrated the formation of **7.20**, which was characterised by the strong absorbance at 475 nm, Figure 7.8.

Figure 7.8: UV/Visible spectra for the reaction of **7.16**, $4 \times 10^{-5} \text{ mol dm}^{-3}$, in 0.5 mol dm^{-3} hydrochloric acid, with sulfite, $1 \times 10^{-4} \text{ mol dm}^{-3}$. Spectra taken every 15 minutes for 60 minutes and finally after 90 minutes.



Data were measured for solutions of constant ionic strength $I (=0.5\sum c_i z_i^2) = 2.0 \text{ mol dm}^{-3}$, using potassium chloride as the compensating electrolyte. Here the effective acid concentration was calculated according to the H_0 acidity function.¹⁹ Data are reported in Table 7.12. It is known¹⁹ that the presence of added potassium chloride increases the acidity of the medium. The change in the H_0 value is given by Equation 7.14.

Equation 7.14: $\Delta H_0 = -0.14[\text{KCl}]$

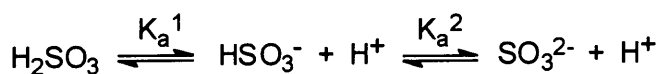
Table 7.12: Effective acid concentration in solution of ionic strength 0.2 mol dm^{-3} .

$[\text{HCl}] / \text{mol dm}^{-3}$	$[\text{KCl}] / \text{mol dm}^{-3}$	H_0	H_0^a	$[\text{H}^+]_{\text{effective}} / \text{mol dm}^{-3}$
0.5	1.5	0.20	-0.01	1.02
1.0	1.0	-0.20	-0.34	2.19
1.5	0.5	-0.47	-0.54	3.46
2.0	0	-0.69	-0.69	4.90

^a Corrected for KCl.

The equilibrium constant for the formation of **7.20** from DNBF and hydrogen sulfite ions was calculated from absorbance measurements at 475 nm. At equilibrium, the

sulfite ion may exist in the protonated or di-protonated forms according to Scheme 7.13. The values of K_a^1 and K_a^2 are $1.54 \times 10^{-2} \text{ mol dm}^{-3}$ and $1 \times 10^{-7} \text{ mol dm}^{-3}$ respectively.¹⁷



Scheme 7.13

The acid dissociation constants may be expressed in terms of the component concentrations at equilibrium, according to Equations 7.15 and 7.16.

$$\text{Equation 7.15: } K_a^1 = \frac{[\text{HSO}_3^-][\text{H}^+]}{[\text{H}_2\text{SO}_3]}$$

$$\text{Equation 7.16: } K_a^2 = \frac{[\text{SO}_3^{2-}][\text{H}^+]}{[\text{HSO}_3^-]}$$

The overall equilibrium constant $K_a^1 K_a^2$ is given by Equation 7.17.

$$\text{Equation 7.17: } K_a^1 K_a^2 = \frac{[\text{H}^+]^2 [\text{SO}_3^{2-}]}{[\text{H}_2\text{SO}_3]}$$

Sulfite can be present in three forms as indicated in Equation 7.18.

$$\text{Equation 7.18: } [\text{SO}_3^{2-}]_{\text{stoich}} = [\text{H}_2\text{SO}_3] + [\text{HSO}_3^-] + [\text{SO}_3^{2-}]$$

At the acidity used in the present work, where $[\text{H}^+]_{\text{effective}} \geq 1 \text{ mol dm}^{-3}$, sulfite is present very largely as H_2SO_3 . For example, use of Equation 7.17 shows that when $[\text{H}^+]_{\text{effective}} = 1.02 \text{ mol dm}^{-3}$, $[\text{SO}_3^{2-}] = 1.5 \times 10^{-9} [\text{SO}_3^{2-}]_{\text{stoich}}$, and use of Equation 7.15 shows that, $[\text{HSO}_3^-] = 0.015 [\text{SO}_3^{2-}]_{\text{stoich}}$.

The equilibrium constant for formation of **7.20**, KHSO_3^- , was defined according to Equation 7.19.

$$\text{Equation 7.19: } \text{KHSO}_3^- = \frac{[\text{7.20}][\text{H}^+]_{\text{effective}}}{[\text{7.16}][\text{HSO}_3^-]}$$

The concentration of hydrogen sulfite ions in solution was calculated according to Equation 7.15, and Equation 7.19 was modified accordingly to give Equation 7.20.

$$\text{Equation 7.20: } K\text{HSO}_3^- = \frac{[\text{7.20}][\text{H}^+]^2_{\text{effective}}}{[\text{7.16}][\text{SO}_3^{2-}]_{\text{stoich}}K_a^{-1}}$$

The relative proportions of 7.20 and 7.16 at equilibrium were determined from absorbance measurements, and Equation 7.20 was modified accordingly to give Equation 7.21, where A_0 is the absorbance due to 7.16, and A_∞ is the absorbance due to 7.20.

$$\text{Equation 7.21: } K\text{HSO}_3^- = \frac{(\text{Abs} - A_0)[\text{H}^+]^2_{\text{effective}}}{(A_\infty - \text{Abs})K_a^{-1}[\text{SO}_3^{2-}]_{\text{stoich}}}$$

Absorbance measurements and kinetic data are reported in Table 7.13, for the reaction of DNBF with hydrogen sulfite ions. The data gave a $K\text{HSO}_3^-$ value of $(1.09 \pm 0.25) \times 10^6$.

Table 7.13: UV/Visible data for the formation of 7.20 at 25 °C.

$10^4 [\text{SO}_3^{2-}]_{\text{stoich}}$ / mol dm ⁻³	$[\text{HCl}]^a$ / mol dm ⁻³	$[\text{H}^+]_{\text{effective}}^b$ / mol dm ⁻³	$10^4 k_{\text{obs}}^c$ / s ⁻¹	A_∞^c	$10^{-6} \text{KHSO}_3^{\text{d}}$
1.0	0.5	1.02	3.05	0.343	0.69
2.0	0.5	1.02	5.17	0.519	1.23
3.0	0.5	1.02	7.49	0.522	0.87
4.0	0.5	1.02	8.73	0.553	0.91
10	0.5	1.02		0.64	
20	0.5	1.02	3.28	0.65	
1.0	1.0	2.19	4.12	0.173	0.93
2.0	1.0	2.19	4.99	0.299	1.2
3.0	1.0	2.19	6.04	0.376	1.3
4.0	1.0	2.19	5.38	0.408	1.2
1.0	1.5	3.46	6.62	0.114	1.2
2.0	1.5	3.46	7.12	0.204	1.5
3.0	1.5	3.46	8.23	0.257	1.5
4.0	1.5	3.46	6.48	0.273	1.3
1.0	2.0	4.90	6.99	0.058	0.74
2.0	2.0	4.90	6.98	0.101	1.0
3.0	2.0	4.90	7.65	0.126	0.95
4.0	2.0	4.90		0.147	0.91

^a Ionic strength, 0.20 mol dm⁻³ using KCl as the compensating electrolyte.^b Values in Table 7.12.^c Measured at 475 nm.^d Calculated according to Equation 7.21, with $A_0 = 0.03$, and $A_\infty = 0.65$.

The kinetic data, reported in Table 7.13 gave linear plots of the observed first order rate constant versus stoichiometric sulfite ion concentration, (at a given hydrogen ion concentration), with positive intercepts, according to Equation 7.22.

Equation 7.22: $k_{\text{obs}} = k\text{HSO}_3^+[\text{HSO}_3^-] + k\text{H}^+[\text{H}^+]$

The measured rate constants are given in Table 7.14, where the dependence of $k\text{HSO}_3^+$ on the acid concentration is evident. They lead to values for $k\text{HSO}_3^+$ $(130 \pm 20) \text{ dm}^3 \text{ mol}^{-1} \text{ s}^{-1}$ and $k\text{H}^+$ $(1.2 \pm 0.1) \times 10^{-4} \text{ dm}^3 \text{ mol}^{-1} \text{ s}^{-1}$.

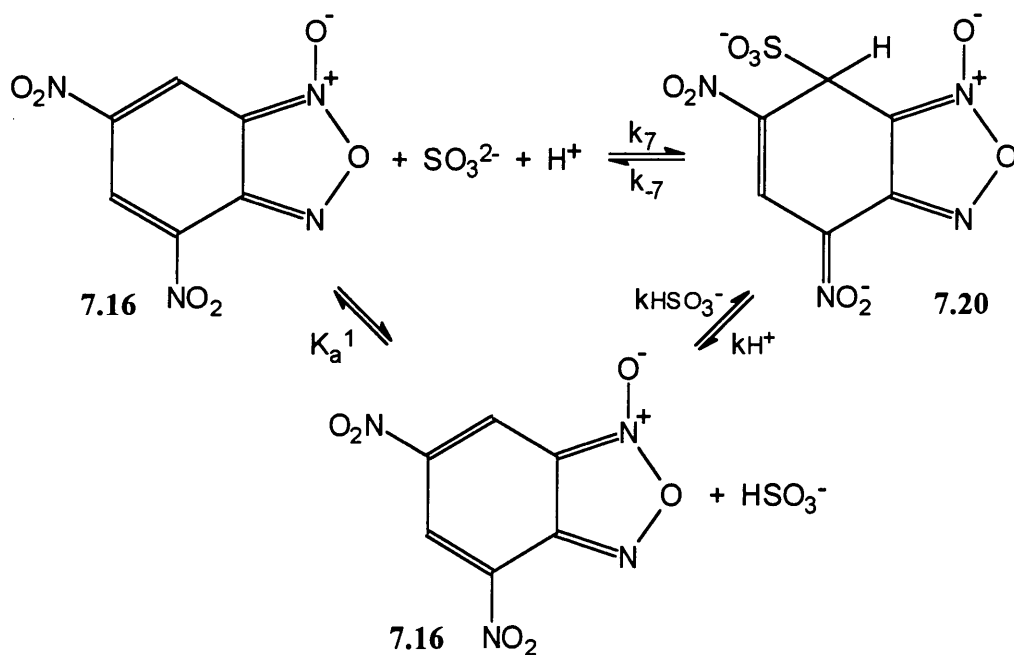
Table 7.14: Rate constants measured for the formation of 7.20 at 25 °C.

$10^4 [\text{SO}_3^{2-}]_{\text{stoich}}$ / mol dm ⁻³	$[\text{H}^+]_{\text{effective}}^{\text{a b}}$ / mol dm ⁻³	$10^6 [\text{HSO}_3^-]^{\text{c}}$ / mol dm ⁻³	$10^4 k_{\text{obs}}^{\text{d}}$ / s ⁻¹	$10^4 k\text{H}^{+\text{e}}/$ dm ³ mol ⁻¹ s ⁻¹	$k\text{HSO}_3^{-\text{e}} /$ dm ³ mol ⁻¹ s ⁻¹
1.0	1.02	1.57	3.05	1.1	125
2.0	1.02	3.14	5.17	1.1	125
3.0	1.02	4.7	7.49	1.1	125
4.0	1.02	6.3	8.73	1.1	125
1.0	2.19	0.70	3.28	1.1	125
2.0	2.19	1.40	4.12	1.1	125
3.0	2.19	2.10	4.99	1.1	125
4.0	2.19	2.80	6.04	1.1	125
1.0	3.46	0.45	5.38	1.4	170
2.0	3.46	0.90	6.62	1.4	170
3.0	3.46	1.3	7.12	1.4	170
4.0	3.46	1.8	8.23	1.4	170
1.0	4.90	0.31	6.48	1.2	150
2.0	4.90	0.63	6.99	1.2	150
3.0	4.90	0.94	6.98	1.2	150
4.0	4.90	1.26	7.65	1.2	150

^a Ionic strength; 0.20 mol dm⁻³, using KCl as a compensating electrolyte.^b Values taken from Table 7.12.^c Calculated from Equation 7.15 using $[\text{H}_2\text{SO}_3] = [\text{SO}_3^{2-}]_{\text{stoich}}$.^d Measured at 475 nm.^e Values of $k\text{H}^+$ and $k\text{HSO}_3^-$ calculated at each acid concentration.

The values in Table 7.14 were calculated assuming that HSO_3^- is the effective nucleophile at the acid concentrations used. The invariance with acid concentration of the values calculated for $k\text{HSO}_3^-$ shows that this assumption is valid. If H_2SO_3 were the reactant, then little variation with acidity of the rate term for the forward reaction would be expected (at these acidities $[\text{H}_2\text{SO}_3] \approx [\text{SO}_3^{2-}]_{\text{stoich}}$). Further, the concentrations of SO_3^{2-} are smaller than 10^{-12} mol dm⁻³. Hence reaction with free sulfite is suppressed.

Using the value obtained for KHSO_3^- it is possible to obtain a value for K_7 , the equilibrium constant for formation of the 1:1 adduct. This uses the cycle shown in Scheme 7.14.



Scheme 7.14

Using Equation 7.23, it can be seen that the value for K_7 is $1.1 \times 10^{13} \text{ dm}^3 \text{ mol}^{-1}$, and Equation 7.24 leads to a value for k_{-7} of $2.1 \times 10^{-6} \text{ s}^{-1}$.

$$\text{Equation 7.23: } K_7 = \frac{K_{\text{HSO}_3^-}}{K_a^1} = \frac{1.1 \times 10^6}{1 \times 10^{-7}} = 1.1 \times 10^{13} \text{ dm}^3 \text{ mol}^{-1}$$

$$\text{Equation 7.24: } k_{-7} = \frac{k_7}{K_7} = \frac{2.3 \times 10^7}{1.1 \times 10^{13}} = 2.1 \times 10^{-6} \text{ s}^{-1}$$

7.4 Comparisons

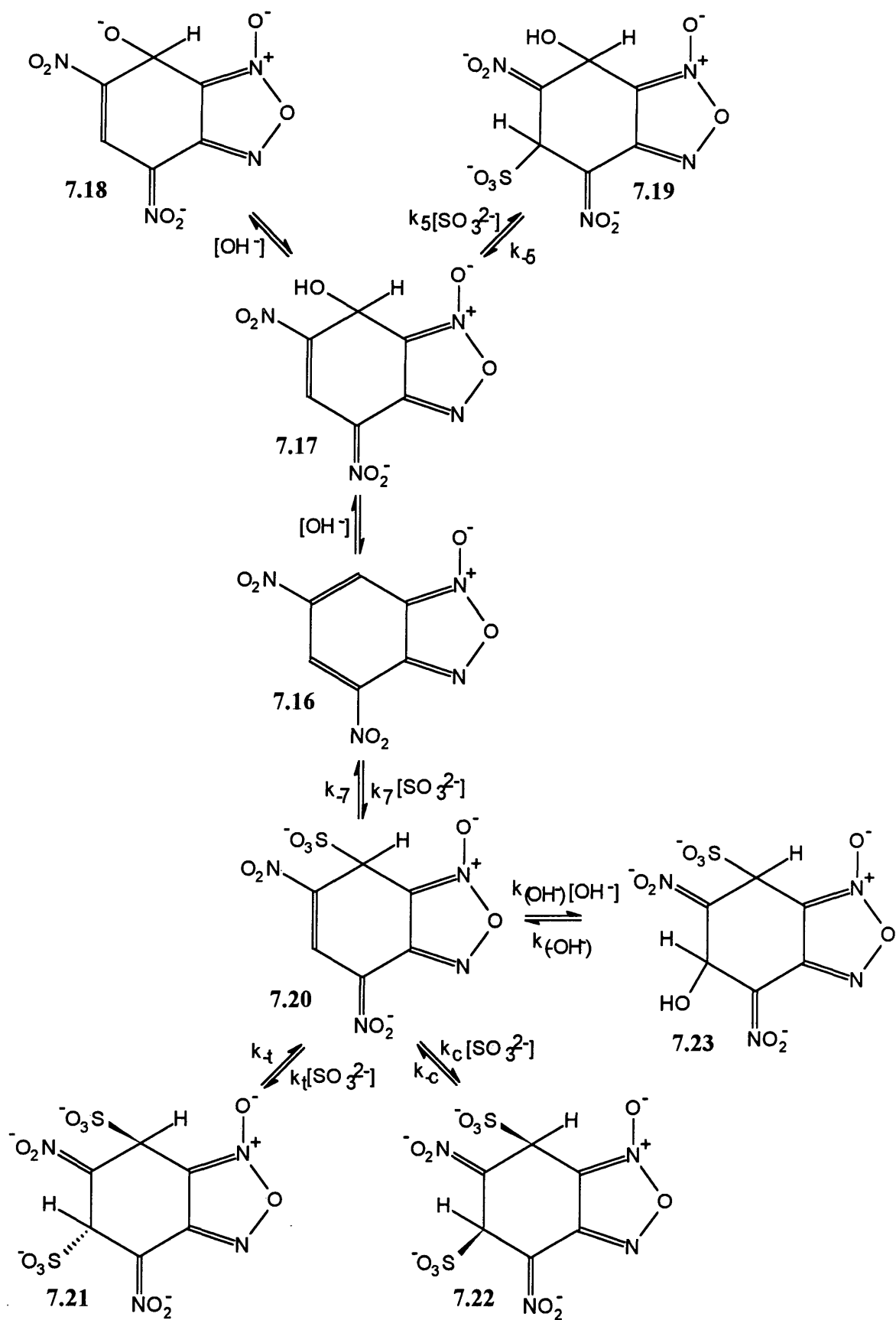
A summary of the rate and equilibrium constants measured is given in Table 7.15, where the individual rate constants correspond to those shown in the overall reaction scheme, described in Scheme 7.15.

Table 7.15: Summary of the rate and equilibrium constants measured at 25 °C.

Adduct	Constant	
7.19	$k_5 / \text{dm}^3 \text{mol}^{-1} \text{s}^{-1}$	1600
	k_{-5} / s^{-1}	1.8
	$K_5 / \text{dm}^3 \text{mol}^{-1}$	890
7.20	$k_7 / \text{dm}^3 \text{mol}^{-1} \text{s}^{-1}$	2.3×10^7
	k_{-7} / s^{-1}	2.1×10^{-6}
	$K_7 / \text{dm}^3 \text{mol}^{-1}$	1.1×10^{13}
7.21	$k_t / \text{dm}^3 \text{mol}^{-1} \text{s}^{-1}$	172
	k_{-t} / s^{-1}	16.2
	$K_T / \text{dm}^3 \text{mol}^{-1}$	11.6
7.22	$k_c / \text{dm}^3 \text{mol}^{-1} \text{s}^{-1}$	0.44
	k_{-c} / s^{-1}	0.06
	$K_C / \text{dm}^3 \text{mol}^{-1}$	7.1
7.23	$k_{(\text{OH}^-)} / \text{dm}^3 \text{mol}^{-1} \text{s}^{-1}$	7.0
	$k_{(-\text{OH}^-)} / \text{s}^{-1}$	0.022
	$K_{(\text{OH}^-)} / \text{dm}^3 \text{mol}^{-1}$	320

Equilibrium constants measured for the di-adducts **7.19** and **7.23**, are much higher than those measured for the isomeric di-sulfite adducts **7.21** and **7.22**. In the di-adducts, both nitro-groups carry negative charges, so that the lower stabilities of **7.21** and **7.22** may reflect unfavourable repulsions between charges on the nitro-groups and the added sulfite groups.

The adduct, **7.19**, is more stable than **7.23**. The major factor here is probably the carbon basicity of sulfite relative to hydroxide. There may also be better charge delocalisation in the transition state to give **7.19**, as there are fewer localised negative charges than in the transition state leading to **7.23**.



Scheme 7.15

The isomeric di-sulfite adducts **7.21** and **7.22**, are of similar stability, but the forward and reverse rate constants for their formation differ greatly. The forward and reverse rate constants for formation of the trans-complex, **7.21**, are greater than for the cis-complex, **7.22**. This is likely to reflect unfavourable repulsion in the transition state for the formation of the cis-isomer between the bound and entering sulfite groups. This repulsion may be partly alleviated by ring distortion in the fully formed cis-complex.

A summary of the rate and equilibrium constants measured for the reaction of sulfite ions with TNB is given in Table 7.16.

Table 7.16: Rate and equilibrium constants for the formation of sulfite adducts with TNB, **7.1** (X = H), at 25 °C.

Adduct	Constant ^a	^b
7.2 (X = H)	$k_1 / \text{dm}^3 \text{ mol}^{-1} \text{ s}^{-1}$	3.54×10^4
	k_{-1} / s^{-1}	125
	$K_1 / \text{dm}^3 \text{ mol}^{-1}$	286
7.11	$k_2 / \text{dm}^3 \text{ mol}^{-1} \text{ s}^{-1}$	195
	k_{-2} / s^{-1}	21
	$K_2 / \text{dm}^3 \text{ mol}^{-1}$	9.3
7.10	$k_3 / \text{dm}^3 \text{ mol}^{-1} \text{ s}^{-1}$	1.2
	k_{-3} / s^{-1}	0.13
	$K_3 / \text{dm}^3 \text{ mol}^{-1}$	9.2

^a Rate constants corresponding to Scheme 7.10.

^b Literature values.⁹

Comparison of the data in Tables 7.15 and 7.16 shows that the 1:1 adduct from DNBF has a stability approximately 10^{11} greater than that formed from TNB. This reflects the higher value for nucleophilic attack $k_7/k_1 \approx 10^3$, and the much lower value for sulfite expulsion, $k_{-7}/k_{-1} \approx 10^{-8}$. A rather similar situation is found in comparison of the hydroxide adducts, where that formed from DNBF has a stability approximately 10^{10} higher than that formed from TNB. These results confirm the highly electrophilic character of DNBF.

Nevertheless, the data in Tables 7.15 and 7.16 show that the 1:2 sulfite adducts from DNBF and TNB have rather similar stabilities. This may reflect the fact that addition of

the second sulfite ion to TNB allows charge to be spread over two nitro groups, while when addition occurs to DNBF only one nitro group remains to accommodate the negative charge.

7.5 Conclusion

The reactions of sulfite with DNBF have produced complexes of 1:1 and 1:2 stoichiometry. The high rates of formation of the 1:1 complexes made impossible a direct measurement of the equilibrium constant, K_7 . However, indirect measurements using Scheme 7.14, gave a value of $1.1 \times 10^{13} \text{ dm}^3 \text{ mol}^{-1}$. This value reflects the very high carbon basicity of the sulfite ion and the highly electrophilic character of DNBF.

The greater stability of the 1:1 complexes formed from DNBF may be attributed to the greater electrophilic character of this compound over TNB. As in the reaction of sulfite with TNB, isomeric complexes were formed in the presence of excess sulfite. The stabilities of the cis- and trans-complexes were found to be similar, although the rates of formation and decomposition varied greatly.

7.6 References

- ¹ M. R. Crampton., *J. Chem. Soc. (B)*., 1978, 343.
- ² D. N. Brooke and M. R. Crampton., *J. Chem. Soc., Perkin Trans. 2.*, 1980, 1850.
- ³ E. Buncel, A. R. Norris, K. E. Russell and P. J. Sheridan., *Can. J. Chem.*, 1974, **52**, 25.
- ⁴ M. R. Crampton and M. J. Willison., *J. Chem. Soc., Perkin Trans. 2.*, 1976, 160.
- ⁵ M. R. Crampton and A. J. Holmes., *J. Phys. Org. Chem.*, 1998, **11**, 787.
- ⁶ M. R. Crampton and C. Greenhalgh., *J. Chem. Soc., Perkin Trans. 2.*, 1985, 599.
- ⁷ A. R. Norris and N. Marendic., *Can. J. Chem.*, 1973, **51**, 3927.
- ⁸ F. Terrier., *Chem. Rev.*, 1982, **82**, 77.
- ⁹ C. F. Bernasconi and R. G. Bergstrom., *J. Am. Chem. Soc.*, 1973, **95**, 3603.
- ¹⁰ M. J. Strauss and S. P. B. Taylor., *J. Am. Chem. Soc.*, 1973, **95**, 3813.
- ¹¹ M. R. Crampton and M. J. Willison., *J. Chem. Soc., Chem. Commun.*, 1973, 215.
- ¹² M. T. Annandale, G. W. vanLoon and E. Buncel., *Can. J. Chem.*, 1998, **76**, 873.
- ¹³ F. Terrier, "Nucleophilic Aromatic Displacement". VCH, New York. 1991.
- ¹⁴ P. Drost., *Liebigs Ann. Chem.*, 1899, **307**, 49.
- ¹⁵ M. R. Crampton., *J. Chem. Soc. (B)*., 1967, 1341.
- ¹⁶ F. Terrier, F. Millot and W. P. Norris., *J. Am. Chem. Soc.*, 1976, **98**, 5883.
- ¹⁷ H. V. Tartar and H. H. Garretson., *J. Am. Chem. Soc.*, 1941, **63**, 808.
- ¹⁸ L. G. Sillen and A. E. Martell., *Chem. Soc. Sp. Publ.* 17, 1964, Table 55.
- ¹⁹ M. A. Paul., *J. Am. Chem. Soc.*, 1954, **76**, 3236.

Chapter 8

Appendix

8 Appendix

8.1 Measurement Techniques

The following sections outline the experimental techniques used to monitor the kinetics of the reactions studied and to elucidate the structures of the intermediates and products formed.

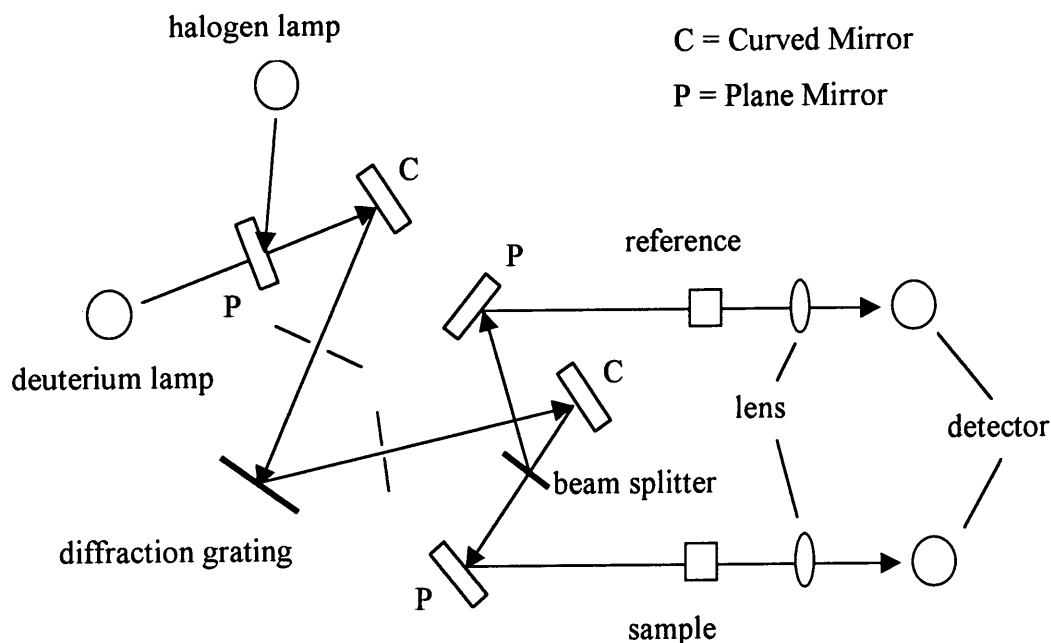
8.1.1 UV/Visible Spectrophotometry

UV/Visible spectra were recorded at 25 °C, in thermostatted, 1 cm path length quartz cuvettes, using freshly prepared solutions. Conventional spectrophotometers were used to measure the kinetics of reactions where the half life, $t_{1/2}$, was greater than 20 seconds, under pseudo first order conditions, with the reagent concentration in large excess of the substrate concentration. Here the Beer-Lambert law may be applied, Equation 8.1, where I_0 is the intensity of the incident light, I the intensity of transmitted light, A is the measured absorbance, ϵ the molar extinction coefficient, c the concentration in mol dm^{-3} , and l is the path length in cm.

$$\text{Equation 8.1: } \log\left(\frac{I_0}{I}\right) = A = \epsilon cl$$

In order to measure the ratio of the intensities of the incident light over the transmitted light, according to the Beer-Lambert law, UV/Visible spectrophotometers use a “double-beam”, where one beam passes through the sample, and the other through a reference cell, Figure 8.1.¹ Two light sources provide a total wavelength range of 200-700 nm, with a deuterium lamp giving UV light (200-300 nm), and a halogen lamp giving visible light (300-700 nm). The light is broken down into its component wavelengths using a monochromator, before being divided into two beams of equal intensity using the application of curved mirrors. The two beams are passed through the sample and reference respectively, before being focussed onto a detector, which measures the ratio of the beam intensities. The difference is converted, and plotted as the absorbance due to the sample. A typical UV/Visible spectrophotometer is shown schematically in Figure 8.1.

Figure 8.1: Schematic representation of a UV/Visible spectrophotometer.



Absorbance data measured over time were analysed using either the data fitting program PECSS, (Perkin Elmer Computerised Spectroscopy Software), or an Excel spreadsheet. Both methods gave consistent results for a standard reaction. The observed first order rate constant, k_{obs} , was determined using a calculation based on the derivation below.

For a first order process, ($X \rightarrow Y$) in which reactant, X is converted to product, Y, the rate of formation of the product is equal to the rate of removal of reactant, Equation 8.2.

Equation 8.2:
$$\frac{d[Y]}{dt} = -\frac{d[X]}{dt} = k_{\text{obs}}[X]$$

Integration of Equation 8.2, according to Equation 8.3, leads to Equation 8.4, which can be rearranged to give an expression for the observed first order rate constant, k_{obs} , Equation 8.5, where $[X]_0$ and $[X]_t$ are the concentrations of X at times $t = 0$ and $t = t$ respectively.

Equation 8.3:
$$-\int_{[X]_0}^{[X]_t} \frac{1}{[X]} d[X] = \int_0^t k_{\text{obs}} dt$$

$$\text{Equation 8.4: } \ln[X]_t - \ln[X]_0 = -k_{\text{obs}}t$$

$$\text{Equation 8.5: } k_{\text{obs}} = -\frac{1}{t} \ln \frac{[X]_t}{[X]_0}$$

Application of the Beer-Lambert law, Equation 8.1, leads to an expression for the absorbance at $t = 0$, where X is the only species present, Equation 8.6, and at $t = t$, where both X and Y are present, Equation 8.7. In both cases, the path length is 1 cm, and $A = \epsilon c \times 1$.

$$\text{Equation 8.6: } A_0 = \epsilon_X[X]_0$$

$$\text{Equation 8.7: } A_t = \epsilon_X[X]_t + \epsilon_Y[Y]_t$$

The concentration of Y at time, t is given by Equation 8.8. Substitution of this equation into Equation 8.7 leads to Equation 8.9, where the absorbance at time, t , is expressed solely in terms of the concentration of reactant X.

$$\text{Equation 8.8: } [Y]_t = [X]_0 - [X]_t$$

$$\text{Equation 8.9: } A_t = \epsilon_X[X]_t + \epsilon_Y[X]_0 - \epsilon_Y[X]_t$$

At the end-point, $t = \infty$, the concentration of the product, Y, is equal to the initial concentration of reactant, X at $t = 0$, and Equation 8.10 may be defined.

$$\text{Equation 8.10: } A_{\infty} = \epsilon_Y[Y]_{\infty} = \epsilon_Y[X]_0$$

Therefore, Equation 8.9 reduces to Equation 8.11, which may be rearranged to give the concentration of the reactant, X at time, t , Equation 8.12.

$$\text{Equation 8.11: } A_t = \epsilon_X[X]_t + A_{\infty} - \epsilon_Y[X]_t$$

$$\text{Equation 8.12: } [X]_t = \frac{(A_{\infty} - A_t)}{(\epsilon_B - \epsilon_A)}$$

Similarly, subtracting Equation 8.6 from Equation 8.10 to give Equation 8.13, followed by rearrangement, gives an expression for the concentration of the reactant X, at time, $t = 0$, Equation 8.14.

$$\text{Equation 8.13: } A_{\infty} - A_0 = \epsilon_Y[X]_0 - \epsilon_X[X]_0$$

$$\text{Equation 8.14: } [X]_0 = \frac{(A_{\infty} - A_0)}{(\epsilon_B - \epsilon_A)}$$

Substitution of Equations 8.12 and 8.14 into Equation 8.5, leads to Equation 8.15, which may be rearranged to give Equation 8.16, where a plot of $\ln(A_{\infty} - A_t)$ versus t is linear with a gradient, $-k_{\text{obs}}$, and intercept, $\ln(A_{\infty} - A_0)$.

$$\text{Equation 8.15: } k_{\text{obs}} = -\frac{1}{t} \ln \frac{(A_{\infty} - A_t)}{(A_{\infty} - A_0)}$$

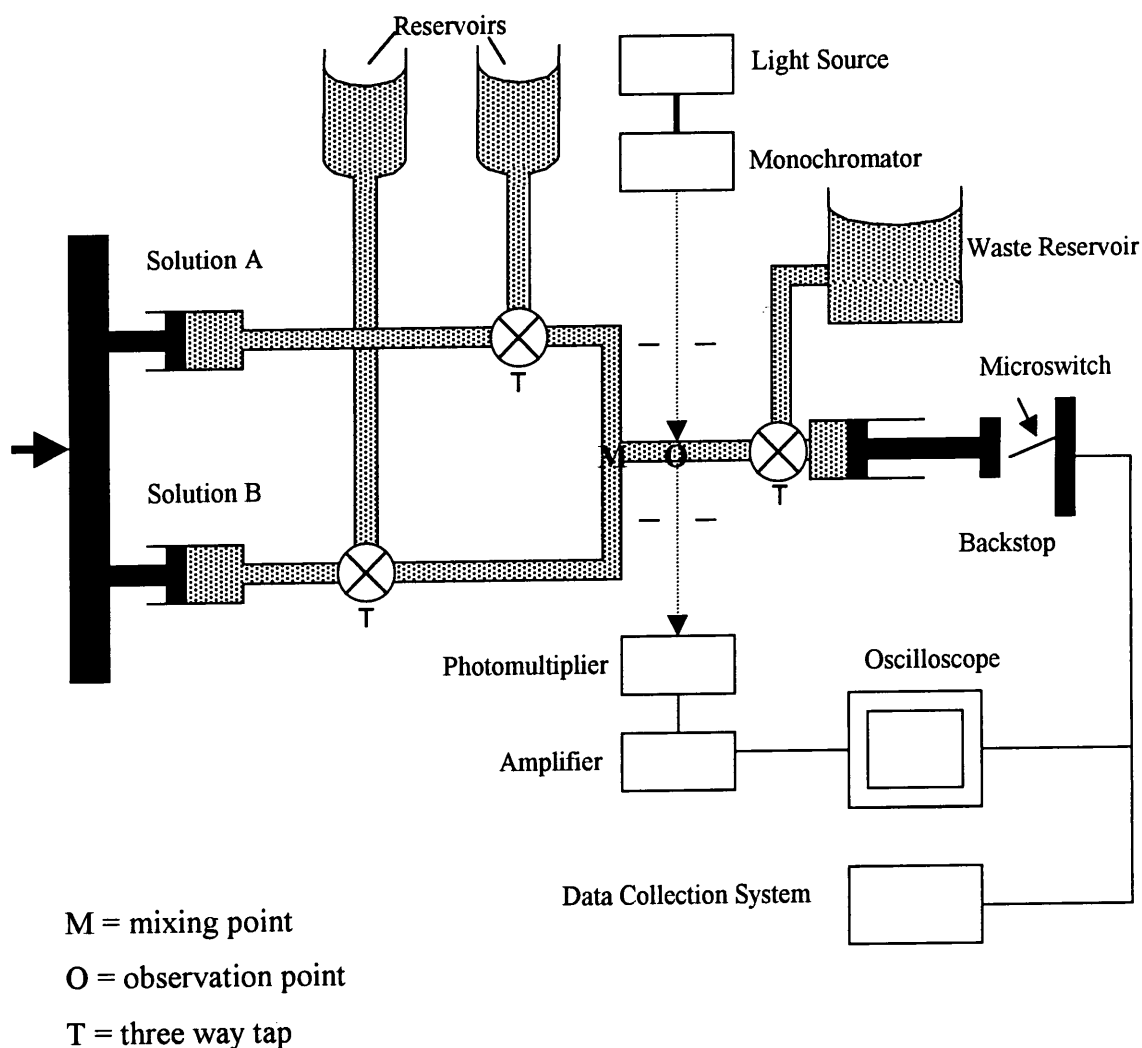
$$\text{Equation 8.16: } \ln(A_{\infty} - A_t) = -k_{\text{obs}}t + \ln(A_{\infty} - A_0)$$

In order to gain an accurate value of k_{obs} , the infinity values, A_{∞} were determined after a period of ten half lives, and the change in absorbance was followed for at least two half lives.

8.1.2 Stopped-flow Spectrophotometry

The stopped-flow technique was used to study the kinetics of reactions in solution with half lives in the range, $2 \text{ ms} < t_{1/2} < 20 \text{ s}$. A schematic representation of the instrument is shown in Figure 8.2.² The two reactant solutions are injected rapidly into a mixing chamber, M, in equal volumes. Mixing requires approximately 2 ms, and this is termed the “dead time”. Hence reactions with half lives of less than 2 ms cannot be measured. After mixing, the solution is allowed to flow into a thermostatted quartz cell at point O, connected to a third syringe. The piston of the third syringe is stopped suddenly by an external stop. The piston of the stopping syringe will also operate a microswitch, S, to trigger the detection system.

Figure 8.2: Schematic of a stopped-flow spectrophotometer



A fibre optic cable is passed through the cell to generate a beam of monochromatic light at the desired wavelength. A photomultiplier is then used to measure the change in voltage caused by absorption of light in the reactant solution. The change in voltage is monitored over time and converted into absorbance data using Equation 8.17. Rate constants, and the associated errors are calculated using expressions derived from Equation 8.16.

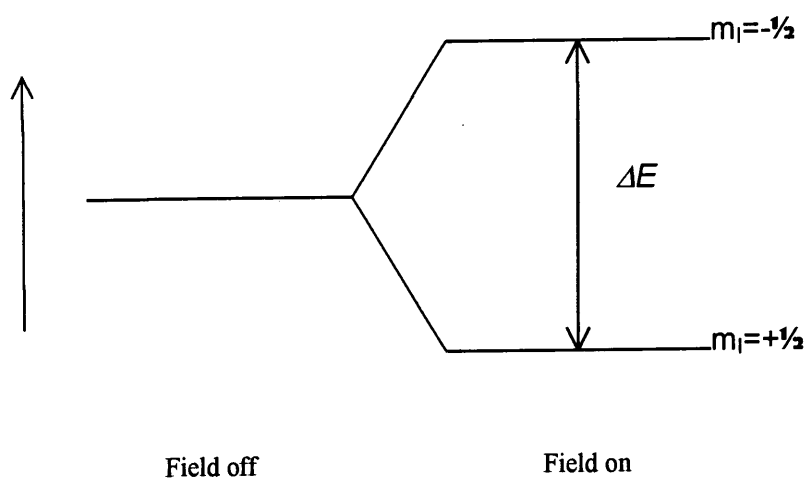
$$\text{Equation 8.17: Absorbance} = \log_{10} \left(\frac{V_0}{V_0 - \Delta V} \right)$$

8.1.3 NMR Spectroscopy

^1H NMR spectroscopy was used to ascertain the site of nucleophilic attack leading to σ -adduct formation, rate parameters and equilibrium constants, through chemical shifts, splitting patterns and coupling constants.

When a nucleus is placed in a magnetic field it will adopt one of a small number of allowed orientations of different energy. A proton ($I = \frac{1}{2}$) has two permitted orientations in a magnetic field, Figure 8.3. The difference in energy, ΔE , is dependent on the strength of the interaction between the nucleus and the field, the nuclear magnetic moment, and the strength of the magnetic field.

Figure 8.3: Energy levels of a hydrogen nucleus in a magnetic field.



The energy separation of the allowed spin orientations is measured by applying radiation of frequency ν . If $\Delta E = h\nu$, the frequency will cause the nuclei to “flip” from the lower to the higher energy level. For a given magnetic field strength and nuclei, the resonance frequency will depend on the chemical environment of the nucleus in the molecule, an effect known as the chemical shift.

The external field applied to a sample, B_0 , causes the electrons to circulate within their atomic orbitals. A small magnetic field, B' , is then induced in the opposite direction to B_0 . The nucleus is shielded from the applied field by the surrounding electrons according to Equation 8.18, where σ is the shielding constant, and B is the effective field experienced.

Equation 8.18: $B = B_0 - B' = B_0(1 - \sigma)$

For high resolution NMR, a magnet must generate a strong, homogeneous and stable magnetic field. Superconducting solenoids of resistance-free alloy supporting a persistent current are used to meet these requirements. A homogeneous field is created by placing shim coils around the sample, and by sample spinning. Magnetic field gradients are generated by the shim coils which will cancel any field gradients generated by the solenoid itself.³

A crucial feature of pulsed NMR, is the ability to excite uniformly and simultaneously all nuclei within a range of chemical shifts. A typical range of ^1H resonance frequencies is 4 kHz, which will excite all protons in the sample, irrespective of their resonance frequency. Pulses of radiofrequency radiation are applied to a probe, (consisting of a coil of wire or foil) which contains the sample, placed inside the magnet. The magnetic nuclei in the sample are excited by the radiofrequency field, and an oscillating voltage is induced in the coil which is passed to a receiver. The oscillating voltage is detected as a function of time after the pulse and is known as the free induction decay (FID). The FID is the sum of the individual nuclei, each with a characteristic offset frequency due to the chemical shift.

After amplification, the NMR signal is mixed with a reference voltage of the same voltage used to excite the spins. A Fourier Transform is then performed to convert the FID from the time domain to the frequency domain.

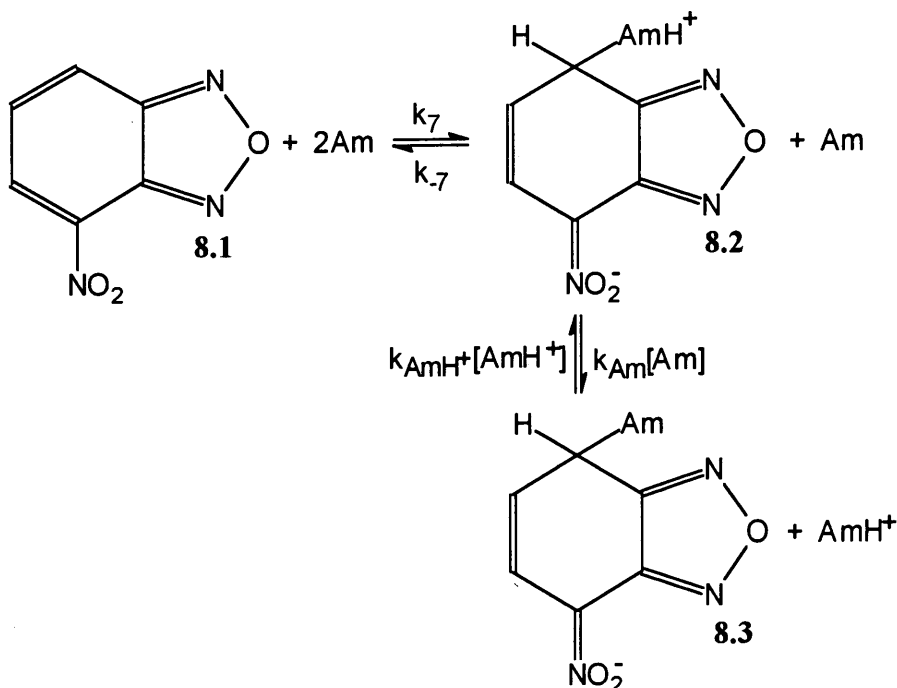
8.1.4 pH Measurements

All pH measurements were performed using a Jenway 3020 pH meter (accurate to 0.02 pH units). The meter was calibrated over the range pH 4.0 to 7.0, or pH 7.0 to 10.0, before use, according to the solution under study.

8.2 Derivation of Rate Equations

8.2.1 Attack at an Unsubstituted Ring Position

The general pathway for amine attack at an unsubstituted position of a benzofurazan derivative, **8.1**, is shown in Scheme 8.1, where attack is at the 7-position.



Scheme 8.1

An expression for the rate of formation of the intermediate, **8.2**, is given in Equation 8.19.

$$\text{Equation 8.19: } \frac{d[\mathbf{8.2}]}{dt} = k_7[\text{Am}][\mathbf{8.1}] + k_{AmH^+}[\text{AmH}^+][\mathbf{8.3}] - (k_{-7} + k_{Am}[\text{Am}])([\mathbf{8.2}])$$

If the zwitterionic intermediate, **8.2**, is treated as a steady-state intermediate, then the concentration is constant over time, and Equation 8.19 may be rearranged to give an expression for the concentration of **8.2**, Equation 8.20.

$$\text{Equation 8.20: } [\mathbf{8.2}] = \frac{k_7[\text{Am}][\mathbf{8.1}] + k_{AmH^+}[\text{AmH}^+][\mathbf{8.3}]}{k_{-7} + k_{Am}[\text{Am}]}$$

The rate of formation of the product, **8.3**, is defined in Equation 8.21.

$$\text{Equation 8.21: } \frac{d[\mathbf{8.3}]}{dt} = k_{Am}[Am][\mathbf{8.2}] - k_{AmH^+}[AmH^+][\mathbf{8.3}]$$

Substituting Equation 8.20 into Equation 8.21 leads to Equation 8.22.

$$\text{Equation 8.22: } \frac{d[\mathbf{8.3}]}{dt} = k_{Am}[Am] \left(\frac{k_7[\mathbf{8.1}][Am] + k_{AmH^+}[AmH^+][\mathbf{8.3}]}{k_{-7} + k_{Am}[Am]} \right) - k_{AmH^+}[AmH^+][\mathbf{8.3}]$$

Rearrangement gives Equation 8.23.

$$\text{Equation 8.23: } \frac{d[\mathbf{8.3}]}{dt} = \frac{k_7 k_{Am}[Am]^2[\mathbf{8.1}] - k_{-7} k_{AmH^+}[AmH^+][\mathbf{8.3}]}{k_{-7} + k_{Am}[Am]}$$

In the reaction solution, the sum of the concentrations of **8.1**, **8.2** and **8.3** is equal to the stoichiometric concentration of **8.1**, Equation 8.24.

$$\text{Equation 8.24: } [\mathbf{8.1}]_0 = [\mathbf{8.1}] + [\mathbf{8.2}] + [\mathbf{8.3}]$$

The concentration of **8.2** is negligible, as proton transfer is rapid, hence Equation 8.24 reduces to Equation 8.25.

$$\text{Equation 8.25: } [\mathbf{8.1}] = [\mathbf{8.1}]_0 - [\mathbf{8.3}]$$

Substitution into Equation 8.23, gives Equation 8.26.

$$\text{Equation 8.26: } \frac{d[\mathbf{8.3}]}{dt} = \frac{k_7 k_{Am}[Am]^2[\mathbf{8.1}]_0 - k_7 k_{Am}[Am]^2[\mathbf{8.3}] - k_{-7} k_{AmH^+}[AmH^+][\mathbf{8.3}]}{k_{-7} + k_{Am}[Am]}$$

At equilibrium, the concentration of **8.3** in solution is constant over time, and $[\mathbf{8.3}] = [\mathbf{8.3}]_{eq}$, resulting in Equation 8.27.

$$\text{Equation 8.27: } 0 = \frac{k_7 k_{Am} [Am]^2 [8.1]_0 - k_7 k_{Am} [Am]^2 [8.3]_{eq} - k_{-7} k_{AmH^+} [AmH^+] [8.3]_{eq}}{k_{-7} + k_{Am} [Am]}$$

Subtracting Equation 8.27 from Equation 8.26 leads to Equation 8.28, which can be rewritten in the form of Equation 8.29.

$$\text{Equation 8.28: } \frac{d[8.3]}{dt} = \left(\frac{k_7 k_{Am} [Am]^2 + k_{-7} k_{AmH^+} [AmH^+]}{k_{-7} + k_{Am} [Am]} \right) ([8.3]_{eq} - [8.3])$$

$$\text{Equation 8.29: } \frac{d[8.3]}{dt} \frac{1}{([8.3]_{eq} - [8.3])} = \left(\frac{k_7 k_{Am} [Am]^2 + k_{-7} k_{AmH^+} [AmH^+]}{k_{-7} + k_{Am} [Am]} \right)$$

As the benzofurazan derivative, **8.1**, does not absorb at the wavelength chosen, and the concentration of the intermediate, **8.2**, is negligible, there is no contribution to the absorbance from either species. Hence the only absorbing species is the product **8.3**. Application of the Beer-Lambert law, Equation 8.1 ($A = \epsilon cl$), results in Equation 8.29, which is the general expression for the absorbance, and Equation 8.30, for the absorbance at equilibrium.

$$\text{Equation 8.29: } A = \epsilon_{8.3} [8.3] \cdot l$$

$$\text{Equation 8.30: } A_{eq} = \epsilon_{8.3} [8.3]_{eq} \cdot l$$

Subtracting Equation 8.29 from Equation 8.30 gives Equation 8.31.

$$\text{Equation 8.31: } A_{eq} - A = \epsilon_{8.3} ([8.3]_{eq} - [8.3]) \cdot l$$

Differentiating Equation 8.29 leads to Equation 8.32.

$$\text{Equation 8.32: } \frac{dA}{dt} = \epsilon_{8.3} \cdot l \cdot \frac{d[8.3]}{dt}$$

Dividing this equation by Equation 8.31 leads to Equation 8.33.

$$\text{Equation 8.33: } \frac{dA}{dt} \frac{1}{(A_{eq} - A)} = \frac{d[\mathbf{8.3}]}{dt} \frac{1}{([\mathbf{8.3}]_{eq} - [\mathbf{8.3}])}$$

The observed first order rate constant is defined in Equation 8.34.

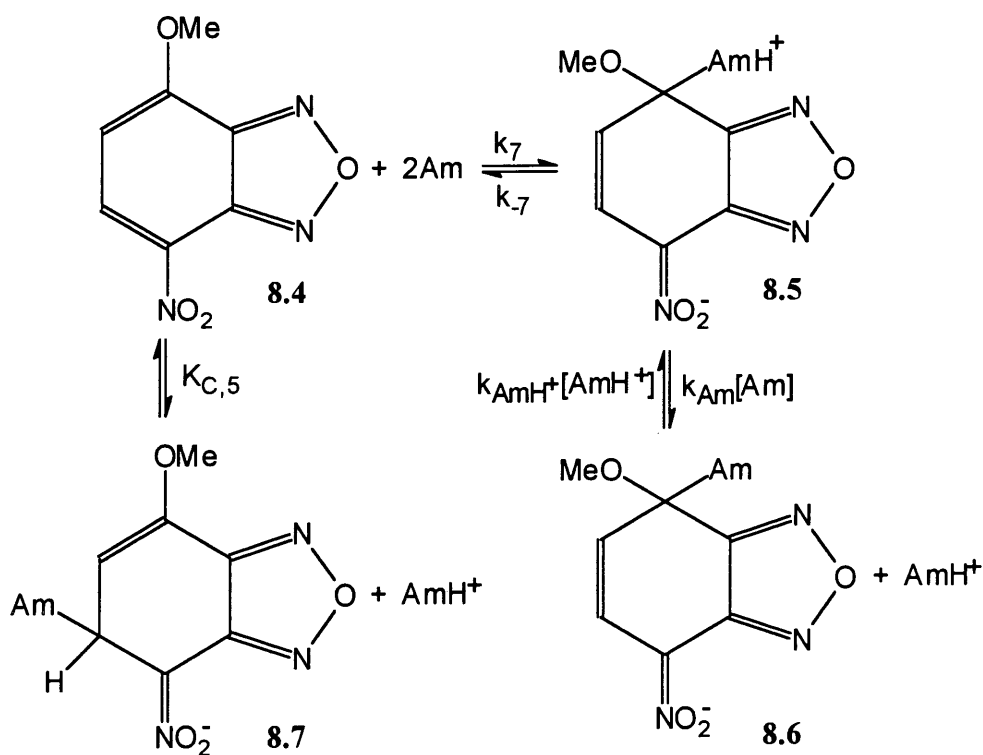
$$\text{Equation 8.34: } k_{obs} = \frac{dA}{dt} \frac{1}{(A_{eq} - A)}$$

Hence, combinations of Equations 8.29, 8.33 and 8.34 yields the expression for the first order rate constant for attack at an unsubstituted ring position of **8.1**, Equation 8.35.

$$\text{Equation 8.35: } k_{obs} = \frac{k_7 k_{Am} [Am]^2 + k_{-7} k_{AmH^+} [AmH^+]}{k_{-7} + k_{Am} [Am]}$$

8.2.2 Attack at a Substituted Ring Position

Scheme 8.2 illustrates the general attack of an amine at a substituted position of a benzofurazan derivative, **8.4**, to give **8.6**. The formation of the 7-adduct, **8.6**, is preceded by the rapid formation of the 5-adduct, **8.7**.



Scheme 8.2

The rate expression for the formation of **8.6** is given in Equation 8.36, derived in the same manner as Equation 8.23 (Section 8.2.1).

$$\text{Equation 8.36: } \frac{d[\mathbf{8.6}]}{dt} = \frac{k_7 k_{\text{Am}} [\text{Am}]^2 [\mathbf{8.4}] + k_{-7} k_{\text{AmH}^+} [\text{AmH}^+] [\mathbf{8.6}]}{k_{-7} + k_{\text{Am}} [\text{Am}]}$$

The stoichiometric concentration of **8.4** is equal to the sum of the concentrations of **8.4**, **8.6** and **8.7** in solution ($[\mathbf{8.5}] \approx 0$), Equation 8.37.

$$\text{Equation 8.37: } [\mathbf{8.4}]_0 = [\mathbf{8.4}] + [\mathbf{8.6}] + [\mathbf{8.7}]$$

The equilibrium constant for the formation of the 5-adduct, **8.7**, is given in Equation 8.38, which can be rearranged to give an expression for the concentration of **8.7**, Equation 8.39.

$$\text{Equation 8.38: } K_{C,5} = \frac{[\mathbf{8.7}][\text{AmH}^+]}{[\mathbf{8.4}][\text{Am}]^2}$$

$$\text{Equation 8.39: } [\mathbf{8.7}] = \frac{K_{C,5}[\mathbf{8.4}][\text{Am}]^2}{[\text{AmH}^+]}$$

Substitution of Equation 8.39 into Equation 8.37 to give Equation 8.40, and subsequent rearrangement to give Equation 8.41, leads to an expression for the concentration of **8.4**, Equation 8.42.

$$\text{Equation 8.40: } [\mathbf{8.4}]_0 = [\mathbf{8.4}] + [\mathbf{8.6}] + \frac{K_{C,5}[\mathbf{8.4}][\text{Am}]^2}{[\text{AmH}^+]}$$

$$\text{Equation 8.41: } [\mathbf{8.4}]_0 = [\mathbf{8.4}] \left(1 + \frac{K_{C,5}[\text{Am}]^2}{[\text{AmH}^+]} \right) + [\mathbf{8.6}]$$

$$\text{Equation 8.42: } [\mathbf{8.4}] = \frac{[\mathbf{8.4}]_0 - [\mathbf{8.6}]}{1 + \left(\frac{K_{C,5}[\text{Am}]^2}{[\text{AmH}^+]} \right)}$$

Substitution of Equation 8.42 into Equation 8.36 leads to Equation 8.43.

$$\text{Equation 8.43: } \frac{d[\mathbf{8.6}]}{dt} = \frac{k_7 k_{\text{Am}} [\text{Am}]^2 ([\mathbf{8.4}]_0 - [\mathbf{8.6}])}{(k - \gamma + k_{\text{Am}} [\text{Am}]) \left(1 + \frac{K_{C,5} [\text{Am}]^2}{[\text{AmH}^+]} \right)} - \frac{k - \gamma k_{\text{AmH}^+} [\text{AmH}^+][\mathbf{8.6}]}{k - \gamma + k_{\text{Am}} [\text{Am}]}$$

At equilibrium, the concentration of **8.6** is constant over time, and $[\mathbf{8.6}] = [\mathbf{8.6}]_{\text{eq}}$. Therefore, equation 8.43 may be written as Equation 8.44.

$$\text{Equation 8.44: } 0 = \frac{k_7 k_{Am} [Am]^2 ([8.4]_0 - [8.6]_{eq})}{(k_{-7} + k_{Am} [Am]) \left(1 + \frac{K_{C,5} [Am]^2}{[AmH^+]} \right)} - \frac{k_{-7} k_{AmH^+} [AmH^+] [8.6]_{eq}}{k_{-7} + k_{Am} [Am]}$$

Subtracting Equation 8.44 from Equation 8.43, results in Equation 8.45, which can be rewritten as Equation 8.46.

$$\text{Equation 8.45: } \frac{d[8.6]}{dt} = \left(\frac{k_7 k_{Am} [Am]^2}{(k_{-7} + k_{Am} [Am]) \left(1 + \frac{K_{C,5} [Am]^2}{[AmH^+]} \right)} - \frac{k_{-7} k_{AmH^+} [AmH^+]}{k_{-7} + k_{Am} [Am]} \right) ([8.6]_{eq} - [8.6])$$

$$\text{Equation 8.46: } \frac{d[8.6]}{dt} \frac{1}{([8.6]_{eq} - [8.6])} = \frac{k_7 k_{Am} [Am]^2}{(k_{-7} + k_{Am} [Am]) \left(1 + \frac{K_{C,5} [Am]^2}{[AmH^+]} \right)} - \frac{k_{-7} k_{AmH^+} [AmH^+]}{k_{-7} + k_{Am} [Am]}$$

If both **8.6** and **8.7** absorb at the wavelength used, application of the Beer-Lambert law yields Equation 8.47.

$$\text{Equation 8.47: } \frac{A}{l} = \epsilon_{8.6} [8.6] + \epsilon_{8.7} [8.7]$$

The concentration of **8.7** may be determined by Equation 8.48.

$$\text{Equation 8.48: } [8.7] = [8.4]_0 - [8.4] - [8.6]$$

Substitution of Equation 8.48 into Equation 8.47 yields Equation 8.49.

$$\text{Equation 8.49: } \frac{A}{l} = \epsilon_{8.6} [8.6] + \epsilon_{8.7} ([8.4]_0 - [8.4] - [8.6])$$

Substitution of the previously described expression for the concentration of **8.4**, Equation 8.42, and subsequent rearrangement leads to Equation 8.50 which can be factorised to give Equation 8.51.

$$\text{Equation 8.50: } \frac{A}{l} = \epsilon_{8.6}[\mathbf{8.6}] + \epsilon_{8.7}[\mathbf{8.4}]_0 - \frac{\epsilon_{8.7}[\mathbf{8.4}]_0[\text{AmH}^+]}{[\text{AmH}^+] + K_{C,5}[\text{Am}]^2} - \epsilon_{8.7}[\mathbf{8.6}] - \frac{\epsilon_{8.7}[\mathbf{8.6}][\text{AmH}^+]}{[\text{AmH}^+] + K_{C,5}[\text{Am}]^2}$$

$$\text{Equation 8.51: } \frac{A}{l} = [\mathbf{8.6}] \left(\epsilon_{8.6} - \frac{\epsilon_{8.7}K_{C,5}[\text{Am}]^2}{[\text{AmH}^+] + K_{C,5}[\text{Am}]^2} \right) + \frac{\epsilon_{8.7}[\mathbf{8.4}]_0K_{C,5}[\text{Am}]^2}{[\text{AmH}^+] + K_{C,5}[\text{Am}]^2}$$

Equation 8.51 may be simplified to give Equation 8.52.

$$\text{Equation 8.52: } \frac{A}{l} = [\mathbf{8.6}]Y + Z$$

At equilibrium, Equation 8.52 takes the form of Equation 8.53.

$$\text{Equation 8.53: } \frac{A_{\text{eq}}}{l} = [\mathbf{8.6}]_{\text{eq}}Y + Z$$

Multiplying both sides of Equations 8.52 and 8.53 by l and subtracting Equation 8.52 from Equation 8.53 leads to Equation 8.54.

$$\text{Equation 8.54: } A_{\text{eq}} - A = ([\mathbf{8.6}]_{\text{eq}} - [\mathbf{8.6}])Y.l$$

Differentiation and rearrangement of Equation 8.52 results in Equation 8.55.

$$\text{Equation 8.55: } \frac{dA}{dt} = l.Y \frac{d[\mathbf{8.6}]}{dt}$$

Dividing Equation 8.54 by Equation 8.55 gives Equation 8.56.

$$\text{Equation 8.56: } \frac{dA}{dt} \frac{1}{(A_{\text{eq}} - A)} = \frac{d[\mathbf{8.6}]}{dt} ([\mathbf{8.6}]_{\text{eq}} - [\mathbf{8.6}])$$

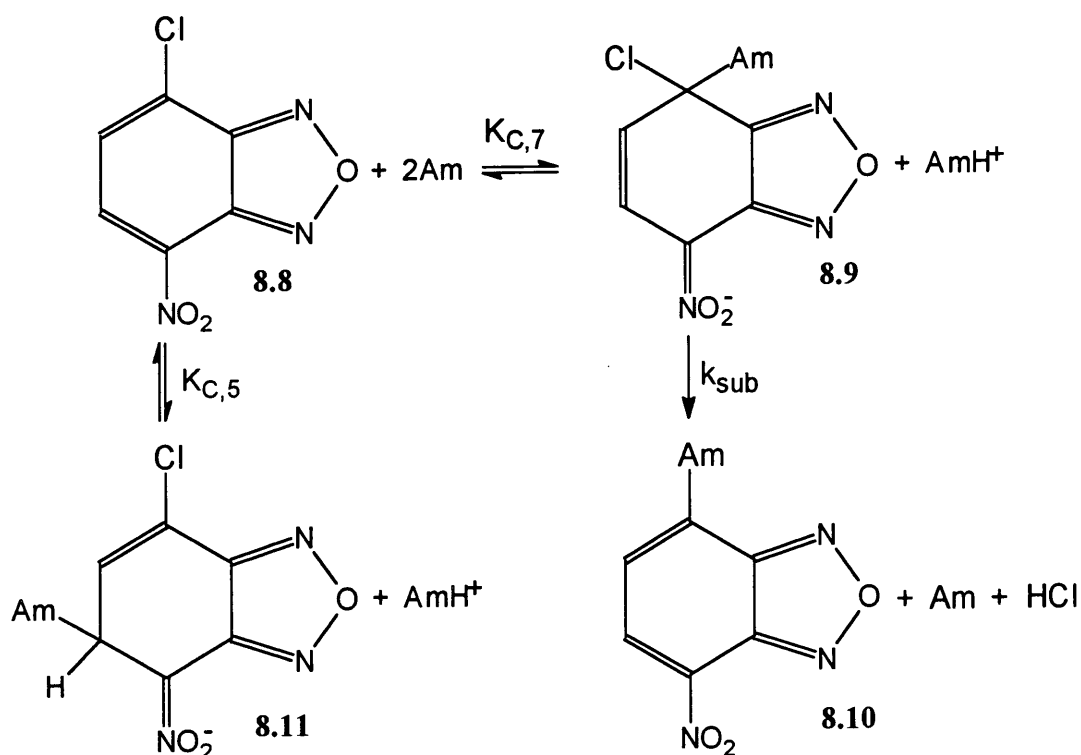
Application of the expression for k_{obs} , Equation 8.34, together with Equations 8.46 and 8.56, results in an expression showing the dependence of k_{obs} on the reagent concentrations

and the rate and equilibrium constants for the individual steps of the reaction, Equation 8.57.

$$\text{Equation 8.57: } k_{\text{obs}} = \frac{k_7 k_{\text{Am}} [\text{Am}]^2}{(k_{-7} + k_{\text{Am}} [\text{Am}]) \left(1 + \frac{K_{\text{C},5} [\text{Am}]^2}{[\text{AmH}^+]} \right)} - \frac{k_{-7} k_{\text{AmH}^+} [\text{AmH}^+]}{k_{-7} + k_{\text{Am}} [\text{Am}]}$$

8.2.3 Formation of the Substitution Product

Scheme 8.3 illustrates the general reaction pathway for formation of the substitution product, **8.10**.



Scheme 8.3

The reaction is followed by monitoring the rate of formation of **8.10**, according to Equation 8.58.

$$\text{Equation 8.58: } \frac{d[\mathbf{8.10}]}{dt} = k_{\text{sub}}[\text{AmH}^+][\mathbf{8.9}]$$

The sum of the concentrations of the species present in the reaction solution is equal to the stoichiometric concentration of **8.8**, Equation 8.59.

$$\text{Equation 8.59: } [\mathbf{8.8}]_0 = [\mathbf{8.8}] + [\mathbf{8.9}] + [\mathbf{8.10}] + [\mathbf{8.11}]$$

The equilibrium constants for the formation of the 5-adduct, **8.11** and the 7-adduct, **8.9**, are given by Equations 8.60 and 8.61 respectively.

$$\text{Equation 8.60: } K_{\text{C},5} = \frac{[\mathbf{8.11}][\text{AmH}^+]}{[\mathbf{8.8}][\text{Am}]^2}$$

$$\text{Equation 8.61: } K_{\text{C},5} = \frac{[\mathbf{8.9}][\text{AmH}^+]}{[\mathbf{8.8}][\text{Am}]^2}$$

Equations 8.60 and 8.61 may be rearranged and substituted into Equation 8.59, to give Equation 8.62.

$$\text{Equation 8.62: } [\mathbf{8.8}]_0 = \frac{[\mathbf{8.9}][\text{AmH}^+]}{K_{\text{C},7}[\text{Am}]^2} + [\mathbf{8.9}] + [\mathbf{8.10}] + \frac{K_{\text{C},5}[\mathbf{8.9}]}{K_{\text{C},7}}$$

Rearranging Equation 8.62, leads to an expression for **8.9**, Equation 8.63.

$$\text{Equation 8.63: } [\mathbf{8.9}] = \frac{K_{\text{C},7}[\text{Am}]^2}{[\text{AmH}^+] + K_{\text{C},7}[\text{Am}]^2 + K_{\text{C},5}[\text{Am}]^2} ([\mathbf{8.8}]_0 - [\mathbf{8.10}])$$

Substitution of Equation 8.63 into Equation 8.58 leads to Equation 8.64.

$$\text{Equation 8.64: } \frac{d[\mathbf{8.10}]}{dt} = \frac{k_{\text{sub}}K_{\text{C},7}[\text{AmH}^+][\text{Am}]^2}{[\text{AmH}^+] + K_{\text{C},7}[\text{Am}]^2 + K_{\text{C},5}[\text{Am}]^2} ([\mathbf{8.8}]_0 - [\mathbf{8.10}])$$

At equilibrium, the concentration of **8.10** is constant with time, and $[\mathbf{8.10}] = [\mathbf{8.10}]_{\text{eq}}$, leading to Equation 8.65.

$$\text{Equation 8.65: } 0 = \frac{k_{\text{sub}}K_{\text{C},7}[\text{AmH}^+][\text{Am}]^2}{[\text{AmH}^+] + K_{\text{C},7}[\text{Am}]^2 + K_{\text{C},5}[\text{Am}]^2} ([\mathbf{8.8}]_0 - [\mathbf{8.10}]_{\text{eq}})$$

Subtracting Equation 8.65 from Equation 8.64, results in Equation 8.66, which can be rearranged to give Equation 8.67.

$$\text{Equation 8.66: } \frac{d[\mathbf{8.10}]}{dt} = \frac{k_{\text{sub}}K_{\text{C},7}[\text{AmH}^+][\text{Am}]^2}{[\text{AmH}^+] + K_{\text{C},7}[\text{Am}]^2 + K_{\text{C},5}[\text{Am}]^2} ([\mathbf{8.10}]_{\text{eq}} - [\mathbf{8.10}])$$

$$\text{Equation 8.67: } \frac{d[\mathbf{8.10}]}{dt} \frac{1}{([\mathbf{8.10}]_{\text{eq}} - [\mathbf{8.10}])} = \frac{k_{\text{sub}}K_{\text{C},7}[\text{AmH}^+][\text{Am}]^2}{[\text{AmH}^+] + K_{\text{C},7}[\text{Am}]^2 + K_{\text{C},5}[\text{Am}]^2}$$

If **8.10** is the only absorbing species at the wavelength under study, application of the Beer-Lambert law leads to Equation 8.68.

$$\text{Equation 8.68: } A = \varepsilon_{\mathbf{8.10}}[\mathbf{8.10}].l$$

At equilibrium, Equation 8.68 is expressed in the form of Equation 8.69.

$$\text{Equation 8.69: } A_{\text{eq}} = \varepsilon_{\mathbf{8.10}}[\mathbf{8.10}]_{\text{eq}}.l$$

Subtracting Equation 8.68 from Equation 8.69 gives Equation 8.70.

$$\text{Equation 8.70: } A_{\text{eq}} - A = \varepsilon_{\mathbf{8.10}}([\mathbf{8.10}]_{\text{eq}} - [\mathbf{8.10}]).l$$

Differentiating Equation 8.68 gives Equation 8.71, and dividing this by Equation 8.70 leads to Equation 8.72.

$$\text{Equation 8.71: } \frac{dA}{dt} = \epsilon_{8.10} \frac{d[8.10]}{dt}$$

$$\text{Equation 8.72: } \frac{dA}{dt} \frac{1}{A_{eq} - A} = \frac{d[8.10]}{dt} \frac{1}{[8.10]_{eq} - [8.10]}$$

The first order rate constant, defined in Equation 8.34, may be defined in terms of the individual rate and equilibrium constants by combination of Equations 8.34, 8.67 and 8.72, according to Equation 8.73.

$$\text{Equation 8.73: } k_{obs} = \frac{k_{sub} K_{c,7} [AmH^+] [Am]^2}{[AmH^+] + K_{c,7} [Am]^2 + K_{c,5} [Am]^2}$$

8.3 Publications, Conferences, Examined Lecture Courses and Colloquia

8.3.1 Research Publications

The following publications have arisen from the work in this thesis,

- 1) M. R. Crampton, L. C. Rabbitt and F. Terrier., *Can. J. Chem.*, 1999, **77**, 639-646.
- 2) M. R. Crampton and L. C. Rabbitt., *J. Chem. Soc., Perkin Trans. 2.*, 1999, 1669-1674.
- 3) M. R. Crampton, J. Delaney and L. C. Rabbitt., *J. Chem. Soc., Perkin Trans. 2.*, 1999, 2473-2480.

8.3.2 Conferences Attended

During the course of my Ph.D., I have attended the following conferences,

- 1) Royal Society of Chemistry, Organic Mechanisms Group, Welwyn Garden City, September 1999.
- 2) 7th European Symposium of Organic Reactivity, (ESOR-7), Ulm, Germany, August 1999.
- 3) 8th Winter School of Organic Reactivity, (WISOR-8), Bressanone, Italy, January 1999.

4) Royal Society of Chemistry, Organic Mechanisms Group, Huddersfield, September 1998.

8.3.3 Examined Lecture Courses

The following lecture courses were undertaken,

- 1) Practical Nuclear-Magnetic Resonance
- 2) Synthetic Methodology in Organometallic and Coordination Chemistry
- 3) Experimental Design and Instrumentation

8.3.4 Colloquia, Lectures and Seminars

1997

- | | |
|-------------|---|
| October 8 | Professor E Atkins, Department of Physics, University of Bristol
Advances in the control of architecture for polyamides: from nylons to genetically engineered silks to monodisperse oligoamides |
| October 15 | Dr R M Ormerod, Department of Chemistry, Keele University
Studying catalysts in action |
| October 21 | Professor A F Johnson, IRC, Leeds
Reactive processing of polymers: science and technology |
| October 22 | Professor R J Puddephatt (RSC Endowed Lecture), University of Western Ontario
Organoplatinum chemistry and catalysis |
| October 23 | Professor M R Bryce, University of Durham, Inaugural Lecture
New Tetrathiafulvalene Derivatives in Molecular, Supramolecular and Macromolecular Chemistry: controlling the electronic properties of organic solids |
| October 29 | Professor R Peacock, University of Glasgow
Probing chirality with circular dichroism |
| October 28 | Professor A P de Silva, The Queen's University, Belfast
Luminescent signalling systems" |
| November 5 | Dr M Hii, Oxford University
Studies of the Heck reaction |
| November 11 | Professor V Gibson, Imperial College, London |

Metallocene polymerisation

- November 12 Dr J Frey, Department of Chemistry, Southampton University
Spectroscopy of liquid interfaces: from bio-organic chemistry to atmospheric chemistry
- November 19 Dr G Morris, Department of Chemistry, Manchester Univ.
Pulsed field gradient NMR techniques: Good news for the Lazy and DOSY
- November 20 Dr L Spiccia, Monash University, Melbourne, Australia
Polynuclear metal complexes
- November 25 Dr R Withnall, University of Greenwich
Illuminated molecules and manuscripts
- November 26 Professor R W Richards, University of Durham, Inaugural Lecture
A random walk in polymer science
- December 2 Dr C J Ludman, University of Durham
Explosions
- December 3 Professor A P Davis, Department of Chemistry, Trinity College Dublin.
Steroid-based frameworks for supramolecular chemistry
- December 10 Sir G Higginson, former Professor of Engineering in Durham and retired Vice-Chancellor of Southampton Univ.
1981 and all that.
- December 10 Professor M Page, Department of Chemistry, University of Huddersfield
The mechanism and inhibition of beta-lactamases
- October 27 Professor W Roper FRS. University of Auckland, New Zealand
- 1998**
- January 14 Professor D Andrews, University of East Anglia
Energy transfer and optical harmonics in molecular systems
- January 20 Professor J Brooke, University of Lancaster
What's in a formula? Some chemical controversies of the 19th century
- January 27 Professor R Jordan, Dept. of Chemistry, Univ. of Iowa, USA.
Cationic transition metal and main group metal alkyl complexes in olefin polymerisation
- January 28 Dr S Rannard, Courtaulds Coatings (Coventry)
The synthesis of dendrimers using highly selective chemical reactions
- February 3 Dr J Beacham, ICI Technology

The chemical industry in the 21st century

- February 4 Professor P Fowler, Department of Chemistry, Exeter University
Classical and non-classical fullerenes
- February 17 Dr S Topham, ICI Chemicals and Polymers
Perception of environmental risk; The River Tees, two different rivers
- February 18 Professor G Hancock, Oxford University
Surprises in the photochemistry of tropospheric ozone
- February 24 Professor R Ramage, University of Edinburgh
The synthesis and folding of proteins
- February 25 Dr C Jones, Swansea University
Low coordination arsenic and antimony chemistry
- March 4 Professor T C B McLeish, IRC of Polymer Science Technology, Leeds University
The polymer physics of pyjama bottoms (or the novel rheological characterisation of long branching in entangled macromolecules)
- March 11 Professor M J Cook, Dept of Chemistry, UEA
How to make phthalocyanine films and what to do with them.
- March 17 Professor V Rotello, University of Massachusetts, Amherst
The interplay of recognition & redox processes - from flavoenzymes to devices
- March 18 Dr J Evans, Oxford University
Materials which contract on heating (from shrinking ceramics to bullet proof vests)
- October 7 Dr S Rimmer, Ctr Polymer, University of Lancaster
New Polymer Colloids
- October 9 Professor M F Hawthorne, Department Chemistry & Biochemistry, UCLA, USA
RSC Endowed Lecture
- October 21 Professor P Unwin, Department of Chemistry, Warwick University
Dynamic Electrochemistry: Small is Beautiful
- October 23 Professor J C Scaiano, Department of Chemistry, University of Ottawa, Canada
In Search of Hypervalent Free Radicals, RSC Endowed Lecture
- October 26 Dr W Peirs, University of Calgary, Alberta, Canada

Reactions of the Highly Electrophilic Boranes $\text{HB}(\text{C}_6\text{F}_5)_2$ and $\text{B}(\text{C}_6\text{F}_5)_3$
with Zirconium and Tantalum Based Metallocenes

- October 27 Professor A Unsworth, University of Durham
What's a joint like this doing in a nice girl like you?
In association with The North East Polymer Association
- October 28 Professor J P S Badyal, Department of Chemistry, University of Durham
Tailoring Solid Surfaces, Inaugural Lecture
- November 4 Dr N Kaltsoyannis, Department of Chemistry, UCL, London
Computational Adventures in d & f Element Chemistry
- November 3 Dr C J Ludman, Chemistry Department, University of Durham
Bonfire night Lecture
- November 10 Dr J S O Evans, Chemistry Department, University of Durham
Shrinking Materials
- November 11 Dr M Wills, Department of Chemistry, University of Warwick
New Methodology for the Asymmetric Transfer Hydrogen of Ketones
- November 12 Professor S Loeb, University of Windsor, Ontario, Canada
From Macrocycles to Metallo-Supramolecular Chemistry
- November 17 Dr J McFarlane
Nothing but Sex and Sudden Death!
- November 18 Dr R Cameron, Department of Materials Science & Metallurgy, Cambridge
University
Biodegradable Polymers
- November 24 Dr B G Davis, Department of Chemistry, University of Durham
Sugars and Enzymes
- December 1 Professor N Billingham, University of Sussex
Plastics in the Environment - Boon or Bane
In association with The North East Polymer Association.
- December 2 Dr M Jaspers, Department of Chemistry, University of Aberdeen
Bioactive Compounds Isolated from Marine Invertebrates and Cyanobacteria
- December 9 Dr M Smith Department. of Chemistry, Warwick University
Multinuclear solid-state magnetic resonance studies of nanocrystalline
oxides and glasses

1999

- January 19 Dr J Mann, University of Reading

The Elusive Magic Bullet and Attempts to find it?

- January 20 Dr A Jones, Department of Chemistry, University of Edinburgh
Luminescence of Large Molecules: from Conducting Polymers to Coral Reefs
- January 27 Professor K Wade, Department of Chemistry, University of Durham
Foresight or Hindsight? Some Borane Lessons and Loose Ends
- February 3 Dr C Schofield, University of Oxford
Studies on the Stereoelectronics of Enzyme Catalysis
- February 9 Professor D J Cole-Hamilton, St. Andrews University
Chemistry and the Future of life on Earth
- February 10 Dr C Bain, University of Oxford
Surfactant Adsorption and Marangoni Flow at Expanding Liquid Surfaces
- February 17 Dr B Horrocks, Department of Chemistry, Newcastle University
Microelectrode techniques for the Study of Enzymes and Nucleic Acids at Interfaces
- February 23 Dr C Viney, Heriot-Watt
Spiders, Slugs And Mutant Bugs
- February 24 Dr. A-K Duhme, University of York
Bioinorganic Aspects of Molybdenum Transport in Nitrogen-Fixing Bacteria
- March 3 Professor B Gilbert, Department of Chemistry, University of York
Biomolecular Damage by Free Radicals: New Insights through ESR Spectroscopy
- March 9 Dr Michael Warhurst, Chemical Policy issues, Friends of the Earth
Is the Chemical Industry Sustainable?
- March 10 Dr A Harrison, Department of Chemistry, The University of Edinburgh
Designing model magnetic materials
- March 17 Dr J Robertson, University of Oxford
Recent Developments in the Synthesis of Heterocyclic Natural Products
- May 11 Dr John Sodeau, University of East Anglia
Ozone Holes and Ozone Hills
- May 12 Dr Duncan Bruce, Exeter University
The Synthesis and Characterisation of Liquid-Crystalline Transition Metal Complexes

- October 12 Dr. S. Beckett (Nestle)
Chocolate for the next Millennium
- October 13 Professor G. Fleet, University of Oxford
Sugar Lactone and Amino Acids
- October 19 Professor K. Gloe, TU Dresden, Germany
Tailor Made Molecules for the Selective binding of Metal Ions
- October 20 Professor S. Lincoln, University of Adelaide
Aspects of Complexation and Supramolecular Chemistry
- October 25 Professor S. Collins, University of Waterloo, Canada
Methacrylate Polymerization Using Zirconium Enolate Initiators:
Polymerization Mechanisms and Control of Polymer Tacticity
- October 26 Dr. D. Hughes (Astra Zeneca)
Perspectives in Agrochemistry
- October 27 Dr. C. Braddock, Imperial College
Novel catalysts for Atom Economic Transformations
- November 3 Professor D.W. Smith, University of Waikato, NZ
The Strengths of C-C and C-H Bonds in Organic and Organometallic
Molecules: Empirical, Semi-empirical and Ab Initio Calculations
- November 10 Dr. I. Samuel, Department of Physics, University of Durham
Improving Organic Light Emitting Diodes by Molecular, Optical and Device
Design
- November 16 Professor A. Holmes
Conjugated Polymers for the Market Place
- November 17 Dr. J. Rourke, University of Warwick
C-H Activation Induced by Water
- November 18 Dr. G. Siligardi, Kings College London
The Use of Circular Dichroism to Detect and Characterise Biomolecular
Interactions in Solution.
- November 23 Professor B. Caddy
Trace evidence - a challenge for the forensic scientist
- November 24 Professor T. Jones, Imperial College
Atomic and Molecular Control of Inorganic and Organic Semiconductor
Thin Films
- November 30 Rev. R. Lancaster
Principles and Practice

- December 8 Professor D. Crout, Department of Chemistry, University of Warwick
More than Simply Sweet: Carbohydrates in Medicine and Biology
- 2000**
- January 12 Professor D. Haddleton, Department of Chemistry, University of Warwick
Atom Transfer Polymerisation - What's all the Hype About?
- January 19 Dr. P.R. Fielden, UMIST
Miniaturised Chemical Analysis (Lab-on-a-Chip): Functional or Merely Fashionable?
- January 25 Professor B. Meijer
From Supramolecular Architecture Towards Functional Materials
- January 26 Professor S. Flisch, University of Edinburgh
The challenges involved in protein glycosylation - synthesis of glycan chains and selective attachment to proteins
- February 1 Professor R. Snaith
Egyptian Mummies - what, why, who & how!
- February 2 Chick Wilson, Head of Crytallography, ISIS, Rutherford Appleton Lab
Protons in motion? Neutron diffraction studies of hydrogen atoms in organic crystal structures.
- February 9 Dr. S. Moratti, University of Cambridge
Shape and Stereoselectivity in Polymer
- February 15 Professor D. Phillips
A Little Light Relief
- February 16 Professor Kocienski, University of Glasgow
Asymmetric Synthesis Using Planar Chiral TT-Allyl Cationic Complexes
- February 23 Dr. N. Clarke, UMIST
The Flow of Polymer Blends
- February 22 Professor G. Stuart
Brewing - Evolution from a Craft into a Technology
- March 1 Professor D. Tildsley, Unilever (Head of Research)
Computer Simulation of Interfaces: Fact and Friction
- March 7 Prof. Motherwell, Unviersity College, London
Curiosity and Simplicity - Essential Ingredients for the Discovery of New Reactions
- March 8 Professor J. Courtieu, Universite de Paris-Sud, Orsay

Chiral Recognition through NMR in Liquid Crystal Solvents: an Order Affair

- March 9 Dr. Antony Fairbanks, Dyson-Perrins Laboratory, Oxford
Selectivity in Glycoside Formation"
- March 20 Professor S Marder, Professor of Chemistry and Optical Sciences,
University of Arizona
Design of Molecules for Two-Photon Absorption and their Application to
3D Polymerization and Imaging
- March 21 Professor E. Rizzardo, CSIRO Mol. Sci. Victoria, Australia
Designed Polymers by Free Radical Addition-Fragmentation Processes
- May 5 Professor R. Hochstrasser, University Pennsylvania, USA
Ultrafast Molecular and Protein Dynamics seen through their Vibrations

8.4 References

-
- ¹ L. M. Harwood and T. D. W. Claridge. "Introduction to Organic Spectroscopy". Oxford Chemistry Primers. 1997.
- ² B. G. Cox. "Modern Liquid Phase Kinetics". Oxford Chemistry Primers. 1996.
- ³ P. J. Hore. "Nuclear Magnetic Resonance". Oxford Chemistry Primers. 1995.

